Use of luminescent proximity-based techniques to investigate IL-23 receptor complex formation, cytokine binding and activation in living cells

Charles Lay, Bsc (Hons).

Thesis submitted to the University of Nottingham

for the degree of Doctor of Philosophy

Abstract

The cytokine IL-23 is a pro-inflammatory messenger molecule, involved in upregulating the immune response after infection by fungal and bacterial pathogens. The pathway is also crucial to the induction and maintenance of several auto-inflammatory diseases, including Psoriatic Arthritis, Plaque Psoriasis, Crohn's Disease and Ulcerative Colitis. Over the last decade anti-IL-23 antibody drugs have been developed and shown to be effective treatments for these conditions. However, despite the proven efficacy of drugs targeting the IL-23 pathway, little is known about the ligand binding and activation mechanism of the receptor, which is made up of the receptor chains IL23R and IL12Rβ1. Further pharmacological characterisation of the receptor could enable the targeting of the receptor with alternative modalities such as small molecule or peptide antagonists.

In this project, proximity-based techniques are utilised to quantify the interaction of IL-23 with its receptor and to probe how engagement of ligand leads to activation of signalling. Initially a NanoBRET ligand binding assay was created and used to quantify the interaction between a fluorescently tagged version of IL-23 and the full-length *N*-terminally NanoLuc labelled receptor components IL23R and IL12Rβ1, expressed individually and together in the membranes of living cells. An intra-receptor NanoBRET assay was also used to measure the formation of receptor complexes and changes in the relative positions of the *N*-terminal domains of the receptor. The results from these experiments demonstrated that the IL-23 receptor complex forms in the absence of ligand, with subsequent binding of cytokine to the high affinity binding site initiating a potent change in the conformation of the *N*-terminal domains of the receptor.

Further study of receptor heteromer formation using split luciferase complementation and measurement of receptor activation with a phospho-STAT3 AlphaLISA assay, confirmed that receptor components formed inactive complexes in the absence of ligand, that could be activated through addition of IL-23. This technique also allowed the induction of ligand independent signalling complexes through the high affinity crosslinking of the receptor *N*-terminal domains in certain conformations.

The assays developed were then utilised to characterise receptor antagonists including a cyclic peptide from an emerging class of IL23R inhibitors, which was subsequently developed into a probe specific to the IL23R:IL-23 interface. Finally, the effect of several disease relevant mutations of IL23R on ligand binding, conformational change and activation were tested, demonstrating that the mechanism of action of the C115Y mutation is disruption of the interaction between IL23R and IL-23.

Publications Arising

- Lay CS, Bridges A, Goulding J, Briddon SJ, Soloviev Z, Craggs PD and Hill SJ**.** (2022) Probing the binding of interleukin-23 to individual receptor components and the IL-23 heteromeric receptor complex in living cells using NanoBRET. Cell Chem Biol, 29: 19-29.
- Lay CS, Kilpatrick LE, Craggs PD & Hill SJ. (2022) Use of NanoBiT and NanoBRET to characterise Interleukin-23 receptor dimer formation in living cells. Br. J. Pharmacol. In press.
- Lay CS, Kilpatrick LE, Isidro-Llobet A, Craggs PD and Hill SJ. Use of a fluorescent cyclic peptide probe specific to the Interleukin-23 receptor subunit IL23R to characterise receptor antagonists and receptor variants. (Under review).

Acknowledgements

This PhD would not have been possible without the generous backing of many scientists and support staff at both GSK and the University of Nottingham, who facilitated the lab work, took part in the many stimulating discussions behind this study and created the friendly and helpful environment in which the project was completed. Firstly, I would like to thank both my academic supervisor Stephen Hill and my industrial supervisor Peter Craggs who were instrumental in the design and facilitation of a highly interesting and fulfilling project. Both Steve and Pete worked tirelessly to support me throughout the process and their guidance and experience allowed me to vastly improve my scientific skillset.

At GSK I would like to thank Chris Larminie, Melanie Leveridge, Ryan Bingham and Andy Powell for their help in originating and facilitating the project, Angela Bridges for molecular biology guidance, Albert Isidro Llobet for help with the synthesis of chemical probes and Zoja Soloviev for her help with the LC-MS experiments.

I would also like to thank the postdoctoral team within the Cell Signalling group at Nottingham and specifically Laura Kilpatrick, Mark Soave, Joelle Goulding and Simon Platt for all the help they gave in training me, engaging in discussions and making the lab a fun place to work during my time at the university.

I would also like to thank Stephen Briddon, Seema Rajani and Tim Self for their training in the FCS and imaging techniques used during the project and Richard Proudman and Marleen Groenen for their help keeping the lab running through the many challenges of the last few years. I am also very grateful to Luisa Martinez-Pomares for her great commitment to being my pastoral supervisor. I am thankful to everyone involved in the COMPARE initiative, especially the team science committee members who enabled the many training and career progression opportunities I was able to take part in.

I would like to thank my friends and family for their various distractions from the lab over the years. Specifically, I'd like to thank Alex Mckenna and his UCL colleagues for allowing me to gate crash their British Society for Immunology conference attending /Golden Eagle spotting and whisky tasting trips and my fellow PhD students at the University of Nottingham who have become some of

my closest friends, including Chloe Peach, Edward Wragg, Lydia Ogrodzinski, Nikki Dijon, Clare Harwood, Sean Cullum, Desislava Nesheva, George Coney and Jack Lochray. You are a diverse group of amazing personalities the like of which it is unlikely will ever be assembled again under one roof, who made Nottingham the place to be. Finally, thank you to Rhiannon for the support, diversion, and advice you have given over the last four rollercoaster years.

Abbreviations

AF488	AlexaFluor-488
ANOVA	Analysis of variance
APC	Antigen presenting cell
AS	Ankylosing Spondylitis
B_{max}	Maximal binding
BSA	Bovine Serum Albumin
CD	Crohn's Disease
CK	Casein Kinase
DMEM	Dulbecco's Modified Eagle Medium
DTT	Dithiothreital
E. coli	*Escherichia coli*
EBI3	Epstein Barr virus Induced gene 3
EC_{50}	Agonist concentration that gives 50% efficacy
ECD	Extracellular domain
ELISA	Enzyme Linked Immunosorbent Assay
EPO	Erythropoietin
FBS	Fetal Bovine Serum
FCS	Fluorescence Correlation Spectroscopy
FRET	Förster Resonance Energy Transfer
GFP	Green Fluorescent Protein
GHR	Growth Hormone Receptor
GPCR	G-protein Coupled Receptor
GWAS	Genome Wide Association Studies
HBSS	Hanks Buffered Saline Solution

HEK293T	Human Embryonic Kidney cell 293T
HiBiT	High affinity fragment of NanoLuc
HT	HaloTag
IBD	Inflammatory Bowel Disease
IC_{50}	Antagonist concentration that gives 50% inhibition
ICD	Intracellular domain
IFN	Interferon
IL	I**nterleukin**
ILC	Innate Lymphoid Cell
ITC	Isothermal Calorimetry
JAK	Janus Kinase
K_D	Dissociation constant
K_I	Inhibition constant
K_{off}	Dissociation rate
K_{on}	Association rate
LB	Lysogeny Broth
LC-MS	Liquid Chromatography coupled Mass Spectrometry
LgBiT	Large fragment of NanoLuc
MAIT	Muscosally Associated Invariant T (cell)
NAM	Negative Allosteric Modulator
NanoBiT	NanoLuc Binary Technology
NanoBRET	NanoLuc Bioluminescence Resonance Energy Transfer
NHS-(Ester)	*N*-Hydroxysuccinimide
NL	NanoLuciferase

P630	Peptide 630
PA	Psoriatic Arthritis
PBS	Phosphate Buffered Saline
PCH	Photon Counting Histogram
PCR	Polymerase Chain Reaction
PDB	Protein Data Bank
PDL	Poly-D-Lysine
PFA	Paraformaldehyde
PTM	Post-translational Modification
RORγT	Retinoic acid receptor Related Orphan Receptor yt
SD	Standard Deviation of the mean
SEM	Standard Error of the Mean
SmBiT	Low affinity fragment of NanoLuc
SNP	Single Nucleotide Polymorphism
SOCS	Suppressor of Cytokine Signalling
SPR	Surface Plasmon Resonance
STAT	Signal Transducer and Activator of Transcription
TAE	Tris Acetic EDTA
TAMRA	Tetramethylrhodamine
TCR	T Cell Receptor
Th17	T helper 17
TIRF-M	Total Internal Refection Fluorescence Microscopy
TMD	Transmembrane domain
TPOR	Thrombopoietin Receptor

TYK2	Tyrosine Kinase 2
UC	Ulcerative Colitis
UV	Ultraviolet

Table of Contents

Chapter 1. Introduction

1.1 General introduction

The cytokine interleukin-23 (IL-23) is a pro-inflammatory signalling molecule involved in the immune system's response to pathogens through the induction and maintenance of pro-inflammatory immune responses (Floss et al., 2015). Loss of function in IL-23 pathway genes can lead to compromised immunity but has also been shown to be protective against auto-inflammatory disorders (Martínez-barricarte et al., 2018; Staels et al., 2022). The cytokine is a successful drug target for anti-IL-23 therapeutics and peptide antagonists of the receptor are in development (Chyuan and Lai, 2020; Sayago et al., 2018). Despite the therapeutic importance of the IL-23 pathway, the mechanism by which ligand binding leads to activation of the receptor remains unclear with a conserved mechanism of activation remaining a matter of controversy in the wider cytokine receptor field (Bloch et al., 2018; Sivanesan et al., 2016).

The IL-23 cytokine is made up of two di-sulphide linked proteins IL23p19 and IL12p40. The IL-23 receptor is formed of two single transmembrane domain proteins; IL23R and IL12Rβ1 which transduce the binding of IL-23 through the trans-phosphorylation of constitutively associated Janus Kinase (JAK) proteins. Signalling is then transduced by the phosphorylation of further signalling molecules, for example STAT3, which are phosphorylated by these activated JAK proteins (Floss et al., 2015).

This project aims to use proximity-based, target engagement techniques to measure the engagement of ligand by the IL-23 receptor expressed on living cells, gain insights into how binding leads to signal transduction and generate tools for further pharmacological study of the receptor.

1.2 Conserved structural features of cytokines and cytokine receptors

The function of cytokines and their receptors is mediated by their specialised structures. In this section the conserved features of cytokines and cytokine receptors will be introduced before the specific structural features of the IL-23 cytokine receptor are discussed in detail.

Cytokines and their receptors are a diverse family of proteins grouped primarily by their function in transmitting intercellular signals relating to the immune response (Brocker et al., 2010). The super family of signalling molecules is broadly split into six families: the interferons, tumour necrosis factors (TNFs), tumour growth factors (TGFs), chemokines, colony stimulating factors (CSFs) and interleukins (Table 1-1; Akdis et al., 2016; Hamilton, 2008; Zlotnik and Yoshie, 2012). Cytokines are generally mono, dimeric or trimeric proteins which signal through single transmembrane domain containing receptors with the exception of the chemokine family which signal using class A G-Protein Coupled Receptors (GPCRs) (Akdis et al., 2016; Zlotnik and Yoshie, 2012). Other than receptor serine/threonine and tyrosine kinases most of these single pass receptors lack intrinsic catalytic activity and instead signal through constitutively associated signal transducers (Vander Ark et al., 2018). The interleukins are the largest and most structurally diverse group of cytokines, made up of four subfamilies grouped by their shared structural features: these are the IL-1 type, class I helical, class II helical and IL-17 types (Akdis et al., 2016; Brocker et al., 2010).

Cytokine Family	Structural Features of Cytokines	Receptors Subtypes	Structural Features of cytokine receptors	Key Signal Transducers
Interferons (Walter, 2020)	Monomeric α-helical bundles	Class II cytokine receptors	Heterodimers of single TMD proteins.	JAK/STAT pathway
TNFs (Dostert et al., 2019)	Homo-trimeric complexes of THR containing proteins	TNF receptors	Trimeric complexes of single TMD proteins.	TRADD/TRAF pathway, FADD, RIPK-1 etc.
TGFs (Hinck, 2012)	Disulphide linked homodimeric complexes	Receptor Serine/Threonine and Tyrosine Kinases	Homodimers with intrinsic catalytic activity	Smads
CSFs (Hamilton, 2008)	Homodimeric and monomeric	Mixed	Hetero and homodimeric Class I Cytokine receptors / homodimeric receptor tyrosine kinase	JAK/STAT pathway
Chemokines (Zlotnik and Yoshie, 2012)	Monomeric peptides with intramolecular disulphide bonds	Class A GPCRs	Seven transmembrane domain containing monomers	Gαi proteins, β arrestin
Interleukins (Brocker et al., 2010)	Monomers and dimers often consisting of α-helical bundles	Class I and II cytokine receptors	Hexamers/dimers of single TMD proteins.	JAK/STAT pathway

Table 1-1: An overview of the structural features of cytokines and their receptors. A table summarising the general features of each Cytokine family. Review articles summarising the structural features of each of the families are included in the first column. TNF = Tumour necrosis factor, TGF = tumour growth factor, CSF = Colony stimulating factor, THR = TNF homology region, TRADD = TNF receptor type 1-associated DEATH domain protein, TRAF = TNF receptor associated factor, FADD = Fas-associated DEATH domain protein and RIPK-1 = Receptor-interacting serine/threonine-protein kinase 1.

A structurally conserved group of single pass receptors termed 'cytokine receptors' sense interleukins, some CSFs and interferons in addition to other hormones such as Erythropoietin (EPO) (Figure 1-1) (Spangler et al., 2015). The cytokine receptor superfamily is divided into class I or class II receptors sub-classes with class I receptors containing a characteristic WSxWS motif (Olsen and Kragelund, 2014). Both receptor classes are characterised by an *N*-terminal structured extracellular domain (ECD), a helical transmembrane domain (TMD) and disordered intracellular domain (ICD) (Pang and Zhou, 2012; Spangler et al., 2015).

The class I or haemopoietic cytokine family is further divided into the homodimeric, γc containing, βc containing and gp130 containing families, with the latter three groups being characterised by the sharing of common receptor chains (Akdis et al., 2016; Spangler et al., 2015). All class I cytokine receptors share at least one cytokine homology region made up of two type III fibronectin domains, containing two disulphide bridges and a WSxWS motif, which has been suggested to interact with the extracellular matrix (Olsen and Kragelund, 2014). The receptors may also exhibit additional fibronectin domains, immunoglobulin domains and stalk regions in their ECDs (Spangler et al., 2015).

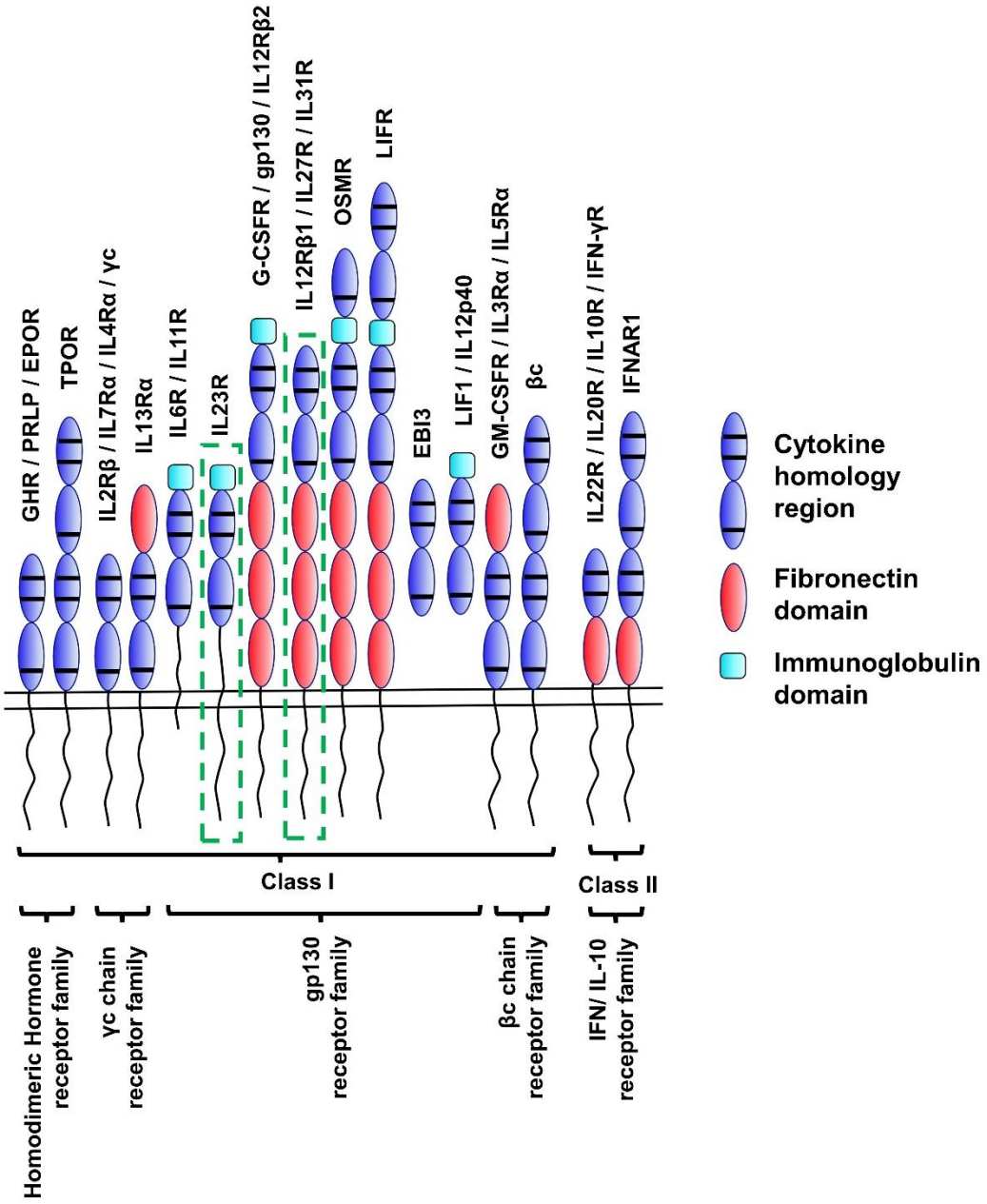

Figure 1-1: Structural features of the cytokine receptor family. Schematic highlighting the conserved structural features of the cytokine receptor family. Each receptor that shares the same series of domains is highlighted at the *N*-terminus of the appropriate cartoon structure. Receptors are separated into sub-groups based on structural homology as shown at the *C*-terminus of the cartoon.

There are limited structures available of the class I cytokine receptors and of cytokine receptors as a whole. A quarter of class I receptors have no solved structures, with six structures of the parts of the ICDs in complex with signal transducers available and the remaining structures being fragments of the ECD (Seiffert et al., 2020). No high-resolution structures have been solved of class I

TMDs although several studies have gained structures using nuclear magnetic resonance (NMR) (Metcalfe et al., 2020; Seiffert et al., 2020).

1.2.1 The IL-6 and IL-12 cytokine and receptor family

Within the gp130 sub-family of cytokine receptor chains, (which are named for their structural homology or shared complexes with the gp130 receptor chain) there is a further division between the IL-6 like and IL-12 like receptor families. The IL-6 like cytokine and receptor family is characterised by a conserved four helix bundle cytokine structure and heteromeric receptors made up of pairings with gp130 (Metcalfe et al., 2020). The IL-6 receptor is made up of two gp130 molecules and two IL6R molecules which collectively engage two IL-6 molecules to form a hexameric complex (Figure 1-2) (Boulanger et al., 2003).

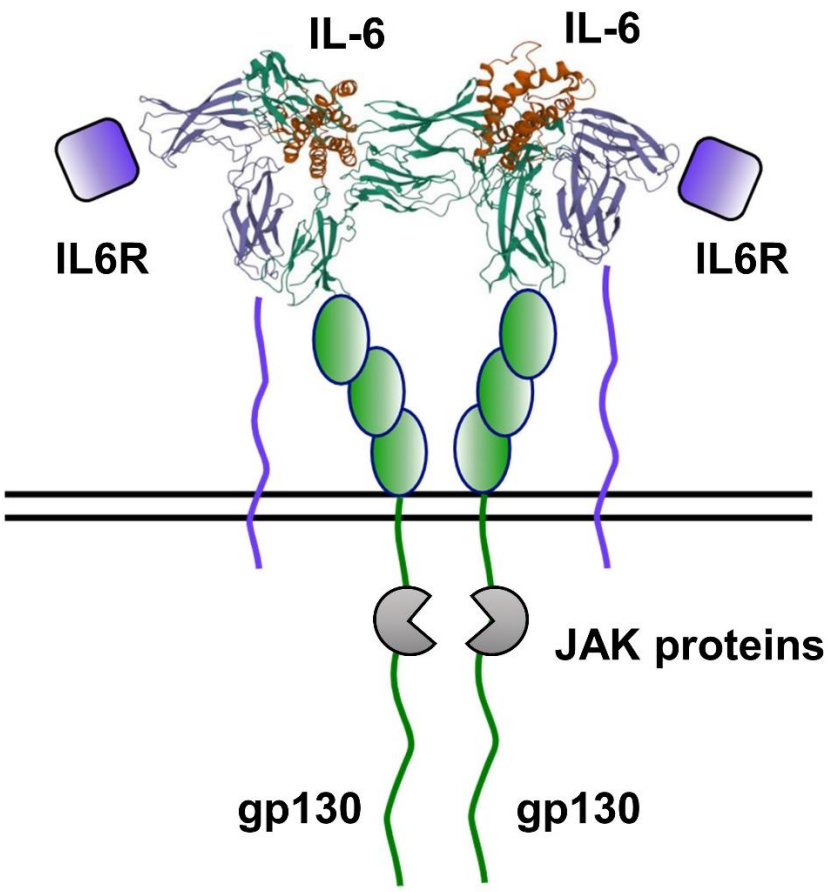

Figure 1-2: The hexameric IL-6 cytokine-receptor complex. A combined cartoon and crystal structure schematic demonstrating the hexameric IL-6 cytokine-receptor complex. The two IL6R receptor chains are shown in purple, the two gp130 receptor chains are shown in green and

the two IL-6 cytokine molecules are shown orange. Crystal structure (A 2:2:2 stochiometry of IL-6, gp130 D1-3 and IL6R D2-3) is PDB:1P9M (Boulanger et al., 2003). The remaining structure is a cartoon with squares representing immunoglobulin domains and ovals demonstrating fibronectin domains.

The IL-12 like cytokine group is characterised by the heterodimeric promiscuous pairing of four helix bundle 'alpha' components homologous to IL-6 with either IL12p40 or Epstein Barr virus induced gene 3 (EBI3) 'beta' components (Figure 1-3) (Vignali and Kuchroo, 2012). These beta components are thought to originate from cytokine receptor chains and are structurally homologous to gp130 (Lupardus and Garcia, 2008). Four heterodimeric IL-12 family members have been observed in humans with a fifth member IL-39 found in mice (Bridgewood et al., 2019; Hasegawa et al., 2016). These are formed of disulphide linked dimers of IL12p40 with IL12p35 (IL-12) and IL12p40 with IL23p19 (IL-23) and non-disulphide linked dimers of IL27p28 with EBI3 (IL-27) and IL12p35 with EBI3 (IL-35) (Figure 1-3; Hasegawa et al., 2016). IL-27 has been reported to have both pro and anti-inflammatory properties and is antagonistic to IL-23 by inhibiting Th17 differentiation (Beizavi et al., 2021; Yoshida and Hunter, 2015). IL-35 has been reported to have immunosuppressive properties and is also thought to act in an antagonistic way to IL-23 by blocking Th17 differentiation (Zhang et al., 2019).

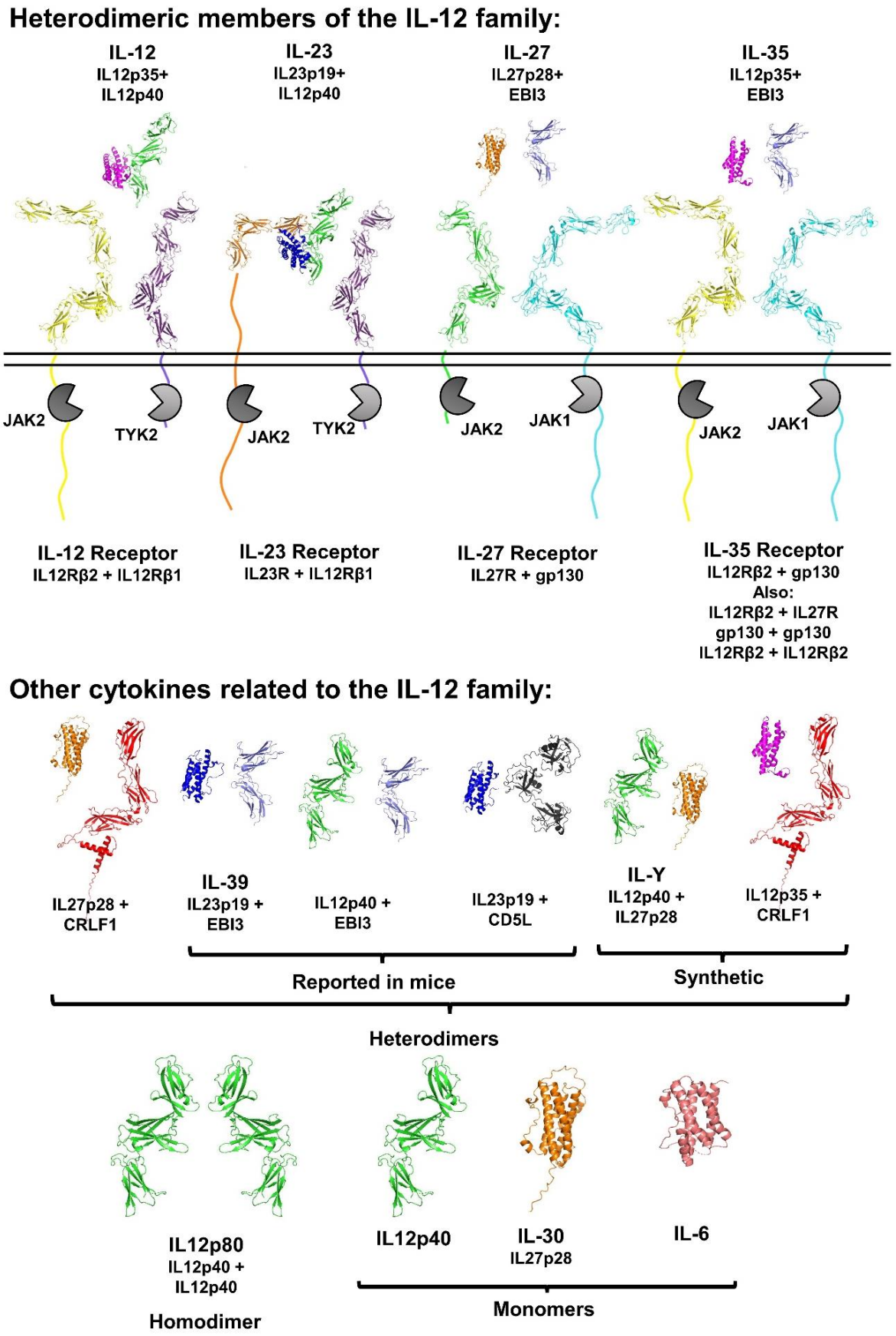
Heterodimeric members of the IL-12 family:
IL-12
IL12p35+
IL12p40
IL-23
IL23p19+
IL12p40
IL-27
IL27p28+
EBI3
IL-35
IL12p35+
EBI3
JAK2
TYK2
JAK2
TYK2
JAK2
JAK1
JAK2
JAK1
IL-12 Receptor
IL12Rβ2 + IL12Rβ1
IL-23 Receptor
IL23R + IL12Rβ1
IL-27 Receptor
IL27R + gp130
IL-35 Receptor
IL12Rβ2 + gp130
Also:
IL12Rβ2 + IL27R
gp130 + gp130
IL12Rβ2 + IL12Rβ2
Other cytokines related to the IL-12 family:
IL27p28 +
CRLF1
IL-39
IL23p19 +
EBI3
IL12p40 +
EBI3
IL23p19 +
CD5L
IL-Y
IL12p40 +
IL27p28
IL12p35 +
CRLF1
Reported in mice
Synthetic
Heterodimers
IL12p80
IL12p40 +
IL12p40
Homodimer
IL12p40
IL-30
IL27p28
IL-6
Monomers

Figure 1-3: The cytokines and receptors of the IL-12 family. IL-12 family member cytokines are shown with their corresponding receptors. The disordered domains, cell membrane and associated JAK proteins are depicted as cartoons. Other cytokines related to the IL-12 family are also shown for reference. Structures shown are models taken from the Alphafold database (www.alphafold.ebi.ac.uk) unless a crystal structure was available (Jumper et al., 2021). Crystal structures used were PDB: 1F45 (IL-12 and IL-12p35), 6WDQ (IL12p40, IL23p19 and IL23R in complex with IL-23), 3L5H (gp130) and 3L5H (IL-6). Where no structure exists of cytokine subunits in complex, subunits are depicted as non-linked pairs.

IL-6 was the first member of the IL-6/IL-12 family to be discovered and is the most studied member of the group. The structural similarity of the family led researchers to hypothesise that the IL-12 family cytokines engaged their receptors in a similar fashion to the hexameric IL-6 complex (Figure 1-2) with both receptor chains engaging the alpha component of the cytokine and the beta chain increasing the affinity of this interaction (Vignali and Kuchroo, 2012). It has now been established however that both IL-23 and IL-12 engage their receptors through interactions with both cytokine components (Glassman et al., 2021). IL-27 has been demonstrated to signal through a complex made up of the receptor components IL27R and gp130 (Yoshida and Hunter, 2015) and IL-35 has been reported to signal through several receptor complexes made up of heteromers of IL-12Rβ2 and gp130 or IL-12Rβ2 and IL27R and homomers of IL-12Rβ2 or gp130 (Collison et al., 2012). IL27p28 has also been shown to interact with the protein Cytokine Receptor Like Factor 1 (CRLF1) to form an additional heterodimeric cytokine which, most likely signals through a trimeric receptor made up of IL6R, IL27R and gp130 (Guilhot et al., 2009).

The promiscuous pairing of the IL-12 cytokine family indicates the possible existence of further heterodimeric cytokines beyond those outlined here, for example the IL23p19/EBI3 heterodimer IL-39 which has been discovered in mice but not yet in humans (Figure 1-3; Bridgewood et al., 2019; Wang et al., 2016). There have been further reports of an murine expressed IL12p40/EBI3 (Lee et al., 2022) and IL23p19/CD5 antigen-like (CD5L) heterodimer (Hasegawa et al., 2016) and the hypothetical combinations of IL12p35 with CRLF1 (Detry et al., 2019) and IL27p28 with IL12p40 (IL-Y) (Flores et al., 2015) have been recombinantly expressed in mammalian cells.

In addition to the heterodimeric members of the IL-12 family, IL12p40 is also found in a homodimeric form IL12p80, which has been reported to have antagonistic activity against IL-12 signalling and to induce its own signalling pathway (Gillessen et al., 1995; Jana and Pahan, 2009; Mondal et al., 2020). IL-12 family cytokine constituents have also been reported to be secreted as monomers, IL12p40 for example has been shown to act as an endogenous antagonist of both IL-12 and IL-23 activity (Mondal et al., 2020) and the cytokine IL-30 is made up of monomeric IL27p28 (Hasegawa et al., 2016). IL-30 is thought to be able to signal in a similar fashion to IL-6, binding to common receptor structures including sIL6R to enable trans-signalling (Garbers et al., 2013). The cytokine component IL23p19 has also been reported to be secreted in isolation and may act as an agonist of STAT3 signalling through interactions with gp130 (Espígol-Frigolé et al., 2016). There are indirect indications that EBI3 can be secreted in isolation, as EBI3 is not disulphide linked to IL27p28 in IL-27 or IL12p35 in IL-35, the peptide may facilitate trans-signalling with these molecules in a similar way to the sIL6R:IL6 complex (Hasegawa et al., 2016). Indeed it has been reported that EBI3 can induce IL-6 trans-signalling by associating with IL-6 and inducing signalling on cells expressing gp130 but not IL6R (Chehboun et al., 2017). It has been demonstrated that IL23R but not IL12Rβ1 surface expression is related to both EBI3 and calnexin expression, indicating that EBI3 acts as a calnexin mediated chaperone of IL23R folding and membrane insertion (Mizoguchi et al., 2020).

1.3 The structure of IL-23 and its receptor

1.3.1 The structure of IL-23

IL23p19 is an 18.7 kDa protein composed of four α helices (termed A, B, C and D). The protein contains an internal disulphide link between Cys58 and Cys70 and is disulphide linked to IL12p40 via Cys54 which is located on the loop between A and B (Lupardus and Garcia, 2008). IL23p19 is homologous to other 4 helical cytokines with the highest similarity to IL-6 (Lupardus and Garcia, 2008). IL12p40 is a 34.7 kDa glycosylated protein composed of three domains (termed D1, D2 and D3), linked to IL23p19 via Cys177 with the binding interface located between D2 and D3 (Lupardus and Garcia, 2008). Several features of the structure of IL12p40 indicate that the protein has an evolutionary

history as a receptor (Yoon et al., 2000). For example D1 of IL12p40 shares strong homology the immuno-globulin domain typically found in type 1 cytokine receptors and contains an internal disulphide link (Lupardus and Garcia, 2008). IL12p40 D2 and D3 represent the cytokine binding region with D2 containing two conserved internal disulphide bridges at Cys109-120 and Cys148-171 that are typical of this domain and D3 containing the signature WSXWS (WSEWAS in IL12p40) motif which is conserved across this receptor type and a further disulphide bridge (Lupardus and Garcia, 2008). The evolutionary origins of IL12p40 as a receptor are likely related to the phenomenon of trans-signalling in which alternative splicing or protein cleavage creates protein isoforms consisting of the soluble receptor extracellular domain. Soluble receptors can then associate with cytokines to enable signalling on cells that only express one receptor subunit, as has been shown for the closely related IL6R (Rose-John, 2012).

Several crystal structures have been solved of the IL-23 cytokine, the first of these resolved the post translational modification of an asparagine linked GlcNAc group emanating from N200 (Bloch et al., 2018). Subsequent studies confirmed this and suggested that glycosylation also occurs at N281 (Beyer et al., 2008). A study measuring the secretion of wildtype and glycosylation null mutants of IL-12 family members by HEK293T cells demonstrated that non-glycosylated IL-23 was still secreted (Bohnacker et al., 2020). The researchers also showed that non-glycosylated IL-23 has no significant change in its ability to stimulate IL-17 production in Peripheral Blood Mononuclear Cells (PBMCs) and a slight decrease in the activation of signalling in a reporter cell line (Bohnacker et al., 2020). The function of IL-23 glycosylation has yet to be determined.

1.3.2 The structure of the IL-23 receptor

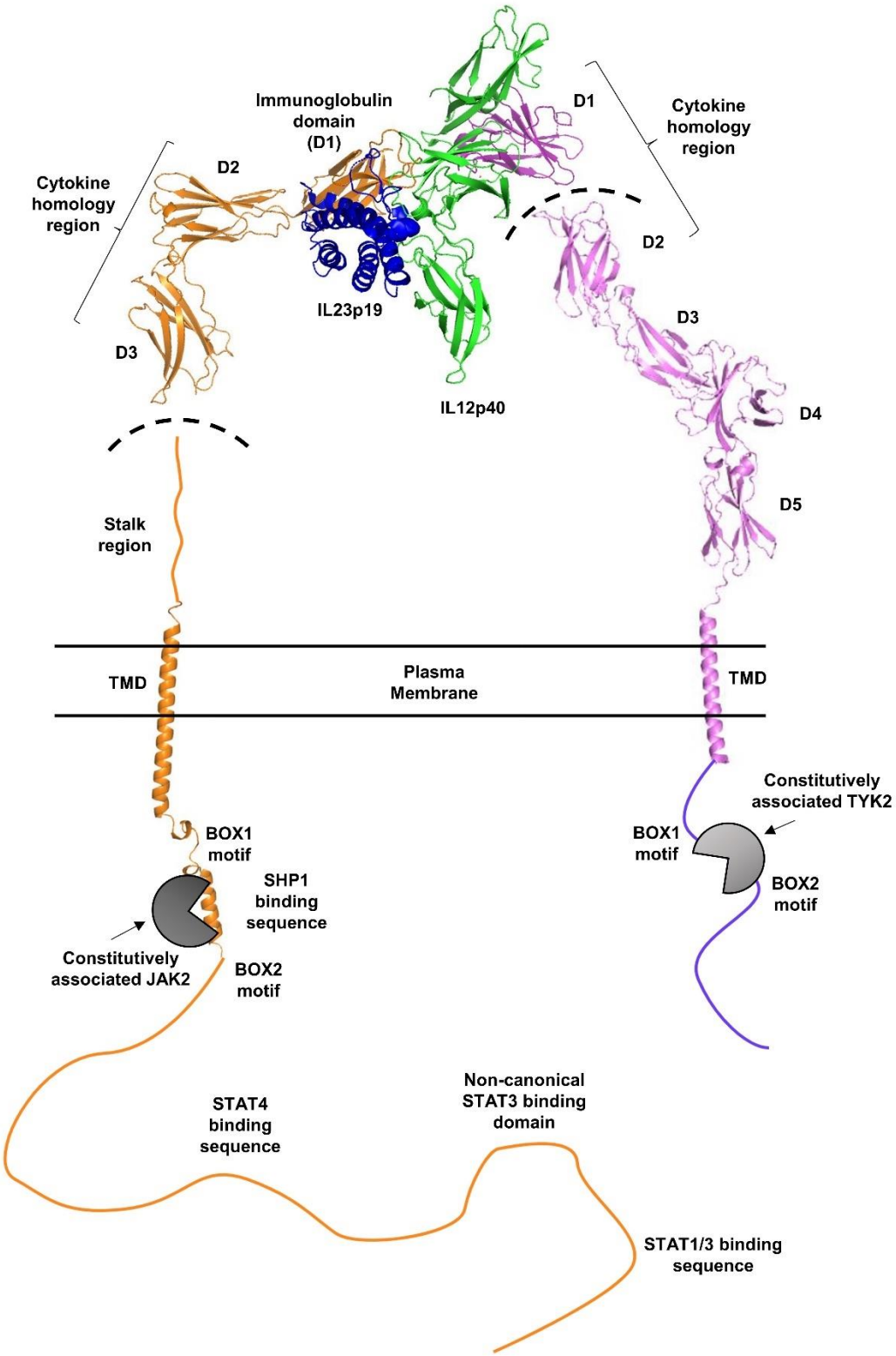

Figure 1-4: Key structural features of the IL-23 cytokine-receptor complex. A schematic containing, AlphaFold modelled, crystal structure and cartoon representations of the IL-23 receptor engaging its ligand. The crystal structure of D1-3 of IL23R and D1 of IL12Rβ1 in complex with IL-23 (PDB: 6WDQ) is shown separated from the remainder of the structure by dashed lines. The Alphafold modelled structures of the IL23R TMD with membrane proximal ICD and IL12Rβ1 D2, 3, 4, 5 and TMD were taken from www.alphafold.ebi.ac.uk (Jumper et al., 2021). The remainder of the structure (IL23R stalk and ICDs) is represented by cartoon lines as an indicator of their disordered nature. IL23R is shown in orange, IL12Rβ1 in purple, IL23p19 in blue, IL12p40 in green and associated JAK proteins in grey. The same colour scheme will be used in cartoons of the receptor throughout this thesis.

The IL-23 receptor is made up of two single TMD receptors IL23R and IL12Rβ1 (Figure 1-4) (Parham et al., 2002). IL12Rβ1 is a class I cytokine receptor made up of 662 amino acids with strong homology to gp130 (a class I cytokine receptor involved in IL-6 signalling) (Chua et al., 1994). Like IL12p40, IL12Rβ1 is also a subunit of the IL-12 cytokine-receptor complex (Chua et al., 1994). IL12Rβ1 has a five-domain ECD spanning from residues 24-545 meaning that the majority of the protein is extracellular (Chua et al., 1994). The ECD of the receptor is made up of five type III fibronectin domains termed D1-5 (Chua et al., 1994). The *N*-terminal domains D1 and D2 have homology to cytokine binding domains with characteristic two disulphide bridge structure in D1 and a WSxWS motif (WSKWS in IL12Rβ1) in D2 (Chua et al., 1994). IL12Rβ1 has a 24 amino acid predicted TMD (Leu546-Leu570) and a 91 amino acid ICD (Chua et al., 1994). IL12Rβ1 has been shown to associate with and signal through the JAK kinase TYK2, the ICD contains a Box 1 region of with a LCPPLPTP motif and a Box 2 motif with an EASLQEALVVE motif (Chua et al., 1994) that have been shown to be essential for TYK2 association and activation in the murine homolog of IL12Rβ1 (Floss et al., 2016). There are no tyrosine residues in the ICD of IL12Rβ1 which indicates that no canonical STAT motifs are present (Floss et al., 2016). There are three potential binding motifs for casein kinase II (CK2) within the *C*-terminal region of IL12Rβ1 at Ser588 (SAIE), Ser612 (SLQE) and Ser651 (SLED) which have been predicted based on the consensus SXXE/D CK2 motif however there have yet to be functional studies on these sites to test their role in CK2 binding.

IL12Rβ1 has been reported to be expressed in two near identical isoforms (isoform 1 and 1b) differing by only 2 *C*-terminal amino acids (van de Vosse et al., 2013), as yet there have been no functional studies to assess differences between these isotypes. A third soluble isoform of IL12Rβ1 (isoform 2) has also been reported to be secreted (Ford et al., 2012; van de Vosse et al., 2013). The expression of this isoform has been reported to be influenced by cell stimulation, with one study showing isoform 2 is downregulated after stimulation of leukocytes with phytohemagglutinin (PHA) (van de Vosse et al., 2013) and other studies showing that challenge of dendritic cells with *M. tuberculosis* led to higher secretion of isoform 2 with this isoform giving greater protection from infection in mice (Ray et al., 2015; Robinson et al., 2010).

IL23R is a 629 amino acid (including a 23 amino acid signal peptide) protein that has homology to other long chain class I cytokine receptors (Parham et al., 2002). The receptor contains an *N*-terminal immunoglobulin domain and two cytokine binding domains in its ECD termed D1, D2 and D3 that include the characteristic twin disulphide bridges in D2 and WSxWS motif in D3, in the case of IL23R this motif manifests as WQPWS (Parham et al., 2002). Although the *N*-terminal region of IL23R shares common domains with other members of the class I cytokine receptor family the protein is atypical due to its three-domain structure, with most receptors in this family exhibiting five extracellular domains, in place of these domains IL23R exhibits a disordered 'stalk' region (Parham et al., 2002). Crystal structures of the D1, D2 and D3 domains of the ECD of IL23R in complex with IL-23, reveal that binding of IL23R to IL-23 is mediated exclusively through an interaction of D1 with IL23p19 (Bloch et al., 2018; Glassman et al., 2021). The critical residues for this interaction have also been confirmed in mutational studies and mapping of the binding interface through Hydrogen Deuterium Exchange (HDX) (Sayago et al., 2018; Schroder et al., 2015).

The TMD of the IL23R receptor is a 23-residue sequence that occurs at position Ile354-Phe376. The ICD of IL23R is a 252 amino acid long region responsible for signal transduction, in contrast to IL12Rβ1 and other cytokine receptors the region contains no clear Box1 and Box2 motifs for JAK binding (Parham et al., 2002). A putative JAK2 binding site was predicted near to the cell membrane at

Ile384-Glu398 (Pidasheva et al., 2011), however an alternative sequence was identified in murine IL23R through functional studies utilising *C*-terminal mutants of the receptor (Floss et al., 2016), which demonstrates homology to the human IL23R region Glu439-Glu459. Further functional studies are needed to confirm the region responsible for human JAK2 association. The non-canonical murine JAK2 binding region, has an atypical position as it lies 60 amino acids from the membrane (Floss et al., 2016). As JAK proteins are normally found associated to domains close to the membrane, the authors of the study hypothesised that this distance may be facilitated by an as yet undefined tertiary structure of the ICD or that JAK2's position in IL23R is an exception (Floss et al., 2016). Further prediction of the JAK2 binding domain has since been undertaken based on the analysis of the crystal structures of IFNAR1, IFNLR1 and IL10RA in complex with their corresponding JAK proteins (Ferrao and Lupardus, 2017). This study suggested that IL23R does in fact contain Box1 and Box2 motifs with Box1 being the ILLLIP motif located at Ile383 and Box2 the ExxLYVDxxxxExxxIFIP motif located at Glu425 (Ferrao and Lupardus, 2017). Although the canonical Box 1 motif for class I cytokine receptors is a region of hydrophobic residues prior to a PxP motif, there is a high level of variation across the cytokine receptor predicted box 1 and 2 domains, with some class II receptors exhibiting PXXP motifs and the majority of class I JAK1 interacting receptors all containing a single Proline in their predicted box 1 regions as in the case for IL-23R (Ferrao et al., 2018). The authors of the study hypothesise that the widespread variation in Box 1 and Box 2 domains may be a mechanism through which cytokine receptors differentiate signals transduced through identical adaptor molecules to disparate downstream functions. Furthermore although this prediction appears to contradict the previous murine mutational studies (Floss et al., 2016), the final motif of the predicted box 2 region (a hydrophobic area comprised of the sequence IFIP), sits within the region homologous to murine non-canonical binding site. However, this IFIP motif is not conserved in the mouse and is instead ISPL.

JAK2 facilitates the binding of further signal transduction molecules to IL23R through phosphorylation of tyrosine residues within the IL23R ICD, for this reason binding sites for transduction molecules have been hypothesised at ICD

tyrosine residues (Floss et al., 2013). The ICD of IL23R contains 7 Tyrosine residues with the closest of these to the membrane being the YEDI motif at Tyr397 which was predicted to be an SHP2 binding site for Mitogen-activated protein kinase (MAPK) and Phosphoinositide 3-kinase (PI3K) signalling (Parham et al., 2002). This prediction is supported by the observation that mutation of the murine IL23R YEDI motif to FEDI, abolishes the phosphorylation of Akt and MAPK (Floss et al., 2013). Tyr429, Tyr450 and Tyr476 are not embedded in conserved binding motifs and have not been predicted to be involved in transduction (Parham et al., 2002). The remaining Tyrosine residues are, Tyr463, Tyr484 and Tyr611. Tyr463 sits in a YPQNS motif which has been compared to STAT and SHP2 binding motifs, however no role for signal transduction has yet been shown for this residue (Floss et al., 2013). Tyr484 sits within a GYKPQ motif which was predicted to be a STAT4 binding site and Tyr611 sits within an YFPQ motif which was predicted to be a STAT1/3 binding site (Parham et al., 2002). It has since been demonstrated however, that human IL23R with both Y484F and Y611F mutations could still phosphorylate STAT3 (Floss et al., 2013). To completely abrogate phosphorylation of STAT3 by murine IL23R, not only were Y484F and Y611F equivalent mutations required but also a deletion of a site spanning Leu554-Gln574 (Floss et al., 2013). This non-canonical STAT3 binding motif is conserved across several mammalian IL23R homologues and its human equivalent Ser539-Gln555, may also act in this fashion. In addition to the aforementioned binding sites, a conserved binding motif for Casein Kinase I (CK1) was predicted at Ser535 (SVSS) (Floss et al., 2013) and potential binding motifs for CK2 at Ser466 (SLFD), 558 (SSPD), 566 (SVEE), 578 (SPSE) and 625 (SLLE) although there have yet to be functional studies to test if any of these sites bind their predicted transducers. The presence of these CK2 binding sites may be significant as CK2 has previously been shown to facilitate STAT3 activation by JAK proteins (Zheng et al., 2011). IL-23 signalling has also been reported to activate pyruvate kinase M2 (PKM2), an additional protein which has been demonstrated to phosphorylate STAT3 (Damasceno et al., 2020; Lochmatter et al., 2016).

Several IL23R isoforms have been reported to be formed by alternative splicing. These include several soluble forms of the receptor that lack TMD and ICD regions that have been theorised to act as endogenously secreted antagonists of IL-23, variants lacking portions of the ICD predicted to have impaired signalling and isoforms lacking specific regions of the ECD (Kan et al., 2008; Mancini et al., 2008; Zhang et al., 2006). There have been no functional studies on these differentially spliced isoforms however their expression has been observed to be tissue specific with variants IL23R2 and IL23R4 expressed at higher levels in certain cancers (Zhang et al., 2006). The soluble forms of IL23R (sIL23R) most likely act in a similar way to IL1R2 which acts as an antagonist of IL-1 signalling (Schlüter et al., 2018). Indeed it has been demonstrated that the truncated extracellular domain of IL23R retains affinity for IL-23 (Bloch et al., 2018; Glassman et al., 2021). There is a possibility that soluble IL23R acts as an agonist in a similar way to soluble IL6R, which allows trans-signalling by enabling the engagement of IL-6 with gp130 (Rose-John, 2012). This however is unlikely, as much of the signal transduction of the IL-23 is thought to be mediated through the ICD of IL23R (Floss et al., 2013). Furthermore it has been shown that the synthetic production of sIL23R by engineered stem cells inhibited IL-17 production by T cells (Rostami et al., 2018). In addition to sIL23R generated by alternative splicing, it has been suggested that a motif in the stalk region of IL23R spanning residues 319-355 acts as a substrate for the metalloprotease ADAM17 and that cleavage at this site constitutes an alternative pathway through which to generate sIL23R (Franke et al., 2016).

1.3.3 IL-23 Signal Transduction

The IL-23 cytokine transduces through several pathways (Listed in Figure 1-5). Initial characterisation of the receptor showed that IL-23 binding led to phosphorylation of JAK2 and TYK2 (Parham et al., 2002), which have since been demonstrated to be constitutively associated with IL23R and IL12Rβ1 respectively (Floss et al., 2016). It is thought that the activation of JAK proteins via trans-phosphorylation causes intracellular IL23R tyrosine residues to be phosphorylated allowing the binding of further signal transducers which are then phosphorylated and activated themselves. The members of the signal transducer and activation of transcription (STAT) family STAT1, STAT3, STAT4 and

STAT5 were shown to be phosphorylated upon the addition of IL-23 and it has been demonstrated that these activated STATs are most likely found as homodimers and STAT3/4 heterodimers (Parham et al., 2002).

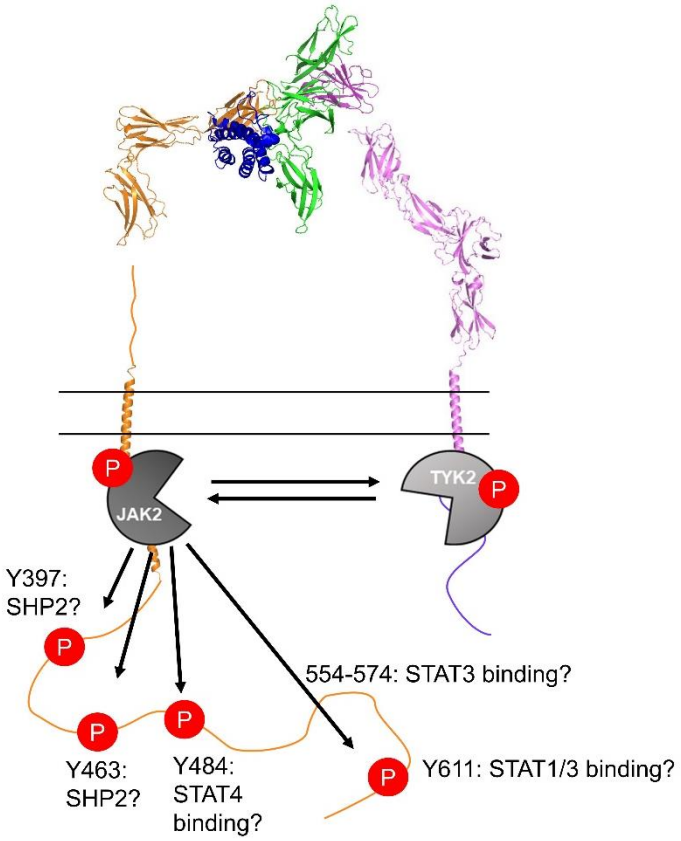

Reported IL-23 signalling tranducers:

- MAPK
- PI3k
- Akt
- STAT1,3,4,5 homodimers
- STAT3/4 heterodimers
- IκBα
- P38
- PKM2
- LASP1
- Ataxin
- ROCK

Figure 1-5: The signalling pathways activated by IL-23. A figure demonstrated the processes induced by IL-23 binding. Constitutively associated JAK proteins trans-phosphorylate each other, followed by phosphorylation of Tyrosine residues within the ICD of IL23R and phosphorylation of further signal transducers. A list of reported IL-23 transducers is also shown.

The transducer protein SHP2 has been predicted to interact with the ICD of IL23R and be activated by associated JAK kinases on IL-23 binding (Parham et al., 2002). SHP2 is a phosphatase that interacts with the MAPK and PI3K pathways in IL-6 signalling by acting as an adaptor for Gab1 and the Grb2/SOS

guanine-nucleotide exchange factor complex (Eulenfeld et al., 2012). It was hypothesised that SHP2 may activate the same pathways through a similar mechanism in IL-23 signalling and it has since been shown that IL-23 stimulation leads to activation of both MAPK and Akt (Engelowski et al., 2018; Floss et al., 2013), however whether this is indeed SHP2 dependant has yet to be demonstrated. In addition to acting as a signal transducer, SHP2 may also play a role in negative feedback against IL-23 signalling through its action as a phosphatase and has previously been shown to deactivate STAT1, 3 and 5 proteins through dephosphorylation (Ke et al., 2006; Wu et al., 2002).

The major feedback mechanism against IL-23 signalling has been suggested to be the Suppressor of Cytokine Signalling 3 (SOCS3) protein (Chen et al., 2006) which can bind to phospho-tyrosines within activated receptors, JAKs and STATs, recruiting the ubiquitination machinery for degradation (Babon et al., 2009). SOCS3 has also been shown to directly inhibit JAKs by acting as a pseudo-substrate (Sasaki et al., 1999). Whilst SOCS3 has been shown to exert a negative feedback effect on downstream IL-23 pathways (Chen et al., 2018, 2006), the protein has yet to be demonstrated to directly interact with the IL-23 receptor, and it has been suggested that the receptor has mechanisms to dampen regulation by SOCS3 leading to prolonged activation compared to IL-6 (Floss et al., 2013). SOCS1, another member of the SOCS family, has been shown to increase IL-23 mediated Th17 cell differentiation, although this is most likely due to inhibition of the antagonistic IFN-γ pathway (Tanaka et al., 2008).

Further reported signal transducers of IL-23 include Nuclear Factor κB (NF-κB) which has been shown to be induced by IL-23 signalling (Cho et al., 2006; Ju et al., 2008). This is most likely due to phosphorylation of the regulatory protein IκBα which is phosphorylated within 15 minutes of IL-23 stimulation of eosinophils (Cheung et al., 2008). The same study also demonstrated that p38 is rapidly phosphorylated within 5 minutes in response to IL-23 stimulation (Cheung et al., 2008).

Phosphoproteomic analysis of murine Th17 cells after IL-23 stimulation demonstrated that myosin regulatory light chain (RLC) was phosphorylated in response to IL-23 and that this was mediated by a Rho-associated protein kinase

(ROCK) kinase (Álvarez-Salamero et al., 2020). The intermediate between ROCK and the IL-23 receptor is yet to be defined however it is known that SHP2 is a regulator of ROCK (Langdon et al., 2012).

The *C*-terminal regions of both IL23R and IL12Rβ1 contain consensus SxxE/D binding motifs for CK2. It is not known if these motifs, which are widespread across proteins (Rabalski et al., 2016), do indeed mediate interaction with CK2, however several studies have shown that CK2 is a key mediator of T cell differentiation to Th17 cells (Gibson et al., 2017; Ulgesa et al., 2016). Treatment of Th17 cells with CK2 specific inhibitors demonstrated that CK2 plays a role in the phosphorylation of STAT3 following combined IL-23 and IL-6 stimulation (Ulgesa et al., 2016). A similar study also demonstrated that CK2 inhibition reduced STAT3 phosphorylation after IL-6 stimulation (Gibson et al., 2017). These studies demonstrated wide-ranging downstream effects of CK2 inhibition on genes and pathways leading to Th17 cell development and a shift towards a Treg phenotype (discussed in more detail in Section 1-5; Gibson et al., 2017; Ulgesa et al., 2016). A hypothesis was made that Akt S179 was a likely substrate for CK2, however neither study discovered which proteins were directly interacting with CK2 (Gibson et al., 2017). Therefore, the direct involvement of CK2 in IL-23 signalling has yet to be demonstrated, although it is likely that CK2 works synergistically with IL-23 to promote Th17 development.

1.3.4 The IL-23 receptor activation mechanism

Whilst it is established that the binding of IL-23 leads to the phosphorylation of JAK2 and TYK2 and the subsequent phosphorylation of transducers (Parham et al., 2002), the precise activation mechanism is less well defined. Originally it was thought that both IL23R and IL12Rβ1 would engage IL23p19 with IL12p40 acting to increase the affinity of the interaction in a similar way to IL-6 and the IL-6 receptor (known as the site 1-2-3 model) (Vignali and Kuchroo, 2012) however, mutational studies showed that IL23R engaged IL23p19 and IL12p40 engaged IL12Rβ1 (Schroder et al., 2015) and this was later confirmed in structural studies (Figure 1-4; Bloch et al., 2018; Glassman et al., 2021).

As IL-23 engages two separate receptor subunits the mechanism of activation could be a simplistic ligand induced dimerisation model in which the cytokine brings IL23R and IL12Rβ1 into proximity enabling the transphosphorylation of associated JAK proteins, or a structural rearrangement caused by IL-23 binding to pre-associated dimers. The first study to confront this issue used a split Renilla luciferase to investigate if the IL-23 receptor existed as a heterodimer prior to ligand binding (Sivanesan et al., 2016). The study fused complementary fragments of Renilla luciferase to the *C*-termini of IL23R and IL12Rβ1 using linkers of differing length, expressed these constructs in live cells and measured the change in luminescence with and without the addition of IL-23. It was demonstrated that whilst the luminescence was comparable between linker lengths in the presence of IL-23, in the absence of the cytokine there was a low signal for the 5 amino acid linker, a high signal almost that of the signal with IL-23 for the 10 amino acid linker in the absence of ligand and an intermediate signal size for the 20 amino acid linker. The authors concluded that the IL-23 receptor formed as a dimer before IL-23 association in a similar fashion to the EPO receptor (EPOR) (Remy et al., 1999) and that binding of IL-23 caused a scissor-like conformational change in receptor structure that brought the *C*-terminal domains together to initiate signalling (Figure 1-6; Sivanesan et al., 2016).

The next study to confront IL-23 receptor activation solved a crystal structure of IL-23 bound to IL23R followed by the use of isothermal calorimetry to measure the affinity of the purified ECDs of both IL23R and IL12Rβ1 for IL-23 (Bloch et al., 2018). Using this method, the group found that there was a much higher affinity of IL-23 for the IL23R over the IL12Rβ1 truncate. The group then showed that the IL23R:IL-23 complex had a much higher affinity for IL12Rβ1 than IL-23 alone. The authors concluded that this demonstrated that IL-23 must first bind to IL23R and then initiate ligand induced dimerization by recruiting IL12Rβ1 (Bloch et al., 2018). Additional evidence relating to IL-23 receptor activation came from a study in which synthetic cytokine receptors were constructed consisting of the ICD, TMD and a short fragment of the ECD of the murine IL23R and IL12Rβ1 receptors expressed with *N*-terminal fusions of nanobodies for either mCherry or Green Fluorescent Protein (GFP) (Engelowski

et al., 2018). These chimeric receptors could then be induced to signal through the addition of a dual antigenic ligand consisting of both mCherry and GFP.

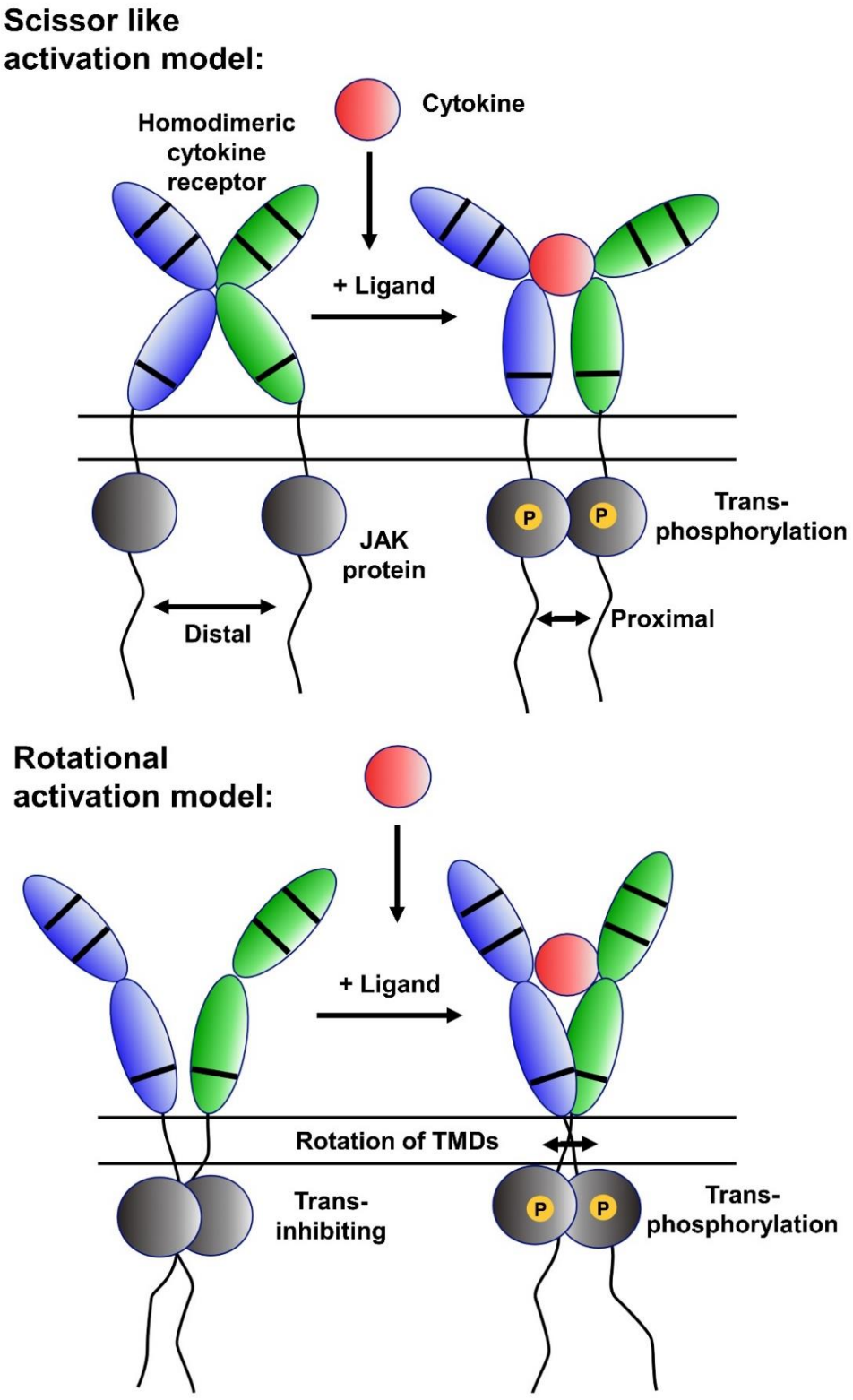

Figure 1-6: Models for the activation of cytokine receptors. Top, ligand binding induces the *C*-terminal domains of the receptor to come into proximity. Bottom, ligand binding induces a

rotation of the TMDs resulting in trans-phosphorylation. Figures adapted from Corbett et al., 2016 and Waters and Brooks, 2015.

The two competing models of ligand induced conformational change and ligand induced dimerization have yet to be further studied within the context of the IL-23 receptor but have been a subject of debate within the wider cytokine receptor family. The initial mechanism suggested for cytokine receptor assembly was that of ligand induced dimerization (Cochet et al., 1988; Fuh et al., 1992). This model suggests that ligands first engage freely diffusing receptor monomers before recruiting secondary receptor chains, thus bringing the ICDs of the receptor chains and their associated kinases into proximity, allowing trans-phosphorylation. This theory is supported by several step-wise cytokine engagement studies in which a cytokine binding site has demonstrated a significantly higher affinity over another (Bloch et al., 2018; Fuh et al., 1992). Further evidence originates from chimeric or antibody engaged receptors that can be made to signal with addition of a ligand for the ECD of the chimeric receptor or in the presence of a bi-specific antibody for both receptor chains (Elliott et al., 1996; Engelowski et al., 2018; Rui et al., 1994). Single particle tracking experiments have also shown that several cytokine receptors exist as monomers when expressed at low levels and can be dimerised with the addition of ligand (Gandhi et al., 2014; Moraga et al., 2015b, 2015a; Wilmes et al., 2020).

The model of activation by ligand induced conformational change has been supported by the observation of inactive unliganded dimers using cross-correlation spectroscopy, co-localisation, resonance energy transfer, co-immunoprecipitation, chemical or antibody crosslinking and structural studies. The observation that cytokine receptors can exist in inactive dimers prior to ligand binding, implies that dimerization alone is not enough to initiate signalling (Couturier and Jockers, 2003; Krause et al., 2013; Livnah et al., 1999; Lu et al., 2006; Malka et al., 2008; Pillet et al., 2010; Tenhumberg et al., 2006). In addition to the reports of inactive IL-23 receptor dimers, co-immunoprecipitation studies have shown that the closely related IL-6 receptor is likely dimeric in the absence of ligand (Schuster et al., 2003) and it has been observed that both IL-12 receptor subunits must be expressed in order to form a high affinity binding site for IL-12 (Chua et al., 1994).

The growing experimental evidence that many single pass receptors can exist as inactive complexes has led researchers to suggest mechanisms for conformational change-based cytokine receptor activation. These mechanisms, developed typically at homodimeric receptors have then been applied more widely across cytokine receptors and single pass receptors more broadly, based on shared observations and structural similarities, for example a conserved proline containing ECD-TMD linker thought to mediate conformational change (Schmidt et al., 2016).

The first mechanism to be suggested was the 'scissor-like' conformational change mechanism, in which the ECDs of unliganded dimerised receptors interact in a conformation that holds the ICDs and hence the associated JAK proteins apart, preventing the initiation of signalling. Binding of ligand causes a re-arrangement of the ECD of the receptor that brings the TMD and ICDs of the receptor together and enables trans-phosphorylation and activation of JAK proteins (Figure 1-6) (Corbett et al., 2016). This mechanism was originally suggested after the structure of the class I cytokine receptor type, EPOR was solved. The researchers observed that dimers of the purified ECDs of EPOR formed both in the presence and absence of ligand, but each had differential conformations with ligand binding bringing the *C*-termini into closer association (Livnah et al., 1999). A further study which utilised the re-complementation of a split enzyme fused to the *C*-termini of EPOR to measure interactions between the receptor subunits expressed on living cells, observed interactions were present both in the liganded and unliganded receptor but that longer linkers were needed to mediate this interaction for the unliganded receptor, indicating that the *C*-termini were further apart in this conformation (Remy et al., 1999). Since these studies, the model has been applied to the IL-7 (McElroy et al., 2012) and IL-23 receptor (Sivanesan et al., 2016), however critics have suggested that more recent evidence contradicts this model (Corbett et al., 2016), for example the observation that JAK proteins are associated in trans-inhibiting complexes, mediated by their functionally inactive pseudokinase domains, when bound to non-liganded dimers of the growth hormone receptor (GHR) (Brooks et al., 2014).

A general model of single pass domain receptor activation has also been suggested that relies on the ligand induced rotation of pre-dimerised TMDs (Figure 1-6) (Maruyama, 2015; Moriki et al., 2001). This model is supported by several studies that show cytokine and other single pass receptors undergo a rotation around their TMD in order to initiate activation (Brown et al., 2005; Matthews et al., 2011; Seubert et al., 2003). A study of GHR suggested that JAK2 proteins, associated to the box 1 and 2 domains of inactive homodimers, formed a trans-inhibiting complex mediated through interactions of kinase and pseudokinase domains (Brooks et al., 2014). The researchers suggested that ligand binding induced a rotation of the TMD, resulting in a re-arrangement in the ICD that allowed the kinase domains to come into proximity thus activating each other through phosphorylation (Brooks et al., 2014). A comprehensive study of GHR, Thrombopoietin receptor (TPOR) and EPOR using Total Internal Fluorescence (TIRF) microscopy, Single Molecule Förster Resonance Energy Transfer (FRET) and Molecular Dynamics (MD) simulations has since been demonstrated that constitutively associated JAK2 acts as a key regulator of class I homodimeric cytokine receptor dimerisation. With introduction of the JAK2 V617F pseudokinase domain mutation (an oncogenic mutation that leads to constitutive activation of GHR) inducing increased levels of ligand independent dimerisation (Wilmes et al., 2020).

It has been proposed that the ligand induced rotational model could be applied to further cytokine receptors, due to the successful activation of chimeric recombinantly expressed receptors made up of the ECD and ICDs from different receptors, by the ligand for the ECD, indicating a common activation mechanism (Waters and Brooks, 2015). In addition, a membrane proximal region of the ECD containing acidic amino acids has been suggested to inhibit ligand independent signalling through mutual repulsion (Brooks et al., 2014). Replacement of these residues with alanine led to a change in the relative position of the subunits and an increase in basal signalling (Brooks et al., 2014). Many other cytokine receptors exhibit acidic residues at this position and it has

been shown that synthetic deletions of the membrane proximal or TMD regions of TPOR, IL23R and IL27R lead to ligand independent signalling (Ding et al., 2009; Hummel et al., 2017; Lambert et al., 2011; Matthews et al., 2011). Oncogenic mutations have also been reported in the IL-7 receptor that substitute amino acids in the membrane proximal ECD for basic residues, leading to hypersensitivity to IL-7 and harmful proliferation (Campos et al., 2019). Oncogenic mutations have also been identified in the IL-6 binding epitope of gp130 that enable ligand independent gp130 homodimer activation by altering the angle of the ECD (Schütt et al., 2013).

Building on the previously suggested models for conformational change based activation, a study that modelled the stimulation of EPOR, GHR and the prolactin receptor, suggested an activation mechanism based on both scissor-like and rotation based conformational change (Pang and Zhou, 2012).

Researchers have proposed that conformational change allows different ligands to influence downstream signalling bias; indeed two studies have shown that the degree of rotation can influence the transduction profile of cytokine receptors (Liu et al., 2009; Seubert et al., 2003). Cytokine receptors have highly disorganised ICDs that contain short recognition sequences for signal transducers, the effect of ligand binding and subsequent modifications on ICD organisation and accessibility is only beginning to be studied (Seiffert et al., 2020).

Whilst there is strong evidence for both ligand induced dimerization and ligand induced conformational change, the latter mechanism would allow cytokine receptors to avoid accidental activation events from non-specific dimerization of diffusing receptor monomers especially at higher expression levels (Maruyama, 2015). If a cytokine receptor is activated by ligand induced conformational change, this does not rule out the presence of an equilibrium between monomers and inactive dimers prior to ligand binding. Whilst there have been reports of cytokine receptors being exported from the endoplasmic reticulum as pre-formed complexes (Gent et al., 2002), the strong evidence of monomeric species from single molecule tracking experiments indicates that some receptors can indeed exist as monomers, especially at low expression

levels (Spangler et al., 2015; Wilmes et al., 2020). It may be that the ratio of inactive dimers, active dimers and monomers could be determined by the intrinsic affinity of the subunits, the concentration of receptors present and the concentration of ligand, as has recently been suggested for receptor tyrosine kinases (RTKs) (Paul and Hristova, 2019). Indeed, it has been proposed that in the absence of ligand the class I homodimeric cytokine receptors GHR, EPOR and TPOR exist in a dynamic equilibrium between monomers and dimers dependent on receptor affinity and membrane concentration, however in this study researchers suggested that these dimers were responsible for basal signalling and that their association was tightly regulated by limited surface expression (Wilmes et al., 2020).

Finally, the signalling of cytokine receptors may also be regulated by the further organisation, for example, clustering of activated receptors and internalisation into signalling vesicles (Westerfield and Barrera, 2020). This aspect of cytokine signalling remains understudied, however there are reports of some cytokine receptors organising into higher order structures upon activation (Pillet et al., 2010) and it is known that many cytokine receptors including IL23R internalise in response to their ligand (Sun et al., 2020).

1.4 The structure and function of JAK and STAT proteins

1.4.1 Structural features and functions of JAK proteins

The IL-23 receptor is constitutively associated with JAK proteins that play a key role in the activation of the receptor by trans-phosphorylating each other after ligand binding. JAKs are a family of four signal transducing kinases, (JAK1, 2, 3 and TYK2), that associate with a variety of receptor subtypes and transmit signals primarily via the phosphorylation of members of the STAT family (Mohr et al., 2012). The enzymes are named after the two faced Roman god Janus as they possess two similar but distinct kinase domains, one responsible for the enzyme's catalytic activity, the kinase domain and one, termed a pseudokinase domain, that acts as a site for regulation (Figure 1-7; Shan et al., 2014). The kinase domain contains an activation loop which is phosphorylated to switch the enzyme into the active state and catalytic motifs that allow the addition of phosphate groups to target proteins (Morris et al., 2018). The pseudokinase domain is thought to be involved in trans-inhibition of partner JAK proteins and

is the site of activating mutations that prevent kinase domain inactivation (Lupardus et al., 2014; Zhao et al., 2005). JAKs are found predominantly in the signalling pathways of class I and II cytokine receptors, but have been shown to be activated by receptor tyrosine kinases, such as Epidermal Growth Factor Receptor (EGFR), and GPCRs such as CXCR4 (Shuai et al., 1993; Vila-Coro et al., 1999).

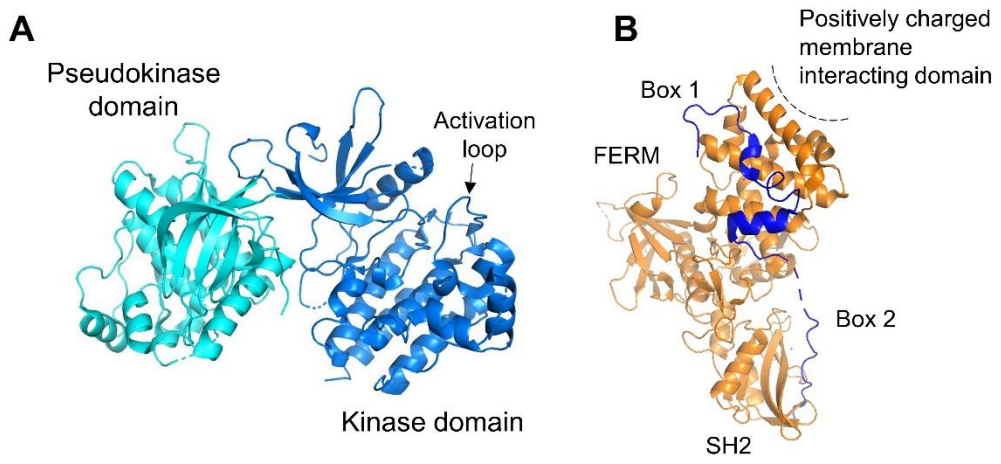

Figure 1-7: The key structural features of JAK proteins. (A) A crystal structure of TYK2 demonstrated the pseudokinase and kinase domains of the protein. (B) The crystal structure of the JAK2 FERM and SH2 domains (orange) in complex with the box 1 and 2 domains of the EPO receptor (blue). Crystal structures are PDB: 4OLI (A; Lupardus et al., 2014) and 6E2Q (B; Ferrao et al., 2018) .

The *N*-terminal domain of JAKs contains a Src Homology 2 (SH2) domain and a 4.1/Ezrin/Radixin/Moesin (FERM) domain. These motifs allow the association of JAKs with the *C*-terminal domain of their cognate receptors through complementary sequences termed box one and two (Figure 1-7; Wallweber et al, 2014). Most cytokine receptors are thought to recruit a specific JAK protein although some receptors have been shown to recruit multiple isoforms (Morris et al., 2018) and a low level of redundancy has been demonstrated when the cognate kinase is knocked out (Engelowski et al., 2018).

JAK2 is associated with many receptor pathways. Although there are no examples of humans with JAK2 deficiency several cases have been reported of humans carrying gain of function mutations, predominantly V617F (Shan et al, 2014). These mutations occur in the pseudokinase regulatory domain and result

in JAK2 overactivity. This induces cytokine independent transduction and leads to myeloproliferative disorders (Zhao et al., 2005). Alongside canonical cytokine signalling, JAK2 has also been shown to directly interact with histones in the nucleus leading to the expression of oncogenes (Dawson et al., 2009).

1.4.2 The structure, function and regulation of STAT proteins

STAT proteins are key signal transducers of cytokine receptor activation. These molecules directly associate with JAK-phosphorylated sites within the *C*-terminal domains of cytokine receptors and are activated via phosphorylation by JAK proteins. After activation STAT proteins translocate to the nucleus and bind to DNA to induce changes in protein expression (Bousoik and Montazeri Aliabadi, 2018).

There are seven human STAT proteins (STAT1, 2, 3, 4, 5a, 5b and 6b) that transduce a wide variety of signals from the cytokine family and are subject to various levels of regulation (Abroun et al., 2015). STAT proteins exist as monomers and inactive dimers prior to phosphorylation (Braunstein et al., 2003). It has also been shown that cytokine stimulation does not change the pre-existing monomer to dimer ratio of STAT3 (a key transducer of IL-23 signalling) (Haan et al., 2015; Kretzschmar et al., 2004; Schröder et al., 2004). STATs have been shown to be basally shuttled to and from the nucleus (Bhattacharya and Schindler, 2003; Zeng et al., 2014). Nuclear concentration of STAT3 has been shown to be independent of phosphorylation however activation does increase the rate of shuttling between the nucleus and the cytosol (Herrmann et al., 2007; Liu et al., 2005).

STAT3 has been shown to be vital to a number of non-cytokine related cellular processes (Abroun et al., 2015). For example the protein has been shown to interact with the microtubule destabilising protein stathmin resulting in stabilisation of the cytoskeleton (Ng et al., 2006). STAT3 has also been found to be vital for the optimal function of the mitochondria, with knock out leading to significant impacts of the activity of complex I and II (Wegrzyn et al., 2009).

1.5 IL-23's function within the immune system

To understand the value of therapeutics targeting the IL-23 pathway the function of IL-23 in the immune system must first be outlined. Antigen presenting cells

(APCs) such as macrophages and dendritic cells patrol the periphery of the body. When they come into contact with pathogens they initiate an immune response through the presentation of pathogenic antigens and the production of pro-inflammatory cytokines including IL-23 (Gaudino and Kumar, 2019).

1.5.1 IL-23 in adaptive immunity

T cells are key mediators of adaptive immunity and have been shown to respond to the production of IL-23. T cells mature within the thymus, to become naïve cells expressing up to 100 million T Cell Receptors (TCRs) (Qi et al., 2014), which are capable of binding to hypothetical foreign antigens (self-reactive naïve T cells are killed in the thymus) (Kumar et al., 2018). After a naïve T cell encounters a foreign antigen presented by a Major Histocompatibility Complex (MHC) expressed on the surface of an APC, the process of clonal expansion begins in which differentiation and multiplication generates a population of effector T cells specific to the antigen presented. Cytokines such as IL-23, along with co-stimulation from the APC, influence the eventual subtype of T cell formed (Hwang et al., 2020; Kumar et al., 2018). The main effector cell types are cluster of differentiation (CD)8+ cells and CD 4+ T helper 1 (Th1), Th2, Th17, Th22 or regulatory T (Treg) cells, with each of the CD4+ subtypes having a differential profile of cytokine production (Bhaumik and Basu, 2017).

Th17 cells, named due to their production of IL-17, are a T cell subtype that has been linked with the IL-23 dependent development of auto-inflammatory disease (Kikly et al., 2006). The cell type exhibit a high degree of plasticity and can be formed by several alternative cytokine stimulation conditions, in addition to the ability to change lineage at late stages of differentiation (Mazzoni et al., 2019). Differentiation of T cells to Th17 cells (Figure 1-8) can be initiated *in vitro* by treatment with IL-6 and either Tumour growth factor-β (TGF-β) or IL-1β (Acosta-Rodriguez et al., 2007; Bhaumik and Basu, 2017). The initial stimulation induces the expression of the IL-23 receptor (Mangan et al., 2006; Zhou et al., 2007), with subsequent exposure to IL-23 enhancing the differentiation and inducing the production of pro-inflammatory cytokines such as Granulocyte Macrophage Colony Stimulating Factor (GM-CSF) (Figure 1-8; El-Behi et al., 2011). It has also been shown that an imbalance in the level of IL-23 and TGF-β in the later stages of differentiation can divert polarisation to Th1

or Th22 (pro-inflammatory cell types with a different cytokine production signature) (Bhaumik and Basu, 2017; Mazzoni et al., 2019) and even fully polarised Th17 cells can become Th1 like, with these 'exTh17', 'Th17/Th1' or 'Th17.1' cells being linked to autoinflammatory disease (Mazzoni et al., 2019). Further cytokines including IL-21 have also been implicated in Th17 differentiation (Yang et al., 2008) and it has been demonstrated that polarisation can be induced in the absence of either IL-6, TGF-β, IL-1β or IL-23, indicating that there is a level of redundancy in the cytokine stimulation required for differentiation (Acosta-Rodriguez et al., 2007; Hu et al., 2011; Mangan et al., 2006). The stabilisation of the Th17 cell type is governed by epigenetic modifications of nuclear DNA, the activation or expression of key transcription factors such as STAT3 and Retinoic acid receptor Related Orphan Receptor yt (RORyt) and downregulation of other factors such as T-bet, GATA3 and Fox3p (Bhaumik and Basu, 2017). As the regulation of these factors is modulated by shared signal transducers that are induced by multiple cytokines, most prominently STAT3, it is likely that a Th17 polarising signalling profile may be induced by several combinations of cytokine and TCR stimulations (Bhaumik and Basu, 2017; Mazzoni et al., 2019). It is also likely that the multiple routes of polarisation allow a 'fine-tuning' of the immune response to different classes of pathogens, as it has been shown that different cytokine profiles give rise to functionally different Th17 cells depending on the origin of the APC stimulation (Mazzoni et al., 2019).

CD8+ T cells can directly kill infected or tumorigenic cells after TCR recognition, by activating apoptosis or using cytotoxic molecules such as granzymes (Zhang and Bevan, 2011). There are several reports that sub-populations of CD8+ cells express the IL-23 receptor and react to stimulation by IL-23 by inducing IL-17 production (Ciric et al., 2009; Curtis et al., 2009).

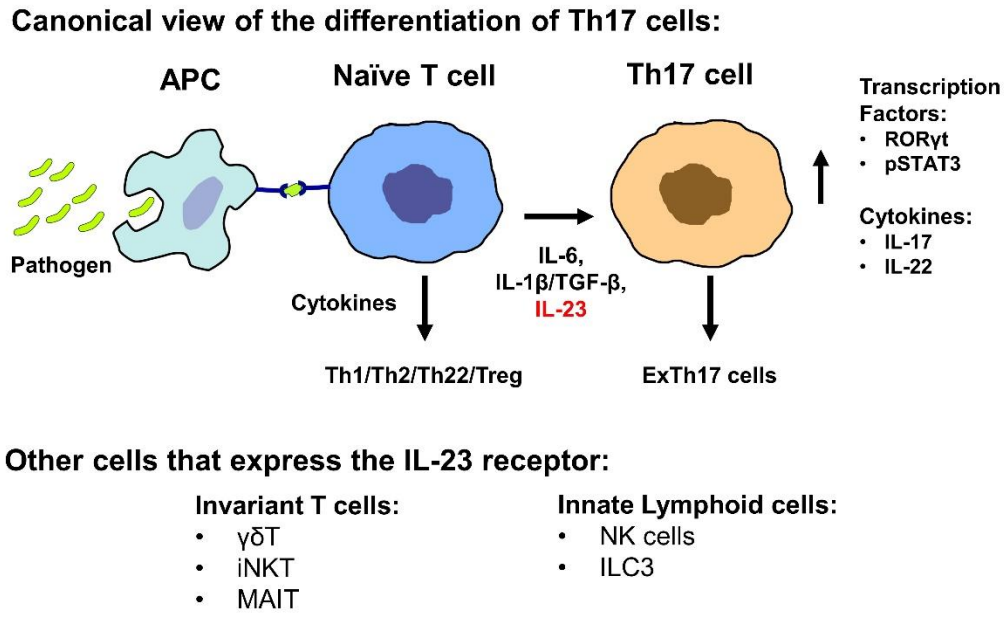

Figure 1-8: The role of IL-23 in Th17 cell differentiation. After Th17 cell differentiation has been initiated by antigen and cytokine stimulation T cells begin to express the IL-23 receptor. Subsequent treatment with IL-23 enhances Th17 cell differentiation through potent activation of phospho-STAT3 and upregulation of transcription factor RORγt. Other classes of immune cells have also been reported to express the IL-23 receptor and respond to IL-23 by promoting inflammation.

1.5.2 IL-23 in innate immunity

Further cell types, linked to innate immunity, express the IL-23 receptor and respond to the production of the cytokine. These include T cell types known as γδT and invariant natural killer T (iNKT) (Cua and Tato, 2010). TCR and Toll Like Receptor (TLR) expressing γδT cells can directly sense pathogenic antigens independent of presentation by MHC complexes (Martin et al., 2009). The TCRs of iNKT are conserved, unlike naïve T cells, and sense bacteria through glycolipids presented by APCs (Doisne et al., 2011). Treatment of γδT and iNKT cells with IL-23 leads to production of pro-inflammatory cytokines such as IL-17 (Cua and Tato, 2010; Doisne et al., 2011). The 'NKT like' mucosally associated invariant T (MAIT) cell type has also been shown to respond to IL-23 stimulation (Wang et al., 2019) and have significantly diminished numbers in a patient with a homozygous IL23R loss function mutation (Staels et al., 2022). MAIT cells sense riboflavin biosynthesis intermediates through their TCR and respond to stimulus by promoting anti-

bacterial and anti-viral immunity through the production of inflammatory cytokines and the killing of infected cells (Hinks and Zhang, 2020).

Further innate lymphoid cell types such as Natural Killer (NK) cells and Innate Lymphoid Cell 3 (ILC3) cells have been shown to express the IL-23 receptor and produce IFN-γ and IL-17 respectively in response to IL-23 treatment (Liu et al., 2019; Takatori et al., 2009; Ziblat et al., 2018). These cell types are mostly tissue resident and respond to cytokines rather than antigen presented by APCs. On stimulation they rapidly initiate an innate immune response through the production of pro-inflammatory cytokines, presentation of antigen and killing of infected cells (Eberl et al., 2015). The expression of RORγt and production of IL-17 by ILC3 cells has led to the suggestion that the cell-type are the non-TCR expressing counterpart of Th17 cells, indeed it is thought that the ILC3 cells also require IL-23 to differentiate (Panda and Colonna, 2019).

Certain myeloid cell types have also been reported to express the IL-23 receptor. Macrophages are known to express IL23R and respond to IL-23 (Cua et al., 2003; Hou et al., 2018), with the presence of IL-23 signalling having been suggested to be a pre-requisite for optimal Pattern Recognition Receptor (PRR) activation (Sun et al., 2020). In addition, eosinophils and dendritic cells have been reported to respond to IL-23 stimulation (Belladonna et al., 2002; Cheung et al., 2008).

Further to IL-23's effect on immune cell stimulation and differentiation, recent research has suggested that IL-23 may have chemoattractant properties and be directly involved in Th17 and γδT migration to locally inflamed areas (Álvarez-Salamero et al., 2020).

1.6 Expression of IL-23 and its receptor

Advances in single cell RNA sequencing have allowed a systematic profiling of gene expression across tissue and cell types (Karlsson et al., 2021). According to these analyses IL23R is expressed in T cells and monocytes, but also has expression in mucosal tissues for example enterocytes and enteroendocrine cells. Surprisingly these results revealed that the highest expression of IL23R in all tissues sampled is in early and late spermatids (Karlsson et al., 2021). Although the IL-23 concentration in semen has been linked to infertility there

have been no mechanistic studies of IL-23's role in reproduction (Duan et al., 2014; Qian et al., 2011). In contrast the IL-23 co-receptor IL12Rβ1 is expressed most highly in blood and immune cells and has low expression in some epithelial cell types.

IL23p19 is widely expressed in many epithelial and immune cell types, in pancreatic endocrine cells and spermatocytes. Conversely IL12p40 expression is limited to certain immune cell types (Karlsson et al., 2021). Physiological IL-23 concentration has been measured in a range of diseases and in several tissues, these are shown in Table 1-2.

Tissue type	**Disease**	**Concentration (pg/mL)**	**Concentration (pM)**	**Reference**
Serum	None	9.87 ± 4.62, 91.6 ± 19.1, 14.8 ± 2.2, 15.5, 372, 21.2 ± 11.0, 582, 54.2 ± 15, 66.4, 166 ± 178	0.176 ± 0.082, 1.63 ± 0.34, 0.264 ± 0.039, 0.277, 6.67, 0.378, 10.4, 0.264 ± 0.268, 1.18, 2.96 ± 3.18	(Atwa et al., 2014; Bilik et al., 2016; Gerenova et al., 2019; Himani et al., 2014; Jaszczura et al., 2019; Lucaciu et al., 2021; Nogueira et al., 2010; Rafat et al., 2022; Rana et al., 2012; Ugur et al., 2015; Youssef et al., 2018)
Serum	Chronic spontaneous urticaria	39.0 ± 27.8	0.696 ± 0.496	(Atwa et al., 2014)
Serum	Ankylosing Spondylitis	334 ± 177	5.96 ± 3.16	(Ugur et al., 2015)

Serum	Systemic lupus erythematosus	108 ± 17, 135 ± 54	1.93 ± 0.31, 2.41 ± 0.96,	(Rafat et al., 2022; Rana et al., 2012)
Serum	Hashimoto's thyroiditis	38.70 ± 3.1	0.691 ± 0.055	(Gerenova et al., 2019)
Serum	Rheumatic Mitral Stenosis	96.7	1.73	(Bilik et al., 2016)
Serum	Crohn's Disease	937	16.7	(Lucaciu et al., 2021)
Serum	Ulcerative Colitis	1370 235 ± 161	24.4 4.19 ± 2.87	(Lucaciu et al., 2021; Youssef et al., 2018)
Serum	Immunoglobulin A vasculitis	700	12.5	(Jaszczura et al., 2019)
Serum	ANCA-associated vasculitis	941	16.8	(Nogueira et al., 2010)
Serum	Rheumatoid Arthritis	2700 ± 1400	48.2 ± 25.0	(Kim et al., 2007)
Synovial fluid	Rheumatoid Arthritis	4430 ± 1490	79.0 ± 26.6	(Kim et al., 2007)
Gingival crevicular fluid	None	2570 ± 700	45.9 ± 12.5	(Himani et al., 2014)
Gingival crevicular fluid	Chronic periodontitis	16400 ± 2050	293 ± 37	(Himani et al., 2014)
Gingival crevicular fluid	Gingivitis	5900 ± 1140	105 ± 20.3	(Himani et al., 2014)

Table 1-2: Reported concentrations of IL-23 in clinical samples taken from healthy and diseased donors. Concentration values were converted to pM from pg/mL using the molecular weight 56050 Da.

Several further RNA analyses focussing on specific immune cell types allow a more precise deconvolution of which cells express the cytokine and receptor. IL23R expression is limited mainly to T cell types with low expression in NK cells. Within T cells expression is higher in memory rather than naive CD4+ and

CD8+ cells and is also prominent in γδT and regulatory T cells (Monaco et al., 2019; Schmiedel et al., 2018; Uhlen et al., 2019). Interestingly, in two separate experiments MAIT cells were by far the highest IL23R expressing cell type sampled (Monaco et al., 2019; Uhlen et al., 2019). IL12Rβ1 was expressed in all the sampled immune cell types. IL23p19 is widely expressed across the cell types sampled including monocytes, B cells, dendritic cells, and most strongly in T cells. IL12p40 conversely has very low expression levels in all cell types and analyses, it may be that activation by pathogens is needed to induce IL12p40 expression (Monaco et al., 2019; Schmiedel et al., 2018; Uhlen et al., 2019).

1.7 Consequences of IL-23 loss of function

Mice lacking the *IL23r* gene retain the ability to initiate systemic T cell driven inflammatory responses, however they have impaired intestinal T cell proliferation and Th17 production (Ahern et al., 2010).

In humans, loss of function mutations in *IL23r* have been shown to cause Mendelian susceptibility to mycobacterial disease (MSMD) (Mahdaviani et al., 2020; Martínez-barricarte et al., 2018; Staels et al., 2022). In this condition, patients suffer opportunistic infections by weakly virulent mycobacterium species, for example bacillus Calmette-Guérin (BCG) or environmental mycobacteria such as *Mycobacterium avium* (Bustamante et al., 2014). The leading cause of MSMD is loss of function in IL12p40 or IL12Rβ1 genes, resulting in the disruption of both IL-23 and IL-12 signalling. Hundreds of patients have been reported who suffer from MSMD and more rarely chronic mucocutaneous candidiasis (CMC) caused by IL12Rβ1 or IL12p40 primary immunodeficiency, in contrast only a handful of cases have been reported caused by IL-12 or IL-23 pathway specific, loss of function (Bustamante et al., 2014; Mahdaviani et al., 2020; Martínez-barricarte et al., 2018; Staels et al., 2022). The frequency of IL12Rβ1, IL12Rβ2 and IL23R loss of function genes in the population is reported to be similar, therefore it has been suggested that IL-12 and IL-23 are partly redundant with each other for protection against mycobacterial disease (Martínez-barricarte et al., 2018). Many clinically significant mutations of the IL-23 receptor have been identified through genome wide association studies (GWAS) studies and through genome sequencing of patients, a subset of which are highlighted in Table 1-3. As this thesis will focus

on analysis of the molecular mechanism of recombinantly expressed receptors, only mutations resulting in amino acid substitutions are highlighted in the table.

Mutation	Location	Disease significance	Functional data
IL23R			
Q3H (reviewed in Floss et al., 2020; rs1884444)	Signal peptide.	Lowered risk of schistomiasis associated immune reconstitution inflammatory syndrome, ulcerative colitis and psoriasis.	None
R86Q (reviewed in Floss et al., 2020; rs76575803)	Extracellular domain 1	Lowered risk of Crohn's disease.	None
C115Y; (rs1646917043)	Extracellular domain 1	Increased susceptibility to mycobacterial disease.	Mutation blocks ligand induced STAT3 phosphorylation (Martínez-barricarte et al., 2018).
G149R (reviewed in Floss et al., 2020; rs76418789)	Extracellular domain 2	Lowered risk of Crohn's disease and ulcerative colitis.	A study shows that mutation increases ER retention and lowers surface expression (Sivanesan et al., 2016).
L310P (reviewed in Floss et al., 2020; rs7530511)	Extracellular domain 3	Lowered risk of psoriasis.	None

V362I (reviewed in Floss et al., 2020; rs41313262)	Transmembrane domain	Lowered risk of Crohn's disease and ulcerative colitis.	A study shows that mutation reduces protein half-life (Sivanesan et al., 2016).
R381Q (reviewed in Floss et al., 2020; rs11209026)	Intracellular domain (membrane proximal)	Lowered risk of Crohn's disease, ulcerative colitis ankylosing spondylitis and psoriasis.	The mutation has been shown to reduce surface expression and half life (Sivanesan et al., 2016). A study in macrophages demonstrated that the mutation led to impaired receptor recycling to the cell surface after activation (Sun et al., 2020).
IL12Rβ1			
R173P (reviewed in van de Vosse et al., 2013)	Extracellular domain 2	Increased susceptibility to mycobacterial disease.	This mutant leads blocks surface expression and response to IL-12 (van de Vosse et al., 2005).
C186S (reviewed in van de Vosse et al., 2013)	Extracellular domain 2	Increased susceptibility to mycobacterial disease.	This mutant leads blocks surface expression and response to IL-12 (van de Vosse et al., 2005).
C198R (reviewed in van de Vosse et	Extracellular domain 2	Increased susceptibility to mycobacterial disease (mild phenotype).	This mutant leads to lowered surface expression and response to IL-12

al., 2013; rs121434495)			(van de Vosse et al., 2005).
R213W (reviewed in van de Vosse et al., 2013; rs121434494)	Extracellular domain 2	Increased susceptibility to mycobacterial disease.	This mutant leads blocks surface expression and response to IL-12 (van de Vosse et al., 2005).
Y367C (reviewed in van de Vosse et al., 2013)	Extracellular domain 3	Increased susceptibility to mycobacterial disease.	This mutant leads blocks surface expression and response to IL-12 (van de Vosse et al., 2005).
R521G (reviewed in van de Vosse et al., 2013)	Extracellular domain 5	Increased susceptibility to mycobacterial disease (mild phenotype).	This mutant leads blocks surface expression and response to IL-12 (Potjewijd et al., 2012).

Table 1-3: Reported clinically significance amino acid substitution mutants of the IL-23 receptor.

1.8 The role of IL-23 in autoinflammatory disease

Before the discovery of IL-23, it was thought that the cytokine IL-12 mediated autoinflammatory diseases due to the protective effect of IL12p40 knock out in murine models of autoinflammatory conditions (Caspi, 1998). Several subsequent studies however, indicated that patients with autoinflammatory conditions demonstrated high levels of IL12p40 without IL12p35 (Fassbender et al., 1998; Shigehara et al., 2003). This was followed by the revelation that IL23p19 but not IL12p35 knockout mice were protected against experimental autoinflammatory disease (Cua et al., 2003). It was subsequently discovered that IL-23 induced the production of pathogenic T cell subsets (Langrish et al., 2005) GWAS found that certain IL23R or IL23p19 variants were protective against Psoriasis, Psoriatic Arthritis (PA), Ankylosing Spondylitis (AS), Uveitis, Crohn's Disease (CD), Ulcerative Colitis (UC) , Bechet's disease, and further

immune diseases (Cargill et al., 2007; Dong et al., 2013; Duerr et al., 2006; Filer et al., 2008; Remmers et al., 2010).

The precise mechanism through which many autoinflammatory diseases are initiated is still a matter of contention with evidence indicating that both genetic and environmental factors can pre-dispose patients towards disease development (Ho et al., 2019; Rahmati et al., 2020). In the case of IL-23 mediated autoinflammatory conditions, it is thought that IL-23 is needed for the activation and differentiation of pathogenic IL-17 producing Th17, γδT and ILC3 cell types (Geremia et al., 2011; Langrish et al., 2005; Sutton et al., 2009). The efficacy of anti-IL-23 therapeutics in psoriasis, PA and CD confirmed the central role of the cytokine in these diseases. Anti-IL-17 therapeutics have also been efficacious in treating auto-inflammatory conditions however the lack of efficacy of anti-IL-23 but not anti-IL-17 therapies in AS, indicate that the applicability of therapeutics targeting the IL-23/IL-17 axis may depend on the specific disease (Baeten and Adamopoulos, 2021; Ruiz de Morales et al., 2020).

1.9 Therapeutic strategies for the IL-23 pathway

1.9.1 Background to cytokine therapeutics

Medications that modulate the immune system date from before the advent of modern medicine, through the traditional use of naturally derived anti-inflammatory molecules such as salicylic acid (Hedner and Everts, 1998). In addition, prior to the discovery of cytokines the production of inflammatory mediators was indirectly modulated using steroids and non-steroidal anti-inflammatory drugs (NSAIDs) (Benedek, 2011; Praveen Rao and Knaus, 2008).

The discovery of cytokines was accompanied by the promise of new, more specific treatments aimed at these messenger molecules. Initially, many researchers suggested the purification and utilisation of cytokines as therapies themselves (Vilček and Feldmann, 2004). The discovery that interferons protected against viral infection and could inhibit tumour growth for example, led to hope that these molecules could be used in the clinic (Gresser, 1977; Isaacs and Lindenmann, 1957; Vilček and Feldmann, 2004). Although recombinant Interferon has shown some promise as an anti-cancer (Mocellin et al., 2010) and anti-viral treatment (Saleki et al., 2021), the therapy has been hampered by

toxicities and has not realised the initial hopes for a highly efficacious treatment (Borg and Isenberg, 2007; Sulkowski et al., 2011). Many cytokines, for example IL-2, TNF, GM-CSF and M-CSF (Dubnika et al., 2018; Hu et al., 2021), are now used therapeutically, however adverse effects remain common and cytokines are more frequently antagonised due to their function in mediating harmful auto-inflammation (Akdis et al., 2016; Scheinecker et al., 2008). Despite this, the administration of cytokine receptor agonists could experience a renaissance with the advent of more selective engineered cytokine therapeutics (Lopes et al., 2020; Ma et al., 2015; Spangler et al., 2015).

Antibody based 'biologic' therapies emerged in the mid-1980s, enabling the sequestration and antagonism of targets that had previously been problematic to drug with small molecules (Lu et al., 2020). The initial indication that antibodies could be effective treatments against cytokine targets was the use of anti-IFN antibodies to prevent choriomeningitis in mice (Riviere et al., 1977). It was hoped that the success of anti-cytokine treatments in *in vivo* models of sepsis would translate into new effective treatments. However, the results of clinical trials were disappointing and the field pivoted to autoinflammatory disease (Dinarello, 2007; Eichacker et al., 2002). The first therapy followed in 1997 when the humanized anti-CD25 (An IL-2 receptor component) drug, Daclizumab was licenced for the treatment of Graft Versus Host Disease (GVHD) (Tsurushita et al., 2005). The following year, the chimeric anti-TNF-α therapy infliximab, was approved for CD (Lu et al., 2020). The development of fully human antibodies using phage display enabled the production of the human anti-TNF-α therapy Adalimumab in 2002 for rheumatoid arthritis (RA) (Lu et al., 2020). Adalimumab became the highest selling drug of all time in 2021 (Urquhart, 2021) and there are now more than 20 licenced antibody therapies that target cytokines and their receptors (Lu et al., 2020).

Whilst antibodies remain the dominant anti-cytokine therapeutics, additional technologies have been developed and are in development. Etanercept, for example is a fusion of human TNF-α receptor with an antibody Fc domain and has been licenced for RA (Goffe and Cather, 2003). Anakinra, a drug approved for several autoinflammatory conditions is a slightly modified version of IL-1 receptor antagonist (IL-1Ra) (Scheinecker et al., 2008; Waugh and Perry, 2005).

New technologies have the potential to give rise to novel cytokine modulating therapeutics, with anti-sense RNA treatments (Jaschinski et al., 2011) and cyclic peptide cytokine-receptor antagonists having been developed (Cheng et al., 2019; Scheide-Noeth et al., 2019).

Whilst some small molecule inhibitors of cytokine receptor interactions have been reported (Bello et al., 2014; Braisted et al., 2003) none have yet made it through clinical trials. Small molecule inhibitors of cytokine signalling proteins have however been successfully developed. The success of early kinase inhibitors such as the anti-cancer therapeutic Imatinib in the early 2000s led to rapid development of kinase inhibitors (Cohen et al., 2021). Antagonists of JAK proteins followed, with the pan-JAK inhibitor Tofacitinib being licenced for the treatment of RA in 2012 (Dhillon, 2017). The ability of Tofacitinib to inhibit multiple cytokine signalling pathways enables broad-acting inhibition in a system where pathogenesis may be influenced by multiple cytokines. Unfortunately this non-specificity, in which multiple non-pathogenic pathways critical to immunity and protective cytokines such as IL-10 are inhibited leads to adverse side effects, such as opportunistic infections (Cohen et al., 2021). Further JAK inhibitors with differing selectivity patterns, have now been licensed; Baricitinib for example is a JAK1 and 2 antagonist and Upadacitinib, Filgotinib and Abrocitinib are JAK1 selective (Angelini et al., 2020; Bieber et al., 2021). It is hypothesised that selective inhibition of JAK1 will reduce side effects by preventing inhibition of JAK1 independent cytokine signalling pathways such as EPO (Namour et al., 2015). Further JAK selective compounds are currently in clinical development for a range of conditions (Hu et al., 2021; Virtanen et al., 2019).

In addition to JAK inhibitors, cytokine signalling can also be inhibited by antagonising STAT proteins. There are 7 human STAT proteins, potentially allowing this approach to be more selective than JAK inhibitors, in addition each cytokine receptor can signal through multiple STATs allowing the potential for selectivity within the outcomes of cytokine signalling (Hu et al., 2021). However, some STATs are known to be involved non-cytokine connected pathways for example in the mitochondria (Bharadwaj et al., 2020). The STAT3 selective antagonist STATTIC was the first small molecule STAT inhibitor to

be reported (Hu et al., 2021; Schust et al., 2006). Since STATTIC's development a range of further STAT3 inhibitors have been developed with a smaller number of STAT5 inhibiting compounds also being reported. No STAT antagonists have yet completed clinical trials with the major hurdle being the high concentrations needed and the associated toxicities (Hu et al., 2021).

Downstream inhibition of cytokine induced transcription factors has also been trialled as a methodology for treating autoinflammatory conditions. Increased expression of the transcription factor RORγt (a transcription factor responsible for inducing pro-inflammatory genes such as IL-17; Capone and Volpe, 2020) is a hallmark of Th17 cell development following IL-23 stimulation, small molecule inverse agonists of RORγt have been developed and are now in clinical trials for psoriasis (Jetten and Cook, 2020).

1.9.2 Anti-IL-23 therapies

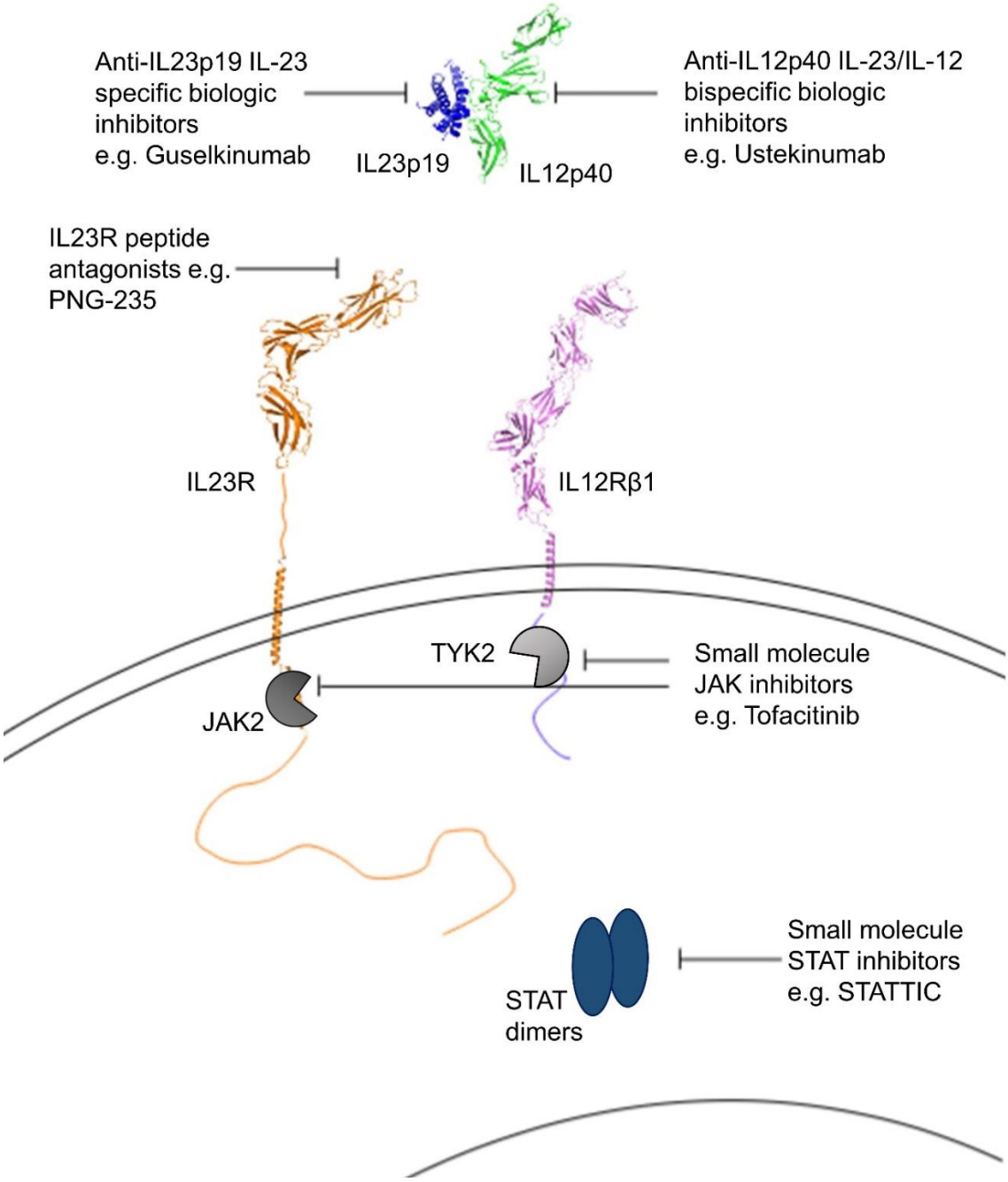

Figure 1-9: IL-23 pathway antagonists. The IL-23 pathway can be antagonised at several stages. Licenced therapeutics antagonise IL-23 and JAK proteins. Drugs are in development that target IL23R and STATs.

Due to the initially held but incorrect hypothesis that IL-12 was the driver of several autoinflammatory diseases, the first anti-IL-23 biological therapies were directed at the IL12p40 subunit and were thus bispecific against both IL-12 and IL-23 (Teng et al., 2015). The first and sole member of this class to be licensed

was Ustekinumab (Jannsen), which was approved by the FDA for the treatment of plaque psoriasis in 2009 after being shown to be effective in reducing at least 75% of the severity of the disease in over two thirds of patients in phase III trials (Yang et al., 2021). The rate of infections was closely monitored in patients treated with the drug and it was found that these were not significantly higher than in the placebo group (Yang et al., 2021). Ustekinumab has since been licenced for PA and CD, however the drug was not effective against AS, systemic lupus erythematosus, multiple sclerosis and RA (Chyuan and Lai, 2020; Pawlak-buś et al., 2021). The unexpected disconnect between the efficacy of anti-IL-23 therapies and anti-IL-17 therapies, which are efficacious in AS but not in CD has been the subject of much debate since the results of these trials (Baeten and Adamopoulos, 2021; Hohenberger et al., 2018; McGonagle et al., 2021). Theories have suggested that IL-23 induces chronic inflammation in AS but is dispensable once chronic inflammation has been established (Baeten and Adamopoulos, 2021). In the case of CD it has been suggested that some populations of IL-23 independent IL-17 producing cells may be protective through their role in barrier immunity (Hohenberger et al., 2018).

Since the successful licencing of Ustekinumab, the anti-IL23p19 specific therapies, Guselkumab (Jannsen), Risankizumab (Boehringer Ingelheim/Abbvie) and Tildrakizumab (Merck) have been developed and licenced for psoriasis, with Guselkumab also being approved for PA (Table 1-4). A meta-analysis of the psoriasis clinical trials for these three therapies and Ustekinumab revealed that there was little difference in terms of efficacy and tolerability between the treatments however Risankizumab and Guselkumab appeared to show slightly higher efficacy than Tildrakizumab, an effect that correlated with the affinities of the antibodies for IL23p19 (Mahil et al., 2020). As anti-IL23p19 antibodies have only been approved recently there is little data on long term tolerability and efficacy. A schematic showing the various stages at which the IL-23 pathway can be inhibited is shown in Figure 1-9.

1.9.3 Peptide IL23R antagonists

Despite the efficacy of biologic therapies for IL-23 there remain some drawbacks to these treatments. Biologic therapies require sub-cutaneous administration which can limit patient adherence and leads to unnecessary

systemic inhibition in diseases that exhibit local inflammation (Arbiser and Elsey, 2018). In addition, tolerance can develop to treatments, due to compensatory adaption in the immune system or development of anti-drug antibodies (Jullien et al., 2015; Khoury and Ilan, 2019).

These issues have led to the continued development of new oral or topical treatments. It is difficult to drug the broad protein to protein interaction interfaces of cytokine receptors with small molecule inhibitors although this has been achieved for IL-2 receptor (Wilson and Arkin, 2010). It has proved easier to design peptide inhibitors of cytokine receptors, with IL23R exhibiting a range of reported peptide antagonists (Table 1-4). The first of these were competitive and non-competitive linear peptides reported by academic groups (Kuchař et al., 2014; Quiniou et al., 2014). These efforts were followed by development of a range of orally bioavailable macrocyclic peptides antagonists IL23R by the company Protagonist (Bourne et al., 2017; Cheng et al., 2019). The company has partnered with Johnson and Johnson to bring three of these compounds into the clinic. The most advanced among these, molecule PN-235/JNJ-77242113 is currently in phase IIb trials as an oral treatment for psoriasis whilst the previous lead candidate PTG-200/JNJ-67864238 was withdrawn from Phase II trials for IBD due to lack of efficacy (Data from www.clinicaltrials.gov accessed on: 25/08/2022). Further cyclic IL23R inhibitors have also been developed by academic groups in demonstrations of novel phage display techniques (Kong et al., 2020; Pandya et al., 2020).

Whilst most peptide antagonists developed have been competitive antagonists of IL23R there is the possibility that cytokine signalling could be blocked by non-competitive, antagonists of receptor dimerization as has been demonstrated for GHR (Rowlinson et al., 1998).

Drug type	Target	Drug Name	Stage of development
Antibodies	IL12p40	Ustekinumab	Approved for: Psoriasis, CD, UC, PA
		Briakinumab	Phase III (discontinued)
	IL23p19	Tildrakizumab	Approved for: PA, Psoriasis
		Guselkumab	Approved for: Psoriasis
		Risankizumab	Approved for: Psoriasis
		Mirikizumab	Phase III
Peptides	IL23R	REX proteins	Reported in (Kuchař et al., 2014)
		TEEEQQLY	Reported in (Quiniou et al., 2014)
		PTG-200	Phase II (discontinued)
		PN-232	Phase I (discontinued)
		PN-235	Phase II
		23-446 and 23-437	Reported in (Pandya et al., 2020)
		Isomer 5	Reported in (Kong et al., 2020)

Table 1-4: Reported IL-23 and IL23R antagonists. Table demonstrating biologic antagonists of IL-23 and peptide antagonists of IL23R.

1.10 Proximity-based techniques in molecular pharmacology

In this project, proximity-based techniques will be used to investigate the ligand binding and activation of the IL-23 receptor with the aim of gaining useful insights for drug discovery projects targeting the IL-23 pathway. Powerful techniques to measure the interactions of ligands, receptors and signal transducers have been developed in recent years to characterise GPCRs (Stoddart et al., 2016) and RTKs (Peach et al., 2021), this project will now apply these to the IL-23 receptor.

1.10.1 Ligand binding assays

The birth of molecular pharmacology was initiated at the beginning of the 20th century with the origination of the receptor theory of drug action by both Paul Erhlich and John Newport Langley (Parascandola and Jasensky, 1974). Whilst receptors were hypothesised to exist from observations made from the effect of compounds on tissues samples or on intact animals, the existence of receptors remained purely theoretical (Maehle, 2004). Despite this, these experiments allowed the establishment of many of the equations used in modern day pharmacological analysis, for example the Hill-Langmuir equation (Gesztelyi et al., 2012).

Mid-way through the 20th century technologies emerged that allowed the radiolabelling of compounds and proteins, typically with the radioactive isotopes H^3, C^{14} or I^{125} (Bylund and Enna, 2018; Paton and Rang, 1965). The rate of decay of these isotopes could be measured through scintillation counters at various time points after radioligands had been mixed with cells, purified receptors, membrane preparations or tissues. By adding an excess of an unlabelled form of a competing compound or protein, specific binding could be measured by the different levels of radioligand present in the two conditions (Maguire et al., 2012). This technique enabled modern molecular pharmacology by allowing the measurement of specific interactions of drug with receptor (Bylund and Enna, 2018). Further technological advances enabled the development of functional assays that enabled the measurement of signalling cascades, for example through quantification of intracellular cyclic Adensone Monophosphate (cAMP) or Ca^{2+} concentration (Miyano et al., 2014).

Whilst radioligand binding revolutionised pharmacology, the use of radioligands has been hampered by safety measures concerning handling of ligands and experimental waste (Stoddart et al., 2016).

1.10.2 Proximity based techniques

Recombinant techniques were developed in the latter part of the 20th century to quantify known interactions of intracellular proteins, and to screen cDNA libraries for novel interactions. These techniques typically involved a split reporter system which can be fused to two proteins of interest to monitor

interactions (Michnick et al., 2000). An early example of this approach is the yeast two-hybrid system in which a pair of proteins are fused to either a DNA interacting protein or a transcription factor activating protein. These fusions are then expressed in yeast, with a transcription factor and a recombinant DNA construct made up of a flexible DNA linker between a transcription factor binding site and an upstream activation signal located at the binding site for the DNA binding protein (Luban and Goff, 1995). Initiation of transcription occurs when the proteins interact and bring the sequences together (Luban and Goff, 1995). Although systems such as the two-hybrid system are highly sensitive, they do not allow measurement of mammalian protein to protein interactions in their native environment. To rectify this, protein complementation assays were created, for example a split version of murine dihydrofolate reductase that could be recombinantly tagged to two proteins of interest and expressed in a mammalian cell line of interest. If the proteins interacted then the enzyme would be reconstituted and the generation of the enzyme's product could be measured (Michnick et al., 2000).

1.10.3 Förster Resonance energy transfer (FRET)

Using a luminescent signal to monitor real time proximity enables dynamic and sensitive monitoring of interactions and can be used to measure distance or orientation of interacting partners (Stoddart et al., 2016). The design and use of fluorescence and luminescence-based techniques requires an understanding of the physics of light. Light is made up of photons which are defined by oscillating waves of both magnetic and electric fields, collectively termed electromagnetic radiation. Bonds within molecules have a particular vibrational frequency in much the same way as the strings of a musical instrument. If a molecule is subjected to photons of the same wavelength as the vibrational frequency of its bonds then they are said to be in resonance and much larger amounts of energy can be absorbed (Learmouth et al., 2009).

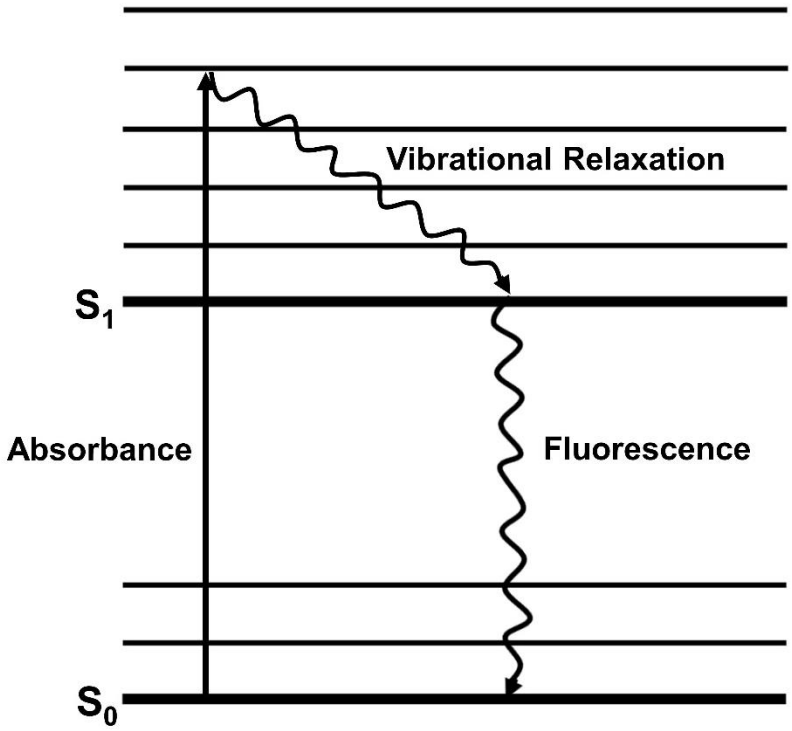

Figure 1-10: A Pierre-Jablonski diagram demonstrating the principles of fluorescence. S_0 represents the ground energy state of an electron and S_1 represents the next highest energy orbital above the ground state.

Fluorescence is a process in which photons of a wavelength in resonance with a molecule, excite its electrons to enter a higher energy orbital state. As the electrons return to their previous orbital state, they release energy in the form of longer wavelength photons, due to some energy being lost as heat in a process called vibrational relaxation. This process can be summarised using a Perrin-Jablonski diagram (Figure 1-10). The excitation wavelength of the fluorophore is dictated by the resonance or vibrational frequency of the bonds within the molecule. The difference between the absorption and emission wavelengths of a fluorophore is known as a Stokes shift (Figure 1-11) and can vary in scale for different molecules based on the amount of vibrational relaxation that occurs as the electron returns to its ground state. Some proteins are intrinsically fluorescent enabling their use as reporters in recombinant biological assays, in addition smaller synthetic fluorescent groups that can chemically bonded to molecules of interest and used to monitor their activity (Learmouth et al., 2009).

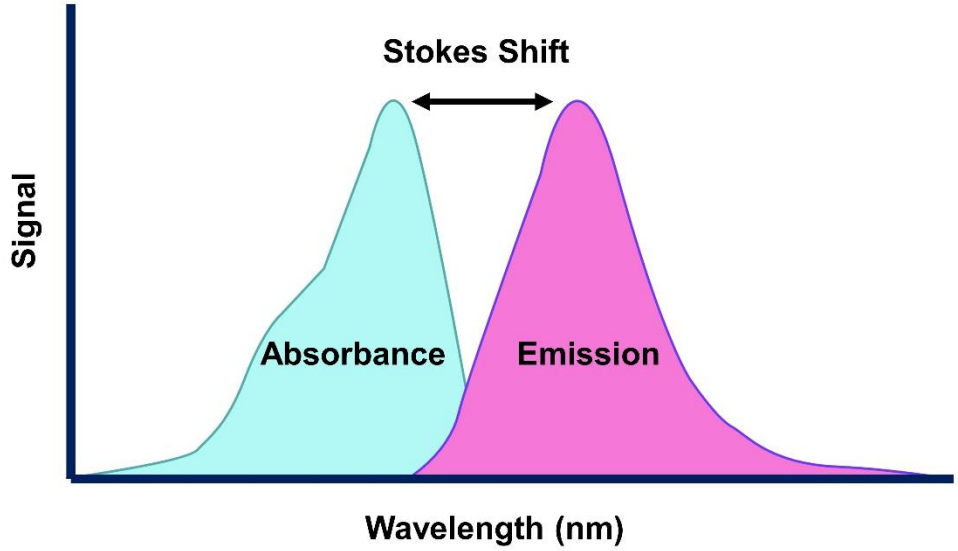

Figure 1-11: The Stokes shift. The absorbance and emission spectra of a hypothetical fluorescent molecule. The difference in wavelength between the peak of the absorbance and emission spectra is termed the Stokes shift.

FRET is a technique that utilises the Stokes shift to measure the proximity of fluorescently tagged molecules. In FRET two molecules of interest are bonded to fluorescent moieties with overlapping emission and excitation wavelengths. The shorter wavelength emission 'donor' molecule is excited by an external light stimulus, the molecule then emits longer wavelength light capable of exciting the 'acceptor' molecule. The ratio of the donor to acceptor emissions is then used as a measure of proximity. The amplitude of the excitation of the acceptor molecule is related to the distance between the donor and acceptor and the orientation of the molecules, due to FRET being more efficient when the dipoles in the molecules are aligned (Clegg, 1995).

One of the advantages of FRET over other proximity-based techniques, is that the read out is immediate and proportional to the interaction, rather than needing time for a reporter to be expressed or a signal transduction cascade to be initiated. This immediacy enables the measurement of kinetic processes for example the association and dissociation of drug-like molecules to a target of interest (Schiele et al., 2015).

1.10.4 Bioluminescence based techniques

The trait of bioluminescence is hypothesised to have evolved independently at least 90 times across the tree of life and is found in wide variety of organisms including insects, fish, fungi and bacteria. Many animals can create their own light, for a range of functions including mating displays, evading predators and attracting prey (Lau and Oakley, 2021). The origin of this bioluminescence is the catalysis, usually an oxidation, of a substrate termed luciferin by bioluminescent enzymes called luciferases. The energy released from the reaction causes the emission of photons from excited electrons in the substrate (Shimomura, 2010).

Many luciferases and luciferins have now been extracted from nature for use in biotechnology. The first use of these enzymes was to act as reporters of gene transcription, with recombinant plasmids encoding the enzymes placed downstream of a binding site for a transcription factor of interest (Roda et al., 2004). Luciferase genes have also been split for use in protein complementation assays (Paulmurugant and Gambhir, 2003).

Whilst FRET is a powerful proximity-based technique, the technology relies on the use of an external high intensity excitation source. This limits the use of FRET in whole cell systems as many biological substances auto-fluoresce and as the excitation can be phototoxic or induce photobleaching. The introduction of luciferases to biological research enabled the use of these enzymes as the excitatory source in a technique known as Bioluminescence Resonance Energy Transfer (BRET). Because this technique utilises a luciferase fused to a target of interest, energy transfer is localised to the molecule, greatly reducing the signal from non-specific auto-fluorescence (Pfleger and Eidne, 2006). Many luciferases and luciferins are now available for use in biological research and have been used to measure real-time interactions with fluorescently tagged compounds and proteins (Dale et al., 2019).

1.11 Aims

The aim of the work described in this thesis was to build a proximity-based assay to measure and quantify the interaction between IL-23 and its full-length receptor subunits expressed in isolation and together on the surface of living

cells. Following this work, the aim was to use similar proximity-based techniques to quantify the association of IL-23 receptor subunits in the presence and absence of cytokine. Furthermore, this project aims to generate novel fluorescent probes and assays to characterise reported IL-23 receptor antagonists and to utilise the assays created to characterise disease linked mutants of IL23R.

Chapter 2. General Materials and Methods

In this section materials used in the project will be presented in a centralised list to enable efficient identification of the origin of reagents and equipment. The methodology of techniques which were utilised in multiple chapters will also be described.

2.1 Materials

Reagent or Resource	**Source**	**Identifier**
Chemicals, Peptides, Recombinant Proteins		
5(6)-TAMRA (5-(and-6)-Carboxytetramethylrhodamine), mixed isomers	ThermoFisher Scientific	Cat# C300
Acetonitrile	Merck	Cat# 34851
Agarose	Merck	Cat# 101614
AF488 Anti-Chicken antibody	ThermoFisher	Cat#A-21441; RRID: AB_2535859
Anti-NanoLuc antibody	Gifted by Promega	
Chicken Serum	Merck	Cat# C5405
Dithiothreitol (DTT)	ThermoFisher Scientific	Cat# R0862
DNA Loading Dye	Promega	Cat# G1881
Dulbecco's Modified Eagle's Medium	Merck	Cat# D6429
Ethidium Bromide	Merck	Cat# 111608
Extracellular NanoLuc inhibitor	Promega	Cat# N235A
Fetal Bovine Serum	Merck	Cat# F2442
Formalin	Merck	Cat# 104002
Formic acid	Fisher Chemical	Cat# F/1900/PB15
FuGENE HD	Promega	Cat# E2312

Glycine	Merck	Cat# G7126
HaloTag Alexa Fluor 488 Ligand	Promega	Cat# G1001
HaloTag NanoBRET 618 Ligand	Promega Corporation	Cat# G9801
IL-12	SinoBiological	Cat# CT050-HNAH
IL12p40	Peprotech	Cat# 200-12p40
IL12p80	Merck	Cat# SRP3075
IL23p19-Fc	SinoBiological	Cat# 13062-H02H
Isopropanol	Merck	Cat# 34863
LB Agar	Merck	Cat# 110283
Lysogeny broth (LB)	Merck	Cat# 110285
Opti-MEM reduced serum medium	ThermoFisher Scientific	Cat# 11058021
P630-TMR	Cambridge Research Biochemicals	Custom Synthesis
Peptide 630 (P630)	Cambridge Research Biochemicals	Custom Synthesis
Phosphate Buffered Saline (PBS)	Merck	Cat# D8537
Poly-D-Lysine hydrobromide	Merck	Cat# P6407
Protease-free Bovine Serum Albumin	Merck	Cat# A7030
Recombinant His-TEV-NanoLuc Protein	D. Veprintsev lab (University of Nottingham; Dr Bradley Hoare)	
Recombinant IL-23 protein	GlaxoSmithKline (Dr Surjit Bains)	
SNAP-Tag AlexaFluor 488 membrane impermeant substrate	New England BioLabs	Cat# S9124S
T4 DNA Ligase	NEB	Cat# M0202L
TAMRA, SE; 5-(and-6)-Carboxytetramethylrhodamine,	ThermoFisher Scientific	Cat# C1171

Succinimidyl Ester (5(6)-TAMRA, SE), mixed isomers		
TEEEQQLY octapeptide	Cambridge Research Biochemicals	Custom Synthesis
Critical Commercial Assays and Kits		
AlphaLISA SureFire Ultra p-STAT3 (Tyr705) Assay Kit	Perkin Elmer	Cat# ALSU-PST3
MycoStrip TM 100	InvivoGen	Cat# rep-mys-100
Nano-Glo luciferase assay system (Furimizine)	Promega Corporation	Cat# N1130
Phusion Site-Directed Mutagenesis Kit	ThermoFisher	Cat# F541
Pureyield Plasmid Maxiprep kit	Promega Corporation	Cat# A2392
Pureyield Plasmid Miniprep kit	Promega Corporation	Cat# A1223
SV Wizard Gel and PCR clean up kit	Promega Corporation	Cat# A9281
Experimental Models: Cell Lines		
Human: HEK293T cells (female)	ATCC (Virginia, USA)	Cat# CRL-3216
Recombinant DNA		
IL12Rβ1 expression plasmid	Origene	Cat# SC303661
IL23R pc3.1 zeo	Genscript	Custom Synthesis
IL23R pc3.1 zeo TMD motif mutant 1	Genscript	Custom Synthesis
IL-23R-MycDDK expression plasmid	Origene	Cat# RC211477
IL-6 secretion signal -HT-TEV-IL12Rβ1	Genscript	Custom synthesis
IL-6 secretion signal -HT-TEV-IL23R	Genscript	Custom synthesis
IL-6 secretion signal -NL-IL-23R	Genscript	Custom synthesis
IL-6 secretion signal-NL-IL12Rβ1	Genscript	Custom synthesis

Pc3.1 *N*-terminal HiBit vector	(Soave et al., 2020a)	
Pc3.1 *N*-terminal m5HT3A Secretion Signal-LgBit vector	(Soave et al., 2020b)	
Pc3.1 *N*-terminal SmBit vector	(Soave et al., 2020a)	
Pc3.1 zeo	Invitrogen	Cat# V86020
Pc3.1 zeo m5HT3A Secretion Signal HiBit-IL12Rβ1	Genscript	Custom Synthesis
Pc3.1 zeo m5HT3A Secretion Signal SNAP-Tag	(Gherbi et al., 2015)	
Software and Algorithms		
Benchling	Benchling	www.benchling.com
Excel	Microsoft	www.microsoft.com
GraphPad Prism 7.02	GraphPad Software	www.graphpad.com
ImageJ Fiji 1.53	National Institute of Health	www.fiji.sc
MARS Data Analysis Software	BMG Labtech	www.bmglabtech.com
MaxEnt1 4.1	Waters	www.waters.com
SnapGene Viewer 6.0.5	SnapGene	www.snapgene.com
Zen 2012	Zeiss	www.zeiss.com
Other		
35 mm glass bottom dish	MatTek	Cat# P35G-1.5-14-C
384 well white Optiplate	Perkin Elmer	Cat# 6007290
DAM negative *E. coli*	Agilent Technologies	Cat# 200247
DH5 alpha *E. coli*	Invitrogen	Cat# 18265017
Mr. Frosty Freezing Container	ThermoFisher Scientific	Cat# 5100
Nunc Lab-Tek 8-well chambered coverslips	ThermoFisher Scientific	Cat# 1554411
PD10 column	Cytiva	Cat# 17085101
Poroshell 300SB-C3 column	Agilent	Cat# PN 821075-924
T4 Ligase	New England BioLabs	Cat# M0202S

Top 10F *E. coli*	Invitrogen	Cat# C303003
White 96-well plates	Greiner Bio-One	Cat# 655089
Xba1 restriction enzyme	Promega Corporation	Cat# R6181
Xho1 restriction enzyme	Promega Corporation	Cat# R6161

2.2 Constituents of buffered solutions

2.2.1 Hank's Buffered Salt Solution (HBSS)

The constituents below were combined to create a 1 L 10x concentrated HBSS stock solution that was adjusted to pH 7.45. This was then autoclaved and had 1.8 g of D-Glucose added. This 10x stock was aliquoted and frozen. Working stocks were then created by thawing these aliquots and adding MilliQ H_2O.

Constituent	**Mass (g)**	**Final Concentration (mM)**
Sodium Pyruvate	0.22	2
NaCl	8.47	145
KCl	0.37	5
$MgSO_4$	0.246	1
HEPES	2.38	10
$CaCl_2$	0.191	1.3
$NaHCO_3$	0.126	1.5

2.2.2 Tris Acetate EDTA (TAE)

Constituent	**Mass (g) / Volume (mL)**	**Final Concentration (mM)**
Tris	242 g	2000
0.5 M EDTA	100 mL	50
Acetic Acid	57.1 mL	1000

2.3 Molecular Biology Techniques

2.3.1 Transformation of *Escherichia coli.*

DH5alpha (or Top10F for site directed mutagenesis) *Escherichia coli* (*E. coli)* were transformed by a heat shock protocol in which a 50 µL bacterial aliquot

was incubated on ice with 20-500 ng of plasmid for 30 minutes followed by a 30 s heat shock at 42 °C and a 5-minute recovery step on ice. Following this 250 µL of LB broth was added to the cells and the sample incubated at 330 rpm and 37 °C for 1 hour. 100 µL of the sample was then spread of a petri dish containing 15 mL of set Lysogeny broth (LB) agar with 50 µg/mL of ampicillin.

2.3.2 Preparation and quantification of plasmid DNA stocks

In order to prepare working stocks of plasmid expression constructs, single colonies of transformed *E. coli* were selected and grown overnight at 37 °C and 330 rpm in either 5 mL or 200 mL of LB broth with 50 µg/mL of ampicillin. DNA was then extracted by alkaline lysis using either a 'Maxiprep' or 'Miniprep' kit depending on the volume of DNA needed. These purifications were carried out according to the manufacturer's (Promega) instructions, the steps used, and their purposes are outlined in Table 2-1.

Description of Step	**Purpose of Step**	**Primary Buffer constituents**
Cultures were centrifuged	To pellet the bacterial cells (which contain the plasmid in their periplasm) and remove growth buffer	N/A
Cells were suspended in 'Cell Re-suspension Buffer'	To resuspend cells to allow homogenous addition of lysis and neutralisation reagents. EDTA prevents the function of DNAases by chelating essential cofactors such as Mg2+, EDTA also aids the destabilisation of the membrane that occurs in the next step. RNase enzyme degrades RNA. Tris buffers the solution to prevent changes in pH. Glycerol prevents changes in osmotic pressure leading to cell lysis.	EDTA, RNase A, Tris,
Cells were treated with 'Lysis Buffer'	To lyse cells to release DNA and denature proteins. SDS lyses cells through its action as a detergent and	NaOH,

	through denaturing proteins in the cell membrane. NaOH lowers the pH, disrupting hydrogen bonds between DNA bases.	Sodium dodecyl sulfate (SDS)
Lysed cells were treated with 'Neutralisation Buffer'	To neutralise the alkaline lysis buffer allowing the hydrogen bonds within plasmid DNA to reform the double stranded DNA. SDS in complex with genomic DNA and linearised proteins reacts with potassium ions to form an insoluble KDS salt, causing the complex to precipitate.	Potassium acetate, Guanidium chloride,
Samples were centrifuged	To separate the cell debris including the genomic DNA from the plasmid DNA in solution.	N/A
The supernatant was run through a silica membrane column	To separate the plasmid DNA from the solution by precipitation on the silica filter (this process is aided by the Guanidium chloride, a chaotropic salt added in the neutralisation buffer, which prevents H_2O from interacting with the DNA).	N/A
'Endotoxin removal wash' was run through the column	To remove endotoxins and salts from the plasmid DNA that could impact subsequent experiments.	Isopropanol, Guanidine HCl,
'Column wash' was run through the column	To remove chaotropic salts from the plasmid DNA	Ethanol
DNA was eluted by addition of H_2O	To dissolve DNA allowing separation from the filter	Distilled H_2O

Table 2-1: General description of the key steps and reagents used in alkaline lysis purification of plasmid DNA from cultures of transformed bacteria (Koontz, 2013)**.**

2.3.3 Generation of new plasmid constructs

2.3.3.1 Restriction cloning

Restriction cloning of new constructs was undertaken when both plasmids containing the gene of interest and vectors with complimentary restriction sites

were available. Dual restriction digests were performed in which 2.5 µg of plasmid was restricted by 2.5 µL of each enzyme in a buffer in which both enzymes had activity, in a volume of 50 µL at 37 °C for 1-2 hours (depending on the activities of the enzymes in the buffer used as described by the manufacturer).

The required DNA fragments were then separated by gel electrophoresis. Briefly restriction reactions were combined with DNA loading dye and added to a gel consisting of 10 mg/mL agarose with 0.2 µg/mL Ethidium Bromide in TAE buffer which was placed in a gel tank and submerging in TAE buffer. The gel was then run at 90 V for 30-45 minutes depending on the size of the fragment. The required DNA fragments were then excised under UV light using a scalpel. Control digests and a DNA ladder were used to confirm that the required fragment was of the correct mass. The excised DNA was purified from the gel using an SV Wizard Gel and PCR clean up kit (Promega) according to the manufacturer's instructions. Briefly these included melting the gel in a 'membrane binding' buffer which contained guanidine isothiocyanate and potassium acetate, binding the DNA to a column and then washing the DNA with a 'membrane wash' buffer which contained potassium acetate, ethanol and EDTA, before eluting the resulting DNA in H_2O.

The concentration and purity of both vector and insert fragments were then quantified using a spectrophotometer (Novix), which measured the absorbance at 260 nm to determine DNA concentration and absorbance at 230 and 280 nm to quantify contamination from salts or ethanol and protein respectively. Ligation reactions were then set up containing 100 ng of DNA at molar ratios of 3:1 5:1 or 7:1 insert to vector ratios, with 1 µL of T4 Ligase and 1 x T4 ligase buffer (which contains $MgCl_2$ and ATP) with a final volume of 20 µL. The reactions were incubated at 16 °C for 16 hours before 10 µL was transformed into DH5alpha *E. coli* as described in 2.3.1.

2.3.3.2 Site directed mutagenesis or deletion

Single nucleotide polymorphisms (SNPs) and deletions were introduced using a Phusion Site-Directed Mutagenesis Kit (ThermoFisher) according to the manufacturer's instructions. Briefly, 5' phosphorylated primers complementary

to the site of interest that incorporated a codon for an alternative amino acid (for SNPs) or had a distance between their complementary sequences (for deletions) were designed and externally synthesised (Merck). A Polymerase Chain Reaction (PCR) was then carried out using the kit's Phusion enzyme, buffer, deoxynucleotide triphosphates (dNTP)s, 5ng of template plasmid, forward primers and reverse primers made up to 20 μL in H_2O. The protocol was then followed according to the manufacturer's instructions and is summarised in Table 2-2.

Step	**Purpose**
PCR reaction heated to 98 °C for 30s	Phusion is a hot start enzyme. This means that the enzyme must first be heated to 98 °C to activate the enzyme by reversibly decoupling an inhibitory ligand that prevents endonuclease activity occurring prior to the start of the PCR.
PCR reaction cycled through 30 cycles of 98 °C for 10s, 55-70 °C (optimised for each primer) for 30s and 72 °C for 225s.	98 °C breaks hydrogen bonds within the DNA strands. The temperature is dropped to a 2-5 °C below the primer melting temperature to allow primers to anneal. Incubation at 72 °C allows elongation of the PCR product.
PCR reaction incubated for 10 minutes at 72 °C.	This step allows incomplete PCR products to be fully elongated.
The PCR products were run on a gel (as described in section 2.3.3.1) with restricted plasmids as controls.	To confirm the successful extension and size of the product.
Samples were digested with the enzyme Dpn1 for 15 minutes at 37 °C.	This enzyme digests methylated (template) DNA that has been grown in *E. coli*.
Samples were ligated by incubation with T4 DNA ligase for 10 minutes at 25 °C.	This joined the blunt ends at the end of the DNA strands. Phosphorylated primers were used to increase the efficiency of this step.

Table 2-2: Summary of site directed mutagenesis procedure.

SnapGene viewer was used to design primers and to predict annealing temperatures. Variations in the annealing temperature, dimethyl sulfoxide (DMSO) concentration (0, 2.5 or 5%) and primer concentration (200 or 500 nM) were used to optimise successful PCRs. Success of PCRs was predicted by measuring the mass of product through gel electrophoresis, after Dpn1 digest and ligation these were transformed in TOP10F *E. coli* (as described in 2.3.1).

2.3.3.3 Characterisation of novel plasmid constructs

The successful generation of plasmid expression constructs was confirmed by Sanger sequencing at the University of Nottingham's Deep Seq facility which utilises a 3130xl ABI PRISM Genetic Analyzer (Life Technologies). Sanger sequencing works by elongating a copy of the template (through PCR with a complementary primer) in the presence of fluorescently coded chain terminating nucleotides (ddNTP). The sequence can then be read by quantifying the sizes and emission of each transcript (França et al., 2002).

Plasmid sequences were then aligned with the expected sequence using www.benchling.com. For site directed mutagenesis or deletion experiments the whole gene was sequenced utilising several primers. In these experiments the successful elongation of the PCR product was confirmed initially by comparing the size of the PCR product with a control vector and then by assessing the expression and function of the construct in a mammalian expression line. In loss of function mutants such as C115Y, the gene was subsequently restricted and removed from the PCR generated plasmid vector and cloned back into the original template vector, to confirm that loss of function was due to the mutation and not the errors in the vector.

2.4 Mammalian cell culture

Human Embryonic Kidney 293T (HEK293T) cells were cultured in Dulbecco's Modified Eagle Medium (DMEM) with 10% Fetal Bovine Serum (FBS) in tissue culture flasks at 37.5 °C and 5% CO_2. Frozen stocks were made by placing cells in FBS with 10% DMSO and lowering the temperature at 1 ºC per minute using a Mr. Frosty^{TM} freezing container containing isopropanol. Cell lines were replaced with these stocks periodically to prevent passage number rising too high. Incubations carried out in DMEM based media were undertaken at 37.5

°C and 5% CO_2 and incubations in HBSS were carried out 37.5 °C without additional CO_2. Mycoplasma testing of cell line stocks was carried out using a mycoStrip TM 100 kit (InvivoGen) which confirmed that the cells were uninfected.

2.5 Transfections

2.5.1 Transient transfections

Unless otherwise stated, HEK293T cells were transfected either by batch transfection (6-well) or single well (96-well) protocols. Batch transfections were used in experiments in which there were a low number of transfection conditions. The advantage of this methodology is that transfected cells are mixed before being added to assay microplates and therefore the expression is more uniform than in 96-well based transfections. Single well transfections were used in experiments with a high number of transfection conditions in which it would be impractical and wasteful to pursue the batch transfection methodology. In addition, the single well methodology reduces experimental artefacts resulting from transfection variation between conditions as each replicate is independently transfected. The transfection methodology was conserved in all experiments where direct comparisons are made between conditions.

2.5.1.1 Batch transfection (6-well)

Cells were seeded into 6-well clear tissue culture plates at $2.5x10^5$ cells per mL followed by an incubation for 4-6 hours. The cells were then transfected through the addition of 100 µL of a transfection mixture containing a 3:1 ratio of FuGENE HD (Promega) to cDNA construct in OptiMEM, which had been incubated for 10-15 minutes. After 24 hours the cells were trypsinised resuspended and centrifuged before being adjusted to the correct concentration and seeded according to the specifications of the experiment.

2.5.1.2 Single well transfections (96-well)

In NanoBRET experiments with a range of transfection conditions HEK293T cells were adjusted to 1.5×10^5 cells/mL and dispensed at 100 µL into a poly-d-lysine (PDL) coated 96-well white microplate. Cells were then incubated for 24 hours before being transfected with 100 ng/well cDNA and 0.3 µL FuGENE HD in 5 µL of OptiMEM per well that had been incubated for 10-15 minutes prior

to addition. Cells were then incubated overnight before the day of the experiment at which point media would be removed and replaced according to the specification of the experiment.

2.6 Imaging

2.6.1 Luminescence imaging

HEK293T cells were seeded at a density of 1. 5x 10^5 cells/mL into PDL coated 35 mm glass bottom plates, in 2 mL of DMEM with 10% FBS and transfected as described in the batch transient transfection section. After transfection the dishes were incubated for 2 days before media was replaced with 3 mL of 37 °C HBSS with 5.13 µM Furimizine. The dishes were then imaged on an LV200 luminescence microscope (Olympus) equipped with a C9100-23B IMAGE EMX2 camera (Hamamatsu) in both brightfield and luminescence settings using a 60x/1.42NA oil immersion objective lens and 0.5x tube lens. Exposure was adjusted to the level of expression (2-15 s). Scale bars were added to luminescence imaging data using Fiji version 1.53 (NIH).

2.7 Storage and handling of ligands and proteins

Lyophilised peptides and proteins were made up in PBS with 1 mg/mL BSA, except for P630 and P630-TMR which were reconstituted in PBS with 10% DMSO to a concentration of 1 mM. Proteins and peptides were stored at -80 °C unless they were from a commercial assay that recommended storage at -20 °C (e.g. LgBit protein). During the preparation of assays, proteins and peptides were thawed and stored on ice.

2.8 STAT3 phosphorylation AlphaLISA experiments

Transfected HEK293T cells were plated into a PDL coated 96 well tissue culture microplate in DMEM with 10% FBS and incubated overnight. The following day media was replaced with serum free DMEM and the cells incubated for 3 hours. Media was then replaced with HBSS containing 1 mg/mL BSA with or without IL-23 and the cells incubated for 30 minutes. An AlphaLISA SureFire Ultra assay was then used to measure STAT3 phosphorylation at residue Tyr705. Assays were performed according to the manufacturer's instructions and the principles are highlighted in Figure 2-1. Briefly, cells were lysed by addition a 1x lysis buffer that released intracellular STAT3 by disruption of the

cell membrane. The resulting lysate was then incubated with both acceptor and donor beads which were conjugated to antibodies for STAT3 and phosphorylated (p)STAT3 (Y705). The level of pSTAT3 was then quantified with the use of a PheraStar FS plate reader equipped with an AlphaLISA 680 615 optic module. This plate reader was equipped with an excitation laser at 680 nm that was used to excite the donor beads causing the emission of singlet oxygen. When the acceptor beads were exposed to singlet oxygen, they were induced to produce a fluorescent signal with peak emission at 615 nm that was recorded by the plate reader.

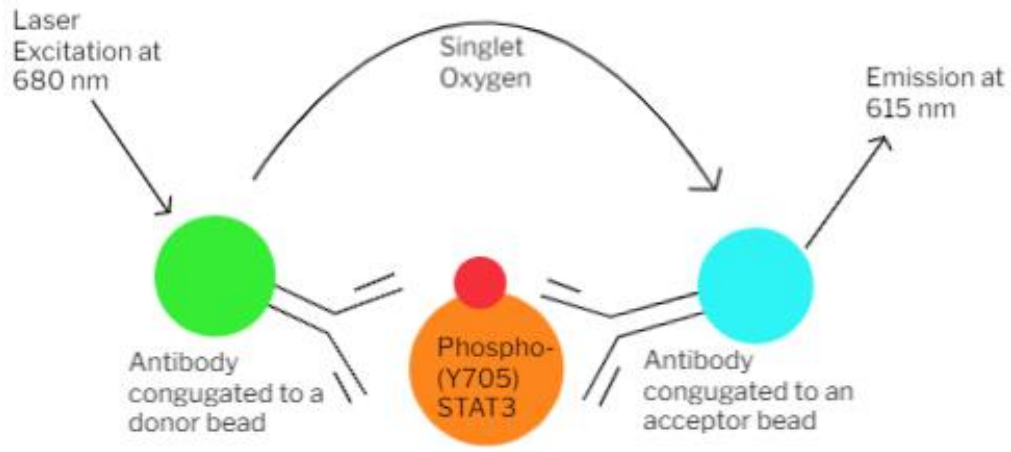

Figure 2-1: The general principles of the pSTAT3 alphaLISA assay. A schematic demonstrating how excitation of an antibody conjugated donor bead can lead to emission from an antibody conjugated acceptor bead via the production of singlet oxygen.

2.9 NanoBRET experiments

NanoBRET is a proximity-based technique that allows the measurement of cellular molecular interactions through the energy transfer from the luciferase NanoLuc to fluorescent molecules. NanoLuc oxidises the substrate furimizine to produce light with the strongest emission at 460 nm. This light can then be used to excite a fluorescent molecule, that has an overlapping excitation wavelength with the emission of NanoLuc and a longer wavelength emission than NanoLuc. The interaction can then be quantified by the production of the fluorescent signal, with the strength of the signal being dependent on both proximity (closer contact allows more efficient energy transfer) and orientation

(due to the alignment of dipoles within the donor and acceptor molecules). In NanoBRET experiments the donor is generally a protein that is expressed with the NanoLuc tag at either the *C* or *N* terminus, the acceptor molecule is either a protein tagged with a fluorescent tag or a synthetic ligand chemically tagged with a fluorescent moiety (Machleidt et al., 2015).

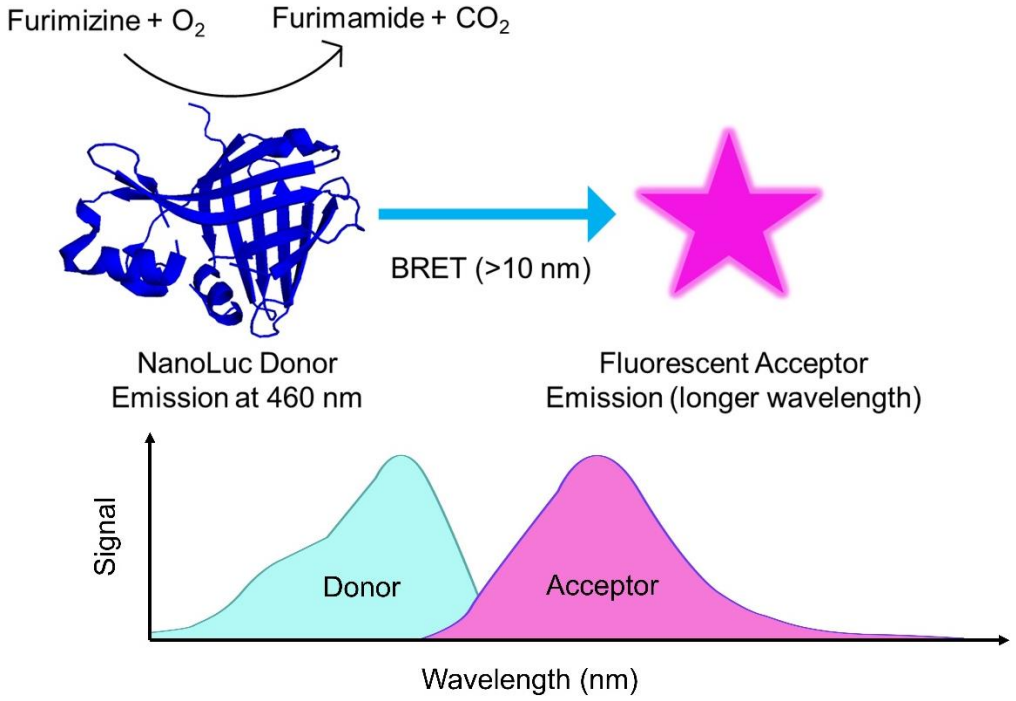

Figure 2-2: The principles of NanoBRET. (Top) A schematic demonstrating the principles of NanoBRET assays. NanoLuc crystal structure is taken from PDB: 5IBO. (Bottom) A cartoon representation of the donor and acceptor wavelengths used to calculate the BRET ratio (acceptor divided by donor signal).

2.9.1 Fluorescent ligand binding and competition experiments

In ligand binding experiments, white 96-well microplates containing transfected HEK293T cells had media removed and replaced with 50 µL per well of increasing concentrations of IL23-TMR or P630-TMR in HBSS with 1 mg/mL BSA either with or without an excess of unlabelled IL-23 (with this varied according to the affinity of IL23-TMR to the constructs expressed, with the concentration used noted in the figure legend) or P630 (10 µM) respectively to quantify non-specific binding. Experiments using P630-TMR were normalised to 0.1% DMSO. In competition binding assays media was replaced with 50 µL per well of increasing concentrations of the test ligand in HBSS with 1 mg/mL BSA and a constant concentration of fluorescent ligand. In both assay formats

plates were incubated for 1-hour before the addition of 5 µL of 77 µM Furimizine per well, followed by a further 4-minute incubation and reading of the microplate on a Pherastar FS plate reader (BMG Labtech) using a 450 nm (30 nm bandpass) and >550 nm filter with gains of 2000 and 3000 respectively.

2.9.2 Kinetic association and dissociation experiments

Batch transfected HEK293T cells had media removed and replaced with 25 µL HBSS with 1 mg/mL BSA containing 15.4 µM furimizine. The cells were incubated for 5 minutes at 37 °C before 25 µL HBSS with 1 mg/mL BSA was added containing IL23-TMR with or without an excess of IL-23 or media with or without 300 pM IL-23 for P630-TMR experiments. The microplate was then immediately transferred to a Pherastar FS plate reader and read repeatedly at 1-minute intervals, for 40 minutes using a 450 nm (30 nm bandpass) and >550 nm filters. The temperature of the plate was maintained at 37°C during the experiment using heating plates within the reader's incubation chamber. Following this the microplate was removed from the reader, had buffer removed and replaced with 50 µL HBSS with 1 mg/mL BSA containing 30 nM IL-23. In P630-TMR experiments 50 µL HBSS with 1 mg/mL BSA containing 75 nM P630-TMR was added at this stage, with or without 750 nM P630, additional iterations of this step were carried out at 40-minute intervals in which media was replaced with an excess of unlabelled competitor or 300 pM IL-23 with 75 nM P630-TMR.

2.10 Data analysis

2.10.1 Ligand binding and transduction experiments

Pherastar plate reader data was analysed using MARS data analysis software (BMG Labtech) including the generation of a BRET ratio, by dividing the acceptor signal at 535 ± 30, <550 or <610 nm by the donor signal at 475 ± 30, 450 ± 30 or 460 ± 80 nm respectively, depending on the filter used.

Data were stored and analysed in Excel (Microsoft). Creation of graphs, fitting of data and statistical tests were carried out using Prism software (GraphPad).

The fitting models used by prism and their purposes in this project are defined below. Numbered equations will be referred to in the legends of figures in which they have been used to fit data.

Affinity measures for fluorescent ligands measured in the presence and absence of an excess of unlabelled inhibitor were determined by fitting specific and non-specific binding simultaneously to prism's 'One site – Total and non-specific binding' model which uses equation 1 with shared parameters for A and C.

Equation 1:

$$BRET\ ratio = \frac{B_{max}.[L]}{([L] + K_d)} + ((A.[B]) + C)$$

Where B_{max} is the maximal specific binding, [L] is the concentration of fluorescent ligand, K_d is the dissociation constant, A is the slope of the non-specific binding component and C is the Y intercept.

The concentration that gave 50% total binding for normalised binding data was generated by fitting data to Prism's 'One site – specific binding' model which used equation 2:

Equation 2:

$$BRET\ ratio = \frac{B_{max}.[L]}{([L] + C)}$$

Where B_{max} is the maximal specific signal of the curve, [L] is the concentration of ligand and C is the concentration of ligand that causes 50% of the specific signal.

In experiments in which it was thought that there may be two binding sites the data was fit to Prism's 'Two sites – specific binding' model which was fitted to a two-site binding equation with equation 3:

Equation 3:

$$Y = \frac{B_{max}1.[L]}{([L]+K_d1)} + \frac{B_{max}2.[L]}{([L]+K_d2)}$$

Where $B_{max}1$, $B_{max}2$ are maximal binding levels are the initial and secondary plateaus and K_d1 and K_d2 are K_d values of the two components.

Competition experiments in which IC_{50} was determined for inhibitors were analysed by fitting the data to Prism's '[Inhibitor vs response – variable slope] (four parameters)' model which used equation 4:

Equation 4:

$$Y = B_{min} + \frac{B_{max} - B_{min}}{1 + \left(\frac{IC_{50}}{[I]}\right)^{C}}$$

Where B_{max} is the maximal signal, B_{min} is the minimum signal, IC_{50} is the compound's 50% inhibitory concentration, [I] is the concentration of competing drug and C is the Hill slope of the curve. When the data was normalised to % inhibition using a high and a low control B_{max} and B_{min} were constrained to 100 and 0 respectively.

Experiments which measured the EC_{50} of signalling induction were analysed by fitting data to Prism's '[Agonist vs response – variable slope] (four parameters)' model which used equation 5:

Equation 5:

$$Y = B_{min} + \frac{[A]^{C}(B_{max} - B_{min})}{[A]^{C} + EC_{50}{}^{C}}$$

Where B_{max} is the maximal signal, B_{min} is the minimum signal, EC_{50} is the log of the compound's 50% activating concentration, [A] is the concentration of agonist and C is the Hill slope of the curve.

If antagonists were determined to act in a competitive manner, K_i values were then generated from IC_{50} measures by using the Cheng-Prusoff equation:

$$K_i = \frac{IC_{50}}{1 + \frac{[L]}{K_d}}$$

Where K_d is the dissociation constant calculated for the fluorescent ligand and [L] is the concentration of fluorescent ligand used.

Linear regression analysis was also performed on the relationship between IC_{50} and fluorescent ligand concentration using a variant of the Cheng-Prusoff equation:

$$IC_{50} = \left([L]\frac{K_i}{K_d}\right) + K_i$$

In which the y intercept gave K_i and the gradient of the slope gave K_i / K_d.

For kinetic experiments in which IL23-TMR associated to the receptor and then was dissociated through replacement of the media with an excess of unlabelled ligand the Prism model 'Association then dissociation' was utilised which uses the equations below:

Equation 6:

$$k_{obs} = ([L].k_{on}) + k_{off}$$

$$K_d = \frac{k_{off}}{k_{on}}$$

$$Y = Bmax(1 - \log(k_{obs}.T))$$

Where [L] is the concentration of IL23-TMR used, B_{max} is the maximal signal and T is time.

To determine the k_{off} of fluoroligands from their dissociation in an excess of an unlabelled competitor the data with fit to the Prism model 'One phase decay' which used equation 7:

Equation 7:

$$BRET\ signal = (Y0 - B_{min}).\log\left(-k_{off}.T\right) + B_{min}$$

Where Y0 is the BRET value at time 0, B_{min} is the plateau of the dissociation, and T is time.

When the dissociation could potentially be two phase the data was fit with Prism's 'two phase decay' model which used equation 8:

Equation 8:

$$A = (Y0 - B_{min}).\%Fast$$

$$B = (Y0 - B_{min}).(100 - \%Fast)$$

$$Y = B_{min} + A.\log(-KFast.X) + B.\log(-KSlow.X)$$

Where %Fast is the fraction of the signal decay due to the fast dissociation step, B_{min} is the plateau of the dissociation, KFast is the rate of the fast dissociation step and KSlow is the rate of the slow dissociation step.

To determine a measure of k_{on} from a single concentration of associating fluoroligand. The k_{obs} of one concentration of associating ligand was first measured using Prism's 'One-phase association' model which utilises the equation 9:

Equation 9:

$$BRET\ signal = Y0 + (B_{max} - Y0)\ (1 - \log(-k_{obs}.T)$$

Where Y0 is the BRET signal at time 0, B_{max} is the maximal BRET signal and T is time.

The equations below were used to convert the k_{obs} and pre-determined value for IL23-TMR K_D to k_{on}:

$$k_{off} = k_{on}.K_D \text{ and } k_{obs} = [L].k_{on} + k_{off}$$

These equations were re-arranged to form Equation 10 as shown below:

(1)

$$k_{obs} = [L].k_{on} + k_{on}.K_D$$

(2)

$$k_{obs} = k_{on}([L] + K_D)$$

(3) Equation 10:

$$k_{on} = \frac{k_{obs}}{[L] + K_D}$$

Where k_{obs} is the rate of association, [L] is the concentration of ligand used and K_D is the pre-determined dissociation constant of IL23-TMR.

To determine a measure of k_{on} or k_{off} from the pre-determined value for IL23-TMR's K_d and the k_{off} or k_{on} measured using equation 7 or 10 respectively the below equation was used:

$$K_D = \frac{k_{off}}{k_{on}}$$

2.10.2 Statistical tests

All statistical tests were carried out using Graphpad prism. Normalcy of data was first confirmed using a Shapiro-Wilk test (all statistically analysed data was found to be parametric).

When two sets of data were tested for statistically significant differences an unpaired t test was used, unless the replicate data were generated from equivalent cells transfected with the same transfection mix on the same day, in which case a paired t test was used.

The significance of differences between multiple conditions were tested using a one-way ANOVA. Analysis of individual differences between multiple conditions were conducted by analysing the ANOVA results with Tukey-Kramer multiple comparison test.

Comparison of fits were made by analysis of the residual sum of squares using the partial F-test as described previously (Cooper et al., 2019).

Chapter 3. Measuring the affinity of IL-23 to full-length receptor subunits and receptor complexes in living cells

3.1 Introduction

The discovery, cloning and engineering of luciferase reporters has been highly enabling for biological research. The first luciferases to be cloned for use in biotechnology were extracted from bacteria, the sea pansy (*Renilla reniformis*) and the firefly (*Photinus pyralis*) (Roda et al., 2004). In 2012 the biotechnology company Promega reported the development of a novel coelenterazine derived substrate named furimazine and a novel luciferase named NanoLuc developed from the deep-sea shrimp (*Oplophorus gracilirostris*) that was smaller (19 kDa vs Renilla luciferase 36 kDa) and brighter than previously available luciferases (Hall et al., 2012). In addition, the parent enzyme was secreted to confuse predators meaning that the modified enzyme was easily exported to the cell surface in recombinant cell systems enabling the *N*-terminal labelling of receptors (Hall et al., 2012).

This new luciferase substrate combination was quickly adapted for use in BRET assays, with this technique termed NanoBRET (Dale et al., 2019). NanoBRET has been used in ligand binding assays with fluorescently labelled probes for both cell surface (Stoddart et al., 2018) and intracellular targets (Robers et al., 2015) and in protein-protein interaction assays (Machleidt et al., 2015). The acceptor fluorophore in fully recombinant protein-protein interaction assays can either be a fluorescent protein or a bio-engineered enzyme capable of binding a specific substrate (Dale et al., 2019). Examples of this class of proteins are SNAP-Tag and HaloTag. SNAP-Tag is an engineered O6-alkylguanine-DNA alkyltransferase enzyme that can irreversibly bind a O6-benzylguanine substrate (Keppler et al., 2003). HaloTag is engineered from an haloalkane dehalogenase enzyme and can covalently bind a chloroalkane substrate (Los et al., 2008). HaloTag has a quicker labelling rate than SNAP-Tag, however it is the larger of the two proteins (33 vs 19.4 kDa) (Hoelzel and Zhang, 2020). HaloTag and SNAP-Tag ligands can be conjugated to a variety of labels including fluorescent dyes which can then be used to measure their interaction with Luciferase labelled

proteins. Labelling proteins with HaloTag or SNAPTag rather than traditional fluorescent proteins is advantageous due to the flexibility of dyes that can then be used including membrane permeable and impermeable varieties (Dale et al., 2019). Using intrinsically fluorescent proteins however, means that no substrate needs to be purchased and the cells need not be subjected to labelling protocols which can lead to loss of cells during wash steps.

The IL-23 receptor is an important drug target for auto-inflammatory diseases however the affinity of the receptor or receptor components for their ligand has not yet been reported in live cells. In addition, there have been conflicting reports as to whether the IL-23 receptor is activated by ligand induced dimerization or conformational change (Bloch et al., 2018; Sivanesan et al., 2016). In this chapter NanoBRET will be used to measure the affinity of IL-23 for its full-length receptor components expressed on living cells and to measure the effect of IL-23 on the proximity of the receptor components.

The IL-23 receptor is a heteromer made up of two single TMD containing proteins. Observations at other closely related cytokine receptors indicate that the anchoring of the TMD in the membrane is likely to be important for the formation and activation of the ligand-receptor complex (Maruyama, 2015; Waters and Brooks, 2015; Westerfield and Barrera, 2020). By utilising an immortalised cell line expressing tagged receptor components, the receptor can be studied in the presence of the membrane and associated signal transducing proteins. Such a cell line should be easily cultured and transfected and not endogenously express IL-23 receptor components. Human Embryonic Kidney 293T (HEK293T) are such a cell line and provide a well validated host system. The expression of project relevant genes in HEK293T cells is demonstrated in Figure 3-1, this transcriptomic analysis indicates that neither IL-23 or its receptor are expressed in this cell line, however RNA for key transducers, including STAT3, TYK2 and JAK2 (albeit at a low level) is present (Uhlen et al., 2019).

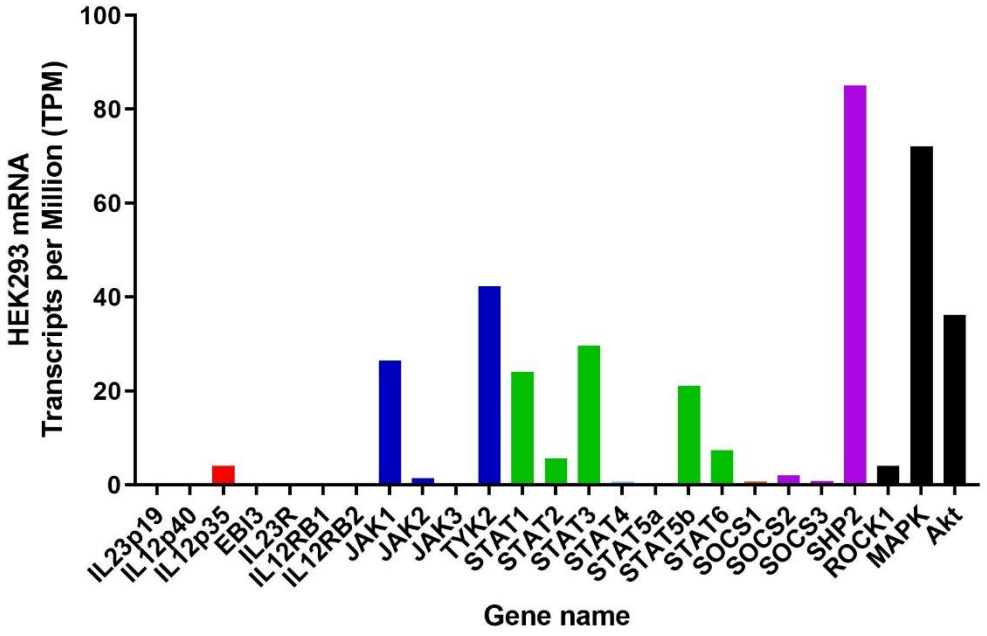

Figure 3-1: Expression of relevant genes in HEK293T cells. HEK293T transcriptomic sequencing performed by the human protein atlas (Uhlen et al., 2019), values taken from www.proteinatlas.org. IL-12 family cytokine genes are coloured red, JAK proteins in blue, STAT proteins in green, negative regulators in purple and additional signal transducers in black.

There are several methodologies through which recombinant tagged genes can be introduced into model cell lines, these include plasmid transfection, viral transduction and CRISPR/Cas9 mediated knock in. IL-23 receptor expression is restricted to a small number of specialist cell types (as discussed in section 1.6). As CRISPR/Cas 9 knock in requires that the genomic product is expressed (Horioka et al., 2020), the restricted expression of the receptor would limit the methodology to cell types requiring specialist culturing conditions, subject to a limited number of passages. In addition, the knock in of large tags such as NL, SNAP or HT may be problematic using this methodology (He et al., 2016).

Plasmid or viral vectors would both be appropriate for this work, however the production of viral vectors is a more complex and time-consuming process, due to the number of planned expression vectors and the ease of HEK293T plasmid transfection, this approach will be used.

Purified IL-23 was donated to this project by GSK, this reagent was originally expressed by suspension HEK293 cells and purified using a his-tag conjugated to IL23p19. This approach would prevent monomeric IL12p40 being purified

which is known to be expressed in isolation. The reagent was purified in 2008 and has since been stored at -80 °C, due to the time elapsed since this original purification the reagent must be characterised before use in the project.

When labelling purified proteins for use in BRET or FRET assays there are two general approaches, namely site specific or non-specific labelling. There are several site-specific labelling approaches, most involving the creation of an expression vector containing a fusion of the protein with a reactive group (Kilpatrick et al., 2017; Thimaradka et al., 2021). This vector is then expressed and purified before being labelled by the addition of a dye specific to the reactive group. In non-specific labelling techniques, dyes are used which react to residues found naturally within the protein, typically lysine or cysteine residues (Kalkhof and Sinz, 2008; Kim et al., 2008). Site specific labelling has the advantage of creating a more consistent reagent with a known labelling site, allowing the intentional positioning of the tag away from binding interfaces and in specific orientations in relation to the donor. Non-specific labelling is a quicker and easier process and does not require protein purification if a stock of pre-existing protein is available.

3.2 Aims

The aims of this chapter were to generate and characterise the reagents needed for the measurement of the interaction of IL-23 with the IL-23 receptor in live cells. As this was the first time that the NanoBRET methodology was used at the IL-23 receptor, a new experimental system with new reagents needed to be generated. It was also essential that these new reagents were validated and characterised to allow confidence in further results, especially as there are no reports of the use of the methodology at other related cytokine receptors. Specifically, this chapter aimed to validate the IL-23 protein donated by GSK using LC-MS, label this IL-23 protein with fluorophore and characterise the fluorescent cytokine using FCS and LC-MS. In addition, this chapter aimed to generate new cDNA constructs needed for the project and to validate these with DNA sequencing. The expression and localisation of *N*-terminally tagged expression constructs was then validated through imaging and comparison to standard curves. The ability of these constructs to transduce following IL-23 binding was also measured using phospho-STAT3 signalling assays.

Using these validated reagents, the chapter aimed to create a NanoBRET ligand binding assay to measure the affinity of IL-23 for its receptor and individual receptor components, expressed in the membrane of living cells. This assay will then be used to characterise the kinetics of the ligand binding interaction and the affinity of the unlabelled ligand. NanoBRET will also be used to create an intra-receptor energy transfer assay to monitor the effect of ligand engagement on the relative position of the *N*-terminal domains of the IL-23 receptor components.

3.3 Methods

3.3.1 Generation of mammalian expression constructs

NanoLuc constructs were custom made at Genscript by synthesis of either IL23R or IL12Rβ1 without their endogenous signal peptides and the subsequent sub-cloning of these, into a pNLF vector (Promega) using Xho1 and Xba1, which previously had an IL-6 secretion signal added to the *N*-terminus of NanoLuc via mutagenesis. The resulting open reading frames encoded an *N*-terminal IL-6 secretion signal followed by NanoLuc then a linker with the amino acid sequence GSR between the NanoLuc fusions and the *N*-terminus of either IL23R or IL12Rβ1. HaloTag constructs were custom synthesised at Genscript by synthesis of cDNAs encoding an *N*-terminal IL-6 secretion signal followed by HaloTag which was fused to either IL23R or IL12Rβ1 by a linker with the sequence EPTTEDLWFQSDN that contained a Tobacco Etch Virus (TEV) protease site. These cDNAs were then sub cloned into pNLF plasmids via Nhe1 and Not1 restriction sites.

SNAP-IL12Rβ1 was cloned into the Xho1 and Xba1 sites of an *N*-terminal SNAP-Tag with an *N*-terminal murine 5-HT3A receptor secretion signal (Gherbi et al., 2015) generated by restriction cloning IL12Rβ1 from an *N*-terminal NanoLuc tagged plasmid (Genscript) this yielded a 20 amino acid linker with the sequence STSPVWWNSADIQHSGGRSR between the SNAP-Tag and IL12Rβ1. The resulting plasmid was sequenced using primers specific for the SNAP plasmid (BGH Reverse) and the insertion of IL12Rβ1 was confirmed through alignment with the parent plasmid.

3.3.2 Transfections

Unless otherwise stated batch transfections were used in which the total DNA concentration was 2 µg per well consisting of 1 µg of one receptor construct and 1 µg of another receptor construct or pc3.1 zeocin plasmid for normalisation. For NL-IL12Rβ1 and IL23R 1:10 DNA ratio experiments, 2.2 µg total DNA per well was used with 2 µg of IL23R construct. Following batch transfections cells were incubated overnight before being re-seeded into assay plates in the afternoon of the following day.

Single well transfections were used for assays in which the concentration of SNAP-IL12Rβ1 DNA was titrated with NL-IL23R (i.e. Figure 3-7 and Figure 3-18).

In fluorescence imaging experiments 2 x 10^5 HEK293T cells were seeded in 300 µL of media into 8-well glass plates coated with PDL and incubated overnight. The following day each well was transfected with a 10 µL transfection mix made up of 200 ng cDNA consisting of 100 ng of each receptor construct and 0.6 µL of FuGENE HD in OptiMEM. 100 ng of pc3.1 zeocin empty vector was included if only one receptor monomer was to be expressed.

3.3.3 Non-specific labelling of purified IL-23

HEK293T purified recombinant IL-23 protein (donated by GSK) was non-specifically labelled via a 2-hour incubation of 100 µg of protein with 21.4 µM of NHS ester coupled TAMRA dye (a 1:3 molar ratio) in 200 µL of Phosphate Buffered Saline (PBS; pH 7.4). Ten of these reactions were then run through PD10 desalting columns (Cytiva) and combined to form the sample used in this study. The concentration of IL-23 in the labelled sample was determined by measuring the UV absorbance at 280 nm with a Nanodrop spectrophotometer (ThermoFisher Scientific) and comparing these to the equivalent value for the unlabelled sample.

3.3.4 Liquid Chromatography coupled Mass Spectrometry

The intact mass of unlabelled and labelled IL-23 was further characterised by liquid chromatography coupled mass spectrometry (LC-MS). Samples were analysed on Reversed-Phase (RP) chromatography (BioResolve RP column (2.1

x 50 mm, 2.7 µM, PN: on BioAccord RDa system (Waters). Samples were desalted by washing with 0.1% formic acid in 25% acetonitrile and eluted using linear gradient with 0.1% formic acid up to 80% acetonitrile at a flow rate of 0.5 mL/min. The eluate was ionised by electrospray ionisation (ESI). The column temperature was maintained at 80 ºC, RDa acquisition was set to high mass range (400-7000 m/z) in positive ion mode with the following source settings: cone voltage - 70 V, capillary voltage - 1.5 kV and the desolvation temperature - 550 ºC. Where samples were reduced to their monomeric subunits prior to LC-MS quantification, Dithiothreitol (DTT) was added to a final concentration of 50 mM prior to injection.

LC-MS data was analysed using UNIFI v1.9.4 (Waters). Chromatography peaks were integrated between 0.5 and 1.5 min and mass spectra of multiply charged state species were de-convoluted to produce mass output using the MaxEnt1 algorithm to the closest Da.

3.3.5 Fluorescence Correlation Spectroscopy analysis

Solution Fluorescence Correlation Spectroscopy (FCS) was carried out as previously described (Briddon et al, 2004; Kilpatrick et al., 2017). Briefly samples were imaged in 8-well chambered Nunc Labtek cover glasses (No. 1.0 borosilicate glass bottom) using an LSM 880 microscope with a 40X c-Apochromat 1.2 NA water-immersion objective (Zeiss) at 24 °C. Samples were excited with a Diode pumped solid state (DPSS) 561 nm laser and emission light collected through a 553-695 nm band pass onto a GaAsP detector using a pinhole set at 1 airy unit. The confocal volume was set to 200 µm above the coverslip surface and beam paths were calibrated using a solution of 20 nM TAMRA (5-6 carboxy mixed isomers; $D = 2.88 \times 10^{-10}$ m^2/s) prepared in high performance liquid chromatography grade H_2O. Calibration measurements were collected using ten 10 s and one 60 s reads. FCS measurements were performed using a range of IL23-TMR concentrations in PBS with or without 1 mg/mL protease-free BSA. Measurements were recorded at 1 kW/cm^2 laser power for four 15 s reads.

FCS analysis was carried out with Zen Black 2012 software (Zeiss). The size of the confocal volume was first measured using the calibration measurement of the diffusion time of TAMRA. Fluctuations of fluorescence caused by the diffusion of TAMRA through the confocal volume were converted to an autocorrelation curve using the equation shown below:

$$G(\tau) = 1 + \frac{< \delta I(T).\delta I(T+\tau) >}{< I >^2}$$

Where δI is the size of the fluctuation in fluorescence intensity, <I> is the mean fluorescence intensity and T is time.

The autocorrelation curve was then fit using a one-component, free 3D, Brownian diffusion model including a pre-exponential for triple state of the fluorophore (Briddon et al., 2004). This analysis yielded both the diffusion time of TAMRA through the confocal volume (the halfway point of the autocorrelation curve) and the structural parameter (the ratio of the height to waist radius) of the confocal volume.

The TAMRA diffusion time allowed the calculation of the radial waist of the confocal volume through the equation:

$$Radial\ waist = \sqrt{4xBxD}$$

Where B is the diffusion time of TAMRA (measured in the calibration read) and D is the literature value for the diffusion coefficient of TAMRA.

The radial waist of the confocal volume could then be used to calculate the size of the confocal volume using the equation:

$$Confocal\ Volume = \ (\pi^{1.5}(w^2(Sxw))1000$$

Where w is the radial waist and S is the structural parameter (measured in the calibration read).

Fluctuations of IL23-TMR diffusing through the confocal volume were then fitted to an autocorrelation curve using the same analysis method used for TAMRA. This analysis yielded the number of particles in the confocal volume which was used to calculate the concentration of fluorescent molecules using the equation:

$$[Fluoroligand] = \frac{A}{(CxN_A)}$$

Where A is number of particles in the confocal volume, C is the size of the confocal volume in liters (which was measured using calibration with TAMRA) and N_A is Avogadro's number.

FCS data were also fitted to a two-component photon counting histogram (PCH) model using an algorithm within the Zen software (Nederveen-Schippers et al., 2021) to derive the ratio of mono to multi-labelled particles. A 20 µs bin time was used (it was confirmed that this bin time was not too short by checking the variability of the data and that it was not too long by checking that there were adequate data points to fully define the curve). A first order correction value to account for deviations from a Gaussian distribution (a value that was determined in the calibration measurements on each experimental day) was used to calibrate the analysis.

3.3.6 Imaging

3.3.6.1 Immuno-cytochemical imaging of NanoLuc fused constructs

HEK293T cells were seeded and transfected in 8-well glass bottom plates as described in the transient transfection section. The following day cells were washed with PBS and fixed with 3% Paraformaldehyde (PFA) for 15 minutes. The cells were then washed three times with PBS and incubated with 30 mg/mL BSA and 10 mg/mL glycine in PBS for 30 minutes. The cells were washed three times with PBS and then incubated in 10% chicken serum in PBS for 30 minutes. This mixture was then replaced with 1000-fold diluted rabbit anti-NanoLuc antibody in PBS with 10% chicken serum. The plates were then incubated overnight at 4°C. The following day the cells were washed three times with PBS, followed by the addition of a 500-fold dilution of AF488 labelled chicken anti-rabbit antibody in PBS with 10% chicken serum. Following an hour-long incubation, cells were washed three times with PBS and 2 mg/mL Hoechst nuclear stain in PBS was added. The plates were incubated for 10 minutes, washed three times with PBS and then imaged using a Zeiss LSM 880 microscope fitted with a 63x PlanAprochromat oil objective (1.4 NA, Zeiss), using an Argon 488 nm laser (2%) and a 405-30 nm diode laser (2%) for excitation. The pinhole was set at 1 Airy Unit. Emission from AF488 and

Hoescht labels were imaged on separate tracks using a 488 nm beamsplitter and 495-630 nm band pass or a 405 nm beamsplitter and a 410-495 nm band pass respectively. All images were taken with 1024 x 1024 pixels per frame with 8 averages.

3.3.6.2 Imaging of SNAP and HT fused constructs

HEK293T cells were seeded and transfected in 8-well glass bottom plates as outlined in the transient transfection section. The following day cells were washed with PBS and then labelled with 500 nM of either AF488 HaloTag ligand or SNAP-Tag AF488 substrate in HBSS and incubated for 30 minutes at 37°C. The cells were then washed three times with HBSS and fixed by incubation with 3% PFA in PBS for 15 minutes. The cells were then washed twice with PBS and then incubated with 2 mg/mL Hoechst stain in PBS for 10 minutes. The cells were then washed three times with PBS before being imaged on a Zeiss LSM 880 microscope as previously described in the immuno-cytochemical imaging section.

3.3.7 Intra-receptor NanoBRET

Cells were plated and single well transfected as previously described, to give varying ratios of NL-IL23R to SNAP-IL12Rβ1. On the day of the experimental read, media was replaced with 50 µL of DMEM with FBS with 0.2 µM SNAPTag-AlexaFluor488 membrane impermeable substrate, cells were then incubated for 30 minutes and washed three times with HBSS. The buffer for the labelled cells was replaced with HBSS with 1 mg/mL BSA with or without 10 nM IL-23 and incubated for one hour. Plates were then read for fluorescent intensity on a PheraStar FS using excitation at 485 nm and emission at 520 nm. Following this 5 µL of 77 µM Furimizine per well was added and a further 4-minute incubation was carried out before plates were read using 475 nm (30 nm bandpass) and 535 nm (30 nm bandpass) filters with gains of 2800 and 3600 respectively on a PheraStar FS.

3.3.8 Ligand induced intra-receptor NanoBRET

To measure agonist induced changes in intra-receptor NanoBRET with a titration of IL-23, HEK293T cells that had previously been batch transfected were re-suspended and adjusted to 2 x 10^5 cells/mL. Cells that expressed

HaloTag fused constructs then had 100 nM HaloTag 618 ligand added. All cells were then dispensed at 100 µL into PDL coated 96-well white clear bottom microplates. On the day of the experimental read, cells transfected with SNAP-Tag fused constructs had media replaced with 50 µL of DMEM with FBS with 0.2 µM SNAPTag-AlexaFluor488 membrane impermeable substrate and were then incubated for 30 minutes followed by three washes with HBSS. The buffer for the labelled cells was then replaced with HBSS with 1 mg/mL BSA with or without increasing concentrations of IL-23 and incubated for one hour. 5 µL of 77 µM Furimizine per well was then added and a further 4-minute incubation before plates were read using a Pherastar FS. Cells labelled with SNAP-Tag AF488 dye were read using 475 nm (30 nm bandpass) and 535 nm (30 nm bandpass) filters with gains of 2800 and 3600 respectively. Cells labelled with Halotag 618 dye were read using 460 nm (80 nm bandpass) and >610 nm longpass filters with gains of 2000 and 3000 respectively.

3.3.9 Standard curves

Standard curves of recombinant NanoLuc (expressed in *E. coli* and purified using an *N*-terminal His-tag was gifted by Dr Bradley Hoare) or SNAP-AF488 substrate (Promega) were conducted by creating serial dilutions of these reagents in 50 µL HBSS with 1 mg/mL BSA in white clear bottom 96-well microplates. The microplate containing the NanoLuc titration had 5 µL of 77 µM Furimizine added to each well and was then incubated at 37°C for 4 minutes. Both micoplates were then read on the same Pherastar plate reader used in cellular NanoBRET experiments, using the equivalent settings.

3.4 Results

3.4.1 Characterisation of NanoLuc fusions of the IL-23 receptor

After receipt of custom synthesised IL23R and IL12Rβ1 NanoLuc fusion expression constructs, their expression was assessed in transiently transfected HEK293T cells using luminescence imaging (Figure 3-2). This experiment showed luminescence emanating from the membrane of HEK293T cells (as compared to the location of the plasma membrane in associated brightfield imaging), demonstrating that both NL-IL23R and NL-IL12Rβ1 localised to the plasma membrane. To add further confirmation that NanoLuc fusions were membrane expressed immuno-cytochemical imaging was carried out on transfected cells labelled with a rabbit anti-NanoLuc antibody (Figure 3-3). These experiments confirmed that NanoLuc fused constructs were surface expressed.

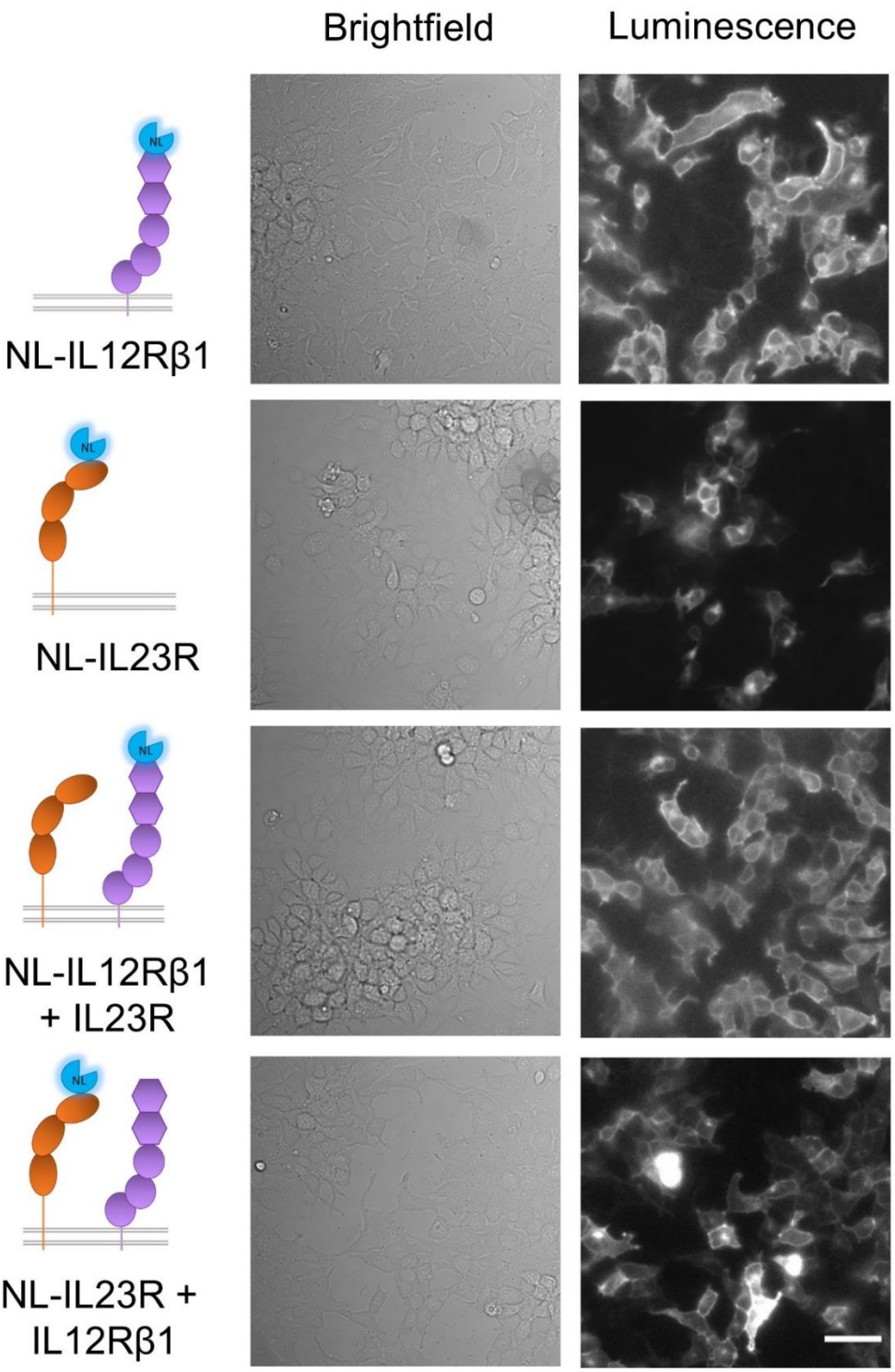

Figure 3-2: Luminescence imaging of NanoLuc fusions of the IL-23 receptor. Brightfield (centre) and luminescence (right) images of HEK293T cells expressing NL-IL12Rβ1, NL-IL-23R, NL-IL12Rβ1 co-expressed with IL23R and NL-IL23R co-expressed with IL12Rβ1 (as depicted in the cartoons on the left). A 3 s exposure was used for NL-IL12Rβ1 transfected cells and a 10 s exposure for NL-IL23R transfected cells. Scale bar represents 50 µm. Images are representative of those collected in five independent experiments.

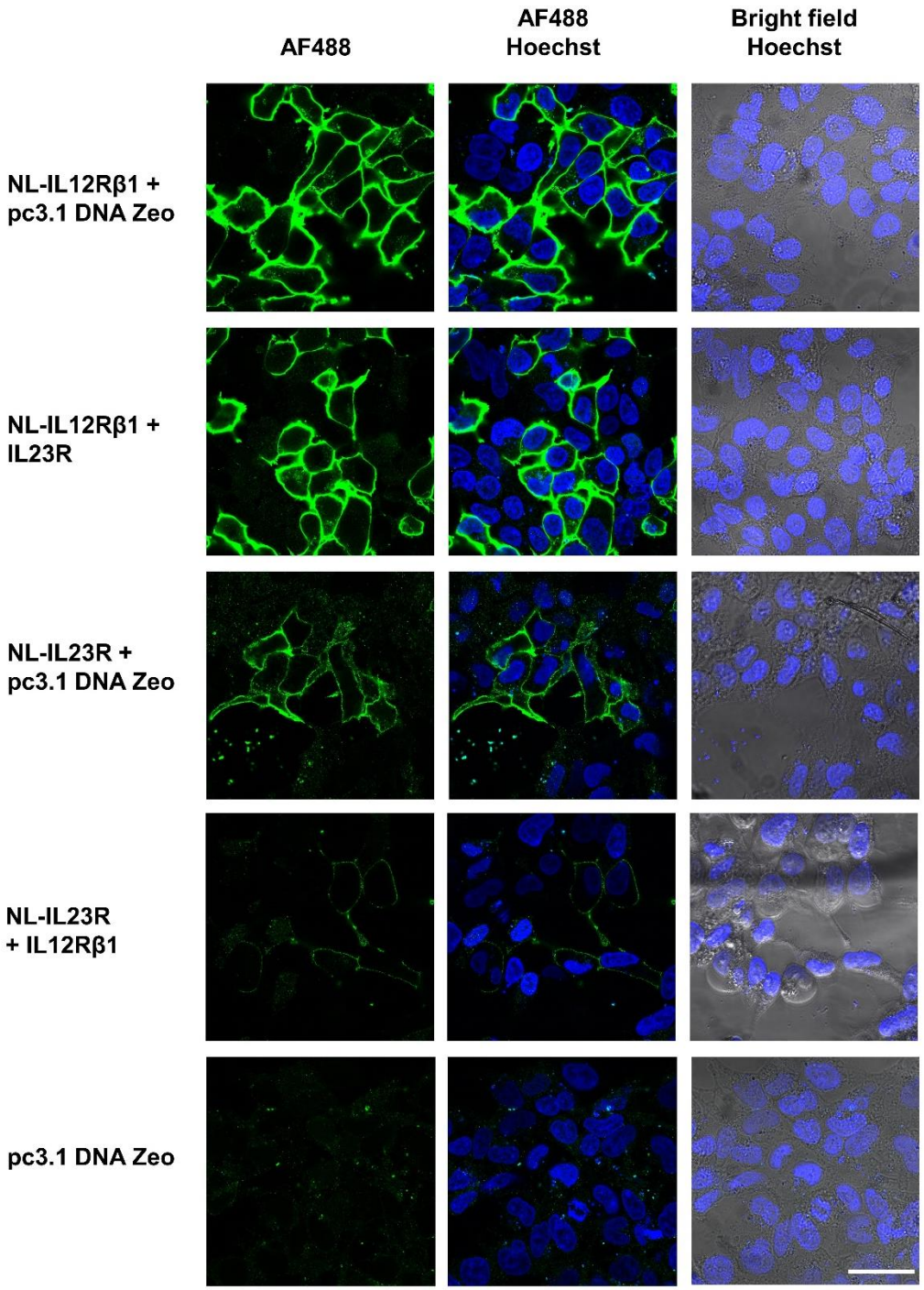

Figure 3-3: Immuno-cytochemical imaging of NanoLuc fusions of the IL-23 receptor. Immuno-cytochemical imaging of transfected HEK293T cells labelled with an anti-NanoLuc antibody presented with (centre) and without (left) Hoechst staining of the nucleus. Brightfield imaging with Hoechst staining (right) is also shown for comparison. Images were taken on the same day using equivalent settings and are representative of those taken in three independent experiments. Scale bar represents 40 µm.

The luminescence and immuno-cytochemical imaging experiments revealed that the cells expressing NL-IL12Rβ1 were brighter than those expressing NL-IL23R (necessitating the variation of exposure times for each condition for the luminescence imaging), indicating that NL-IL12Rβ1 was expressed at a higher level than NL-IL-23R. To further explore this and to allow the approximation of the concentration of NanoLuc labelled constructs expressed in subsequent NanoBRET experiments, a standard curve of purified NanoLuc was created (Figure 3-4A). Linear regression of this standard curve demonstrated that there was a linear relationship ($R^2 = 0.91$) between purified NanoLuc concentration and luminescence up to the concentration of 0.0833 pmol/well NanoLuc. The lack of a linear relationship after 1.66 nM was most likely due to depletion of the Furimizine substrate being increased at the higher concentrations of enzyme.

The standard curve was then used to approximate the concentration of NanoLuc expressed in subsequent NanoBRET experiments (Figure 3-4B). This analysis demonstrated that with equivalent cDNA concentrations used in transfections, NL-IL12Rβ1 had a higher expression than NL-IL23R (0.0518 ± 0.0067 and 0.0125 ± 0.0027 pmol/well respectively). When each of these plasmids were expressed with their corresponding co-receptor the concentration of NL-IL12Rβ1 was increased (1.20-fold) and NL-IL23R was decreased (2.90-fold) to 0.0620 ± 0.0080 and 0.00430 ± 0.00124 pmol/well respectively. The increase of NL-IL12Rβ1 expression with IL23R was found to be non-significant but the decrease in NL-IL23R expression with IL12Rβ1 co-expression was significant (unpaired t test; p value = >0.05 and <0.05 respectively; discussed in section 3.5).

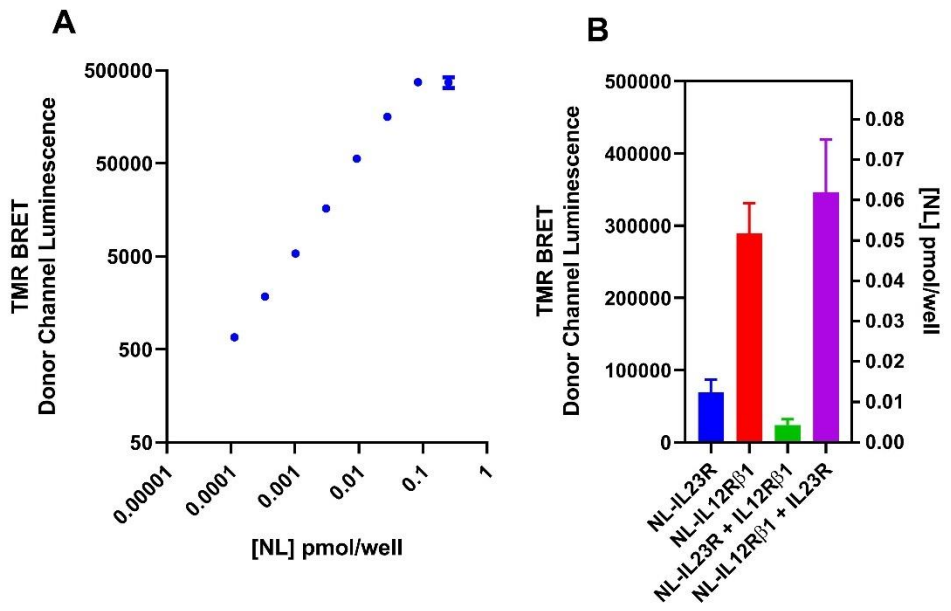

Figure 3-4: Approximation of the concentration of NanoLuc expressed in NanoBRET assays. (A) The luminescence of a standard curve of purified NanoLuc measured with the same furimizine concentration, incubation time and reader settings as were used in NanoBRET experiments. Data are mean ± SEM from three independent quintuplicate experiments. (B) The mean luminescence values for each transfection condition used in subsequent NanoBRET ligand binding experiments (in each condition a total 2 µg of cDNA was used per well of a 6 well plate, with 1 µg of each receptor subunit cDNA used and the total cDNA content normalised by the addition of pc3.1 zeocin vector) with the approximate concentration of NanoLuc shown on the right y axis for comparison. Data are mean ± SEM from five or three (NL-IL12Rβ1+IL-23R) independent experiments.

3.4.2 Characterisation of HT and SNAP tagged IL-23 receptor components

Following the synthesis of the SNAP-IL12Rβ1 plasmid and the receipt of custom synthesised HT-IL12Rβ1 expression plasmids, the cellular localisation of the constructs was assessed by imaging. Cells transiently expressing these constructs were labelled by incubation with membrane impermeant AlexaFluor (AF)488 fused to HaloTag (Figure 3-5) or SNAP-Tag (Figure 3-6) substrate before being fixed and imaged by confocal microscopy. The imaging revealed that both constructs reached the cell surface when expressed in isolation and with unlabelled IL23R.

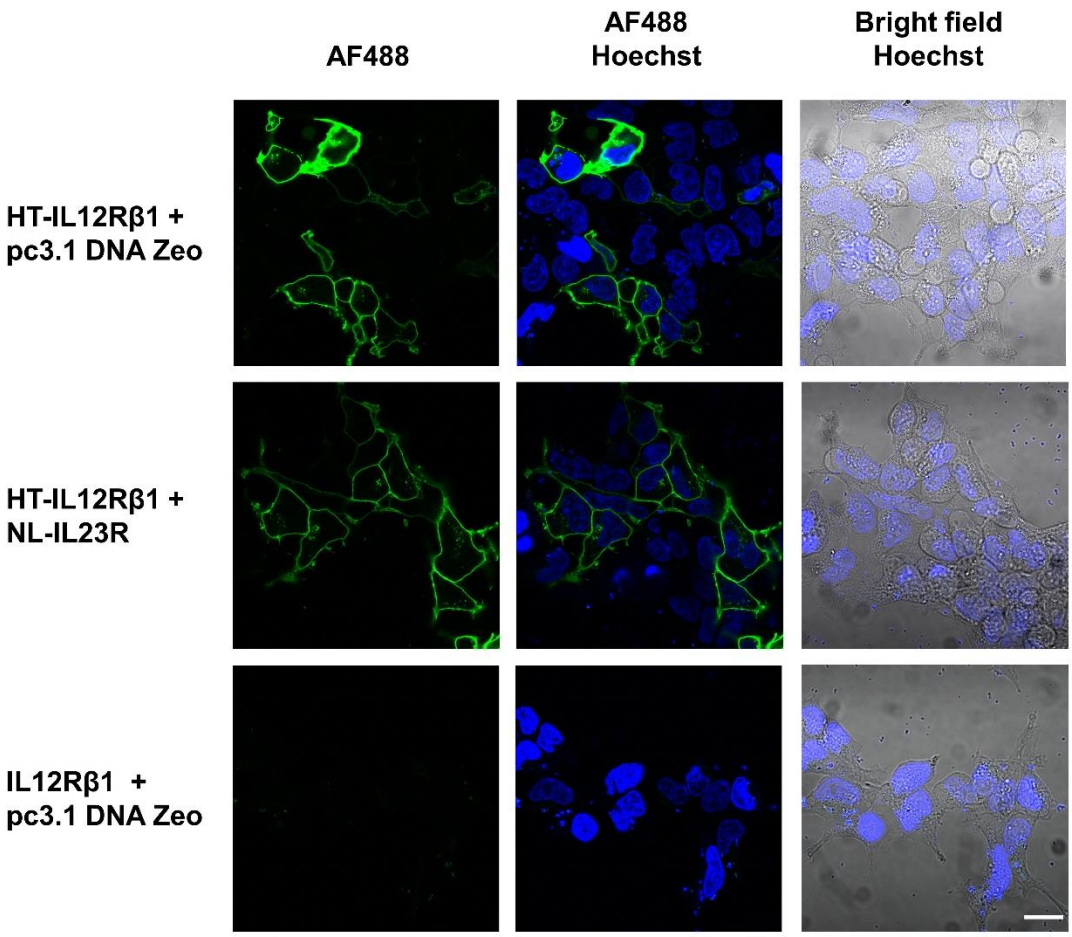

Figure 3-5: Confocal fluorescence microscopy of cells labelled with HT-AF488. HEK293T cells were transiently transfected with the plasmids shown on the left, fixed with PFA and labelled with both Hoechst nuclear stain and HT-AF488. Imaging was carried out using a Zeiss 880F confocal microscope. Scale bar indicates 20 μm.

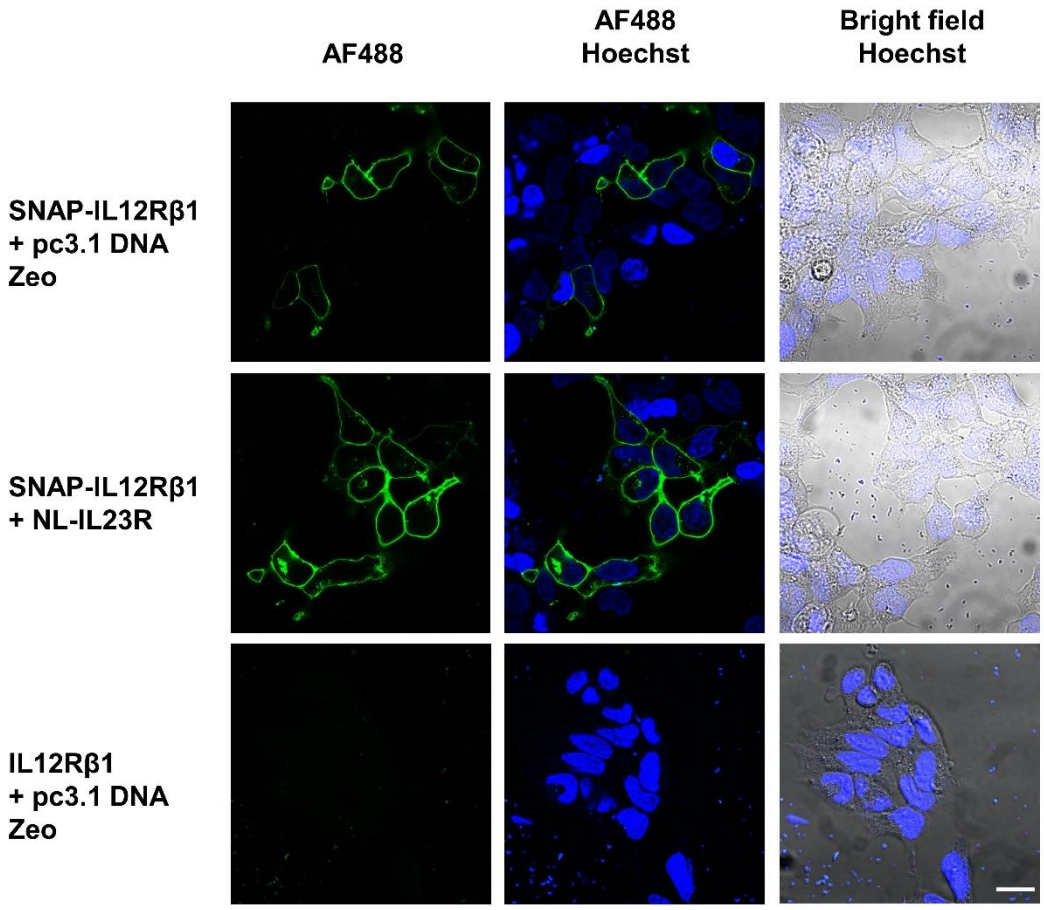

Figure 3-6: Confocal fluorescence imaging of cells labelled with SNAP-AF488. HEK293T cells were transiently transfected with the plasmids shown on the left, fixed with PFA and labelled with both Hoescht nuclear stain (33342) and SNAP-AF488. Imaging was carried out using a Zeiss 880F confocal microscope. Scale bar indicates 20 μm.

To calibrate AF488 fluorescent intensity values in order to estimate expression levels, the fluorescence intensity of a standard curve of purified SNAP-AF488 substrate was measured using the same protocol that would be used in further experiments (Figure 3-7).

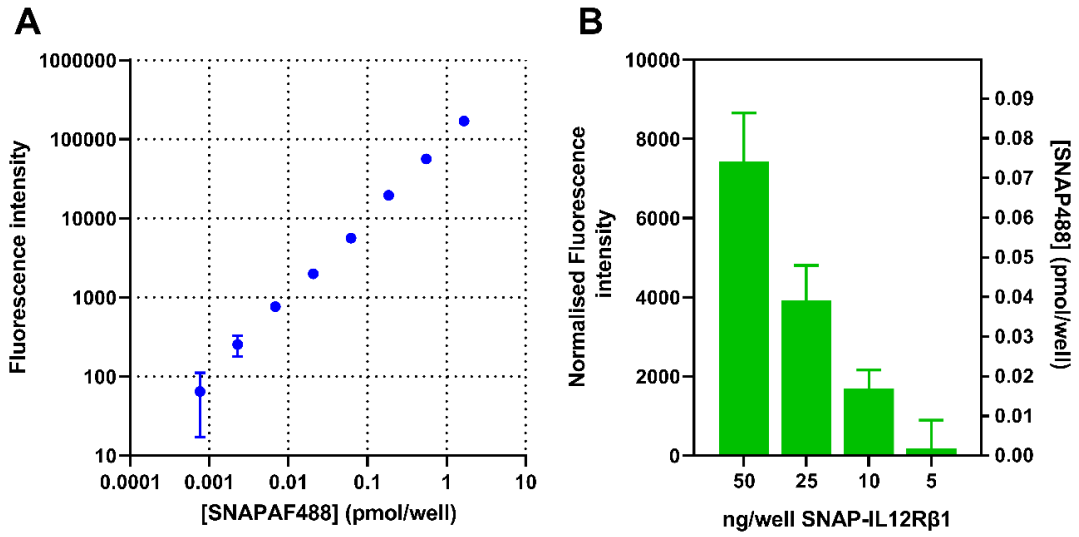

Figure 3-7: Estimation of SNAP construct expression from using a standard curve of SNAPAF488. (A) The fluorescence intensity of a standard curve of SNAPAF488 substrate measured under equivalent conditions to those used to measure the expression of SNAP-IL12Rβ1 (Mean and SEM from four independent experiments). (B) The estimated pmol/well expression of SNAP-IL12Rβ1 when HEK293T cells were transfected with 50 ng/well of NL-IL23R and varying concentrations of SNAP-IL12Rβ1 cDNA (Mean and SEM from five independent experiments).

3.4.3 Signal transduction of tagged receptor constructs

To ascertain whether the *N*-terminal IL-23 receptor fusions had any effect on signal transduction in HEK293T cells, phosphorylation of the transcription factor STAT3 was monitored. Co-expression of the wild-type IL-23 receptor heteromer (IL23R and IL12Rβ1), followed by stimulation with varying concentrations of IL-23, led to the determination of an EC_{50} of 269 ± 106 (n=4) pM for cytokine stimulation of phosphorylated STAT3 (pSTAT3). This experiment was replicated utilising co-transient transfections of either NL-IL23R and IL12Rβ1 or NL-IL23R and SNAP-Tag fused IL12Rβ1 (SNAP-IL12Rβ1) or NL-IL23R and HaloTag fused IL12Rβ1, which led to the determination of potency values of 154 ± 46 (n=4), 150 ± 43 (n=4) pM and 199 ± 33 pM respectively, for IL-23 stimulation of pSTAT3 (Figure 3-8). These results demonstrated that use of these fusion constructs did not significantly ($p>0.05$; one-way ANOVA) alter the EC_{50} of signal transduction induced by IL-23.

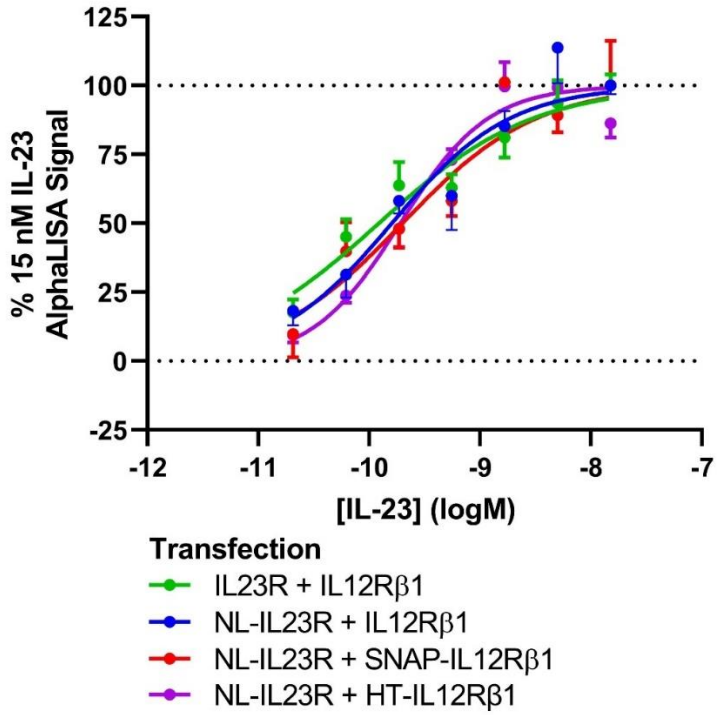

Figure 3-8: Signal transduction is unchanged by the addition of *N*-terminal tags to the IL-23 receptor. STAT3 phosphorylation induced in HEK293T cells transfected with different tagged variants of the IL-23 receptor after a 30-minute incubation with increasing concentrations of IL-23. Data are expressed as a percentage of the response obtained with 15 nM IL-23. Values are mean ± SEM from four independent experiments and are normalised a percentage of the highest signal concentration in each experimental condition. Data were fit with equation 5.

3.4.4 Fluorescent labelling and characterisation of IL-23

Preparation of fluorescently labelled IL-23 was carried out via incubation of purified recombinant IL-23 with NHS-ester linked TAMRA as outlined in Section 3.3.3 (a summary of the reaction is shown in Figure 3-9). The NHS-ester labelling efficiency is related to the protonation of lysine residues in the protein, which in turn is related to the pH of the reaction buffer (Nanda and Lorsch, 2014). During the initial optimisation of the labelling procedure IL-23 protein was dialysed overnight at 4 °C into an alkaline buffer at pH 9. Unfortunately, subsequent LC-MS analysis revealed this procedure resulted in the reduction of

the linking di-sulphide bond within IL-23. Due to this observation the final labelling protocol was carried out at a pH of 7.4.

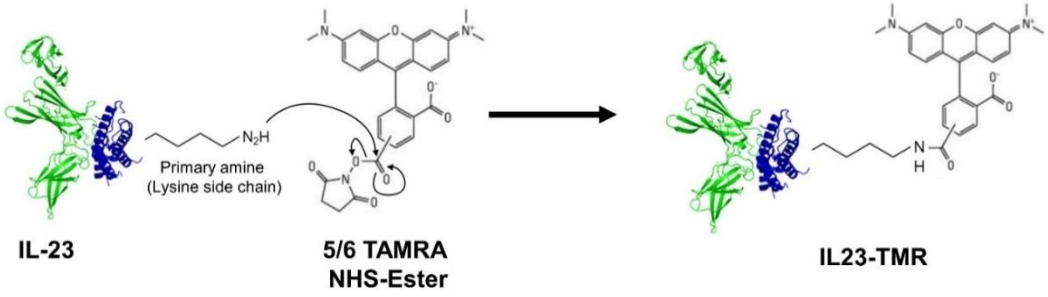

Figure 3-9: Reaction scheme for non-specific TAMRA labelling of IL-23. A nucleophilic substitution is shown in which lysine residues in IL-23 react with NHS ester linked TAMRA to form IL23-TMR. The TAMRA reagent is a racemic mix of isomers labelled with NHS-ester either at ring position 5 or 6.

Following removal of the un-reacted labelling reagent using a desalting column, the TAMRA conjugated IL-23 (hereon referred to as IL23-TMR) and the unlabelled IL-23 were assessed using liquid chromatography coupled mass spectrometry (LC-MS; Figure 3-10 and Figure 3-11). This analysis revealed that both the labelled and unlabelled cytokine samples were heterodimeric and uncontaminated with IL12p40 or IL23p19 monomers (Figure 3-11). Furthermore, upon the application of Dithiothreitol (DTT), the protein could be split into its constituent monomers by reduction of the linking disulphide bond (Figure 3-10). Whilst the IL23p19 subunit closely matched it's predicted molecular weight, the IL12p40 subunit gave several peaks differing by 162 Da, all with masses higher than that predicted from the protein's amino acid sequence (Table 3-1). This most likely corresponded to varying levels of post translational modification (PTM) by *N*-linked glycosylation, a modification that has been previously reported for the IL12p40 subunit (Bohnacker et al., 2020). The unlabelled IL-23 heterodimeric complex also exhibited the previously described heterogeneous pattern, with the most abundant peak corresponding to a 56050 Da species (Figure 3-11).

Protein name	Predicted MW (Da)	Observed mass (Da)	Suspected Post-Translational Modifications (PTM)s
IL23p19-HisTag	19499.8	19499	none
IL12p40	34696.6	36555 (most abundant)	Mannose *N*-linked glycosylation
IL-23 complex	54181.2	56050 (most abundant)	Mannose *N*-linked glycosylation

Table 3-1: The masses of recombinant purified IL-23 subunits and heterodimeric complex used in the study as determined by LC-MS. Predicted molecular weights were generated from the amino acid sequences of the proteins, assuming the reduction of internal disulphide bridges for the cytokine subunits.

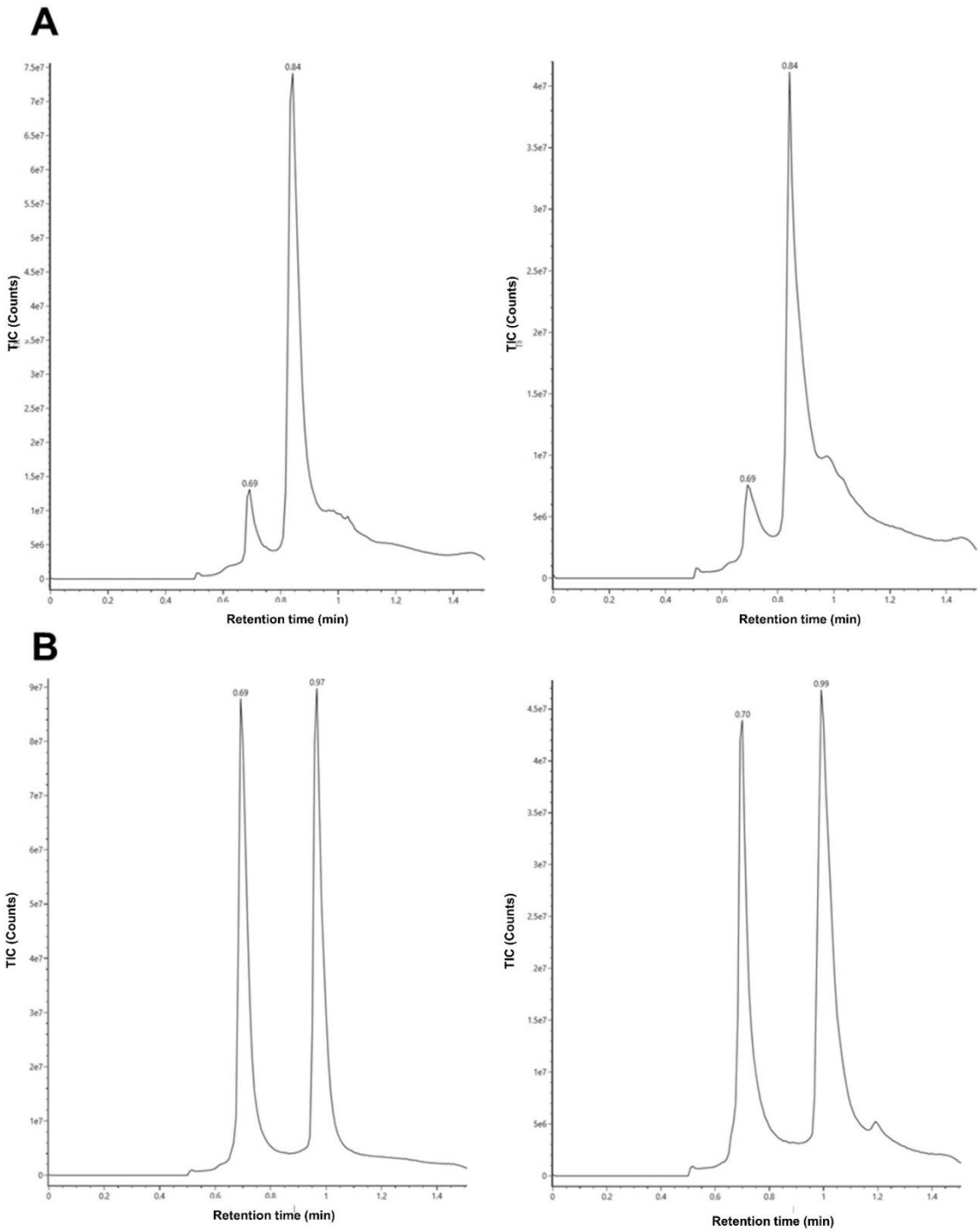

Figure 3-10: Reversed-Phase chromatography demonstrates heterodimeric IL-23 is reduced to its subunits by addition of DTT. (A) Total Ion Count (TIC) chromatograms of IL-23 (left) and IL23-TMR (right). (B) Total ion count chromatograms of IL-23 (left) and IL23-TMR (right), in the presence of 50 mM DTT.

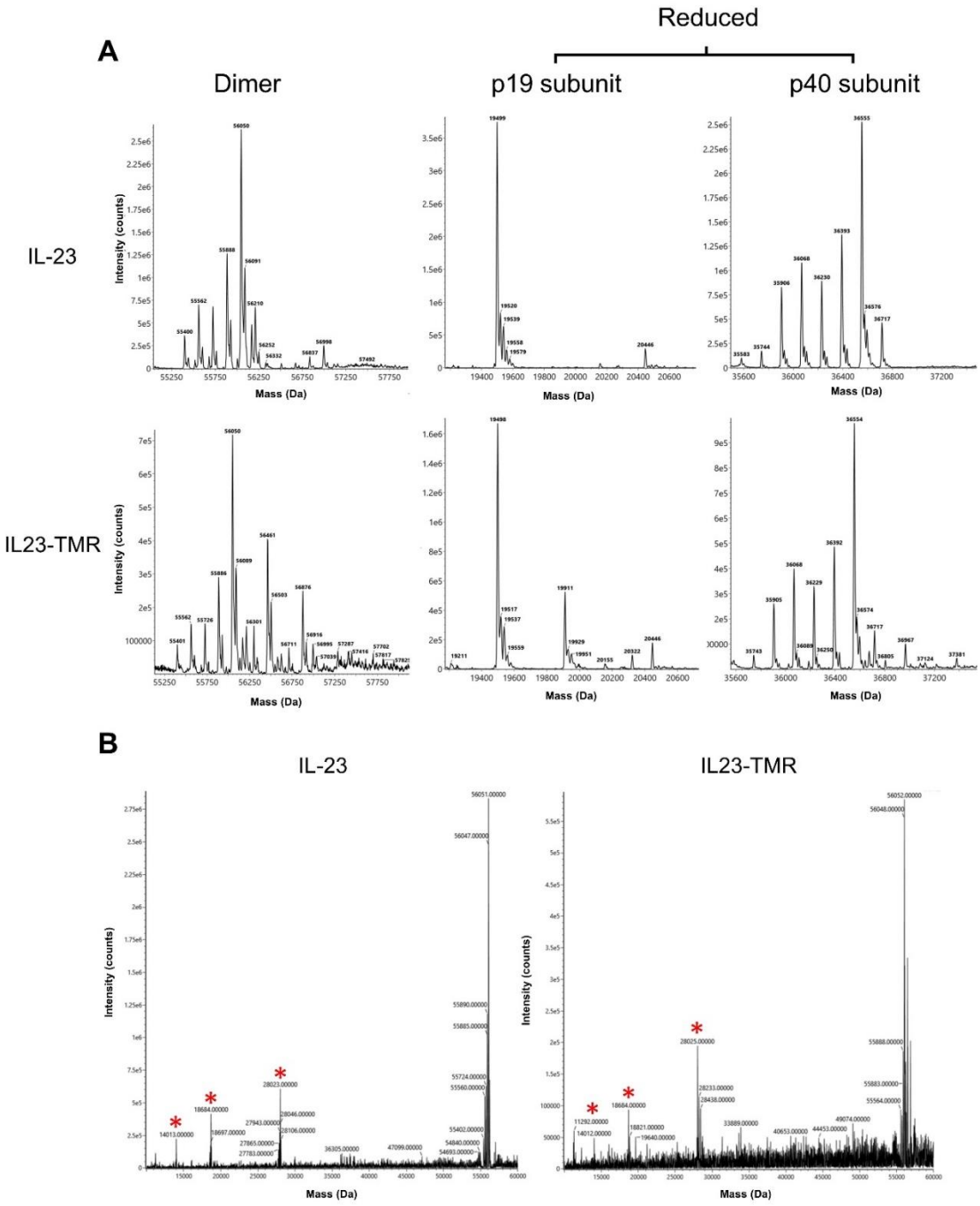

Figure 3-11: LC-MS analysis of IL23-TMR. (A) De-convolved LC-MS spectra of IL-23 (top) and IL23-TMR (bottom), demonstrating both the DTT reduced, p19 and p40 subunits (centre and right respectively) and the non-reduced dimeric cytokine (left). (B) De-convolved LC-MS spectra of IL-23 (left) and IL23-TMR (right) over a broad mass range. Artefact peaks created by resonance effects are denoted by a red asterisk. These peaks are a half, third or fourth the mass of the most abundant ion.

In the IL23-TMR sample the most abundant species remained the unlabelled IL-23 at 56050 Da, however a single TAMRA labelled 56461 Da species and a double labelled 56876 Da species were also present. Trace amounts of three and four labelled species were also apparent from low abundance peaks at 57287 and 57702 respectively (Figure 3-11A). Reduction of the IL23-TMR sample with DTT revealed that the IL23p19 subunit was labelled to a greater extent than the IL12p40 subunit (Figure 3-11A), with peak intensity analysis demonstrating that 64.9% of TAMRA labels were located on IL23p19. The primary constituents of the heterodimeric IL23-TMR fraction were determined by the relative abundance of the most intense PTM variant to be 52.3% unlabelled, 29.5% single labelled and 18.2% double labelled.

To gain a further quantitative measure of the constituents of the labelled IL-23 mixture, fluorescence correlation spectroscopy (FCS) (Briddon et al, 2004) was used, essentially as described by Kilpatrick and colleagues (Kilpatrick et al., 2017). To measure the concentration of TAMRA labelled particles in solution, FCS fluctuations were collected from freely diffusing IL23-TMR in a confocal measurement volume (Figure 3-12A). Subsequent autocorrelation analysis (Figure 3-12B), allowed calculation of the concentration of fluorescent particles (Briddon et al., 2004; Kilpatrick et al., 2017). Measured IL23-TMR concentrations were substantially lower than predicted, but the addition of 1 mg/mL BSA, which prevents non-specific interactions of the protein with the plate, (Kilpatrick et al., 2017) increased the observed concentration (Figure 3-12D). Consequently, 1 mg/mL BSA was included in all subsequent IL-23 and IL23-TMR experiments. FCS measurements of IL23-TMR in the presence of BSA displayed a single diffusing species with a diffusion coefficient of 37.9 ± 1.8 $\mu m^2/s$ whilst that for TAMRA alone was 280 $\mu m^2/s$. By comparing the measured concentration of this IL23-TMR fluorescent species to the total concentration of IL-23 measured in the sample via absorbance at 280 nm it was demonstrated that 51.5% of the IL-23 in the sample was fluorescently labelled with TAMRA.

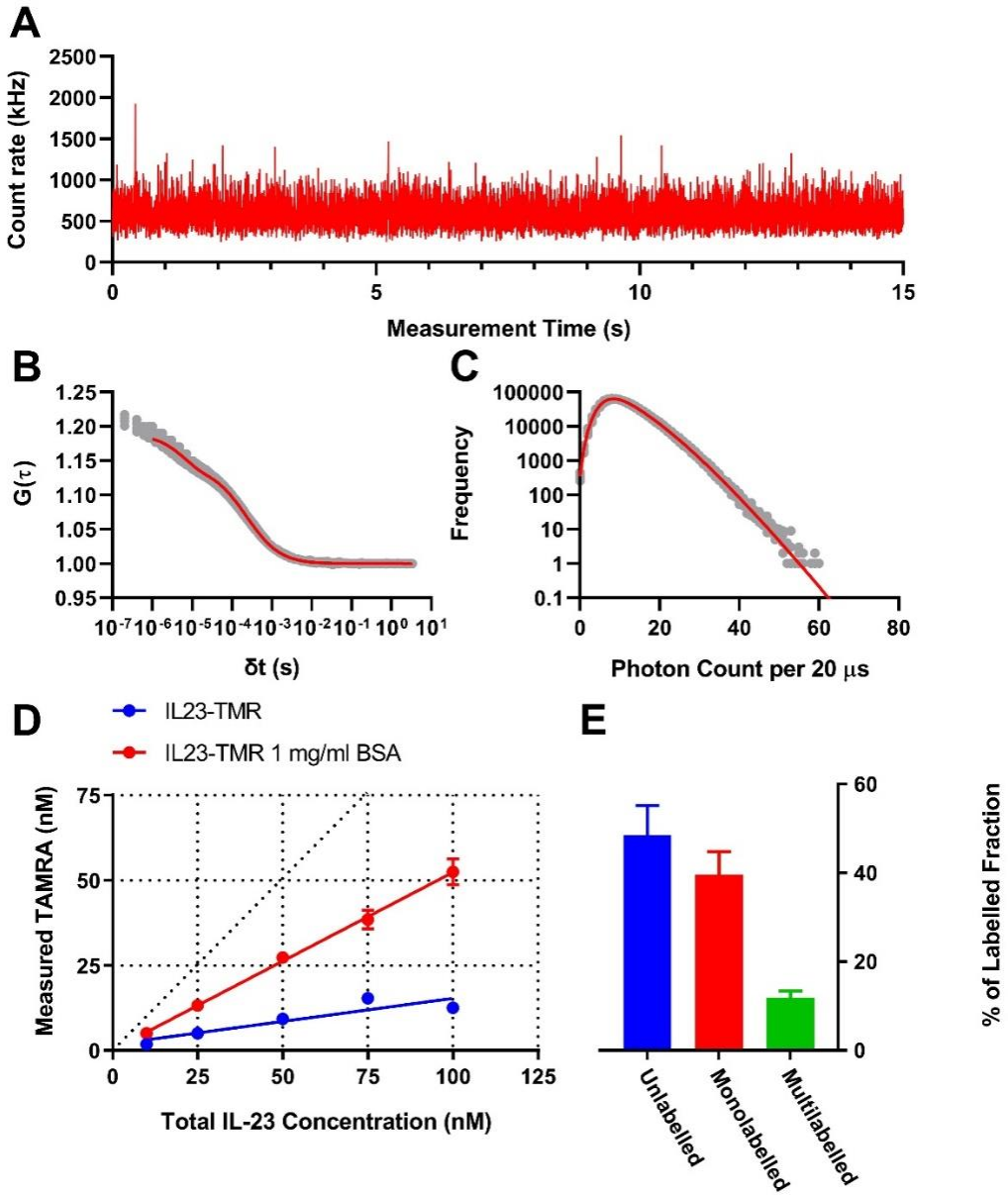

Figure 3-12: Characterisation of labelled IL23-TMR using fluorescence correlation spectroscopy (FCS) and photon counting histogram (PCH) analysis. (A) Example of the fluorescence fluctuations obtained over time for 100 nM IL23-TMR in the presence of 1 mg/mL BSA. (B) Autocorrelation curves for four concurrently collected replicate FCS readings of 100 nM IL23-TMR in the presence of 1 mg/mL BSA with a red line denoting the one component free 3D fit of the data. (C) A Photon counting histogram of the data presented in (B) fit with a two-component model (red line). (D) Analysis of IL23-TMR showing the concentration of TAMRA labelled molecules measured by FCS in (B) vs the total concentration of IL-23 (initially quantified by absorbance at 280 nm), in the presence (red) or absence (blue) of 1 mg/mL BSA. Diagonal dotted line represents x=y. Each data point represents mean value ± SEM of 20 measurements from five independent experiments. (E) The proportion of labelled IL-23 species. Total concentration of IL-23 was quantified by UV absorbance at 280 nm, total concentration of TMR-labelled IL-23 was determined using the autocorrelation analysis demonstrated in (B).

The proportion of different populations of labelled species was quantified using the two component PCH analysis demonstrated in (C). Data shown are mean ± SEM of values obtained in five independent experiments.

The ratio of mono to multi-labelled IL23-TMR particles was determined by calculating the average molecular brightness of individual fluorescent particles using a two component photon counting histogram analysis from the same intensity fluctuations (Chen et al., 1999; Figure 3-10C) . It was found that the IL23-TMR fraction was 77% composed of a 163983 ± 2537 cpm.s^{-1} brightness fraction and 23% composed of a 589772 ± 5557 cpm s^{-1} brightness fraction. The brightness of unconjugated TAMRA under these conditions was determined to be 301461 ± 10764 cpm s^{-1}. As the LC-MS spectra showed that the majority of labelled IL-23 is bound to just one TAMRA molecule, this demonstrated that the reaction of the fluorophore with IL-23 caused significant quenching of its brightness with a mean value almost 2-fold lower than that of unbound TAMRA. The second brightness component likely represents a mixture of IL-23 species, bound to two or more TAMRA molecules with a mean brightness formed both from variable label number and differing degrees of fluorescence quenching. As a result, these components are here-on referred to as mono and multi-labelled IL-23. The overall proportions of these components when compared to the previously established total labelled IL-23 concentration were determined to be 39.6% mono-labelled and 11.9% multi-labelled IL-23 with a remaining 48.5% of the mixture being made up of unlabelled IL-23 (Figure 3-12E; discussed in section 3.5).

3.4.5 Measuring the affinity of IL23-TMR to NanoLuc fused IL-23 receptor constituents

A NanoBRET IL23-TMR binding assay using HEK293T cells transiently expressing NanoLuc fusions of IL23R or IL12Rβ1 in the presence and absence of the corresponding untagged co-receptor was then created. Increasing concentrations of IL23-TMR resulted in an increase in the BRET signal that was comprised of saturable specific and linear non-specific binding components (Figure 3-13). Non-specific binding was determined in the presence of an excess of unlabelled IL-23. When the constructs were expressed in isolation, IL23-TMR had a greater affinity for NL-IL12Rβ1 (K_d = 30.1 ± 5.5 nM; n=5) than NL-

IL23R (K_d = 222 ± 71 nM; n=5) (Figure 3-13A and B). However, when NL-IL23R was co-expressed with unlabelled IL12Rβ1 the affinity of IL23-TMR to the heteromeric receptor complex was strengthened by 3250-fold to 27.0 ± 3.6 pM (n=5) which was significantly different to the affinity of IL23-TMR to cells expressing NanoLuc fused monomers (unpaired t test; Figure 3-13C).

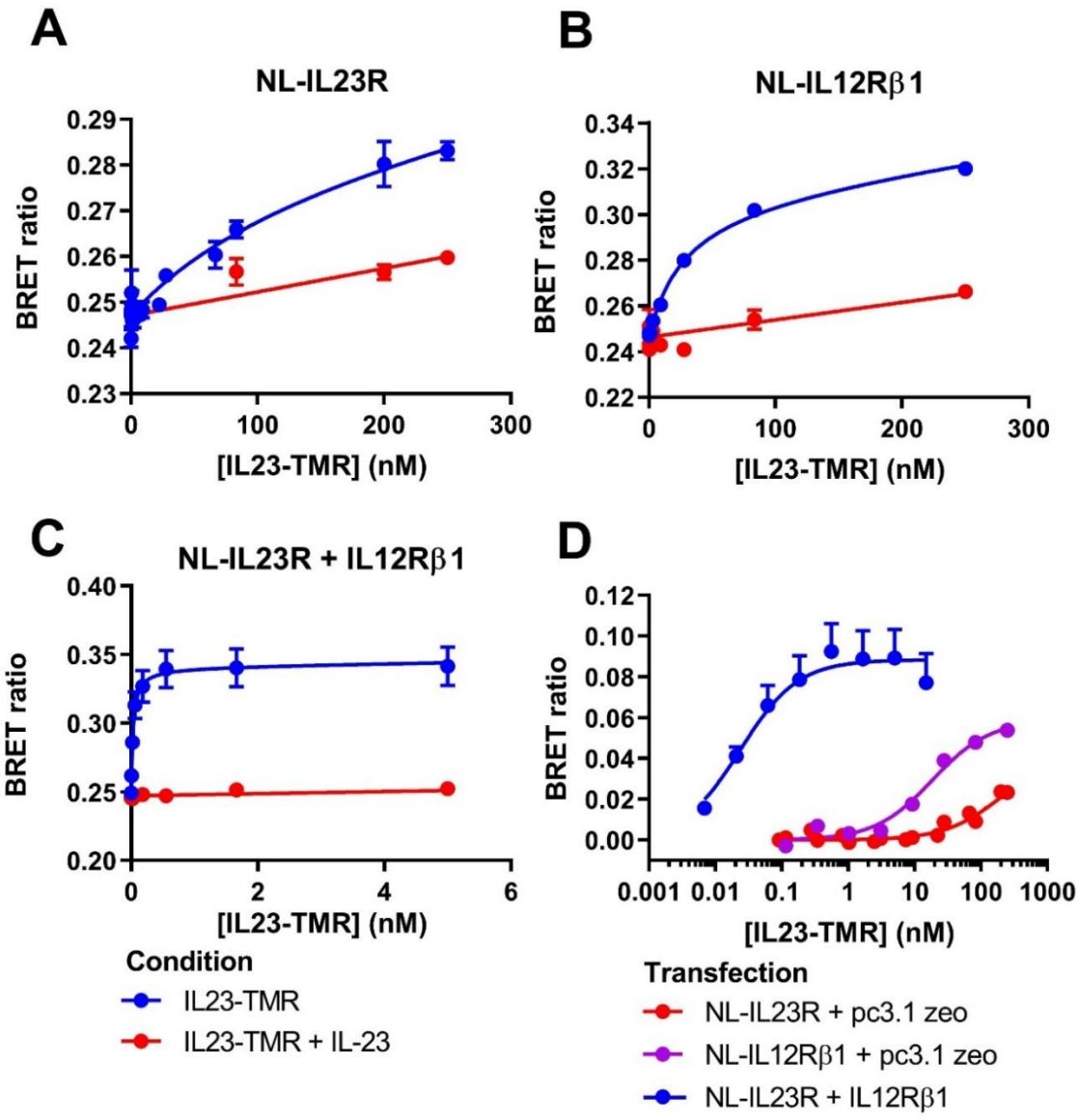

Figure 3-13: Binding of IL23-TMR to NL-IL12Rβ1, NL-IL23R and NL-IL23R co-expressed with untagged IL12Rβ1. (A-C) The binding of increasing concentrations of IL23-TMR to HEK293T cells expressing either (A) NL-IL23R, (B) NL-IL12Rβ1 or (C) NL-IL23R and IL12Rβ1 in the presence (red) or absence (blue) of an excess of unlabelled IL-23. The concentration of unlabelled IL-23 used was 1 µM (A-B) and 50 nM (C). Data points are mean raw BRET ratio values ± SEM from five independent experiments. (D) The combined specific binding data from (A-C) after subtraction of non-specific binding expressed on a logarithmic scale for clarity. Data in (A-C) were fit with equation 1 and data in (D) were fit with equation 2.

The dissociation constant obtained for IL23-TMR binding to NL-IL12Rβ1 in the presence of unlabelled IL23R was higher (46.7 ± 16.1 nM; n=3; Figure 3-14) than that of the interaction of IL23-TMR with NL-IL23R co-expressed with IL12Rβ1 (Figure 3-13; 1730-fold) and similar to the value obtained for the interaction with NL-IL12Rβ1 alone (1.55-fold). However, comparison of the luminescence intensities of cells expressing either NL-IL12Rβ1 or NL-IL23R in isolation indicated that NL-IL12Rβ1 achieved a much higher expression level in transient transfections than that obtained with NL-IL23R (0.0518 ± 0.0066 vs 0.0125 ± 0.0027 pmol/well respectively; Figure 3-4). The higher dissociation constant obtained for NL-IL12Rβ1 in the presence of unlabelled IL23R is therefore likely to be a consequence of the NL-IL12Rβ1:IL23R complex only representing a small proportion of the total binding of IL23-TMR to NL-IL12Rβ1. To investigate this further, transfections with a lower (1:10) transfection ratio of NL-IL12Rβ1 and IL23R were used. The affinity of IL23-TMR under these conditions was 19-fold greater (K_d = 647 ± 79.5 pM; n=5; Figure 3-14B) and consistent with a higher proportion of NL-IL12Rβ1:IL23R complexes present under these experimental conditions.

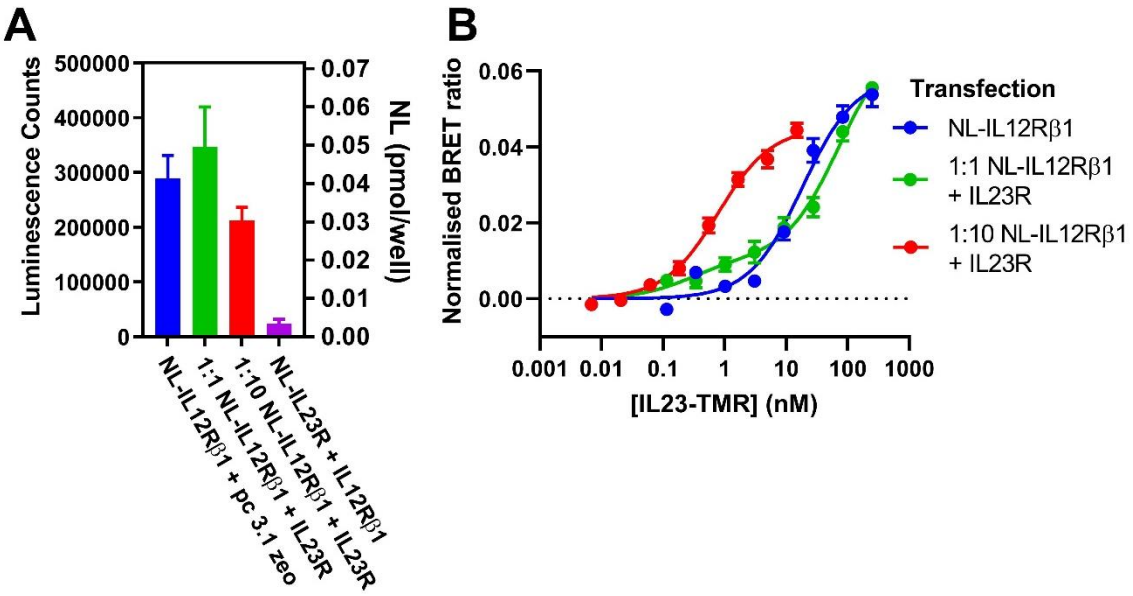

Figure 3-14: Impact of expression level on the observation of ligand-binding characteristics of NL-IL12Rβ1. (A) The luminescence signal measured from HEK293T cells following transient transfection. Corresponding NanoLuc (pmol/well) levels are calculated from a purified NanoLuc standard curve (Figure 3-4). Values are expressed as mean ± SEM from five or three (1:1 NL-IL12Rβ1+IL23R) independent experiments. (B) The binding of IL23-TMR to combinations of NL-IL12Rβ1 and IL23R at different transfection ratios in HEK293T cells. Values show mean ± SEM cells of the BRET ratios obtained after subtraction of non-specific binding. The concentration of IL-23 used to define non-specific binding was 1 µM (blue and green) and 100 nM (red). Data were obtained from 3 (green) or 5 (red and blue) separate experiments. The data for 1:1 NL-IL12Rβ1+IL23R (green circles) were fitted to a two-site binding curve which yielded K_d values of 28 pM and 72 nM with the high affinity site accounting for 16.2% of the maximum specific binding. For these data, the two-site binding curve (Equation 3) was a significantly better fit than to a single site saturation curve (Equation 2) ($p<0.0001$; Partial F test).

3.4.6 Competition experiments with unlabelled IL-23

To measure the affinity of unlabelled IL-23 for the IL-23 receptor complex, NanoBRET competition experiments were undertaken using HEK293T cells transiently transfected with NL-IL23R and IL12Rβ1. This assay was carried out using several concentrations of IL23-TMR and increasing concentration of unlabelled IL-23, the IC_{50} determined for unlabelled IL-23 was shifted to higher concentrations (with increasing concentrations of IL23-TMR) consistent with a competitive interaction (Figure 3-15; Cheng and Prusoff, 1973). However, at

the highest concentration of IL-23 used (3 nM) the decrease in potency reached a limiting value indicative of a more complex interaction (Figure 3-15). Analysis of the data obtained with lower concentrations of IL23-TMR yielded a mean K_i for IL-23 of 31.6 ± 7.7 pM (n=13), which was not significantly different from the pre-determined value for the K_d of IL23-TMR (unpaired t test). In addition, a K_i for IL-23 of 27.2 pM and a K_d for IL23-TMR of 35.1 pM were obtained from a linear plot of the relationship between IL23-TMR concentration and the corresponding IC_{50} values of unlabelled IL-23 (Figure 3-15B).

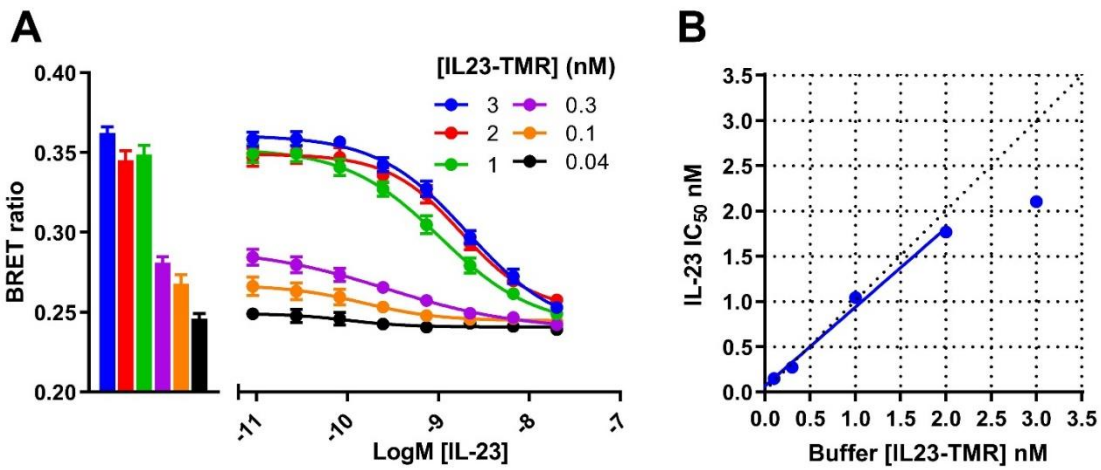

Figure 3-15: Determining the affinity of unlabelled IL-23 for the IL-23 receptor. (A) HEK293T cells expressing NL-IL23R and IL12Rβ1 were incubated with varying concentrations of IL23-TMR as shown in the bar chart (left) and increasing concentrations of unlabelled IL-23 (right). Data represent mean ± SEM of the raw BRET ratios obtained from five independent experiments. Data are fit with equation 4. (B) The IL-23 IC_{50} values derived in (A) plotted against the buffer concentration of IL23-TMR, with all points except that for 3 nM IL23-TMR fitted by linear regression.

3.4.7 Kinetics of IL23-TMR binding.

To observe the association of IL23-TMR to the IL-23 receptor, IL23-TMR was added to cells expressing NL-IL23R and IL12Rβ1 and the increase in BRET ratio measured in real time (Figure 3-16A). It was observed that 300 pM of IL23-TMR took approximately 20 minutes to reach equilibrium, at which point the BRET ratio remained stable (Figure 3-16A). To measure the dissociation rate of IL23-TMR, the probe was allowed to equilibrate with the receptor for 40 minutes followed by replacement of the media with a solution containing 30 nM IL-23, resulting in a decrease in the BRET ratio (Figure 3-16C). The dissociation rate (k_{off}) was measured to be 0.0503 ± 0.0036 min^{-1} (mean ± SEM; n=4) when

fit using a one phase dissociation model. When the association and dissociation were fitted together (Figure 3-16B) the association (k_{on}) and dissociation (k_{off}) rates were found to be 3.96 ± 0.35 x 10^9 M^{-1} min^{-1} and 0.0228 ± 0.0028 min^{-1} respectively (mean ± SEM; n=4). The combined association and dissociation model used to calculate these values (Figure 3-16A) fitted the association phase of the curve well but the dissociation phase of the curve poorly. Despite the poor fit of the dissociation rate the kinetic rates generated by the combined model gave a value for K_d that was similar to that previously measured at equilibrium for IL23-TMR (Table 3-2). Due to the poor fit the k_{on} was also measured by using the k_{obs} of the association curve shown in Figure 3-16B with the pre-determined K_d value measured for IL23-TMR using equation 10. This analysis yielded a similar value for k_{on} (1.06-fold slower).

When both a single-phase and two-phase dissociation model were used to fit IL23-TMR's dissociation (Figure 3-16C-D) the two-phase decay model was shown to be the preferred model using a partial F test (p = <0.0001). A value for IL23-TMR k_{on} was also generated from the previously measured equilibrium K_d and the k_{off} generated from the single-phase decay fit (Figure 3-16C and Table 3-2).

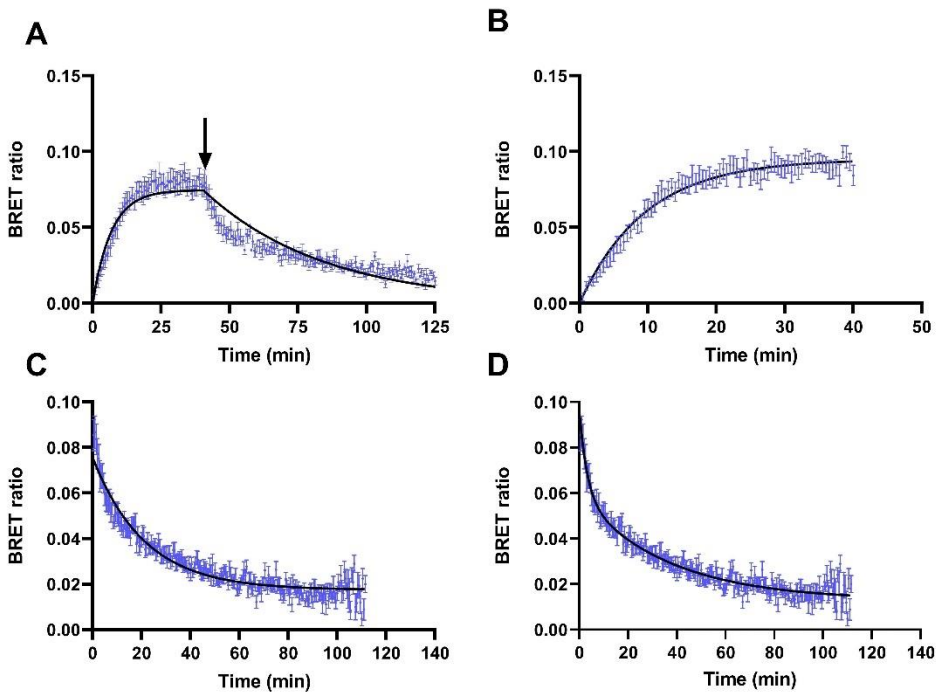

Figure 3-16: Kinetic characterisation of IL23-TMR. (A) The specific association of 300 pM IL23-TMR to HEK293T cells expressing NL-IL23R and IL12Rβ1, followed by dissociation of IL23-TMR by replacement of media with 30 nM IL-23. An arrow indicates the time-point at which media was replaced. The data were fit with Equation 6. (B) The specific association of 300 pM of IL23-TMR plotted fit with Equation 10. (B) (C) The dissociation shown in (B) fit with a one-phase decay model (Equation 7). (D) The data from (C) fit with a two-phase decay model (Equation 8). Data are mean ± SEM from four independent quadruplicate experiments.

Model	k_{on} (M^{-1} min^{-1})	k_{off} (min^{-1})	Residence time (min)	K_d (pM)
Association then dissociation (Equation 6)	3.96 ± 0.35 x 10^8	0.0228 ± 0.0028	46.5 ± 5.4	58.1 ± 6.1
Single phase decay (Equation 7)	1.86 ± 0.13 x 10^9 (Calculated from k_{off} and equilibrium affinity)	0.0503 ± 0.0036	20.3 ± 1.6	N/A
Two phase decay (Equation 8)	N/A	K_{fast} = 0.358 ± 0.0512 % fast = 44.0 ± 1.1 K_{slow} = 0.0122 ± 0.006 % slow = 56.9 ± 0.1	Fast = 3.07 ± 0.50 Slow = 44.0 ± 11.5	N/A
One phase association (Equation 10)	3.73 ± 0.46 x 10^8	0.0101 ± 0.0012 (Calculated from k_{on} and equilibrium affinity)	106 ± 15	
Equilibrium binding (Equation 1)	N/A	N/A	N/A	27.0 ± 3.6

Table 3-2: IL23-TMR kinetic parameters measured in Figure 3-16 (Equilibrium values are from Figure 3-13). Values are Mean ± SEM.

3.4.8 Validation of SNAP and HT-IL12Rβ1 IL23-TMR binding

Before SNAP and HT labelled IL12Rβ1 constructs could be used to measure intra-receptor BRET, ligand binding assays were carried out to confirm that the labelling of IL12Rβ1 did not prevent IL-23 engagement with the receptor. When increasing concentrations of IL23-TMR was applied to HEK293T cells transiently expressing NL-IL23R and SNAP or HT labelled IL12Rβ1 it was observed that specific binding occurred in both cases (Figure 3-17). The affinity

of IL23-TMR was 454 ± 43 pM for NL-IL23R expressed with SNAP-IL12Rβ1 and 179 ± 8 pM for NL-IL23R with HT-IL12Rβ1, which was a 16.8 and 6.6-fold decrease in affinity respectively from the affinity of IL23-TMR binding to NL-IL23R and IL12Rβ1.

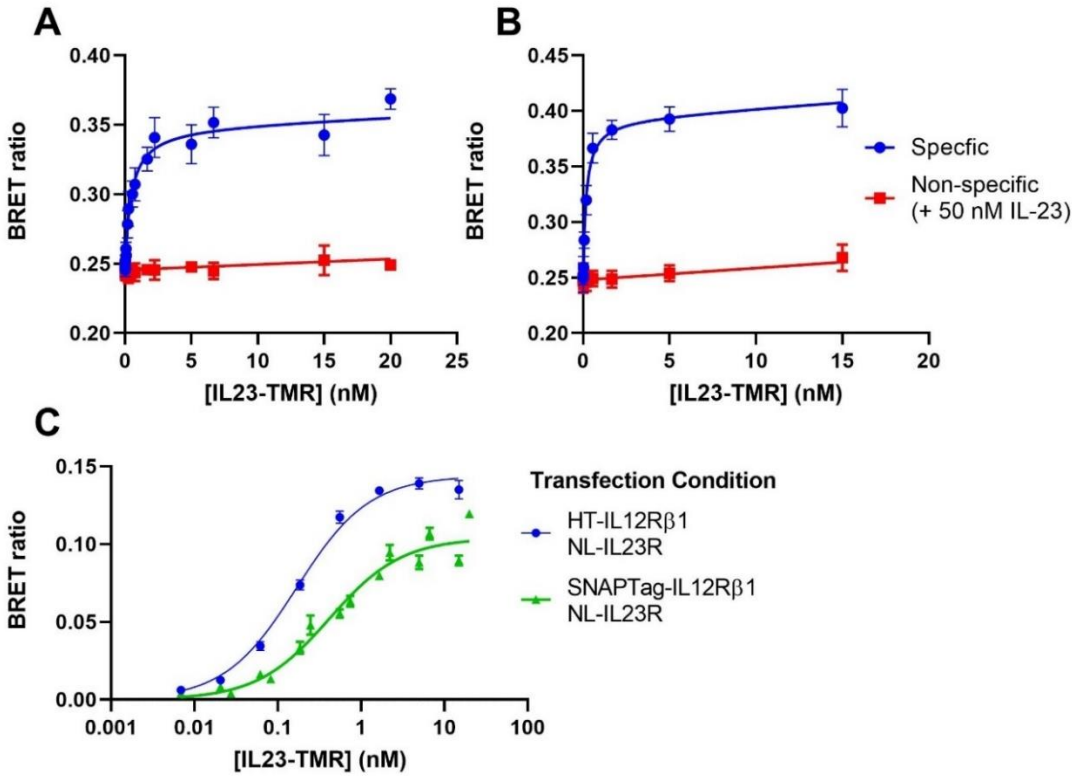

Figure 3-17: Fusion of SNAP-Tag or HaloTag to IL12Rβ1 does not block ligand binding. (A-B) The binding of IL23-TMR to cells expressing NL-IL23R and either HaloTag (A) or SNAPTag (B) fused IL12Rβ1, in the presence or absence of 50 nM unlabelled IL-23. Data are mean with SEM from five (A) or three (B) independent experiments and are fit with Equation 1. (C) The specific binding data shown in (A) and (B) with non-specific subtracted, fit with Equation 2.

3.4.9 Measuring the ligand independent association of IL23R and IL12Rβ1

To ascertain the level of constitutive association between IL12Rβ1 and IL23R, HEK293T cells were transfected with varying concentrations of *N*-terminal fused SNAP-IL12Rβ1 plasmid with a constant concentration of NL-IL23R plasmid. The BRET signal between NanoLuc and AF488 bound to the SNAP-Tag was then measured in the presence and absence of 5 nM IL-23. BRET was observed between the subunits both with and without IL-23 with the signal amplitude in the absence of IL-23 being 54.5 ± 3.9% that of the signal with IL-23 (Figure 3-18A). The level of SNAP-IL12Rβ1 expression increased in a linear

fashion with plasmid concentration (Figure 3-18B), as quantified by fluorescence intensity measurements before NanoLuc substrate addition, however the BRET signal was saturable with increasing SNAP-IL12Rβ1 plasmid concentration (Figure 3-18C). This demonstrated that the increase in BRET signal was due to specific interactions of the constructs rather than non-specific BRET in the membrane. The BRET ratio obtained for the interaction between NL-IL23R and SNAP-IL12Rβ1 was significantly increased by 5 nM IL-23 ($p<0.0001$; t test). The ng/well of SNAP-IL12Rβ1 transfected per well could be further transformed into pmol/well of SNAP-IL12Rβ1 construct using the SNAP-Tag AF488 curve outlined in Figure 3-7A. Whilst the data shown in Figure 3-18D and E was fitted with a specific binding model accurate prediction of the pmol/well of SNAP-IL12Rβ1 required to saturate NL-IL23R was complicated due to the inability to measure the effect of bi-standard on the cell surface and hence correct for a linear increase in signal with increasing expression. The lack of full saturation, especially in the absence of IL-23 meant that the fitting model could not accurately predict the B_{max} of the curve, giving $BRET_{50}$ predictions of 0.0167 ± 0.0094 and 0.0840 ± 0.0409 pmol/well SNAP-IL12Rβ1 in the presence and absence of 5 nM IL-23 respectively. There can be no confidence in the latter value as it is outside of the concentration range tested. An F test used to compare with K_d values predicted by the fitting models suggested that they were significantly different (p value = 0.0037).

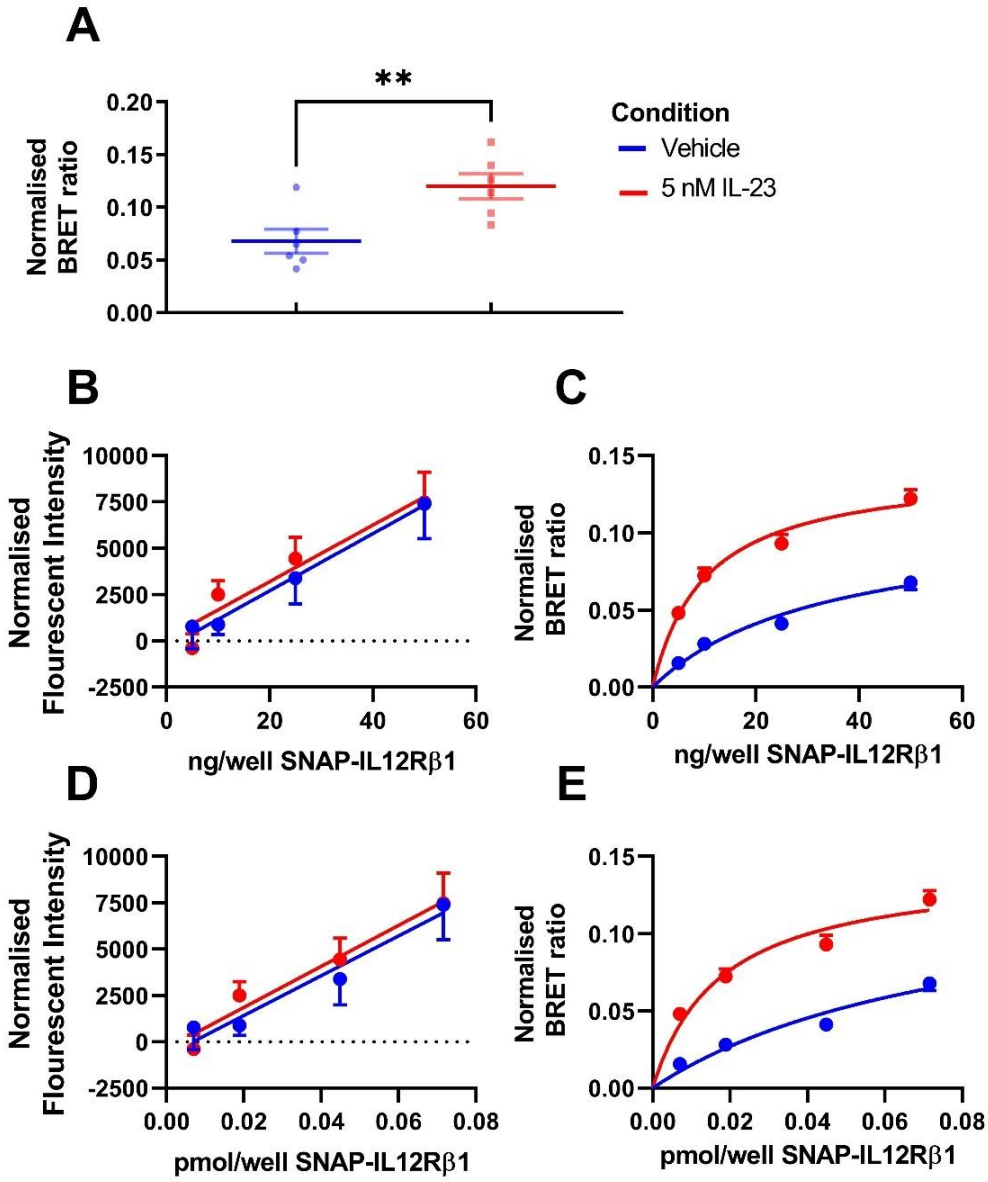

Figure 3-18: Association of IL12Rβ1 and IL23R in the absence of IL-23. (A) The BRET values generated from cells transfected with 50ng of both NL-IL23R and SNAP-IL12Rβ1 and labelled with SNAPTag AF488 substrate, ** denotes a p value of less than 0.005 (unpaired T test). (B) The fluorescence intensity of cells transfected with 50ng of NL-IL23R and increasing concentrations of SNAP-IL12Rβ1 cDNA and labelled with SNAP-AF488 substrate, normalised to the signal from cells expressing NL-IL23R in isolation. (C) The normalised BRET ratio generated from the cells used in (B) after furimizine was added (fit with Equation 2). (D) and (E) the data shown in (B) and (C) respectively with the X axis transformed to pmol/well SNAP-IL12Rβ1 as calculated from the normalised fluorescent intensity values using a SNAP-AF488 substrate standard curve (Figure 3-7). Data are mean ± SEM from five independent experiments.

3.4.10 Ligand induced changes in intra-receptor BRET

To determine how the receptor-subunit *N*-terminal proximity or orientation changed during the formation of the ligand bound IL-23 receptor complex, a BRET assay was carried out in which HEK293T cells were co-transfected with equal concentrations of NL-IL23R and *N*-terminal SNAP-Tag or HaloTag fused IL12Rβ1 plasmids. The receptor was fluorescently labelled by addition of SNAP-Tag AF488 substrate to the SNAP-Tag or HaloTag 618 (HT618) ligand to the HaloTag. Incubation with increasing concentrations of IL-23 led to changes in the BRET ratio with EC_{50} values of 42.9 ± 10.3 (n=5) and 43.6 ± 15.8 (n=5) pM for the SNAP-Tag and HaloTag assays respectively (No statistical difference; unpaired t test; Figure 3-19A). However, whilst the SNAP-IL12Rβ1 assay gave an increase in BRET signal following addition of IL-23, in the HaloTag-IL12Rβ1 assay BRET signal decreased with increasing concentrations of IL-23. A comparable BRET assay was also established using HEK293T cells transfected with both NL-IL12Rβ1 and HaloTag-IL23R. This assay demonstrated an increase in BRET with addition of IL-23 but gave a higher EC_{50} value of 457 ± 209 pM (Figure 3-19C-D). Taken together, these data are consistent with a change in conformation of the IL23R:IL12Rβ1 complex rather than an increase in the formation of these complexes following agonist addition. In all tagging conformations there was a statistically significant change in BRET ratio after incubation with IL-23 (Figure 3-19E-G; results discussed in section 3.5).

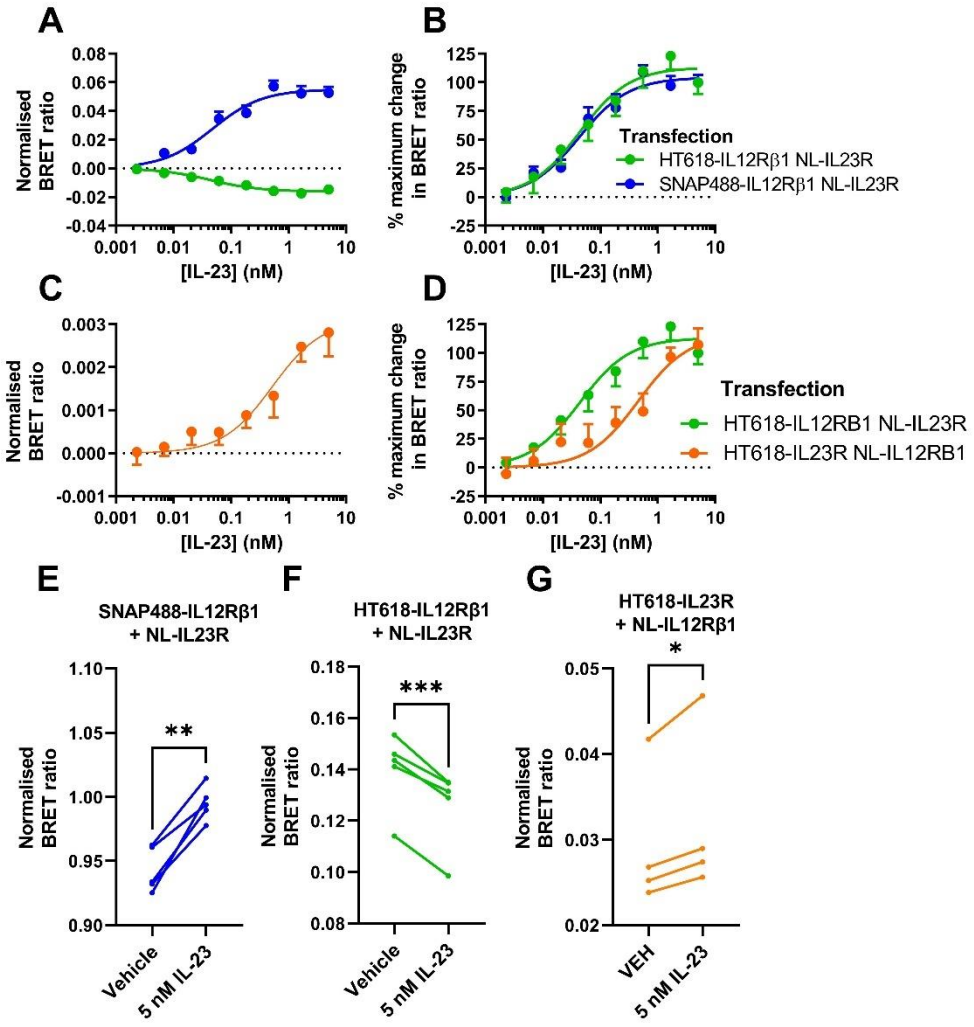

Figure 3-19: Changes in the position of the *N*-terminal regions of IL12Rβ1 and IL23R following binding of IL-23. (A) The intra-receptor BRET between HT618-IL12Rβ1 (green) or SNAP488-IL12Rβ1 (blue) co-expressed with NL-IL23R on HEK293T cells after incubation with increasing concentrations of IL-23. Data show mean ± SEM of background-corrected BRET signals from five independent experiments. (B) The data from (A) normalised to % of the maximum inhibition or induction of BRET. (C) The effect of IL-23 on the intra-receptor BRET between HT618-IL23R co-expressed with NL-IL12Rβ1. Data show mean ± SEM of background-corrected BRET signals from four independent experiments. (D) The data from (C) normalised to % of the maximum inhibition or induction of BRET with the equivalent data for HT-IL12Rβ1 and NL-IL23R plotted for comparison. All data were fit to Equation 2. (E-F) The statistical significance (paired t test) of the changes in BRET measured when 5 nM IL-23 is applied to the cells used in A-C. *** denotes a p value of 0.005, ** denotes a p value of 0.05 and * denotes a p value of <0.5.

3.5 Discussion

The IL-23 cytokine and its receptor are important therapeutic targets (Verreck et al., 2004; Werner et al., 2011). However, many aspects relating to the mechanisms by which the IL-23:IL23R:IL12Rβ1 protein complex is formed remain to be fully elucidated. In this chapter, NanoBRET was utilised to measure the affinity of fluorescently labelled IL-23 to NanoLuc fusions of the full-length individual IL23R and IL12Rβ1 receptor subunits and the full-length IL-23 receptor heteromeric complex in living cells.

Before NanoBRET assays were carried out, reagents needed to be designed, created, and characterised. Mammalian plasmid expression constructs containing NanoLuc tagged IL23R and IL12Rβ1 were generated by custom synthesis and their cellular surface expression was confirmed by luminescence and immunocytochemical imaging. A standard curve of NanoLuc allowed the estimation of receptor expression level in units of pmol/well of the 96-well assay microplate. Interestingly it was observed that NL-IL12Rβ1 was expressed at a higher level than NL-IL23R after transfection of HEK293T cells with an equivalent mass of expression plasmid. This observation corresponds to immune cell RNA-seq datasets available from www.proteinatlas.org which demonstrate that in all tested cell types there is a higher number of IL12Rβ1 transcripts than that of IL23R (Karlsson et al., 2021; Monaco et al., 2019; Schmiedel et al., 2018). In addition, it was observed that co-expression of IL12Rβ1 decreased NL-IL23R expression, an effect that could be explained by an increased burden on the cellular protein synthesis and secretary machinery. However, co-expression of IL23R with NL-IL12Rβ1 increased the expression of NL-IL12Rβ1 possibly indicating that IL23R expression has a chaperone like effect on IL12Rβ1 expression, by aiding protein folding and/or surface expression. An example for how this effect could be mediated is the interaction between EBI3 (an IL-12 family cytokine component) and IL23R, in which EBI3 reduces IL23R misfolding via interaction with the Endoplasmic Reticulum (ER) resident chaperone calnexin, thereby increasing expression (Mizoguchi et al., 2020). Regulation of surface expression by interacting membrane proteins has previously been described for several receptor types, for example the interaction

between the sulfonylurea receptor and the potassium channel subunit Kir6 (Chan et al., 2003).

The transiently transfected HEK293T methodology is an overexpression system in which the IL-23 receptor components are strongly expressed by a viral Cytomegalovirus (CMV) promoter rather than the endogenous promoter in a cell line that does not normally express the proteins (evidenced by the lack of RNA transcripts measured in experiments by the Human Protein Atlas; Uhlen et al., 2019). This is useful as it allows the measurement of interactions with receptor subunits expressed in isolation and prevents artefacts from endogenous protein, however, it is important to be mindful of the limitations of this approach as a model of disease relevant cell types. It is difficult to compare the expression of IL-23 receptor components in the NanoBRET system to that of endogenous cell lines due to a lack of published data for IL23R and IL12Rβ1 expression. The level of IL-12 binding sites on activated human lymphocytes has been measured to be 1-9 x 10^3 per cell (Chizzonite et al., 1992), although there may be more IL12Rβ1 expressed on these cells than the number of receptor complexes. In the intra-receptor NanoBRET experiment there were 4.5 x 10^4 NL-IL23R receptors per seeded cell and 1.2 x 10^5 or 1.2 x 10^6 SNAP-IL12Rβ1 receptors per seeded cell when cells were transfected with 5 or 50 ng/well of plasmid respectively. As the cells had 24 hours to multiply after seeding and transfection efficiency will not be 100%, it is difficult to estimate the exact number of receptors per cell at the time of the experiment.

Fluorescent IL-23 was generated via a non-specific labelling protocol that coupled TAMRA moieties to amine groups within the protein (lysine residues and the *N*-termini). There are 3 lysines in IL23p19 and 26 lysines in IL12p40. The efficiency of coupling is related to the protonation of these lysine residues which can be affected by the microenvironment of the residue within the protein, resulting in different levels of modification at different residues within the protein (Nanda and Lorsch, 2014). Interestingly LC-MS data demonstrated that the majority of TAMRA residues (64.9%) were located on IL23p19 despite the lower level of lysine residues within this protein. This result indicated that one or more residues within IL23p19 may be preferentially labelled. It has been demonstrated that the IL23p19 lysine residue K164 is a key mediator of

interactions with IL23R (Bloch et al., 2018), the observation that IL23-TMR has comparable affinity to IL-23 for the IL-23 receptor, indicated that K164 was not modified, and so the preferentially labelled residue is likely to be the *N*-terminus K39 and/or K102 (possible labelling sites are shown in Figure 3-20).

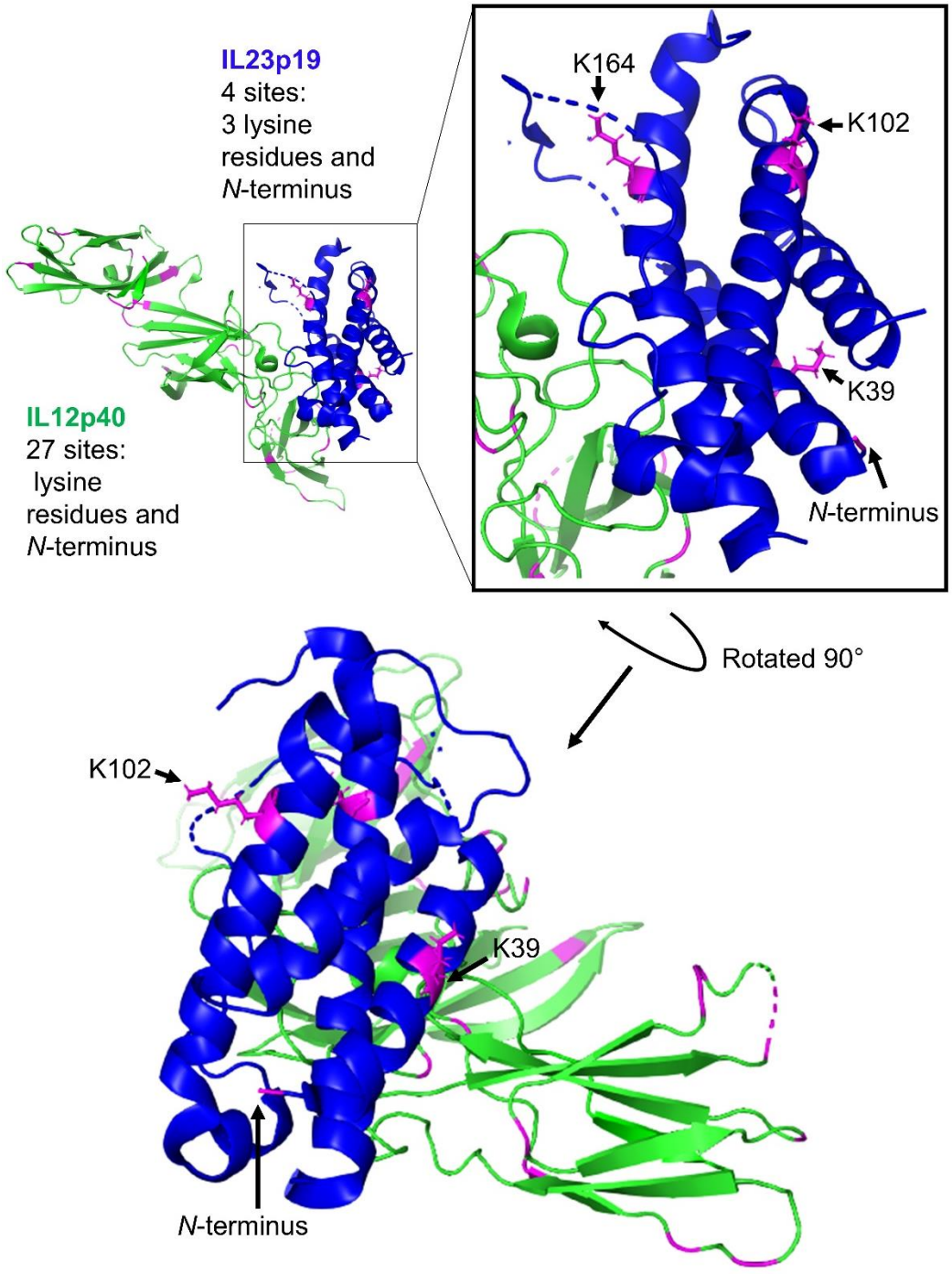

Figure 3-20: The potential NHS-TAMRA labelling sites in IL-23. A crystal structure of IL-23 (PDB: 5MZV) is shown with IL23p19 in blue and IL12p40 in green. Potential labelling sites (lysine residues and the *N*-termini) are shown in purple. As LC-MS data demonstrated that IL23p19 was the predominant labelling site, this subunit is focussed on,

A previous study that characterised the interaction of IL-23 with the purified extracellular domains of the IL23R and IL12Rβ1 receptor subunits using isothermal calorimetry, indicated that IL-23 has a much higher affinity for the extracellular domain of IL23R (44 nM) than the extracellular domain of IL12Rβ1 (2 μM) (Bloch et al., 2018). These observations led Bloch and colleagues to suggest that the binding of IL-23 involved a sequential mechanism whereby IL-23 binds first to the IL23R subunit and then induces a dimerization step between the IL23R:IL-23 complex and IL12Rβ1 leading to the formation of the active cytokine:receptor complex (Bloch et al., 2018).

In this chapter, the dissociation constant of IL23-TMR binding to full-length cell surface expressed NL-IL23R was determined to be 222.2 ± 71.1 nM. However, the dissociation constant of IL23-TMR binding to the full-length NL-IL12Rβ1 in intact cells was 30.1 ± 5.5 nM. This is nearly an order of magnitude lower than the value obtained for IL23R and suggests that the sequence of events suggested using purified protein may need to be re-evaluated when considering results from cell expressed proteins. The higher affinity of IL23-TMR for IL12Rβ1 in live cells is consistent with previous reports that cells expressing IL12Rβ1 have a 2-5 nM affinity for the IL-12 cytokine (Chua et al., 1994). This observation is pertinent to the results presented in this chapter, given that IL-12 and IL-23 heteromers share the IL12p40 cytokine subunit and have both been shown to engage their receptors in a similar manner (Glassman et al., 2021).

When NL-IL23R was co-expressed in cells alongside unlabelled IL12Rβ1, the affinity for IL23-TMR was increased by nearly four orders of magnitude to 27.0 ± 3.6 pM (see Figure 3-13). This suggests that a high affinity binding site for IL23-TMR is formed by oligomeric complexes containing both IL23R and IL12Rβ1 on the cell surface. To further characterise this binding site, the affinity of unlabelled IL-23 in cells expressing both NL-IL23R and IL12Rβ1 was measured using a competition binding assay. The results of these competition experiments (see Figure 3-15) confirmed that the IL23R:IL12Rβ1 complex had a high affinity for the untagged IL-23 cytokine, K_d = 31.6 pM, which was similar to that measured for IL23-TMR, indicating that the labelling of IL-23 had not influenced its affinity for the receptor. The affinity of IL23-TMR for cells expressing NL-IL12Rβ1 and IL23R (measured using a 1:10 expression ratio)

was 24-fold weaker than that measured for cells expressing NL-IL23R and IL12Rβ1. This may be due to an excess of monomeric NL-IL12Rβ1 contributing to a weaker affinity, which is supported by the measurement of both 28 pM and 72 nM affinity components when the interaction of IL23-TMR with cells expressing a 1:1 ratio of NL-IL12Rβ1 and IL23R was fit using a two binding site model (see Figure 3-14). However, this weakened affinity could also be the result of an interference of the NanoLuc tag with IL23-TMR binding when positioned on the *N*-terminus of IL12Rβ1.

The binding kinetics of IL23-TMR were also measured utilising a real-time NanoBRET experimental set up (see Figure 3-16). Previously, the binding kinetics of IL-23 to the purified and immobilised extracellular regions of the IL-23 receptor proteins together and in isolation was measured using Surface Plasmon Resonance (SPR) and reported in a patent filing (Bourne, et al., 2017). Interestingly this experiment contradicted the previous ITC data generated using purified protein and demonstrated a higher affinity of IL-23 for IL12Rβ1 over IL23R. When the association and dissociation of IL-23 was measured for the extracellular portions of both IL23R and IL12Rβ1 immobilised to the same chip, the k_{on} was reported to be 3.79 x 10^7 M^{-1} min^{-1} which is 29.8-fold slower than the rate measured for IL23-TMR associating to live cells expressing the full-length receptor in this chapter. The corresponding SPR k_{off} value was 0.0069 min^{-1} which was 5.30-fold slower than the NanoBRET live cell measurement. These values are remarkably similar considering the differences between the techniques used, indeed, the SPR rates predict an affinity for IL-23 only 6.62-fold weaker than the affinity of IL23-TMR for receptor expressed on live cells. Interestingly, the dissociation of IL23-TMR from the receptor appeared to be biphasic this may be the result of the dissociation being made up of both fast and slow components or could potentially be explained by a co-operative mechanism in which the unlabelled IL-23 increases the rate of IL23-TMR dissociation.

To determine whether IL23R and IL12Rβ1 proteins can form constitutive heterodimers in the absence of ligand in HEK293T cells, and to what extent this is influenced by agonist treatment, BRET was measured between NL-tagged IL23R and a fluorescently labelled SNAP-Tag fusion of IL12Rβ1 (see Figure 3-18). These experiments demonstrated that IL12Rβ1 and IL23R form dimers in

the absence of IL-23, as demonstrated by the saturable increase in BRET ratio obtained with increasing amounts of transfected SNAP-IL12Rβ1. Furthermore, following the addition of IL-23 (5 nM) there was an increase in the BRET ratio obtained for the interaction between NL-IL23R and SNAP-IL12Rβ1. Addition of IL-23 produced a concentration-dependent increase in BRET ratio in HEK293T cells transfected with a 1:1 ratio of NL-IL23R and SNAP-IL12Rβ1. This interaction had an EC_{50} value of 42.9 pM that was consistent with the high affinity binding site measured in the IL-23 competition assays (K_d = 31.6 pM) when both NL-IL23R and IL12Rβ1 were expressed together in the same cells. However, whilst in the SNAP-IL12Rβ1 assay the BRET signal increased with IL-23 binding, in the HaloTag-IL12Rβ1 assay the BRET signal decreased following ligand binding (see Figure 3-19). The IC_{50} value for this inhibitory effect of IL-23 was very similar (43.6 pM) to the EC_{50} value obtained for the increase in BRET signal in the SNAP-IL12Rβ1 assay. Furthermore, when the HaloTag was fused to IL23R and the NanoLuc tag added to IL12Rβ1, this IL-23 induced decrease in BRET was changed to a large increase in the BRET signal. Cells transfected with this tagging conformation demonstrated a 14.5-fold decrease in the potency of IL-23 induced conformational change as compared to the competitive affinity of IL-23, most likely due to interference of the *N*-terminal tags with ligand binding or the subsequent conformational change.

The resonance energy transfer that occurs between two labelled proteins depends on both proximity (<10nm) and the orientation of the acceptor and donor species (Dacres et al., 2012). In the case of receptors that are labelled with both a donor and acceptor species this can lead to agonist-induced increases or decreases in BRET as a consequence of conformational changes induced by agonist binding (for example; Kowalski-Jahn et al., 2021). Taken together, the observations made in this chapter indicate that the binding of IL-23 to a high affinity binding site formed by an oligomeric complex of IL23R and IL12Rβ1 triggers a change in the relative position of the *N*-terminal domains of the IL-23 receptor components. This is the simplest explanation for the positive and negative BRET signals obtained following IL-23 addition in the intra-receptor BRET assays and is consistent with a conformational change such as a rotation,

in which there is only a minor change in the distance between the components. The SNAP-Tag is a 19.4 kDa protein and the HaloTag is a 33 kDa protein (Crivat and Taraska, 2012) and have different linkers (Table 3-3), it is therefore likely that their orientation with respect to the 19 kDa NanoLuc on tagged proteins can change in different ways as a result of conformational changes induced by IL-23.

Construct	**Tag size (kDa)**	**Linker length (# of amino acids)**	**Linker sequence**
SNAP-IL12Rβ1	19.4	20	STSPVWWNSADIQHSGGRSR
HT-IL12Rβ1	33	13	EPTTEDLYFQSDN
HT-IL23R	33	13	EPTTEDLYFQSDN

Table 3-3: Properties of *N*-terminal tags and their linkers used in intra-receptor BRET assays.

Despite the potential for subtle effects of the NanoLuc fusions and fluorescent labelling on IL-23 binding affinity, the NanoBRET technique has enabled the detection of binding events that are at a far higher order of affinity than any of those previously measured using untagged but truncated purified protein (Bloch et al., 2018). Furthermore, it has been demonstrated that SNAP fusions of IL12Rβ1 and NanoLuc fusions of IL23R do not abrogate the ability of the receptor to initiate signal transduction through the phosphorylation of STAT3. The high affinity binding site identified in this work is in agreement with the EC_{50} values that were measured for downstream phosphorylation of STAT3 and values that others have measured for the IL-23 induced phosphorylation of STAT5 (e.g. Varghese et al., 2020; EC_{50} = 28 pM).

A consensus mechanism of receptor activation for the wider IL-12 cytokine family of receptors has yet to be elucidated. Within the cytokine receptor family, initial suggestions of ligand-induced dimerization (Cochet et al., 1988) have been contradicted by the discovery of pre-formed inactive dimeric receptor complexes (Chua et al., 1994; Couturier and Jockers, 2003; Gent et al., 2002; Schuster et al., 2003). Inactive receptor complexes could be activated by ligand induced conformational change, for example a rotation of the transmembrane domains (reviewed by Maruyama, 2015) resulting in the rearrangement of pre-dimerised trans-inhibiting JAKs allowing phosphorylation and signalling

(Waters et al., 2014). If this is the case for the IL-23 receptor, it is unlikely that the interaction occurs within the extracellular domains of the receptor subunits alone, as it has previously been demonstrated that purified IL23R and IL12Rβ1 extracellular domains have no affinity for each other (Bloch et al., 2018) and even that these domains can be replaced entirely by nanobodies and still initiate signalling with the addition of a synthetic dual antigenic ligand (Engelowski et al., 2018).

Whilst this chapter's results contradict the previous affinity values used to suggest the ligand induced dimerisation of the IL-23 receptor, the observations are consistent with previous reports of pre-dimerised inactive receptor complexes of the IL-23 receptor, within the wider IL-12 family and at other closely related receptors. A study by Sivenesan et al. used IL-23 receptor *C*-terminal fusions of split Renilla Luciferase expressed in HEK293 cells to demonstrate luminescence in the absence of IL-23 and used this as evidence of constitutive association in the absence of ligand (Sivanesan et al., 2016). The authors suggested that IL-23 binding leads to a 'scissor-like' conformational change resulting in activation, similar to the related Erythropoietin Receptor (Remy et al., 1999; Sivanesan et al., 2016).

The initial study outlining the discovery of the IL-12 receptor reported cytokine binding sites of three different affinities on live cells, the authors proposed that the highest affinity 5 to 20 pM site was formed by a pre-formed receptor dimer (Chua et al., 1994). In addition, the deletion of the extracellular stalk region of IL23R has been shown to cause the formation of IL23R receptor subunit complexes that signal in the absence of ligand (Hummel et al., 2017); this observation could be evidence for an inhibitory domain that ordinarily prevents signalling in constitutively formed dimers. The closely related IL-6 receptor, which includes a gp130 subunit highly homologous to IL12Rβ1 (Chua et al., 1994) has also been shown to undergo ligand independent dimerisation (Schuster et al., 2003).

The successful application of NanoBRET technology to the IL-23 receptor, which is the first heterodimeric cytokine receptor and third cytokine receptor to be studied with the technique (after EPOR and TPOR; Jia et al., 2021; Pecquet

et al., 2019), highlights its utility to measure similar interactions at other related cytokine receptors which remain equally under-investigated.

The IL-23 cytokine and its receptor are a target of high therapeutic interest, however the binding mechanism, an important piece of information for drug discovery, had not yet been defined on living cells. This chapter defines the affinity of IL-23 to its full-length receptor in living cells for the first time, demonstrating that dimerisation alone is not sufficient to activate the receptor and indicating that IL-23 binding induces a conformational change in pre-formed receptor complexes. The direct implication of these observations for drug discovery are that a novel potentially druggable interface may exist between IL23R and IL12Rβ1. In further chapters NanoBRET and other proximity-based techniques will be further applied to gain insights into receptor assembly, to characterise peptide antagonists of the receptor and to assess any differences in interactions caused by disease relevant mutations.

Chapter 4. Probing the constitutive association of the IL-23 receptor using NanoLuc Binary Technology

4.1 Introduction

NanoLuc Binary Technology (NanoBiT) is a technique based on a split version of NanoLuc. The enzyme is divided into a large (18 kDa) fragment (LgBiT) and smaller (1.3 kDa) high affinity (HiBit) or low affinity (SmBit) peptides (shown in Table 4-1; Dixon et al., 2016). Fusions of NanoBiT fragments to the termini of targets of interest can be used to monitor the formation and disruption of protein complexes through changes in the production of bioluminescence by the complemented enzyme (Dale et al., 2019). The concentration of HiBit tagged target in a sample can be measured by the addition of purified LgBit component and extracellular protein can be specifically monitored due to the non-permeable nature of exogenous LgBit protein (Soave et al., 2020a).

NanoBiT fragment	**Sequence**	K_d **(M)**
Native peptide	GVTGWRLCERILA	7.0×10^{-9}
HiBit	VSGWRLFKKIS	9.0×10^{-7}
sMBit	VTGYRLFEEIL	1.9×10^{-4}

Table 4-1: Sequences of NanoBiT fragments used in this chapter with native peptide shown for comparison. K_d values are taken from (Dixon et al., 2016).

Understanding of the mechanism of activation of the IL-23 receptor and cytokine receptors more generally is limited. In particular, the way by which extracellular binding translates to JAK activation is not clear. Studies on purified truncated proteins indicated that the IL-23 receptor is activated through a ligand induced dimerization mechanism, whereby IL-23 is first bound by IL23R followed by the recruitment of IL12Rβ1 to the IL-23:IL23R complex (Bloch et al., 2018). However, NanoBRET studies in Chapter 3 utilizing a recombinant cellular system, indicated that the receptor may be activated by the conformational change of pre-associated complexes.

In this chapter, NanoBiT will be utilised to measure the formation of IL-23 receptor complexes in the presence and absence of IL-23 and to assess if heteromers form on the cell surface prior to ligand engagement. Use of NanoBiT complemented receptor complexes as donors for BRET studies will also enable

the study of IL-23's interaction with binary complexes. A summary of the approach is shown in Figure 4-1.

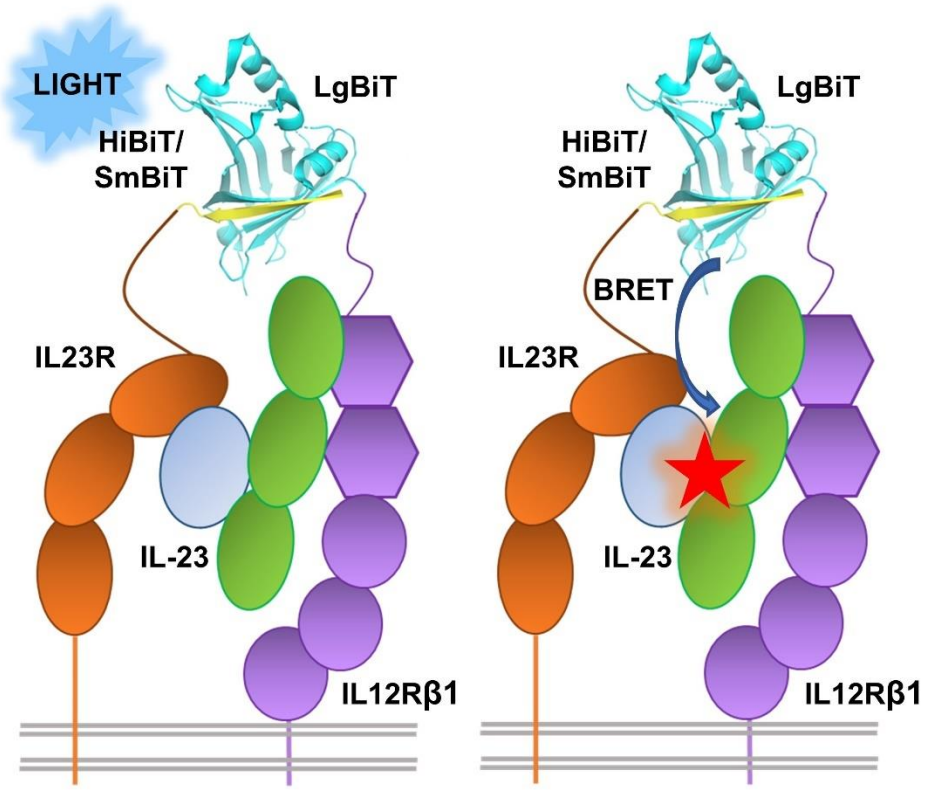

Figure 4-1: A schematic of the planned experimental approaches to be used in chapter 4. The schematic on the left demonstrates how NanoBiT complementation can be used to measure complex formation. The schematic on the right demonstrates how the complemented luciferase can be used to measure interactions with IL23-TMR through BRET. **T**he crystal structure of NanoLuciferase (PDB: 5IBO) is shown, with fragment used to develop HiBit and SmBit coloured yellow.

4.2 Aims

This chapter aimed to utilise NanoBiT technology to quantify IL-23 receptor complex formation in the membrane of living cells in the presence and absence of ligand. The chapter also aimed to construct NanoBiT BRET assays in which complemented receptor complexes were used as donors to measure interactions with fluorescent IL-23. AlphaLISA assays were then used to quantify if NanoBiT tagging or complementation affects phospho-STAT3 signalling in the presence and absence of IL-23. The chapter aimed to use NanoBiT

complementation to probe receptor *N*-terminal position through complementation with exogenous purified protein. Finally, NanoBiT tagged receptor complementation was used to monitor competition between receptor monomers to form receptor complexes.

4.3 Methods

4.3.1.1 NanoBiT constructs

HiBit-IL23R and SmBit-IL23R expression constructs were generated by restriction cloning IL23R into pcDNA.3.1 expression vectors containing *N*-terminal HiBit or SmBit tags (kindly donated by Dr Mark Soave; Soave et al., 2020), using restriction enzymes Xba1 and BamH1. This resulted in linkers with the sequence SSGGSSGGSTSPVWWNSADIQHSGGRSR. LgBit-IL23R and LgBit-IL12Rβ1 expression plasmids were generated in a similar manner by restriction cloning IL23R and IL12Rβ1 into a pcDNA 3.1 expression vector containing *N*-terminal LgBit with a murine 5-HT3A receptor secretion signal (kindly donated by Dr Mark Soave; Soave et al., 2020b), again using Xba1 and BamH1. This procedure left a linker with the sequence GSSGEDLYFQSGSTSPVWWNSADIQHSGGRSR. HiBit-IL23R with a truncated linker was created by site directed deletion of an 18-amino acid portion of the linker from the previously generated HiBit-IL23R plasmid using a site-directed mutagenesis kit and phosphorylated primers specific to the regions adjacent to the deletion (as described in section 2.3.3.2). The resulting construct had a linker with the sequence SSGGSSGGST. Successful insertion of the genes and completion of the planned deletions were confirmed by sanger sequencing (as described in section 2.3.3.3).

4.3.2 Transfections.

HEK293T cells were transiently transfected using both the batch (see section 2.5.1.1) and single well (see section 2.5.1.2) methodologies. To equalise the expression of IL23R and IL12Rβ1 constructs, transfection mixes were made up containing a 1:4 ratio of IL12Rβ1 to IL23R constructs.

The batch transfection protocol was employed for experiments in which cells were treated with increasing concentrations of protein, except for the experiments which assessed the IL23R C115Y mutation. All other experiments utilized the 96-well transfection methodology.

4.3.3 Measurement of luminescence and BRET from NanoBiT complemented cells.

96-well microplates containing transfected cells had media removed and replaced with HBSS with 1 mg/mL Bovine Serum Albumin (BSA) with or without purified IL-23, HiBit or LgBit protein. Cells were then incubated for 1 hour, before 5 µL of 77 µM furimizine was added to each well. The microplate was incubated for 5-minutes before a white plate back was added and luminescence readings were measured using a PheraStar FS plate reader with gains of 3600.

When BRET signal was measured from NanoBiT construct expressing cells, a white plate back was added to the microplate and the signal measured on a PheraStar FS plate reader using a 450 nm (30 nm bandpass) and >550 nm filter with gains of 2800 and 3600 respectively.

4.3.4 Measurement of HaloTag fluorescence intensity.

Cells were incubated with media containing 200 nM Alexa Fluor (AF) 488 HaloTag ligand for 30 minutes. Cells were then washed three times with 50 µL HBSS followed by the addition of 50 µL HBSS with 1 mg/mL BSA and measurement of fluorescence intensity using a PheraStar FS plate reader using an excitation laser at 485 nm and emission at 520 nm.

4.4 Results

4.4.1 Luminescence generated by *N*-terminal NanoBiT fusion constructs

Plasmid DNA constructs containing *N*-terminal HiBit, SmBit and LgBit fusions of IL23R and a LgBit fusion of IL12Rβ1 were transiently expressed in HEK293T cells. Figure 4-2A demonstrates that each of these constructs generated little luminescence when expressed alone and supplied with the NanoLuc substrate furimizine. To test whether the constructs were surface expressed and retained the ability to be complemented by corresponding NanoBiT fragments, exogenous purified HiBit or LgBit protein was added. It was observed that luminescence was produced when the corresponding fragment was expressed on the *N*-termini of an IL-23 receptor monomer. The highest signal was observed for HiBit-IL23R complemented with LgBit, with a lower signal observed for the SmBit-IL23R construct due to the lower affinity of SmBit for LgBit.

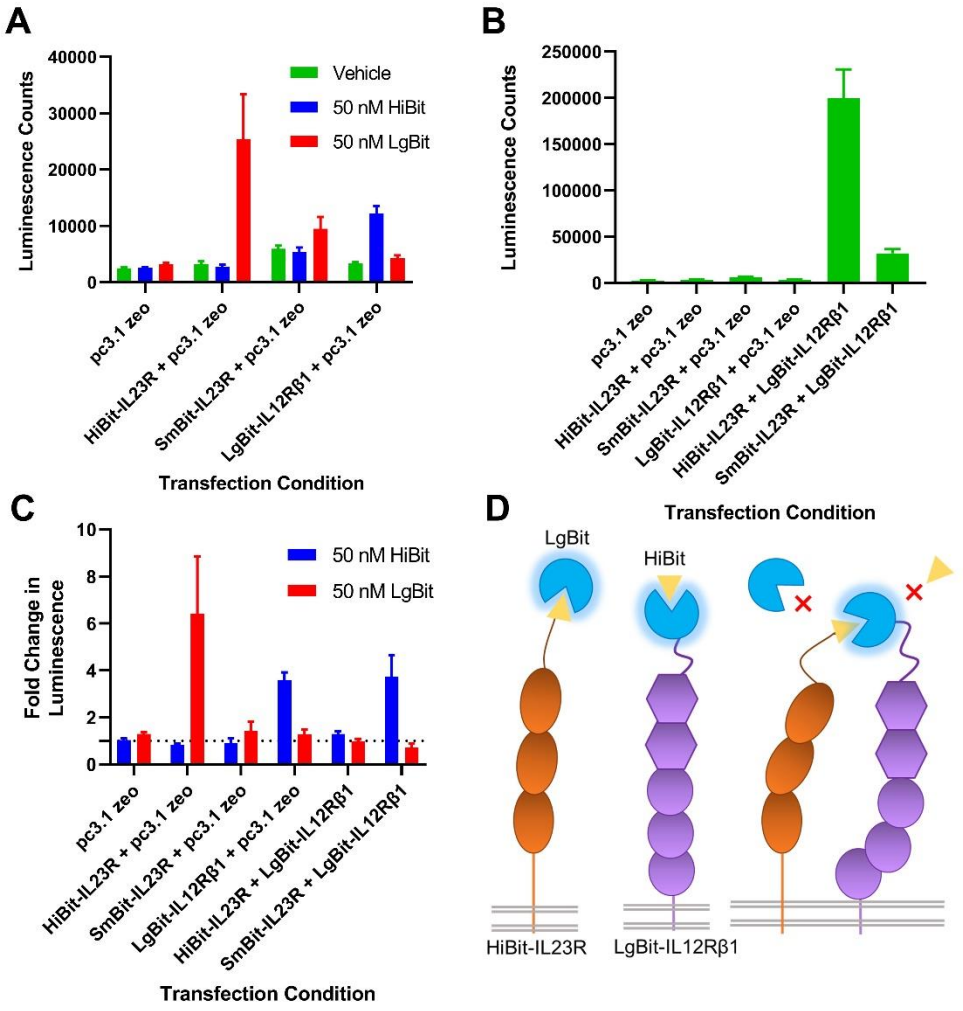

Figure 4-2: NanoBiT tagged IL-23 receptor complexes associate on the cell surface in the absence of ligand. (A) The luminescence generated when HEK293T cells transiently transfected with NanoBiT conjugated IL-23 receptor constructs were incubated with purified NanoBiT reagents. (B) The luminescence signal observed when complementarily tagged NanoBiT constructs were co-expressed together. (C) The fold change in luminescence from the signal observed in (B) when cells were incubated with purified HiBit or LgBit protein. (D) a schematic demonstrating the results of (C). Data are mean ± SEM from five independent experiments which each contained quadruplicate determinations.

When HiBit-IL23R was co-expressed with LgBit-IL12Rβ1, a strong luminescent signal was observed (73.3-fold that of the mean of the receptor constructs expressed in isolation). When an equivalent pairing was expressed containing SmBit-IL23R the signal was weaker (6.19-fold lower), however remained higher than that of the monomers complemented with exogenous protein and was 10.3-fold higher than the mean of receptor constructs expressed in isolation (Figure 4-2B). Finally, when cells expressing the complemented

receptor pairs were exposed to purified HiBit and LgBit protein (Figure 4-2C, D), there was no increase in luminescence in either condition for HiBit-IL23R containing heteromers. There was however an increase in luminescence equivalent to that observed for LgBit-IL12Rβ1 expressed alone when purified HiBit was added to cells expressing the SmBit-IL23R containing heteromer, indicating that this construct had a lower affinity for LgBit-IL12Rβ1 than the equivalent HiBit construct.

4.4.2 Affinity of *N*-terminal NanoBiT fusion constructs for their purified partner

To investigate the affinity of purified HiBit and LgBit to membrane expressed LgBit-IL12Rβ1 or HiBit-IL23R constructs, increasing concentrations of purified protein were added to cells expressing the tagged receptor monomers (Figure 4-3A). HiBit-IL23R had an affinity of 15.2 ± 1.6 nM (n=5) for purified LgBit which was 21.7-fold weaker than the value quoted for HiBit alone (Dixon et al., 2016). When the affinity of purified HiBit control protein for LgBit-IL12Rβ1 was measured it was found that whilst the luminescence signal increased with concentration this signal did not saturate over the concentration range tested (highest concentration equal to 1 μM), which was limited by the stock concentration of commercially available HiBit control protein. The affinity of purified LgBit for cells expressing SmBit-IL23R was also tested, however no luminescence signal was detected over the concentration range used (Figure 4-3B). This observation was expected as the reported affinity for the interaction of SmBit with LgBit is 190 μM (Dixon et al., 2016).

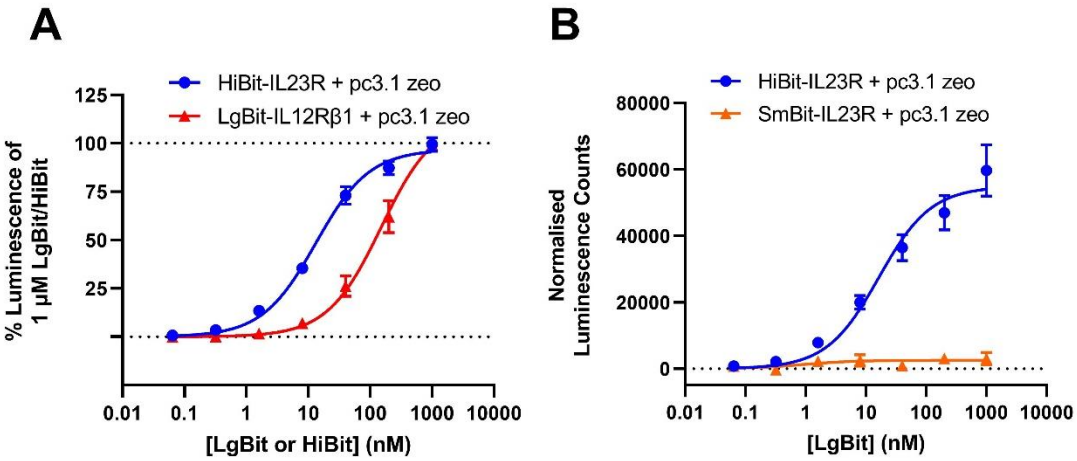

Figure 4-3: The affinity of NanoBiT tagged receptor constructs for purified HiBit or LgBit protein. (A) The normalised luminescence signal generated when increasing concentations of purified complementary NanoBiT fragment were applied to cells transiently expressing HiBit-IL23R or LgBit-IL12Rβ1 in isolation. (B) The luminescence signal generated when increasing concentrations of LgBit were applied to cells expressing either HiBit or SmBit conjugated IL23R. Data are mean ± SEM from five or six (SmBit-IL23R) independent triplicate experiments. Data were fit with Equation 2.

4.4.3 Luminescence imaging of cells expressing NanoBiT complemented receptor

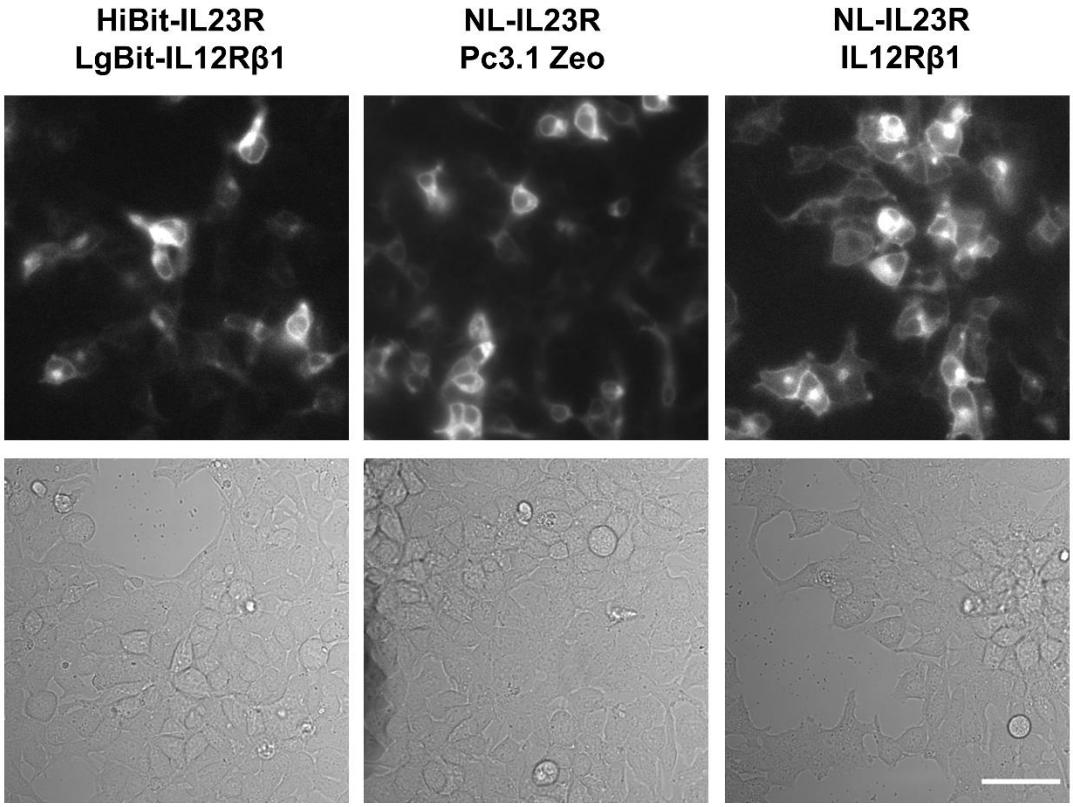

Figure 4-4: Luminescence microscopy demonstrates localisation of NanoBiT heteromers. Luminescence (top) and brightfield (bottom) images of HEK293T cells transiently expressing IL-23 receptor fusions. Images are representative of four (HiBit-IL23R + LgBit-IL12Rβ1) or five independent experiments. Scale bar represents 50 μm.

To assess the localisation of NanoBiT complemented heteromers, luminescence images were taken of cells expressing HiBit-IL23R and LgBit-IL12Rβ1. These images demonstrated luminescence at the periphery of the cell and at intracellular localisations, these observations were similar to NL-IL23R when imaged with IL12Rβ1 under equivalent conditions (Figure 4-4).

4.4.4 Monitoring interactions of IL-23 with binary NanoBiT complemented receptor complexes using BRET

4.4.4.1 Using BRET to measure the binding of IL23-TMR to binary complexes

To test if the NanoBiT heteromers were able to bind cytokine, IL23-TMR was applied to cells expressing HiBit or SmBit-IL23R and LgBit-IL12Rβ1 before measuring the BRET signal generated between the complemented luciferase and IL23-TMR. The luminescence signal generated from the SmBit heteromer was

too low to produce a reliable BRET ratio, however a robust BRET signal was generated using cells transfected with the HiBit heteromer which could be abolished through the addition of unlabelled IL-23. To test whether the affinity of IL23-TMR to exclusively at heteromeric species was increased, the BRET signal was measured after increasing concentrations of IL23-TMR were applied to cells expressing HiBit-IL23R and LgBit-IL12Rβ1 (Figure 4-5), which gave an affinity of 234 ± 40 pM. This value was between that of the previously measured values for IL23-TMR binding to HEK293T cells expressing NL-IL23R and IL12Rβ1 (27.0 ± 3.6 pM; Figure 3-13) and cells expressing IL23R and NL-IL12Rβ1 (647 ± 80 pM; Figure 3-14).

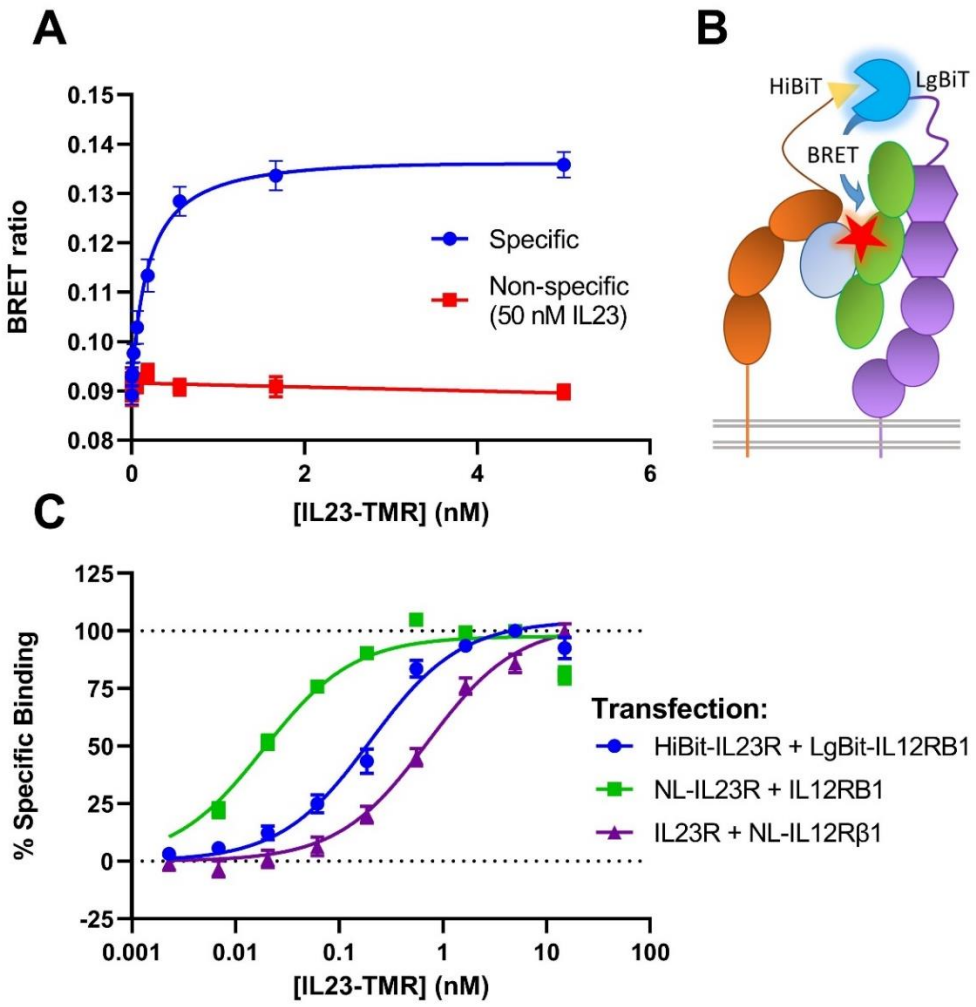

Figure 4-5: NanoBiT complemented IL-23 receptor heteromers bind IL23-TMR with similar affinity to NanoLuc tagged heteromers. (A) The NanoBRET signal generated when increasing concentrations of IL23-TMR were applied to cells expressing HiBit-IL23R and LgBit-IL12Rβ1 (fit with Equation 1). (B) A schematic depicting the assay used in (A). Data are mean ± SEM from five independent experiments which each contained triplicate determinations. (C) The affinity of IL23-TMR for NanoBiT heteromers from (A) plotted against specific binding traces from Figure 3-13 and Figure 3-14 (fit with Equation 2).

4.4.4.2 Confirming the binding of IL-23 to NanoBiT complemented heteromers and measuring the effect on complex formation

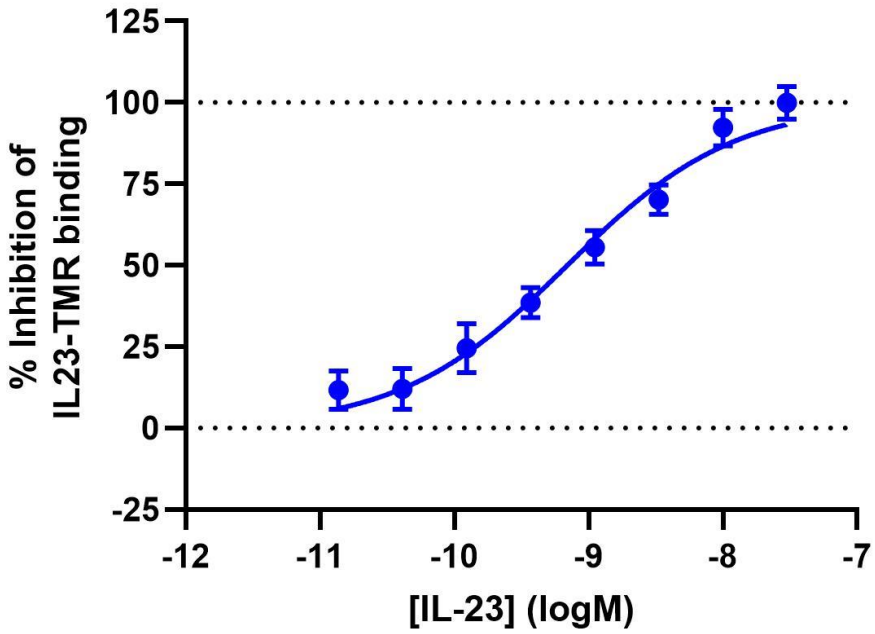

Figure 4-6: Unlabelled IL-23 binds to NanoBiT heteromers. The inhibition of 300 pM IL23-TMR binding to cells expressing HiBit-IL23R and LgBit-IL12Rβ1 by increasing concentrations of unlabelled IL-23. Data are mean ± SEM from five independent experiments and are fit with Equation 4.

To confirm that non-modified IL-23 could also bind to the NanoBiT complemented heteromers, a NanoBRET competition assay was carried out to measure the displacement of 300 pM IL23-TMR from cells expressing HiBit-IL23R and LgBit-IL12Rβ1 by increasing concentrations of IL-23 (Figure 4-6). An IL-23 affinity of 352 ± 155 pM (n=5) was measured, which was comparable to that measured for IL23-TMR. Whilst it was confirmed that both IL23-TMR and IL-23 bound to the NanoBiT heteromers, there was no increase in NanoBiT complementation when IL-23 was added to either SmBit or HiBit heteromers (Figure 4-7). Conversely the addition of IL-23 to cells expressing SmBit complemented heteromers significantly reduced association (paired t test; $p = <0.05$; discussed in section 4.5).

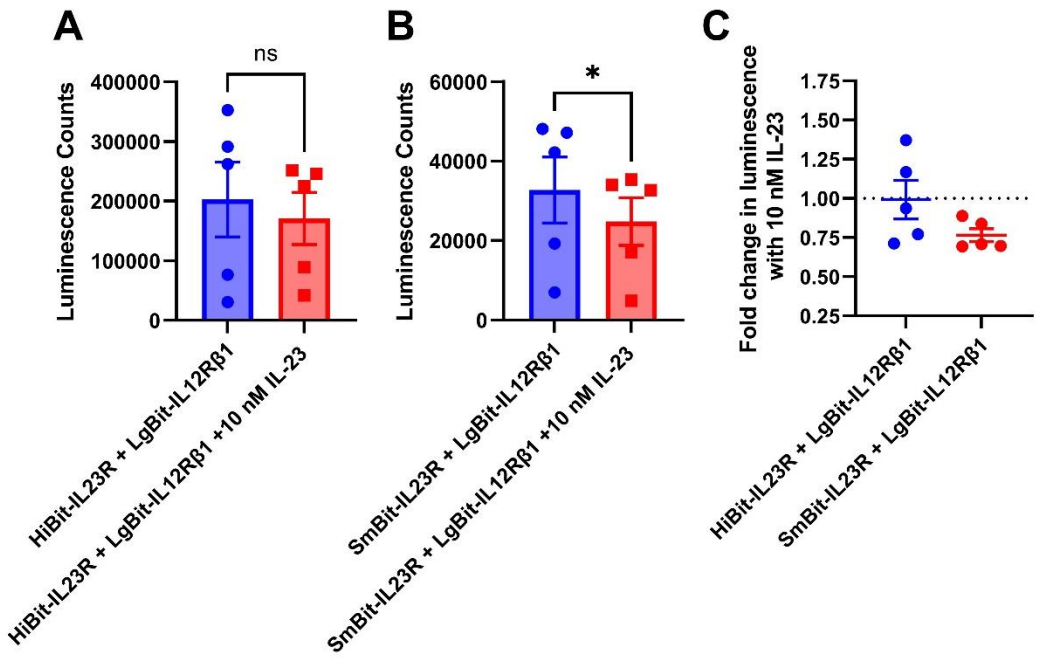

Figure 4-7: NanoBiT heteromers bind IL-23 without any increase in complex formation. (A-B) The luminescence of cells expressing (A) HiBit-IL23R or (B) SmBit-IL23R and LgBit-IL12Rβ1 with or without treatment with 10 nM IL-23. Statistical significance (p = <0.05; paired t test) is indicated by *. (C) The fold change in luminescence generated when cells expressing HiBit or SmBit containing NanoBiT complemented heteromers are incubated with 10 nM IL-23. Data are mean from five independent experiments conducted in quadruplicate with overall mean ± SEM superimposed.

4.4.4.3 The binding kinetics of IL23-TMR engaging binary complexes

To measure the kinetics of IL-23 binding to binary complexes of IL23R and IL12Rβ1, real time BRET measurements were made of IL23-TMR associating with cells co-expressing HiBit-IL23R and LgBit-IL12Rβ1 (Figure 4-8), in an analogous manner to the determination of IL23-TMR kinetics to non-complemented receptors in Chapter 3. After IL23-TMR reached equilibrium, dissociation was initiated by replacement of media with a high concentration of unlabelled IL-23 (Figure 4-8B). Due to the lower BRET signal in this system the association and dissociation fit failed to give reproducible values. However, the k_{off} value was determined from the dissociation plot alone (Figure 4-8B) to be 0.0272 ± 0.0019 min^{-1} (a 1.85-fold slower dissociation than that previously measured from non-complemented receptor). This enabled the calculation of a k_{on} value from IL23-TMR equilibrium K_d (Table 4-2) that was 16.0-fold slower

than the value measured in chapter 3 for IL23-TMR's association to non-complemented receptor indicating that the reduction in affinity of IL23-TMR at the NanoBiT complemented receptor was driven by a reduction in association rate. Interestingly, whilst the dissociation of IL23-TMR from non-complemented receptor was biphasic, this effect was much less pronounced at the NanoBiT complemented receptor. This was demonstrated by a partial F test recommending a monophasic fit for the 300 pM concentration and a biphasic fit with a 29.9% Kfast component for the 2 nM concentration.

The dissociation and association rates were also calculated from the k_{obs} of the association of single concentrations of associating ligand (Figure 4-8A) using Equations 9 and 10. This analysis yielded values that were similar to the association (1.22-fold faster) and dissociation (1.22-fold slower) rates calculated from the dissociation plot. As more than one concentration of IL23-TMR was used, a global fit of association data could have been used (Prism's 'Association kinetics - Two or more conc. of hot.' Analysis). However, when data was analysed using this methodology the results were unstable, most likely due to the low number of concentrations used and variability in the data.

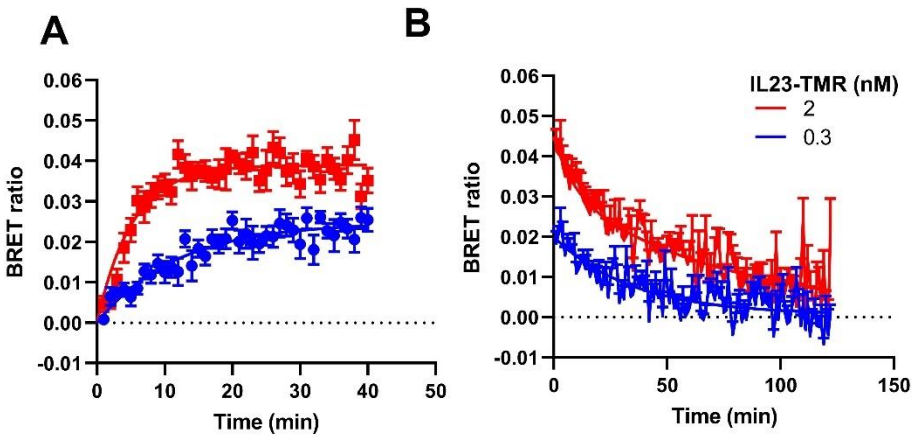

Figure 4-8: The kinetics of IL23-TMR binding to NanoBiT complemented IL-23 receptor. (A) The specific association of IL23-TMR, fit with a one phase association (Equation 9). (B) The dissociation traces of IL23-TMR after the association shown in (A) by replacement of the media with 30 nM of unlabelled IL-23, fit with a single-phase decay equation (Equation 7). Data are mean ± SEM from four (300 pM) or three (2 nM) independent experiments with triplicate determinations.

Model	k_{on} (M^{-1} min^{-1})	k_{off} (min^{-1})	Residence time (min)	K_d (pM)
Single phase decay (Equation 7)	1.17 ± 0.09 x 10^8 (Calculated from k_{off} and equilibrium affinity)	0.0272 ± 0.0019	36.8	N/A
Single phase association (using equations 9 and 10)	1.42 ± 0.21 x 10^8	0.0332 ± 0.0049 (Calculated from k_{on} and equilibrium affinity)	30.1	N/A
Equilibrium binding	N/A	N/A		234 ± 40

Table 4-2: The kinetic rates measured for IL23-TMR associating to NanoBiT complemented heteromers. Data are mean ± SEM from four 300 pM and three 2 nM experiments.

4.4.5 Homodimeric and heterotrimeric complexes

To test if homomeric receptor complexes or multimeric species containing more than one of each receptor unit were formed, the luminescent signal generated by homomeric pairings of IL23R and IL12Rβ1 were also tested (Figure 4-9A). A luminescent signal was generated by both the HiBit and SmBit homomeric pairings of IL23R indicating that complexes were forming containing at least two IL23R proteins, however the luminescence signal was half the amplitude (HiBit 2.12-fold and SmBit 2.18-fold) of the equivalent heteromeric condition. As with heteromeric pairings the HiBit homomer signal was stronger (6.36-fold) than that of the SmBit homomer. Co-expression of IL12Rβ1 with HiBit complemented IL23R homomers reduced the signal measured (6.73-fold). Homomeric HiBit complemented pairings of IL12Rβ1 produced a greater signal than that of heteromeric pairings (1.91 or 2.13-fold for HiBit-IL12Rβ1 or HiBit-IL23R containing heteromers respectively). The co-expression of IL23R with these homomers moderately reduced the signal measured (0.29-fold). Treatment

of homomers with IL-23 in the presence or absence of their co-receptors did not lead to significant changes in luminescence (paired t test Figure 4-9B).

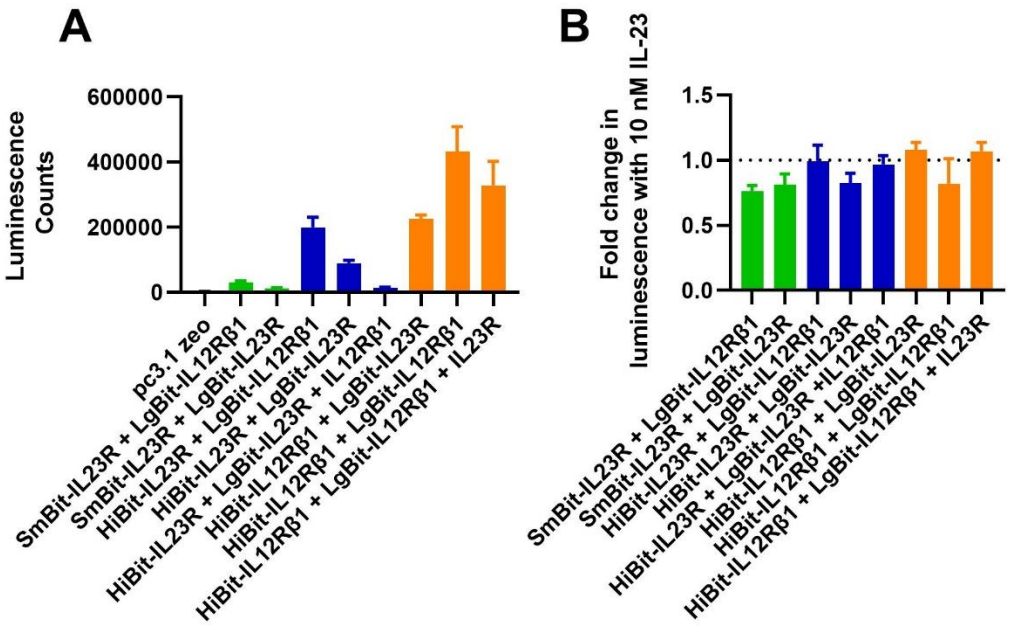

Figure 4-9: Formation of NanoBiT linked homomers of IL23R and IL12Rβ1. (A) The luminescence generated from cells transfected with different combinations of NanoBiT constructs. (B) The fold change in luminescence when the cells from conditions in (A) are treated with 10 nM IL-23. Data are mean ± SEM from five quadruplicate or three triplicate (HiBit-IL12Rβ1 containing conditions) independent experiments.

The addition of purified HiBit and LgBit to cells expressing HiBit complemented homomers of IL23R revealed that there were no reserve of either uncomplemented receptor construct, however when the homomers were expressed with IL12Rβ1 both LgBit and HiBit tagged IL23R could interact with purified protein, indicating that IL12Rβ1 directly disrupted these complexes (Figure 4-10A). Homomers of HiBit-IL23R and LgBit-IL23R did not generate a BRET signal when treated with 10 nM IL23-TMR, however when cells were co-transfected with HiBit-IL23R, LgBit-IL23R and IL12Rβ1 a BRET signal was generated that could be displaced by IL-23 (Figure 4-10B). These trimeric or multimeric species had an affinity of 36.2 ± 16.5 pM for IL23-TMR and 140 ± 67 pM for IL-23 (Figure 4-10D and E). IL12Rβ1 homomers could not engage IL23-TMR in the presence or absence of IL23R (Figure 4-10C).

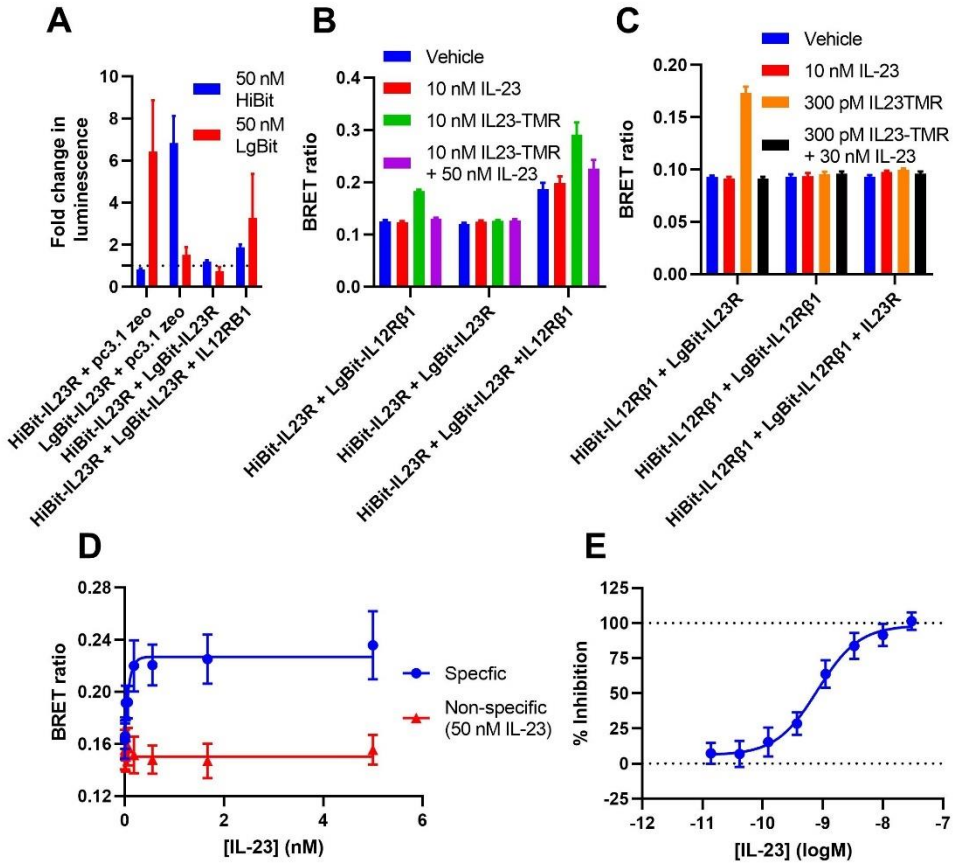

Figure 4-10: NanoBiT linked homomers of IL23R but not IL12Rβ1 can engage IL-23 when co-expressed with their co-receptor. (A) The fold change in luminescence generated when transfected cells were treated with either HiBit or LgBit. (B and C) The BRET ratio generated when transfected cells are treated with IL23-TMR. (D) The BRET signal generated when cells expressing HiBit-IL23R, LgBit-IL23R and IL12Rβ1 were treated with increasing concentrations of IL23-TMR. Data are fit with Equation 1. (E) The inhibition of 300 pM IL23-TMR binding to cells expressing HiBit-IL23R, LgBit-IL23R and IL12Rβ1 by increasing concentrations of IL-23, fit with Equation 4. Data are mean ± from five quadruplicate (A-B) or triplicate (C-D) experiments.

4.4.6 Creation of semi-active receptor complexes by NanoBiT complementation

An AlphaLISA assay for STAT3 phosphorylation, was used to test the effect of NanoBiT complementation on signal transduction. The results demonstrated that both HiBit and SmBit heteromers induced STAT3 phosphorylation when cells were treated with IL-23 (Figure 4-11A). When increasing concentrations of IL-23 were applied to cells expressing HiBit-IL23R and LgBit-IL12Rβ1 the EC_{50} of STAT3 phosphorylation was measured to be 193 ± 69 pM (n=4; Figure

4-11B) which was similar to the value measured in chapter 3 for cells transfected with wildtype receptor in an equivalent assay (269 ± 106 pM; Figure 3-8).

It was observed that in the absence of ligand, cells transfected with HiBit-IL23R but not SmBit-IL23R containing heteromers had significantly higher (one-ANOVA, p = <0.05) basal levels of phospho-STAT3 than cells expressing wildtype receptor (Figure 4-11C). To investigate if this effect was mediated by HiBit complementation, cells expressing the HiBit heteromer were treated with 5 μM purified HiBit. This reduced the basal STAT3 phosphorylation of the cells by 0.493 ± 0.144 fold (mean ± SEM, n=4; Figure 4-11D). Next to test if this effect was directly related to the proximity of the *N*-terminal domains of the receptor, the basal STAT3 phosphorylation of cells transfected with an equivalent NanoBiT heteromer in which the linker between HiBit and IL23R had been shortened by 18 amino acids (from 28 to 10) was tested. In this tagging conformation the basal transduction remained significantly higher than that of wildtype receptor transfected cells (Figure 4-11E). Finally, to test if the synthetic signalling was due to the specific orientation of the *N*-terminal domains rather than constraint alone, cells were transfected with a HiBit linked heteromer in which the tagging conformation had been switched so that HiBit was conjugated to IL12Rβ1. This led to a significant decrease in basal STAT3 signalling that was comparable to that measured in wildtype transfected cells (Figure 4-11F). The luminescence produced by cells transfected by this heteromer was measured and confirmed to be equivalent to cells expressing HiBit-IL23R containing heteromer (Figure 4-9).

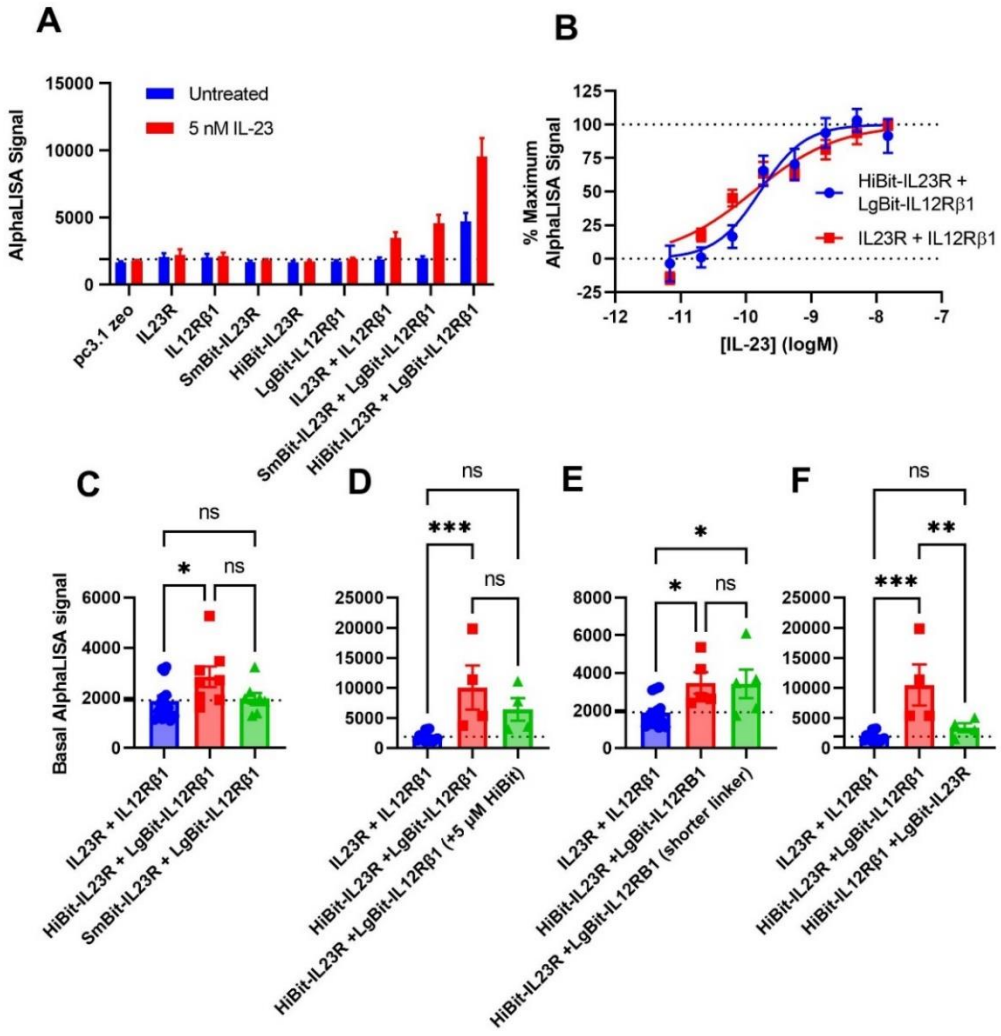

Figure 4-11: High affinity NanoBiT complementation induces ligand independent signalling. (A) The phospho-STAT3 AlphaLISA signal generated from cells transfected with NanoBiT constructs and treated with IL-23 for 30 minutes. Data are mean ± SEM from 4 (monomers), 14 (wildtype), 17 (HiBit-IL23R and LgBit-IL12Rβ1) or 8 triplicate experiments. (B) The phospho-STAT3 AlphaLISA signal generated when increasing concentrations of IL-23 were applied to cells expressing NanoBiT complemented receptor with the previously measured curve for wildtype receptor (**Figure 3-8**) plotted for comparison. Data are mean ± SEM from four triplicate experiments and are fit with Equation 5. (C-F) Comparison of the basal pSTAT3 signalling of cells expressing HiBit-IL23R and LgBit-IL12Rβ1 with either (C) cells expressing SmBit-IL23R and LgBit-IL12Rβ1, (D) equivalent cells treated with 5 μM purified HiBit, (E) cells expressing LgBit-IL12Rβ1 and a HiBit-IL23R with an 18 amino acid truncated linker and (F) cells expressing HiBit-IL12Rβ1 with LgBit-IL23R. (D-F) show mean values generated in eight (C), four (D and F) or five (E) independent matched experiments with previously generated wildtype data for comparison, overall mean and SEM are also plotted. A one-way ANOVA was used to measure the statistical significance of differences. * Signifies a p value of lower than <0.05, ** signifies a p value of <0.005 and *** signifies a p value of <0.0005.

It was observed that cells transfected with HiBit-IL23R containing heteromers also had a higher IL-23 induced amplitude of signalling that wildtype transfected cells (Figure 4-12). Treatment with purified HiBit or shortening of the HiBit linker did not disrupt this effect (Figure 4-12A-B), however switching of the tags did significantly (one-way ANOVA p = <0.0001; Figure 4-12C) reduce signal amplitude to a level analogous to that observed in cells transfected with wildtype receptor.

The AlphaLISA assay also allowed the confirmation that cells transfected with IL12Rβ1 homomers and IL23R could induce STAT3 phosphorylation (Figure 4-12D).

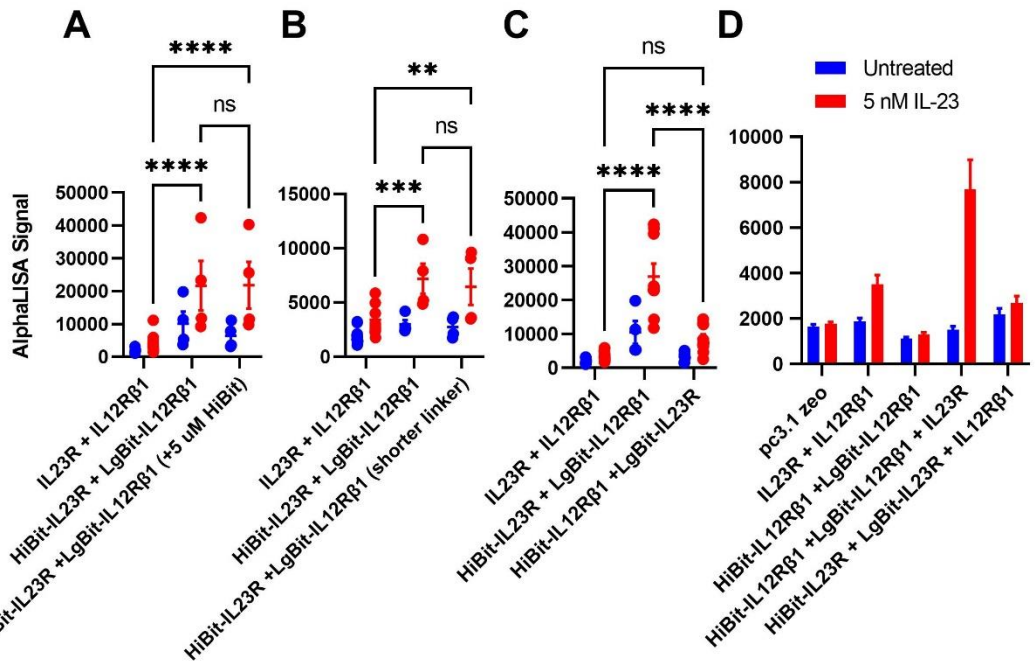

Figure 4-12: IL-23 induced STAT3 phosphorylation of NanoBiT complemented receptors. (A-C) The phospho-STAT3 AlphaLISA signal generated when cells from **Figure 4-11** are treated with 5 nM IL-23 for 30 minutes. Data are mean values from four (A and C) or five (B) independent triplicate experiments, with overall mean and SEM also plotted. A one-way ANOVA was used to measure the statistical significance of differences. ** signifies a p value of <0.005, *** signifies a p value of <0.0005 and **** signifies a p value of <0.0001. (D) The phospho-STAT3 AlphaLISA signal generated when cells expressing NanoBiT tagged homomers with or without their co-receptor are treated with IL-23. Data are mean ± SEM from three (HiBit-IL12Rβ1 and LgBit-IL12Rβ1) or four independent triplicate experiments.

4.4.7 The affinity of LgBit for HiBit-IL23R in different receptor states

To assess whether receptor heteromerization and ligand binding alter the position of the *N*-terminal regions of the IL-23 receptor subunits, the affinity of purified LgBit was measured to HiBit-IL23R in isolation, when co-expressed with IL12Rβ1 and in the presence and absence of IL-23. The affinity of LgBit for HiBit-IL23R expressed in isolation, with addition of 5 nM IL-23 was 25.9 ± 7.9 nM (n=5; Figure 4-13) which was not statistically different from the HiBit dissociation constant measured in the absence of IL-23 (unpaired t test). This is expected as the affinity of IL23-TMR for NL-IL23R was previously determined to be 222 nM (Figure 3-13). In contrast, when HiBit-IL23R was co-expressed with IL12Rβ1 the affinity of LgBit was decreased, to similar degree both in the presence and absence of IL-23, to a level where there was no clear saturation in luminescence signal at the highest concentration used in the assay (1 µM; Figure 4-13).

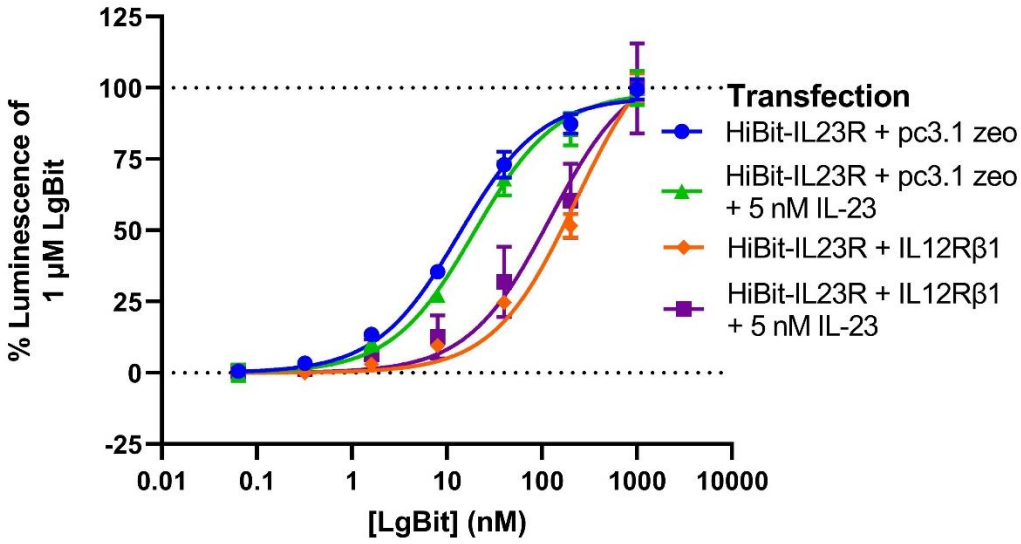

Figure 4-13: Heteromerisation but not ligand engagement decreases the affinity of exogenous purified LgBit for HiBit-IL23R. The luminescence signal generated by the application of increasing concentrations of purified LgBit protein to cells expressing HiBit-IL23R in the presence or absence of co-expressed IL12Rβ1 and with or without IL-23. Data are mean ± SEM from five independent triplicate experiments.

4.4.8 Disrupting NanoBiT complexes with increasing expression of IL12Rβ1

Finally, to test if NanoBiT heteromers of SmBit-IL23R and LgBit-IL12Rβ1 could be disrupted by increasing expression levels of non-NanoBiT component

labelled IL12Rβ1, cells were transfected with 40 ng of SmBit-IL23R, 10 ng of LgBit-IL12Rβ1 and increasing concentrations of HT-IL12Rβ1 cDNA, with the total DNA concentration normalised to 100 ng with pc3.1 zeo plasmid. Two parallel experiments were carried out, in one luminescence measurements were made in the presence and absence of IL-23, in the second the cells were fluorescently labelled by incubation with HT-AF488 substrate, followed by the measurement of fluorescence intensity. These measurements showed that increasing concentrations of HT-IL12Rβ1 cDNA led to a linear increase in HT-IL12Rβ1 expression (Figure 4-14A) and that this increased expression correlated with a decrease in NanoBiT complementation (Figure 4-14B). Control experiments were carried out to monitor the effect of increasing the expression of IL12Rβ1 on the expression of 10ng of HT-IL12Rβ1 or 40ng HT-IL23R cDNA (Figure 4-15). These experiments showed that, whilst there was some decrease in expression especially in HT-IL12Rβ1 when IL12Rβ1 expression was increased from 0 to 2.5 ng per well, the expression of receptor monomers remained relatively stable over the concentration range tested.

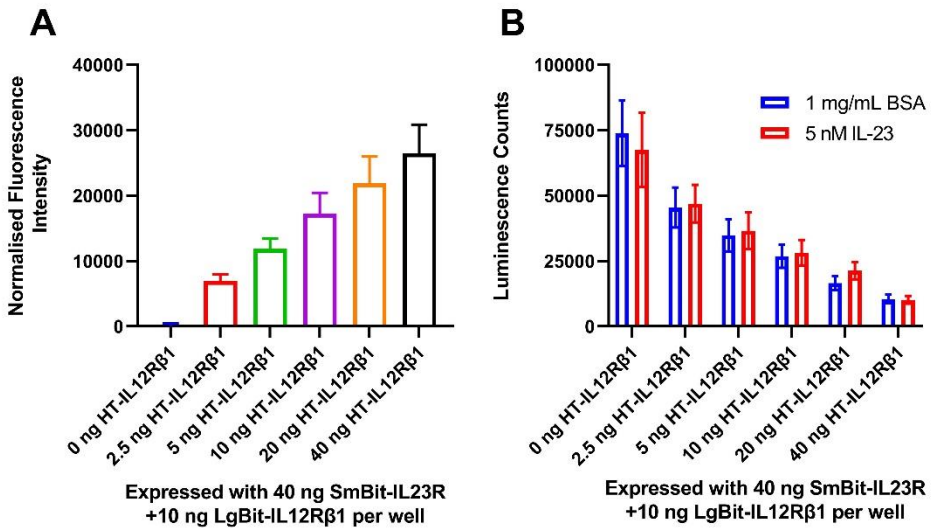

Figure 4-14: HT-IL12Rβ1 competes with LgBit-IL12Rβ1 for SmBit-IL23R in a ligand independent manner. (A) The fluorescence intensity of cells expressing 40 ng SmBit-IL23R with 10 ng LgBit-IL12Rβ1 and increasing amounts of HT-IL12Rβ1 cDNA, that have been labelled with HT-AF488 ligand. (B) The luminescence signal from cells transfected as in (A; without HT-AF488 labelling) in the presence and absence of IL-23. Data are mean ± SEM from five quadruplicate experiments.

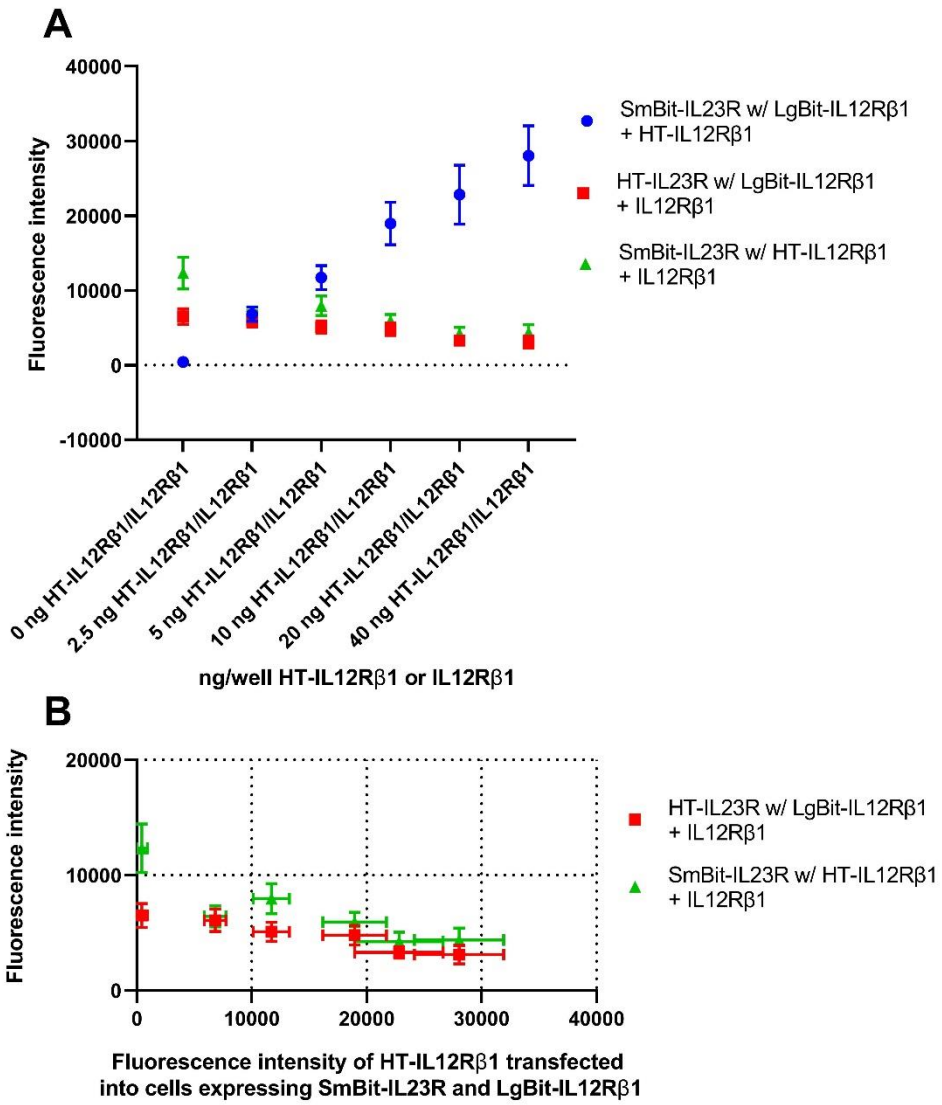

Figure 4-15: Increasing expression of IL12Rβ1 leads to a modest reduction in the expression of HT-IL23R and HT-IL12Rβ1. (A) The fluorescence intensity generated from cells labelled with HT-AF488 and expressing 40ng SmBit-IL23R cDNA, 10ng LgBit-IL12Rβ1 cDNA and increasing concentrations of HT-IL12Rβ1 (blue circles), or cells expressing increasing concentrations of IL12Rβ1 and HT-IL23R with LgBit-IL12Rβ1 (red squares) or SmBit-IL23R with HT-IL12Rβ1 (green triangles). Data are normalised to the background signal observed in the 0 ng HT-IL12Rβ1 condition. (B) the correlation between increasing expression of HT-IL12Rβ1 (fluorescence intensity measurements of cells transfected with different levels of HT-IL12Rβ1 are plotted on the x axis) and the expression of 40ng HT-IL23R or 10 ng HT-IL12Rβ1 cDNA (as quantified by fluorescence intensity and plotted on the y axis). Data are mean ± SEM from five quadruplicate experiments.

4.5 Discussion

The results from Chapter 3 suggested that the IL-23 receptor associates in the absence of ligand. In this chapter the formation of inactive and semi-active receptor heteromers in the absence of ligand was confirmed by the observation of a luminescence signal when *N*-terminal domains of the receptor are labelled with corresponding NanoBiT fragments and co-expressed in HEK293T cells. A strong luminescent signal was observed for cells expressing HiBit-IL23R and LgBit-IL12Rβ1 and a weaker signal for cells expressing SmBit-IL23R and LgBit-IL12Rβ1. The difference in signal is likely to be the result of the greater affinity of HiBit for LgBit than SmBit and has previously been described (Peach et al., 2021). The lack of subsequent STAT3 phosphorylation observed for SmBit-IL23R:LgBit-L12Rβ1 heteromeric complexes in the absence of ligand confirms that heteromerization alone is not sufficient to induce signalling. Furthermore, the confirmation that IL-23 could bind these receptor heteromers made using NanoBRET and phospho-STAT3 transduction assays, taken together with the observation that treatment of HiBit-IL23R:LgBit-L12Rβ1 or SmBit-IL23R:LgBit-L12Rβ1 heteromeric complexes with IL-23 did not lead to an increase in luminescence, indicates that dimerisation is not sufficient in itself to initiate receptor activation.

A 1:4 expression ratio of IL12Rβ1 to IL23R based constructs was used throughout this chapter due to the observation in chapter 3 that NL-IL12Rβ1 was expressed at approximately 4-fold the level as NL-IL23R when cells were transfected with equivalent amounts of DNA. This approach was shown to yield a near equal ratio of fully complemented receptor components, as the addition of purified HiBit or LgBit to cells co-expressing HiBit-IL23R and LgBit-IL12Rβ1 yielded no increase in luminescence (see Figure 4-2), indicating there was not a significant uncomplemented reserve of either protein.

Whilst the possibility that HiBit:LgBit interactions were contributing to complex formation could not be completely ruled out, it was found that the affinity of HiBit and LgBit for their corresponding NanoBiT fragment was greatly reduced when fused to IL-23 receptor monomers (see Figure 4-3). The effect was most marked for LgBit-IL12Rβ1 which did not generate a saturable luminescence signal with increasing concentrations of purified HiBit over the concentration

range tested, having a likely affinity in the order of 100-1000 nM, making this the limiting affinity for NanoBiT complementation driven heteromer formation.

Utilising a NanoBiT BRET binding assay, in which light generated from complemented receptors was used to excite fluorophore conjugated IL-23 (IL23-TMR), it was possible to monitor binding interactions of IL-23 solely to pre-formed heteromers (see Figure 4-5). This approach demonstrated an affinity of pre-formed IL23R-IL12Rβ1 heteromers for IL23-TMR that was similar to that previously measured for IL23-TMR binding to NanoLuc tagged receptor heteromers. Interestingly, the equilibrium dissociation constant measured was between that of IL23-TMR binding to cells expressing NL-IL23R and IL12Rβ1 and those expressing (a 1:10 ratio of) NL-IL12Rβ1 and IL23R. The difference in these affinities is possibly because the tagging of IL12Rβ1 with NanoLuc leads to a greater steric interference in the binding of IL23-TMR. A NanoBiT heteromer binding affinity mid-way between these values suggests that the position of the complemented luciferase interferes less in binding than NanoLuc fused to IL12Rβ1, but more than NanoLuc fused to IL23R. As the affinity of IL23-TMR binding to NanoBiT complemented heteromers is equivalent to the affinities measured for the interaction of the probe with NL-tagged heteromers, and as IL-23 does not induce heteromerization, it is most likely that heteromers are pre-formed prior to ligand binding in both experiments.

The kinetic characterisation of IL23-TMR binding to HiBit-IL23R and LgBit-IL12Rβ1 was also undertaken (see Figure 4-8). These experiments demonstrated that the NanoBiT tagging of the receptor caused a mild reduction in k_{off} rate (1.84-fold) combined with a larger reduction in k_{on} (16.0-fold) which is most likely the main driver behind IL23-TMR's weakened affinity at the NanoBiT tagged receptor complex. Interestingly whilst the dissociation of IL23-TMR from NL-IL23R and IL12Rβ1 was made up of a fast and slow rate step, the dissociation of IL23-TMR from binary complexes appeared to be monophasic and was closer to the slow rate step measured in chapter 3. This observation may indicate that the fast dissociation phase was a result of dissociation from monomeric NL-IL23R.

A NanoBiT BRET competition assay demonstrated that unlabelled IL-23 also bound NanoBiT complemented heteromers with high affinity. Furthermore, an AlphaLISA assay for STAT3 phosphorylation confirmed that both HiBit and SmBit containing heteromers were able to mediate ligand induced signal transduction. It has previously been suggested the IL-23 receptor is activated through a ligand induced dimerisation mechanism (Bloch et al., 2018). However, in this study, despite the clear evidence that the NanoBiT receptor heteromers were engaging IL-23, the addition of IL-23 did not lead to an increase in complex formation in SmBit or HiBit containing heteromers and therefore these results are not consistent with a ligand induced dimerisation mechanism. These results instead indicate that inactive receptor complexes can form in the absence of ligand and are most likely activated by a subsequent ligand induced conformational change.

Measurement of basal STAT3 phosphorylation in the absence of ligand stimulation demonstrated that cells transfected with HiBit-IL23R and LgBit-IL12Rβ1 had higher levels of phospho-STAT3 than untagged receptor or SmBit-IL23R and LgBit-IL12Rβ1 transfected cells (see Figure 4-11). This observation and the reduction in basal signalling induced by treatment with purified HiBit indicate that basal signalling is most likely a result of the *N*-termini of the receptor monomers being constrained by the NanoBiT complementation in a favourable conformation for ligand independent activation. The observation that the level of STAT3 phosphorylation can be raised further by the introduction of IL-23 indicates that these complexes are not locked in a fully active conformation. Lack of a reduction in basal signalling when the linker between the HiBit tag and IL23R was truncated, indicate that this effect is not directly related to *N*-terminal proximity. Instead, the disruption of basal signalling caused by the switching of the tag positions indicates that the relative orientation of the *N*-terminal domains is vital for receptor activation. The cause of the higher amplitude of IL-23 induced STAT3 phosphorylation observed for cells expressing HiBit-IL23R and LgBit-IL12Rβ1 are unclear. A possible hypothesis could be that the ligand independent STAT3 activation leads to upregulation of pathway components resulting in a higher maximal signal when cells are treated

with ligand. This is precedented by the previous observation that STAT3 signalling upregulates IL23R expression in T cells (Ghoreschi et al., 2010).

It would be interesting to study the transduction profile of the semi-activated crosslinked receptor in a disease relevant cell line, as it has also previously been shown that synthetic agonists of cytokine signalling at the Erythropoietin receptor (EpoR) can exhibit differential signalling profiles depending on the conformation of the dimer that is stabilised (Moraga et al., 2015a).

It was shown in chapter 3 that the *N*-terminal domains of the IL-23 receptor undergo a re-arrangement on ligand binding. There has also been a report of ligand induced re-arrangement occurring at the *C*-terminal domains of the receptor (Sivanesan et al., 2016). The observations at the *C*-terminus of the receptor led to the suggestion that the IL-23 receptor is activated through a 'scissor-like' conformational change, in a similar manner to EpoR, in which the *C*-terminal domains of the receptor are brought into closer proximity allowing transphosphorylation of JAK proteins (Sivanesan et al., 2016). This study's observation of ligand independent signalling when the *N*-terminal domains of the receptor are constrained in certain conformations is consistent with this hypothesis. This finding may indicate that the wildtype IL-23 receptor could be activated by a synthetic bitopic ligand capable of constraining the *N*-terminal domains of the receptor. Indeed, it has previously been shown that a chimeric IL-23 receptor containing receptor ICDs, TMDs and *N*-terminal nanobodies for mCherry and GFP could be activated by the application of a bitopic ligand consisting of a fusion of the respective fluoro-proteins (Engelowski et al., 2018).

The formation of heteromers containing more than one IL23R molecule in the absence of ligand was also tested. These experiments demonstrated that complexes containing HiBit-IL23R or SmBit-IL23R and LgBit-IL23R gave half the signal of complexes containing HiBit or SmBit-IL23R and LgBit-IL12Rβ1. The ability of these complexes to engage ligand was also tested, revealing that when co-expressed with IL12Rβ1 the majority of homomers were disrupted, however the remaining complexes could engage IL23-TMR. As the experiments in Chapter 3 demonstrated that IL23R and IL12Rβ1 must be present to form the high affinity IL-23 binding site, it must be assumed that a multimeric species

consisting of at least two IL23R molecules and IL12Rβ1 are engaging IL-23 in this situation. Homomeric complexes of IL12Rβ1 were also observed to form in the absence of ligand, however these homomers could not engage IL23-TMR when co-expressed with IL23R but could induce STAT3 phosphorylation when treated with IL-23, indicating that signalling was mediated by non-complemented complexes. Previously it has been shown that trimeric species of chimeric IL-23 receptor components can be induced to form using synthetic ligands and that these species can trans-phosphorylate each other to induce signalling (Engelowski et al., 2018). The experiments outlined in this chapter suggest that multimeric IL-23 receptor species containing multiple IL23R but not IL12Rβ1 monomers can be induced to form with no reduction in ligand binding affinity, therefore the formation of higher order receptor structures, as is the case for other closely related receptors (Ward et al., 1994) cannot be ruled out.

To gain insights into how receptor heteromerization and ligand binding affects the *N*-terminal domain of IL23R, the affinity of purified LgBit for HiBit-IL23R in the different receptor configurations was measured. The results demonstrated that the affinity of LgBit was significantly decreased when HiBit-IL23R was co-expressed with IL12Rβ1 and that this effect was not altered by the presence or absence of IL-23. This finding indicates that the heteromeric structure of the IL-23 receptor shields the *N*-termini of HiBit-IL23R to some degree from complementation with LgBit and that this heteromer forms independently of IL-23. As the *N*-terminus of IL23R is shielded by IL12Rβ1 to a similar degree both in the presence and absence of IL-23, it is likely that in both conformations the *N*-terminal domain of IL23R is in proximity to IL12Rβ1.

The effect of increasing expression of HT-IL12Rβ1 on the formation of SmBit containing NanoBiT heteromers was also tested. This experiment demonstrated that HT-IL12Rβ1 could compete with LgBit-IL12Rβ1 for SmBit-IL23R and that this effect was independent of the presence of IL-23, further supporting the possible presence of inactivated receptor complexes in the absence of ligand. The successful disruption of IL-23 receptor heteromers raises the possibility of the development of peptide blockers of heteromerization based on the structure of IL12Rβ1. Numerous examples of membrane-spanning blocking peptides

have been reported that act as allosteric inhibitors of complex formation (Stone and Deber, 2017). Such molecules could be useful tools to further study heteromer formation, and a potential novel therapeutic tactic to antagonise IL-23 signalling at the heteromeric interface. A crucial piece of information for this approach is the location of the formation of heteromeric receptor species. In chapter 3 luminescence was observed at intracellular foci and on the cell membrane when imaging cells expressing HiBit-IL23R and LgBit-IL12Rβ1. Other cytokine receptors such as the Growth Hormone receptor have been shown to be exported from the endoplasmic reticulum as a dimer (Gent et al., 2002), however studies on IL23R have shown that the molecule is internalised after ligand stimulation and recycled to the cell surface in the absence of IL12Rβ1 (Sun et al., 2020).

This chapter has demonstrated that inactive IL-23 receptor complexes form prior to cytokine engagement, with the *N*-terminal domains of the receptor in proximity. Furthermore, it has been demonstrated that ligand binding leads to no increase in association between receptor monomers and does not decrease the IL12Rβ1 mediated shielding of the IL23R *N*-terminus. In addition, this chapter revealed that constraint of the *N*-terminal domains of the receptor in specific orientations can lead to ligand independent activation, with a 10-amino acid change in the distance between the *N*-terminal domains not affecting the formation of the semi-activated state. Finally, this chapter has demonstrated that receptor complex formation could be inhibited by increasing concentrations of competing receptor monomers in a ligand independent manner, highlighting a route for allosteric modulation of IL-23 signalling by the disruption of receptor complex formation.

Chapter 5. Creation and characterisation of a fluorescent peptide probe for IL23R

5.1 Introduction

Fluorescently labelled probes are key tools for the discovery and characterisation of receptor antagonists (Huber, 2017; Schürmann et al., 2016; Soave et al., 2020c). The interaction of GPCRs and their ligands have been extensively characterised through this approach, using techniques such as Fluorescence Polarisation (FP), FRET or BRET, to construct competition assays (Stoddart et al., 2016). These assays facilitate screens to identify new binders and enable the characterisation and development of novel drug-like molecules (Jin et al., 2020; Rectenwald et al., 2019). In addition, fluorescent probes can be used to label targets and are especially useful when antibodies specific for a receptor are difficult to create (Borgarelli et al., 2021).

Cytokine receptors are a large group of single transmembrane domain (TMD) containing proteins (Liongue et al., 2016). Despite many cytokines being important drug targets, for example Interleukin-4 (IL-4), IL-5 and IL-6, (Hassani and Koenderman, 2018; Jones and Jenkins, 2018; Oh et al., 2010) there has been limited development of peptide or small molecule receptor antagonists (Schreiber and Walter, 2010). Instead, the development of biologic cytokine antagonists and small molecule signalling inhibitors has been pursued (Baker and Isaacs, 2018). Whilst biologic therapies have been highly effective, they are expensive to produce, do not cross the blood brain barrier and are usually confined to systemic administration through sub-cutaneous injection (Dömling and Li, 2022). Small molecule inhibitors of cytokine signal transducers, for example JAK proteins, suffer from numerous side effects due to the protein's function in multiple pathways (Virtanen et al., 2019). Small molecule or peptide antagonists of cytokine receptors would enable specific inhibition, simplified synthesis and local administration, for example through a topical or gut restricted treatment for diseases such as psoriasis or Crohn's disease respectively.

The IL-23 pathway is a key drug target for the treatment of autoinflammatory diseases and is currently antagonised by highly effective biologic treatments specific to either the IL23p19 or IL12p40 subunits of the IL-23 cytokine (Parigi and Iacucci, 2022). Despite the reports of several classes of IL23R peptide antagonists, including linear and cyclic peptides with competitive and non-competitive binding mechanisms (Bourne et al., 2017; Kong et al., 2020; Kuchař et al., 2014; Pandya et al., 2020), no probes have yet been outlined and validated to characterise this nascent drug class's interaction with the receptor. Instead, these peptides have been validated using either, functional read-outs which do not allow detailed pharmacological characterisation of the peptide's binding mechanism or immobilised purified protein techniques such as ELISA and SPR which do not allow the measurement of the interactions with the full-length dimeric receptor expressed in the cell membrane (Bourne et al., 2017; Kong et al., 2020; Kuchař et al., 2014; Pandya et al., 2020; Quiniou et al., 2014). This second point is important as it was demonstrated in Chapter 3 that when the subunits of the IL-23 receptor are expressed in the cell membrane, as opposed to being studied as purified truncates, their affinity for IL-23 is markedly increased (Bloch et al., 2018).

5.2 Aims

The aims of this chapter were to use IL23-TMR to characterise reported antagonists of the IL-23 receptor. The aim was then to develop and characterise a fluorescent probe from a peptide antagonist of the receptor and to use this reagent to measure the activity of further antagonists. In parallel the chapter aimed to characterise the mechanism of action of reported disease relevant mutants of IL23R, including a variant likely to block the IL23R:IL23p19 interaction interface. This aim was to then use this variant to define the binding site of the developed fluoroprobe.

5.3 Methods

5.3.1 Site directed mutagenesis

Amino acid substitutions in IL23R were introduced into untagged and *N*-terminal NanoLuc tagged IL23R plasmids using site directed mutagenesis (as

described in section 2.3.3.2). The successful substitutions were confirmed by sequencing (as described in section 2.3.3.3).

5.3.2 Transient transfections

Batch transfections (see section 2.5.1.1) were utilised for the majority of experiments. The single well transfection technique (see section 2.5.1.2) was used for experiments involving mutant IL23R. A 4:1 ratio of IL23R to IL12Rβ1 constructs was utilised in all experiments.

5.3.3 Total and surface expression quantification

Total expression was quantified by measuring the luminescence from transfected cells treated with 7.7 μM furimizine in 50 μL HBSS for 10 minutes using a PheraStar FS plate reader. To quantify what proportion of this luminescence was a result of surface expressed protein, half of these cells were supplemented with 60 μM NanoLuc extracellular inhibitor during the 10-minute incubation prior to the measurement of luminescence.

5.3.4 Intra-receptor NanoBRET experiments

Transfected cells had media replaced with DMEM with 10% FBS containing 100 nM HaloTag 618 ligand (Promega) and were incubated for 5 hours at 37 °C with 5% CO_2. Media was then replaced with HBSS with or without 5 nM IL-23 and the cells were incubated for a further hour in the absence of CO_2. Following this 5 μL of HBSS with 77 μM furimizine was added to each well and the BRET signal was measured on a PheraStar FS plate reader using 460 nm (80 nm bandpass) and >610 nm long pass filters.

5.4 Results

5.4.1 Using IL23-TMR to characterise IL-23 receptor antagonists

In chapter 3 it was demonstrated that IL23-TMR can be competitively displaced by unlabelled IL-23. To assess if IL23-TMR can be displaced by further IL-23 receptor antagonists, several reported inhibitors were tested using this IL23-TMR competition assay (Figure 5-1). IL12p40, a subunit of IL-23 which is endogenously secreted as a monomer and acts as an antagonist of both IL-23 and IL-12 signalling (Mondal et al., 2020), displaced IL23-TMR with a K_i of 12.4 ± 1.4 nM (n=5; 392-fold weaker than IL-23). An octapeptide with the sequence TEEEQQLY that was reported to be a negative allosteric modulator

(NAM) of the IL-23 receptor (Quiniou et al., 2014) was also tested and found not to displace IL23-TMR. Finally a cyclic peptide, known as Peptide 630 (P630) reported in a patent filing describing oral IL23R antagonists was tested (Bourne et al., 2017). P630 competitively displaced IL23-TMR with a K_i of 21.8 ± 3.4 nM (n=5; 690-fold weaker than IL-23).

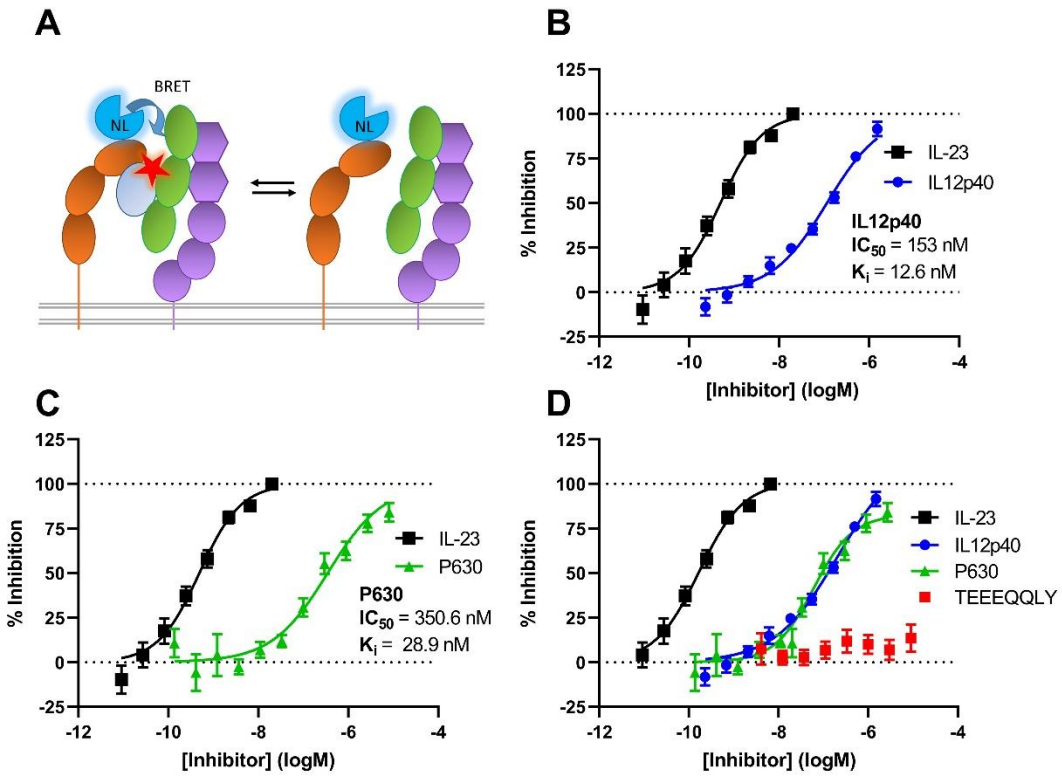

Figure 5-1: Using IL23-TMR to characterise IL-23 receptor antagonists. (A) A schematic demonstrated the principles of the BRET competition assay using IL12p40 as an example. (B-C) The competitive inhibition of the binding of 300 pM IL23-TMR to cells expressing NL-IL23R and IL12Rβ1 by increasing concentrations of (B) IL12p40 and (C) P630 with previously generated (**Figure 3-15**) IL-23 competition data for comparison. (D) The data from B and C plotted with the inhibition caused by TEEEQQLY. Data are mean ± SEM from five independent experiments conducted in triplicate and are fit with Equation 4.

5.4.2 Design and characterisation of P630-TMR

With the aim of creating a peptide fluorescent probe for IL23R, a TAMRA labelled version of P630 was designed and synthesised. The resulting labelled probe P630-TMR, consisted of P630 conjugated to TAMRA via a lysine residue bound to the *C*-terminus of the peptide (distal to the cyclised portion of the molecule; Figure 5-2B). To test whether the binding of P630-TMR to the receptor could be measured via BRET, increasing concentrations of the probe

were applied to cells expressing NL-IL23R with IL12Rβ1, NL-IL23R alone and NL-IL12Rβ1 with IL23R (Figure 5-2B-D). It was observed that P630-TMR bound specifically with comparable affinity (Mean ± SEM, n=5; K_d = 51.1 ± 7.3, 101 ± 4 and 55.2 ± 10.5 nM respectively) to cells expressing each of these combinations of constructs (Figure 5-2C to 2E; Table 5-1). Whilst P630-TMR bound each of the receptor combinations with similar affinities, the maximum binding (B_{max}) BRET ratio was different depending on the constructs expressed (Figure 5-2G and F) with the highest B_{max} measured for the interaction with NL-IL23R expressed in isolation (4.04-fold higher than NL-IL23R with IL12Rβ1), and the lowest B_{max} measured for the interaction with cells expressing NL-IL12Rβ1 with IL23R (42.5-fold lower than NL-IL23R with IL12Rβ1).

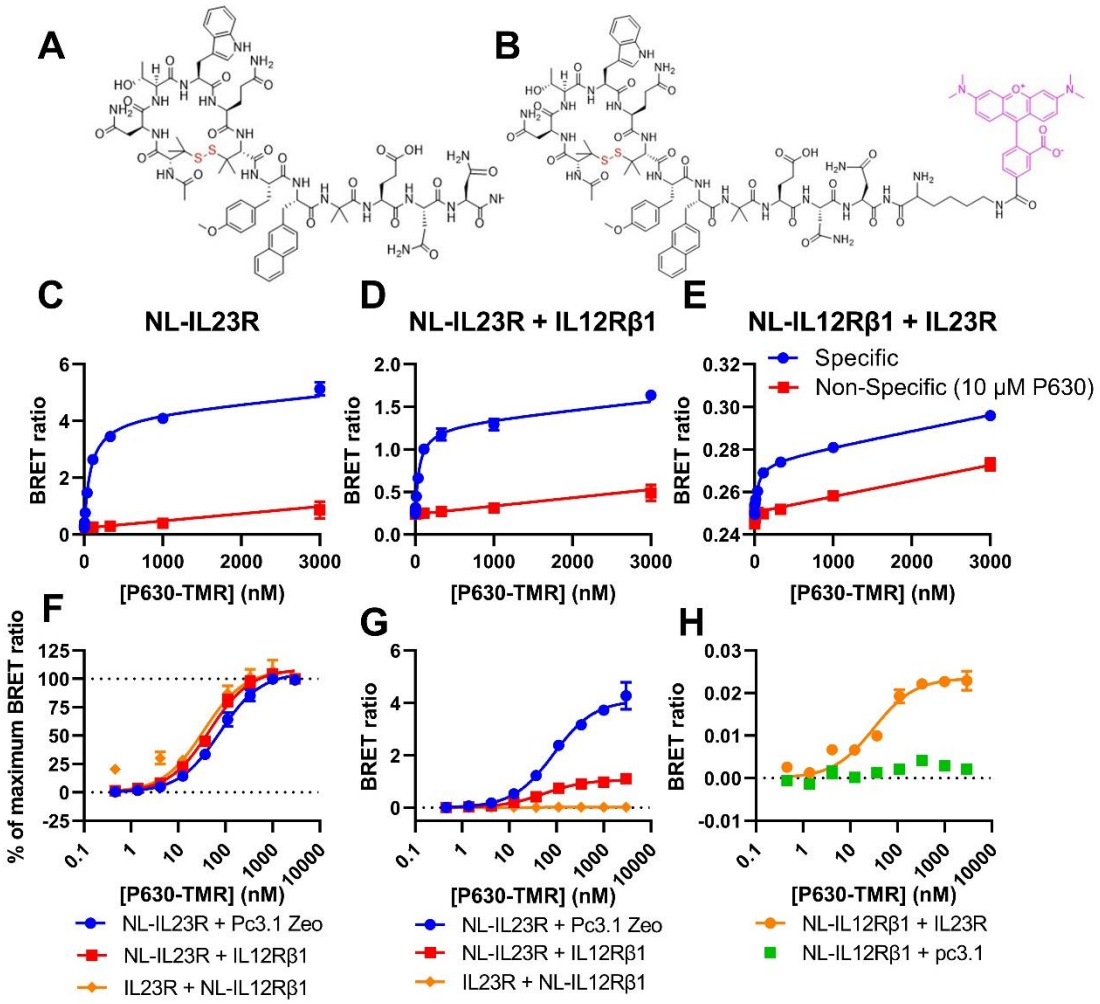

Figure 5-2: Creation and characterisation of a fluorescent cyclic peptide probe for IL23R. (A-B) The chemical structures of (A) P630 and (B) P630-TMR. (C-E) The BRET ratio measured when increasing concentrations of P630-TMR were applied to (A) cells expressing (C) NL-IL23R alone, (D) NL-IL23R with IL12Rβ1 or (E) NL-IL12Rβ1 and IL23R in the presence or absence of 10 μM P630 (fit with Equation 1). (F) The data shown in C-E normalised to % maximum BRET ratio. (G) The BRET data shown in C-E with non-specific binding subtracted. (H) The specific binding of P630-TMR to cells expressing NL-IL12Rβ1 in the presence or absence of IL23R (F-G are fit with Equation 2). Data are mean ± SEM from five independent experiments.

The P630 peptide was originally reported in a patent for molecules that block IL-23:IL23R binding (Bourne et al., 2017) and another peptide from the patent has been mapped to the IL23R:IL-23 interface (Sayago et al., 2018), therefore P630-TMR is likely to bind specifically to the IL23R subunit. To test this hypothesis, the binding affinity of P630-TMR to cells expressing NL-IL12Rβ1

in isolation was measured (Figure 5-2G) demonstrating that in the absence of IL23R expression there was no specific binding. Finally, the NanoBiT BRET system outlined in Chapter 4 was utilised to assess the affinity of P630-TMR binding to binary IL-23 receptor complexes (Figure 5-3). P630-TMR specifically bound to these binary complexes with a similar affinity (K_d = 53.5 ± 4.4 nM; mean ± SEM, n=3) to that measured for the previously measured tagged receptor combinations (Figure 5-2; Table 5-1).

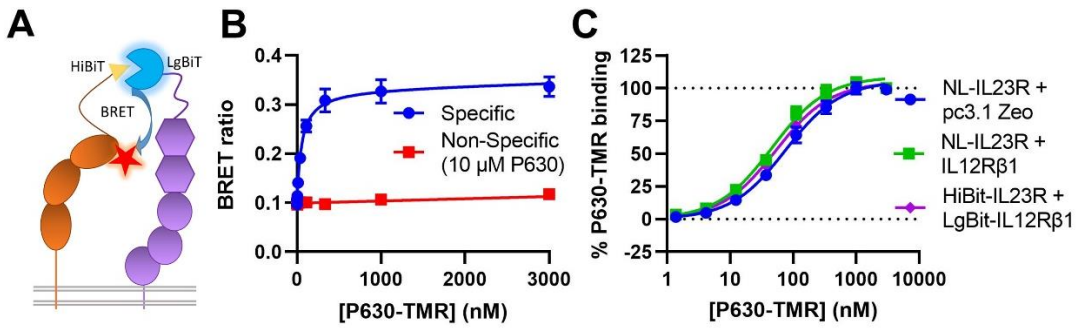

Figure 5-3: P630-TMR binding to binary NanoBiT IL-23 receptor complexes. (A) A schematic depicting the NanoBit assay methodology. (B) The BRET ratio generated when increasing concentrations of P630-TMR were applied to cells expressing NanoBiT complemented receptors. Data are mean ± SEM from three independent experiments conducted in triplicate and are fitted with Equation 1. (C) The data from (B) normalised to % of P630-TMR specific plateau and plotted with Equation 2 alongside data generated in Figure 5-2 for reference.

5.4.3 Using P630-TMR to characterise IL23R antagonists

To test if P630-TMR displacement could be used to measure the affinity of unlabelled IL-23, a competition assay was undertaken in which P630-TMR was displaced by increasing concentrations of IL-23 from cells expressing either NL-IL23R in isolation or NL-IL23R co-expressed with IL12Rβ1. It was observed that IL-23 displaced P630 with a much lower K_i when both subunits of the receptor were co-expressed (Figure 5-4). When NL-IL23R was expressed alone P630-TMR was not fully displaced over the concentration of IL-23 tested. When NL-IL23R was co-expressed with IL12Rβ1 a K_i of 22.6 ± 5.2 pM (mean ± SEM, n=5) was measured for IL-23 which was similar to the value measured in Chapter 3 for the displacement of IL23-TMR (31.6 ± 7.7 pM).

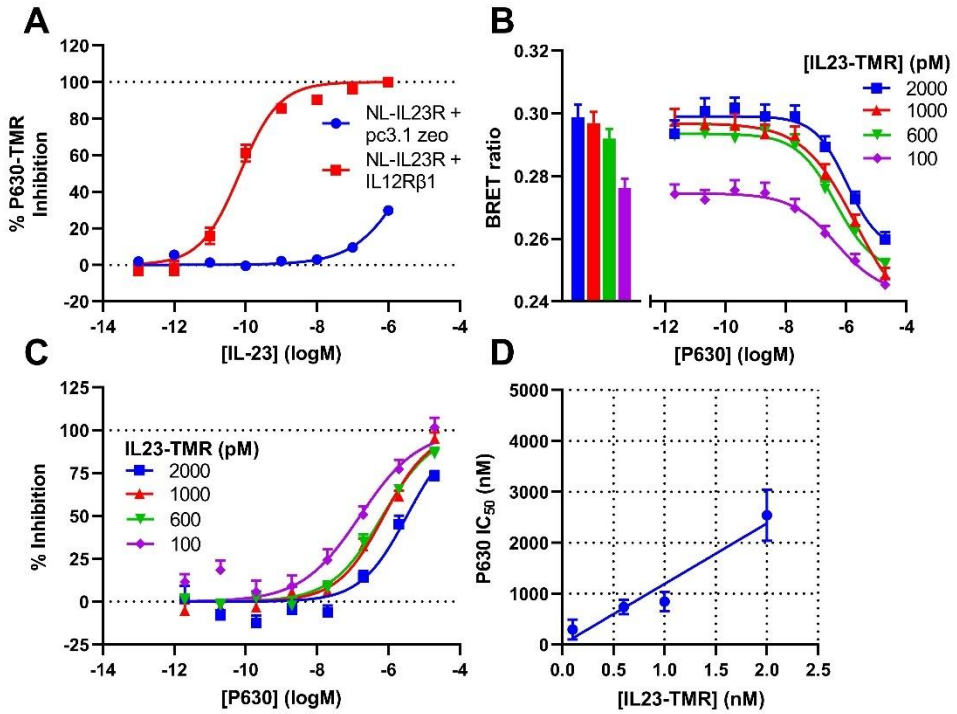

Figure 5-4: The displacement of P630-TMR by IL-23 is dependent on the co-expression of IL12Rβ1 with IL23R. (A) The displacement of 75 nM P630-TMR by increasing concentrations of IL-23 from cells expressing NL-IL23R in the presence or absence of IL12Rβ1. (B) The displacement of different concentrations of IL23-TMR by increasing concentrations of P630. (C) The data shown in (B) normalised to % inhibition (total inhibition was defined by an excess of IL-23). (D) the relationship between P630 IC_{50} determined in (C) and the concentration of IL23-TMR used. Data are mean ± SEM from four (A: NL-IL23R + pc3.1 zeo) or five independent experiments performed in triplicate. Data in (A-C) were fit with Equation 4.

To assess if the interaction of P630 with IL-23 was competitive, multiple concentrations of IL23-TMR were displaced by P630. Consistent with a competitive interaction increasing concentrations of IL23-TMR shifted the measured P630 IC_{50} to higher levels (Figure 5-4B). The mean value generated for P630 K_i was 38.0 ± 9.0 nM (± SEM, n=25). The Cheng-Prusoff equation was then used to generate an IL23-TMR K_d value of 32.0 pM from the gradient of the linear regression of the data plotted in Figure 5-4D and the measured P630 K_i value. The experiment was also repeated with different concentrations of P630-TMR being competed by IL-23 (Figure 5-5A). Interestingly, in this assay configuration, there was not a significant change in the measured IL-23 IC_{50} over the concentration range of P630-TMR tested (Figure 5-5B).

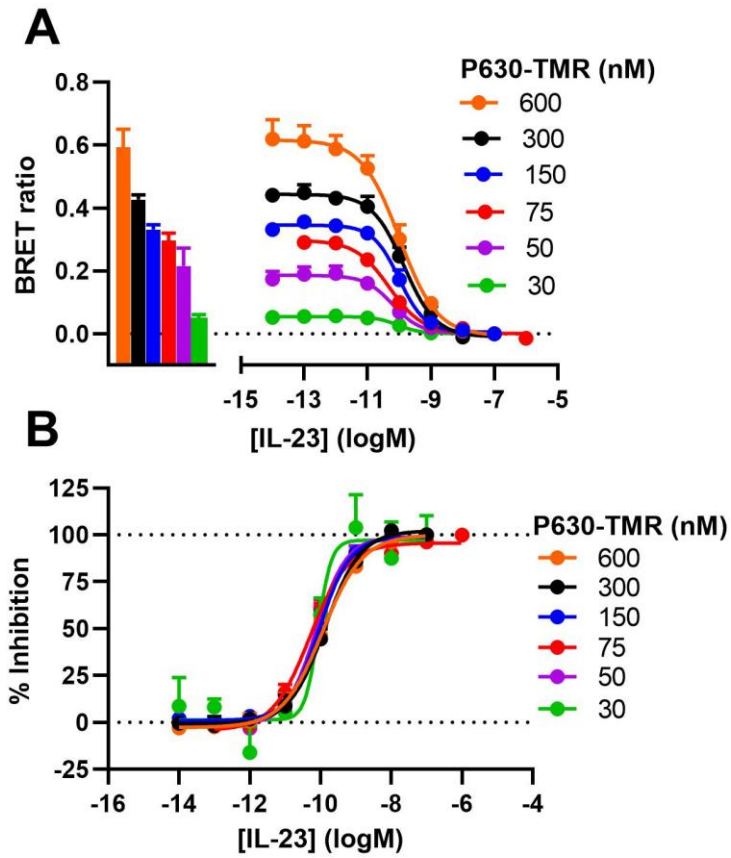

Figure 5-5: Unlike the interaction between IL23-TMR and P630 the interaction between IL-23 and P630-TMR is non-competitive. (A) Displacement of several concentrations of P630-TMR by increasing concentrations of IL-23. (B) The data from (A) normalised to % of the maximum inhibition of the BRET signal. Data are mean ± SEM from five independent experiments performed in triplicate and are fit with Equation 4.

The ability of P630-TMR to characterise other reported IL-23 receptor antagonists was then tested using cells expressing NL-IL23R and IL12Rβ1 (Figure 5-6A). Unlabelled P630 was able to displace P630-TMR yielding a K_i of 6.32 ± 1.06 nM which was similar to the value measured using IL23-TMR (21.8 ± 3.4 nM; Figure 5-1). TEEEQQLY and IL12p40 did not displace P630-TMR (see schematic shown in Figure 5-6A and B). Given that IL12p40 displaced IL23-TMR but not P630-TMR, single concentrations of an IL23p19-Fc fusion protein, IL12p80 (a homodimer of IL12p40) and IL-12 (a heterodimeric cytokine made up of IL1240 and IL12p35) were tested to see if there were any differences in the displacement of these molecules (Figure 5-6B). A 200 nM concentration of IL23p19-Fc exhibited a low level of inhibition of

both IL23-TMR and P630-TMR. Both IL12p80 and IL-12 displaced IL23-TMR to a much greater degree than P630-TMR, with IL-12 giving no inhibition of P630-TMR and IL12p80 treatment leading to mild inhibition. Interestingly, the level of IL23-TMR displacement by 50 nM of IL12p80 was higher than that of 500 nM IL-12 and comparable to that induced by 500nM IL12p40. This result indicates that homodimerisation of IL12p40 enhances the protein's ability to inhibit IL-23 binding.

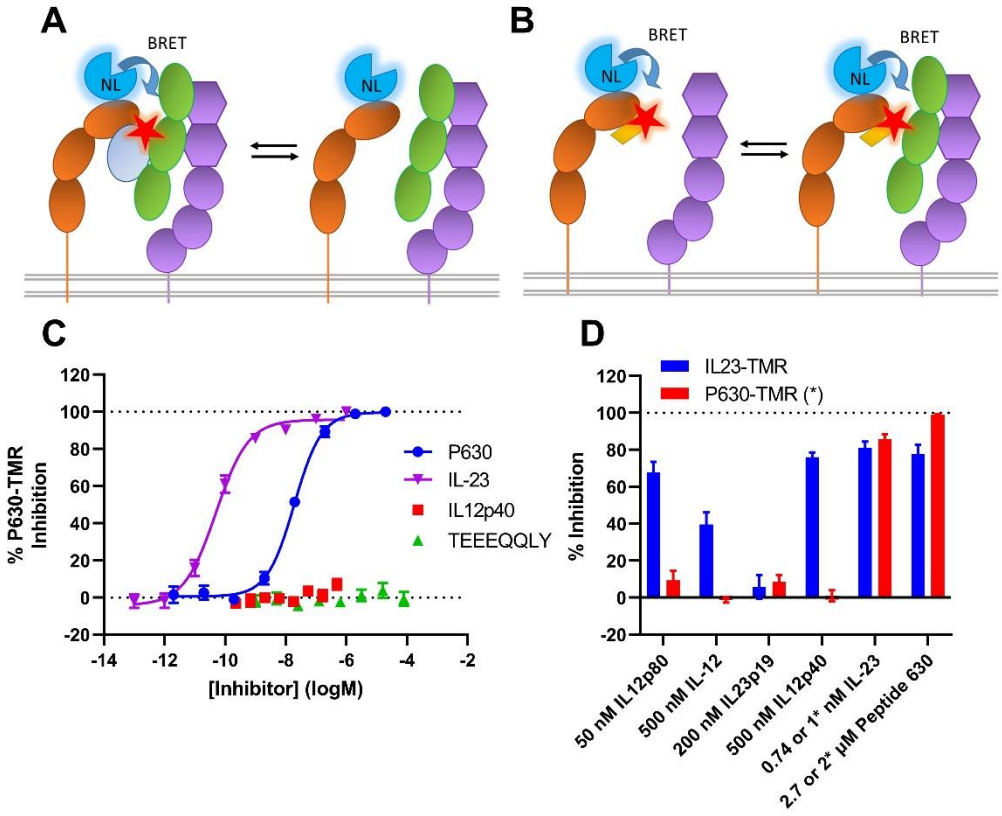

Figure 5-6: P630-TMR measures antagonism at the IL23R/IL23p19 interface. (A) A schematic demonstrating the competitive displacement of IL23-TMR by IL12p40. (B) A schematic demonstrating how P630-TMR is not displaced when IL12p40 binds to IL12Rβ1. (C) The displacement of 75 nM P630-TMR by increasing concentrations of various IL-23 receptor binders (fit with equation 4). (D) the displacement of either P630-TMR or IL23-TMR by a single concentration of various IL23R or IL12Rβ1 binders. An * indicates a concentration that was used for P630-TMR inhibition. Data are mean ± SEM from three (C: TEEEQQLY) or five independent experiments performed in triplicate.

Probe	Assay	Constructs expressed	K_i or K_d
IL12p40	IL23-TMR Competition (Figure 5-1B)	NL-IL23R and IL12Rβ1	12.4 ± 1.4 nM
	P630-TMR Competition (Figure 5-6A)		Did not displace probe
TEEEQQLY	IL23-TMR Competition (Figure 5-1D)	NL-IL23R and IL12Rβ1	Did not displace probe
	P630-TMR Competition (Figure 5-6A)		Did not displace probe
P630	IL23-TMR Competition (Figure 5-1C)	NL-IL23R and IL12Rβ1	21.8 ± 3.4 nM
	P630-TMR Competition (Figure 5-6A)		6.32 ± 1.06 nM
IL-23	IL23-TMR Competition (Figure 3-15A)	NL-IL23R and IL12Rβ1	31.6 ± 7.7 pM (Chapter 3)
	P630-TMR Competition (Figure 5-4A)		22.6 ± 5.2 pM
P630-TMR	Binding assay (Figure 5-2C-E and 5-3B)	NL-IL23R and IL12Rβ1	51.1 ± 7.3 nM
		NL-IL23R	101 ± 4 nM
		NL-IL12Rβ1 and IL23R	55.2 ± 10.5 nM
		NL-IL12Rβ1	No observable binding
		HiBit-IL23R and LgBit- IL12Rβ1	53.5 ± 4.4 nM

Table 5-1: The affinities of antagonists and labelled probes described in this chapter.

5.4.4 Kinetic characterisation of P630-TMR

The kinetic binding properties of P630-TMR were also investigated (Figure 5-7). It was observed that treatment of cells transfected with NL-IL23R and IL12Rβ1 with 75 nM P630-TMR led to a rapid association followed by a biphasic decay in signal. Interestingly, incubation of cells with 300 pM IL-23 prior to the addition of P630-TMR resulted in a rapid association that was not followed by this characteristic decay phase. In addition, replacement of media with 300 pM IL-23 and 75 nM P630-TMR at later time points also reduced the BRET ratio to a similar level and abolished this decay.

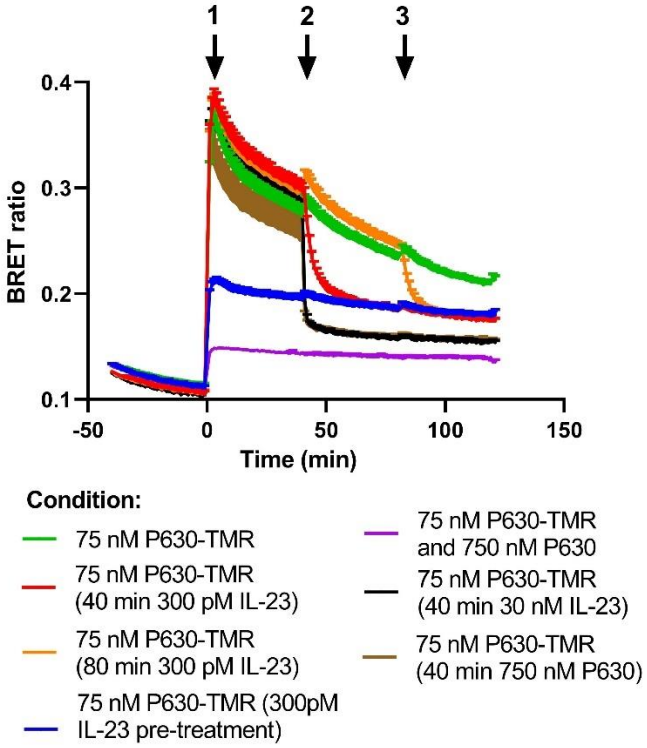

Figure 5-7: The kinetic properties of P630-TMR. The BRET signal measured when HEK293T cells transiently transfected with NL-IL23R and IL12Rβ1 were treated with P630-TMR in the presence and absence of competitors. Numbered arrows indicate time points at which additions were made. At time point 1 (following a 40-minute pre-incubation) media was replaced with 75 nM P630-TMR. At time point 2 (40 minutes after time point 1) certain conditions had media replaced with an excess of IL-23 or P630 or 300 pM IL-23 with 75 nM P630-TMR. At time point 3 (40 minutes after time point 2) in one condition media was replaced with 300 pM IL-23 and 75 nM P630-TMR. Data are mean ± SEM from three (addition of excess of IL-23 or P630), four (addition of 300pM IL-23 and P630-TMR) or five independent experiments conducted in triplicate.

When the media was replaced with an excess of unlabelled IL-23 or P630, P630-TMR rapidly dissociated. When the rate of this dissociation was quantified, a P630-TMR dissociation rate of 1.51 ± 0.20 min^{-1} was given from which an association rate of 2.96 ± 0.38 x 10^7 M^{-1} min^{-1} could be calculated using the pre-determined equilibrium affinity value Table 5-2.

Model	k_{on} (M^{-1} min^{-1})	k_{off} (min^{-1})	Residence time (min)	K_d (nM)
Single phase decay	2.96 ± 0.38 x 10^7 (Calculated from K_{off} and equilibrium affinity)	1.51 ± 0.20	0.701 ± 0.105	N/A
Equilibrium binding	N/A	N/A	N/A	51.1 ± 7.3 (Figure 5-2D)

Table 5-2: The kinetic properties of P630-TMR.

5.4.5 Defining the mechanism of action of the IL23R C115Y loss of function mutation

A single nucleotide polymorphism resulting in a cysteine to tyrosine mutation in the *N*-terminal domain of IL23R was previously reported in patients demonstrating a deficient immune response to Mycobacterial pathogens, with this mutation shown to block IL-23 induced STAT3 phosphorylation (Martínez-barricarte et al., 2018). Due to the position of the C115Y mutation at the IL23R:IL23p19 interface (Figure 5-8A) and the residue's role in tethering a 'hook-like' projection of IL23R that interacts with IL23p19 (Bloch et al., 2018), it was hypothesised that the loss of function of the C115Y mutant could be due to impaired binding of IL-23. To test this, untagged and NanoLuc tagged versions of the C115Y IL23R variant were created. When signal transduction of these mutants were tested, it was found that, as previously reported (Martínez-barricarte et al., 2018), the mutation blocked STAT3 phosphorylation (Figure 5-8B). Using the NanoLuc tag as a marker of expression it was demonstrated that the C115Y mutation could be successfully surface expressed in HEK293T cells, although the mutation resulted in a 40.8% reduction in total NL-IL23R and a

37.3% reduction in the proportion of NL-IL23R on the cell surface as compared to wildtype (Figure 5-8C and D). The fraction of NanoLuc tagged protein on the cell surface was defined by addition of 60 μM Extracellular NanoLuc inhibitor, a compound with a reported affinity of less than 10 nM (Walker et al., 2017). Using the intra-receptor NanoBRET assay to measure the basal association of receptor subunits, as described in Chapter 3, it was discovered that the C115Y mutant still associated with fluorescently labelled HT-IL12Rβ1 although this was reduced by 50.1% from the level of association measured for wildtype IL23R, a reduction consistent with the protein's reduced total and surface expression (Figure 5-8E).

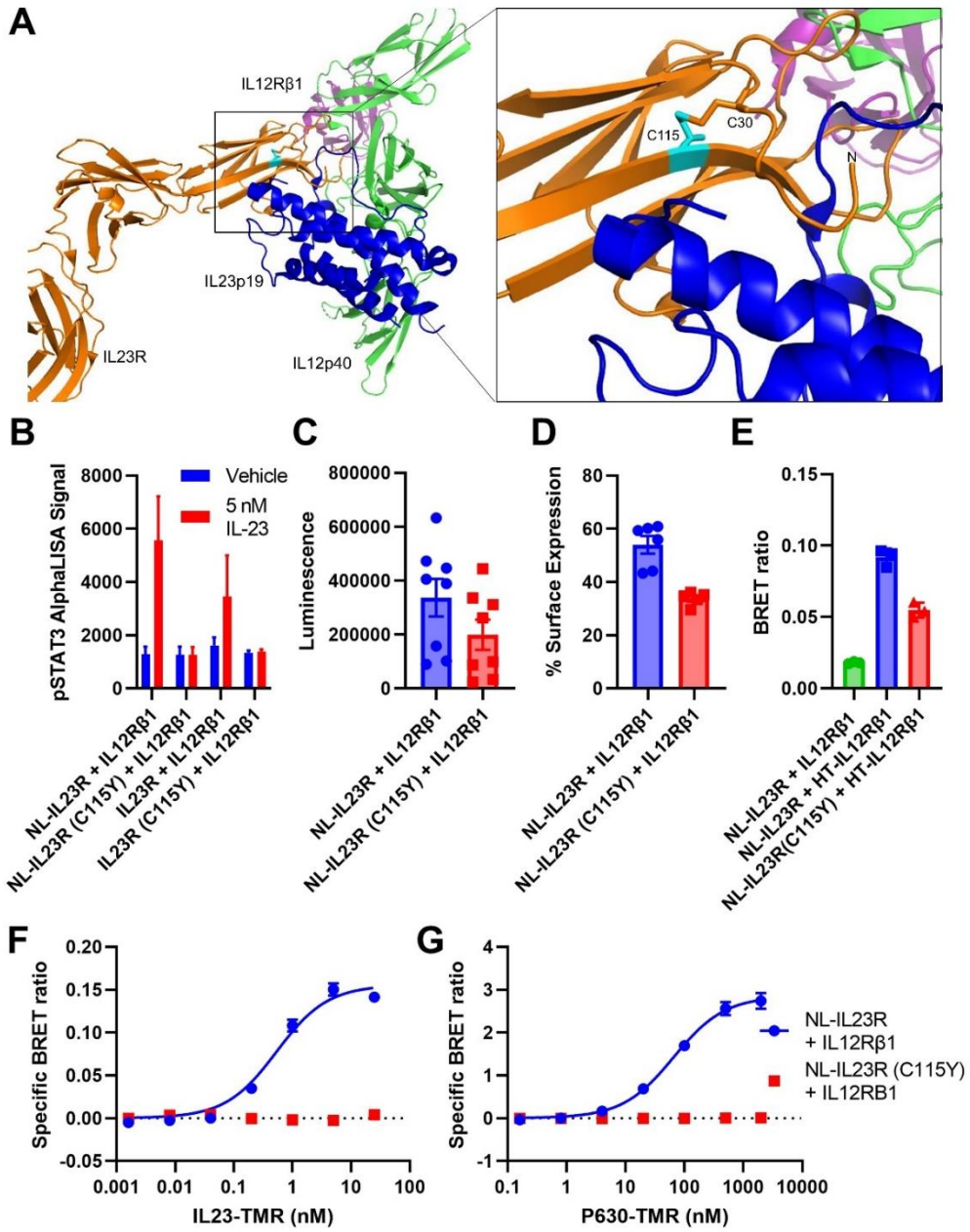

Figure 5-8: A single nucleotide polymorphism in the *N*-terminal domain of IL23R, linked to immunodeficiency, blocks binding of both IL23-TMR and P630-TMR. (A) Left: A crystal structure of the *N*-terminal domains 1-3 of IL23R (orange) in complex with IL-23 (IL23p19 = blue, IL12p40 = green) and the *N*-terminal domain 1 of IL12Rβ1 (PDB: 6WDQ; Glassman et al., 2021). Right: The magnified interaction interface between IL23R and IL23p19, with C115 coloured cyan. (B) The phospho-STAT3 alphaLISA signal generated when cells expressing IL12Rβ1 and different IL23R constructs are treated with 5 nM IL-23. Data are mean ± SEM from six (untagged) or three (NanoLuc tagged) independent experiments conducted in triplicate. (C) The luminescence signal measured when IL12Rβ1 is expressed with either NL-IL23R wildtype or the C115Y mutant. Data are mean ± SEM generated from the mean luminescence values from eight independent experiments performed in pentuplicate. (D) The proportion of luminescence from (C) that emanated from extracellular protein (as defined by the reduction in

luminescence after treatment with 60 μM NanoLuc extracellular inhibitor). (E) The BRET ratio generated when NL-tagged wildtype or C115Y IL23R were co-expressed with HaloTag-618 ligand labelled HT-IL12Rβ1. Data are mean ± SEM generated from the mean BRET values of three independent experiments performed in pentuplicate. (F-G) The BRET ratio generated when increasing concentrations of (F) IL23-TMR or (G) P630-TMR were applied to cells expressing wildtype (pink) or C115Y (black) mutant receptor (fit with Equation 2). Data are mean ± SEM from five (C115Y) or four (wildtype) independent experiments conducted in triplicate.

The ability of the C115Y mutant to bind IL23-TMR was also tested (Figure 5-8F), demonstrating that whilst a specific BRET signal was measured from control cells expressing the wildtype receptor, IL23-TMR did not bind to C115Y mutated IL23R. To test if P630-TMR and IL23-TMR shared a common binding epitope in the *N*-terminal region of IL23R the binding of P630-TMR to cells expressing wildtype and mutant receptor was also measured, demonstrating that the C115Y mutation also blocked specific binding of P630-TMR (Figure 5-8G).

The properties of two further disease associated IL23R mutants were also measured and compared to C115Y and wildtype protein. These mutants (V362I and R381Q; locations highlighted in Figure 5-9A) had both been identified to lower the risk of autoinflammatory diseases through genome wide association studies (GWAS) (Sivanesan et al., 2016). Whilst the V362I mutant had similar properties to wildtype IL23R, it was observed that the R381Q mutant resulted in lower surface expression and a subsequent lowered association with HT-IL12Rβ1 (Figure 5-9B-D). Despite this reduced surface expression, the R381Q mutant generated a similar amplitude of STAT3 phosphorylation to wildtype IL23R after cytokine stimulation and bound IL23-TMR with a comparable affinity to wildtype IL23R (Figure 5-9E and F).

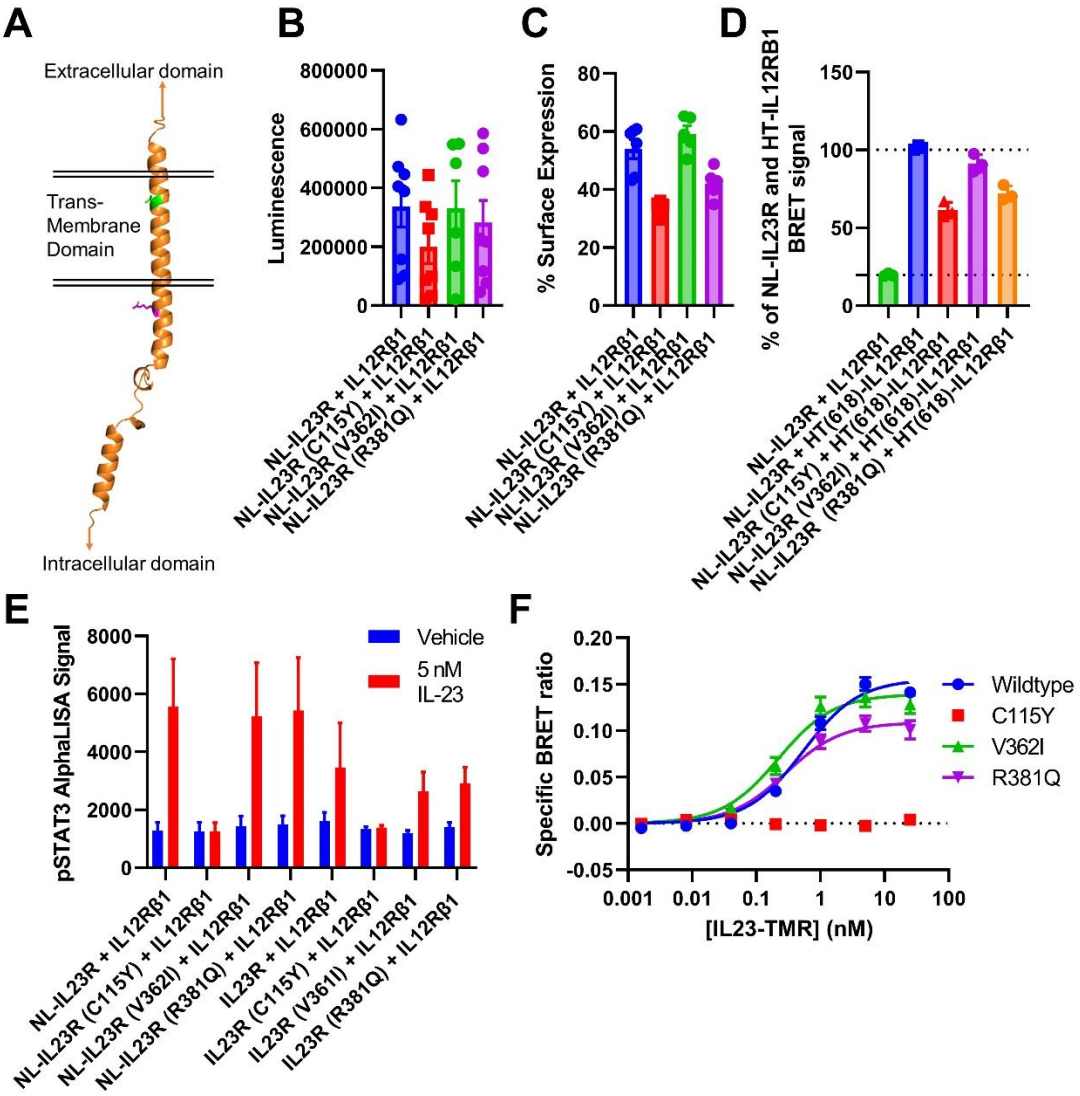

Figure 5-9: Comparison of the properties of the C115Y IL23R mutant with IL23R variants associated with protection from autoinflammatory diseases. (A) The Alphafold predicted structure of the transmembrane and membrane proximal regions of IL23R with the V362 and R381 residues shown in green and magenta respectively (Jumper et al., 2021). (B) The luminescence measured when NanoLuc tagged mutants of IL23R are transiently expressed with IL12Rβ1 (C) The proportion of the luminescent signal generated in (B) that originated from extracellular protein (defined by the reduction in luminescence after treatment with 60 μM NanoLuc extracellular inhibitor). Data are mean ± SEM generated from six (V362I) or eight independent experiments performed in pentuplicate. (D) The intra-receptor BRET signal when NanoLuc tagged IL23R variants were co-expressed with HaloTag-618 ligand labelled HT-IL12Rβ1. Data are mean ± SEM generated from three independent experiments performed in pentuplicate. (E) The phosphorylation of STAT3 when cells expressing IL23R variants and IL12Rβ1 are treated with 5 nM IL-23. Data are mean ± SEM from six (untagged) or three (NanoLuc tagged) independent experiments conducted in triplicate. (F) The BRET signal measured when increasing concentrations of IL23-TMR were applied to cells expressing

NanoLuc tagged IL23R variants with IL12Rβ1. Data are mean ± SEM from five or four (wildtype) independent experiments conducted in triplicate and are fit with Equation 2.

Despite the association of the C115Y mutant with HT-IL12Rβ1, when these receptor complexes were treated with IL-23, the characteristic decrease in BRET (observed for wildtype IL23R in chapter 3-19) was not observed, indicating that there was no ligand induced conformational change (Figure 5-10). When the same assay was performed on the V362I and R381Q mutants, a ligand dependent decrease in BRET was observed for both isoforms, with a reduced change associated with the R381Q mutant.

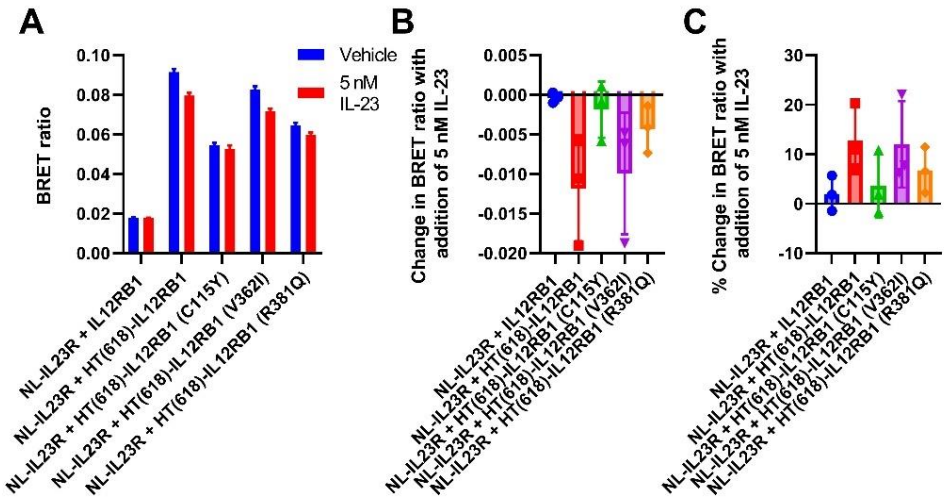

Figure 5-10: The C115Y mutant of IL23R associates with IL12Rβ1 but does not undergo ligand induced conformational change. (A) The BRET ratio generated by transiently transfected cells labelled with HT618 ligand in the presence and absence of IL-23. (B) the data from (A) expressed as mean change in BRET ratio with IL-23. (C) the data from (A) transformed to % change in BRET signal with IL-23 addition. Data are mean ± SEM from three independent experiments conducted in pentuplicate.

5.5 Discussion

The availability of validated chemical probes is a vital resource for the interrogation of emerging drug targets. Whilst there are few reports of small molecule antagonists of cytokine receptors, a growing list of cyclic peptide inhibitors of the IL-23 receptor indicates that the target may be tractable for antagonists beyond traditional antibody-based drugs (Cheng et al., 2019; Kong

et al., 2020; Kuchař et al., 2014; Pandya et al., 2020; Quiniou et al., 2014). In this chapter a fluorescently tagged version of IL-23 was used to measure antagonism of the IL-23 receptor by IL12p40, an endogenous protein antagonist (Mondal et al., 2020) and P630, a peptide from an emerging class of cyclic peptide IL23R inhibitors (Bourne et al., 2017). P630 was then developed into a novel fluorescent probe for the IL-23 receptor termed P630-TMR, through conjugation with the fluorophore TAMRA.

By measuring the binding of P630-TMR to cells expressing the cytokine subunits in isolation and together, using NanoBRET ligand binding assays, it was determined that P630-TMR bound specifically to IL23R. The mechanism of action of the IL23R C115Y loss of function mutation was then established to be a disruption of the IL23R:IL23p19 binding epitope with this result used to demonstrate that the IL23R binding epitope for P630-TMR and IL23-TMR is most likely conserved, as both probes cannot bind this mutant (see Figure 5-8).

It was observed that whilst P630-TMR bound with comparable affinity to cells expressing NL-IL23R in isolation or with IL12Rβ1, the BRET efficiency was much higher in the absence of IL12Rβ1 (see Figure 5-2). It has been demonstrated in previous chapters that the IL-23 receptor subunits associate in the absence of ligand with the *N*-termini in proximity. A possible explanation for the observed IL12Rβ1 driven reduction in BRET efficiency is a modulation of the position of the IL23R conjugated NL-tag by the *N*-terminus of IL12Rβ1 within an inactive receptor complex. The further reduction in BRET efficiency observed when the NanoLuc tag is placed on the *N*-terminus of IL12Rβ1 is most likely due to the increased distance between the *N*-terminus of IL12Rβ1 and the P630-TMR binding epitope, however the successful measurement of a BRET signal is consistent with the receptor subunits forming a complex in the absence of IL-23.

Fluoroprobes are useful tools in drug discovery as they can be used to identify the competitive binding of molecules that share a common binding site. It was found that P630-TMR could be displaced by IL-23, unlabelled P630 and to a low degree with an IL23p19-Fc fusion protein (see Figure 5-6), therefore it is likely P630-TMR could be used to characterise novel binders of the

IL23p19:IL23R interface. Furthermore, by positioning the NanoLuc tag on the *N*-terminus of IL12Rβ1, displacement of P630-TMR could be measured from unlabelled IL23R. This would be advantageous as structural studies have demonstrated that the *N*-terminal domain of IL23R is closely involved in ligand binding. Using this approach, the interaction of unmodified IL23R binders with untagged full-length IL23R could be measured in the membranes of living cells, enabling a more accurate recapitulation of *in vivo* drug-target interactions.

In this chapter it was demonstrated that the interaction between IL23-TMR and P630 is competitive, reinforcing the hypothesis that P630 binds to a shared epitope with IL-23. However, the lack of a conventional competitive interaction when P630-TMR was displaced with IL-23 indicates that observations of the interaction at the IL23R interface may be biased by the presence of the additional IL-23 binding site on IL12Rβ1, which acts as an additional allosteric site from which P630 cannot displace IL-23.

The IL-23 binding site is made up of interfaces on two proteins which have been shown to associate prior to ligand binding in this experimental model. It is therefore possible that IL-23 can first bind the IL12Rβ1 half of the binding site subsequently displacing P630-TMR either through constraint in the region of the IL23R epitope or a cooperative effect that displaces P630-TMR. This would explain why increasing concentrations of P630-TMR did not raise the IC_{50} of IL-23 (see Figure 5-5), as this effect would be dependent on the initial interaction with IL12Rβ1. However, this model conflicts with the observation that increasing concentrations of P630 led to increasing displacement of IL23-TMR (see Figure 5-4). Perhaps this effect could be explained by the existence of a threshold above which P630 is able to displace IL23-TMR, although the IL23-TMR displacement by P630 appear to be mono-phasic and the affinity of P630 is similar when measured with P630-TMR or IL23-TMR. A further factor that may influence the results could be modulation of the interaction between P630 and IL-23 brought on by the addition of the TMR moiety to P630, or the concentration ranges used in both experiments. To probe the differences observed here in more detail it would be useful to study the competition of IL-23 with P630-TMR at NL-IL23R expressed in isolation. To ascertain if in the absence of IL12Rβ1 the interaction becomes competitive. In addition, the

experiment could be conducted with an excess of P630-TMR to see if a threshold exists beyond which IL-23 can be competitively displaced.

IL-23 engages its receptor in a bivalent interaction in which IL23R specifically engages IL23p19 and IL12Rβ1 specifically interacts with IL12p40 (Glassman et al., 2021; Schroder et al., 2015). This means that potential competitive antagonists could be directed to either the IL12Rβ1 or IL23R epitopes, however due to the promiscuous pairing of IL12Rβ1 with IL12Rβ2 to form the IL-12 receptor complex, all IL23R antagonists reported thus far have been directed at the IL23R interface, making them specific to IL-23 signalling. Using fluoro-labelled IL-23 it was possible to measure antagonism at both the IL23R and IL12Rβ1 interfaces, as shown by the displacement of IL23-TMR but not P630-TMR by IL12p40, a protein that specifically binds to IL12Rβ1 (Glassman et al., 2021). IL-12 was able to displace IL23-TMR but not P630-TMR, presumably through competition at the IL12p40:IL12Rβ1 interface. This finding may represent an endogenous mechanism through which IL-23 signalling is regulated by the presence of IL-12, through competition for IL12Rβ1.

IL12p80, a homodimer of IL12p40 reported to act as an antagonist of IL-12 signalling and to have its own functional responses (Jana et al., 2009; Mondal et al., 2020), also inhibited IL23-TMR binding. This is presumably through the IL12p40:IL12Rβ1 interface as P630-TMR was not heavily displaced by an equivalent concentration of IL12p80. The low level of displacement of P630-TMR by IL12p80 and not IL12p40, at concentrations that led to an equivalent displacement of IL23-TMR, could imply that IL12p80 was able to displace P630-TMR through a steric interaction when the larger molecule bound to the closely associated IL12Rβ1 subunit, if IL12p80 is able to displace IL23p19 in a similar fashion this may explain the molecule's more potent displacement of IL23-TMR. Another interesting observation was the equivalent inhibition of IL23-TMR by IL12p40 and a 10-fold lower concentration of IL12p80. Although IL12p80 contains two IL12p40 molecules this does not account for the increase in competition. Taken together with previous reports of murine IL12p80's increased inhibition of IL-12 binding compared to IL12p40 (Gillessen et al., 1995), this observation indicates that homodimerization of IL12p40 increases the molecule's ability to displace heterodimeric IL12Rβ1 engaging cytokines.

The competitive displacement of an octapeptide that is a reported allosteric antagonist of the IL-23 receptor (TEEEQQLY) was also tested, demonstrating that it did not displace IL23-TMR or P630-TMR (see Figure 5-1 and 5-6). As the inhibition of functional response by this molecule was not tested, the efficacy of the molecule as an IL-23 receptor antagonist cannot be assessed, however the results indicate that, as reported, the peptide does not competitively bind to either of the IL-23 binding epitopes (Quiniou et al., 2014).

The binding kinetics of P630-TMR were also investigated. Whilst it was demonstrated in Chapter 3 that 300 pM of IL23-TMR reached a stable equilibrium after approximately 20-minutes, P630-TMR had a much more rapid association (62.9-fold the k_{on} of IL23-TMR), with 75 nM of the probe reaching its maximum association within 5-minutes and then undergoing a biphasic reduction in the observed BRET signal (see Figure 5-7). This reduction in signal is unlikely to be a result of substrate depletion, evaporation or another assay artefact as it is not observed for the equivalent interaction with IL23-TMR, meaning the phenomena is most likely specific to P630-TMR. Furthermore, when cells were pre-incubated with 300 pM unlabelled IL-23, P630-TMR bound with no decrease in signal over time. A possible hypothesis to explain these observations is that P630-TMR has a two-step binding mode in which an initial binding event is followed by a re-arrangement in which the secondary position has a less favourable orientation for BRET. The dissociation rate of P630-TMR was also measured, demonstrating that the probe exhibited a rapid dissociation from the receptor (30.1-fold faster than IL23-TMR). These results demonstrate that the P630-TMR probe has much quicker association and dissociation rates than IL-23, with the higher affinity of IL-23 driven by the elongated residence time of the IL-23 cytokine at the receptor.

A disadvantage of using a fluoroprobe competition assay in drug discovery, is that allosteric interactions may not be identified if they do not displace the probe used. A good example in this study is the lack of displacement of P630-TMR by IL12p40, a known binder of IL12Rβ1. The advantageous nature of the approach described in this chapter, is that by screening potential antagonists through both P630-TMR and IL23-TMR competition assays, ‘hits’ can be further sorted into IL23p19 competitive (if they displace P630-TMR and IL23-TMR) or IL12p40

competitive or allosteric (if they only displace IL23-TMR). If an allosteric molecule binds to the receptor, preventing activation by IL-23 but not impacting IL23-TMR binding, this could be identified by one of the many functional assays that have been described for the pathway (for example; Fereshteh et al., 2016; Varghese et al., 2020). Currently drug discovery efforts targeting the IL-23 receptor would either need to screen molecules against purified protein in a biochemical assay, an approach which does not accurately represent the activity of the receptor constituents on the cell surface, or screen 'hits' found in functional assays for activity against signal transducers that could result in non-specific inhibition of the pathway.

Several disease linked mutants of IL23R were also profiled using the previously validated NanoBRET and AlphaLISA assays. The experiments conducted indicated that the R381Q mutation reduced surface expression, as had previously been reported in the literature (Sun et al., 2020) and demonstrated that both the V362I and R381Q mutants maintained a similar affinity for IL-23 (Figure 5-9). The immunodeficiency linked C115Y mutation however, completely blocked binding of IL23-TMR which is likely the mechanism through which responsiveness to IL-23 is lost in patients with the mutation (Martínez-barricarte et al., 2018). Both R381Q and V362I mutants have been identified as protective against the development of auto-inflammatory disease and have been shown to maintain functionality in cellular models (Sivanesan et al., 2016). The maintenance of unmodified ligand binding and signalling demonstrated here indicate that there is a more subtle mechanism by which propensity for auto-inflammatory disease is modulated.

This chapter describes the use of IL23-TMR and the novel fluorescent peptide P630-TMR as competitive probes to define IL-23 receptor antagonists, however this is not the only application for a membrane receptor specific fluorescent probe. Examples of further applications of P630-TMR include the fluorescent labelling of cells for imaging or flowcytometry experiments (Borgarelli et al., 2021). The approach outlined in this study to measure competitive interactions at IL23R should enable better characterisation of an emerging class of peptide inhibitors. As the tractability of further cytokine receptors for peptide or small molecule antagonism is established (for example; Bello et al., 2014; Scheide-

Noeth et al., 2019) this technology could be applied in a similar way to further under-characterised drug targets.

Chapter 6. General Discussion

The IL-23 receptor is an important therapeutic target for auto-inflammatory conditions such as Crohn's disease and psoriasis, however the mechanism of receptor activation has yet to be fully defined. Using NanoBRET this project measured the interaction of IL23-TMR with NanoLuc fusions of the full-length IL-23 receptor subunits expressed in live cells and reported that IL23-TMR had a higher affinity for NL-IL12Rβ1 compared to that for NL-IL23R. In addition, it was observed that co-expression of NL-IL23R with IL12Rβ1 created a binding site with an affinity far higher than those measured for NL-IL23R or NL-IL12Rβ1 alone (Figure 3-13). Intra-receptor NanoBRET experiments indicated that this heteromeric complex could be formed in the absence of added ligand and demonstrated that the binding of IL-23 induced a potent change in the relative positions of the *N*-terminal domains of the receptor in a manner consistent with a conformational change (Figure 3-19). These experiments contradicted the existing literature model of receptor activation which stated that IL-23 first engages IL23R leading to the binding of IL12Rβ1 by the IL-23:IL23R complex (Bloch et al., 2018). However, as the previous experiments were conducted using purified truncates of the receptor extracellular domains, it was unsurprising that the proteins functioned differently when expressed at their full-length within the cell membrane. Another important factor are the reports that interactions between cytokine receptor subunits may be partly mediated through constitutively associated JAK proteins, whose effects would only be observed in an intact cellular system (Waters and Brooks, 2015; Wilmes et al., 2020).

To further explore the constitutive association of the IL-23 receptor components, complex formation was monitored using NanoBiT complementation. In these assays, receptor subunit association was measured by the reconstitution of NanoLuc from complementary fragments appended to the *N*-terminal domains of the receptor. This technique, which does not use resonance energy transfer and so is not influenced by dipole-dipole interactions, has lower sensitivity to changes in orientation when compared to the intra-receptor BRET assay and therefore allows a focus on proximity. The methodology also enabled the establishment of a donor for subsequent BRET binding studies to measure the

engagement of IL23-TMR to binary receptor complexes. This approach confirmed that in a transient transfection system the IL-23 receptor heteromer associates in the absence of ligand. Despite the constitutive association, STAT3 signalling could only be induced by addition of ligand or by specific conformations of high affinity complementation (Figure 4-11). This observation indicated that receptor activation is not driven by dimerisation alone and that a further ligand induced conformational change is most likely necessary for activation of the receptor.

A universal model for cytokine receptor activation remains controversial; many publications have reported that cytokine receptor subunits associate in the absence of ligand (Couturier and Jockers, 2003; Krause et al., 2013; Livnah et al., 1999; Lu et al., 2006; Malka et al., 2008; Pillet et al., 2010; Tenhumberg et al., 2006). In addition, detailed studies have investigated the specific mechanisms of the subsequent conformational change necessary for activation, demonstrating that dimerization alone is not sufficient to induce signalling (Brooks et al., 2014; Pillet et al., 2010). Importantly, many of these studies include evidence from experiments conducted at physiologically relevant receptor expression levels (Couturier and Jockers, 2003; Pillet et al., 2010; Tenhumberg et al., 2006). In parallel several studies using single molecule imaging techniques have reported convincing evidence that cytokine receptor subunits are induced to dimerise and signal through the addition of ligand (Gandhi et al., 2014; Moraga et al., 2015b, 2015a; Wilmes et al., 2015). There may not be a single shared mechanism for cytokine receptor activation, meaning some of the disagreement may be due to differential mechanisms between receptors. However, there are notable examples such as the growth hormone receptor, in which persuasive evidence for both ligand induced dimerization (Wilmes et al., 2020) and ligand induced conformational change have been reported (Brooks et al., 2014).

In this study, the major limitation of the approach used is the transient transfection based HEK293T overexpression system. The system was essential as it allowed a versatile platform to perform a wide variety of experiments under analogous conditions together with a greater recapitulation of the *in vivo* environment of the receptor, when compared to previous purified protein

methodologies (Bloch et al., 2018). However, some crucial factors were not recapitulated in this system. The first is equivalent expression levels of relevant pathway genes as those in disease states and the second is the endogenous expression level of IL23R and IL12Rβ1 themselves. In particular, the effect of *C*-terminally associated JAK proteins on cytokine receptor association and activation, is an important aspect of IL-23 receptor biology that needs further study. The findings here could be built on by repetition of the experiments in JAK knock out, mutant and overexpressing cell lines.

In an ideal assay system, the association and activation of the IL-23 receptor would be tested in various types of primary immune cells under endogenous promoter-driven expression. The overexpression system in the present study likely leads to a higher expression of IL-23 receptor components than that seen in endogenous cell types, although this is difficult to quantify without reported levels of IL-23 receptor component expression. In the membrane, where diffusion is limited to a 2D plane, overexpression could plausibly lead to a shift towards dimerization in any equilibrium between monomer and dimer that exists endogenously. For this reason, the results presented here should not be construed as direct evidence that the IL-23 receptor is found purely as a dimer under *in vivo* conditions. Despite this the study presents compelling evidence that the IL-23 receptor can associate to form a complex that is only activated after the addition of ligand. Furthermore, this ligand induced activation causes a change in the positions of the *N*-terminal domains of the receptor and can be synthetically replicated by constraint of the *N*-terminal domains in specific conformations. This evidence strongly indicates that ligand induced conformational change is an integral part of the IL-23 receptor activation mechanism.

The results outlined here lead to the suggestion of two possible IL-23 receptor activation mechanisms (outlined in Figure 6-1). In the first, IL23R and IL12Rβ1 are constitutively associated in the membrane, IL-23 then binds and activates the receptor through conformational change. In the second, an equilibrium between monomers and dimers of IL23R and IL12Rβ1 exists under endogenous conditions, related to membrane concentration and inter-receptor chain affinity. This equilibrium is then shifted towards complex formation by the binding of

IL-23, but the final activation is dependent on a conformational change in the receptor heteromer. There are several plausible reasons as to why the second explanation could be evolutionarily advantageous; firstly under low ligand concentrations the initial equilibrium provides a further stage of regulation through which a threshold of expression must be reached before the high affinity binding site is formed, but under high ligand concentrations and low expression levels, ligand induced dimerisation could be instigated through the binding of medium and low affinity binding sites on IL12Rβ1 and IL23R respectively. Secondly, as shown by the success of anti-IL-23 therapeutics in treating auto-inflammatory diseases, aberrant IL-23 signalling can be highly pathogenic. By requiring a final ligand induced conformational change for activation, unintentional signalling events caused by random collisions of receptor subunits can be avoided. Finally, an equilibrium between unliganded IL23R and IL12Rβ1 would allow rapid switching of receptor chains between different cytokine receptor complexes, for example formation of IL-12 receptor complexes through association with IL12Rβ2.

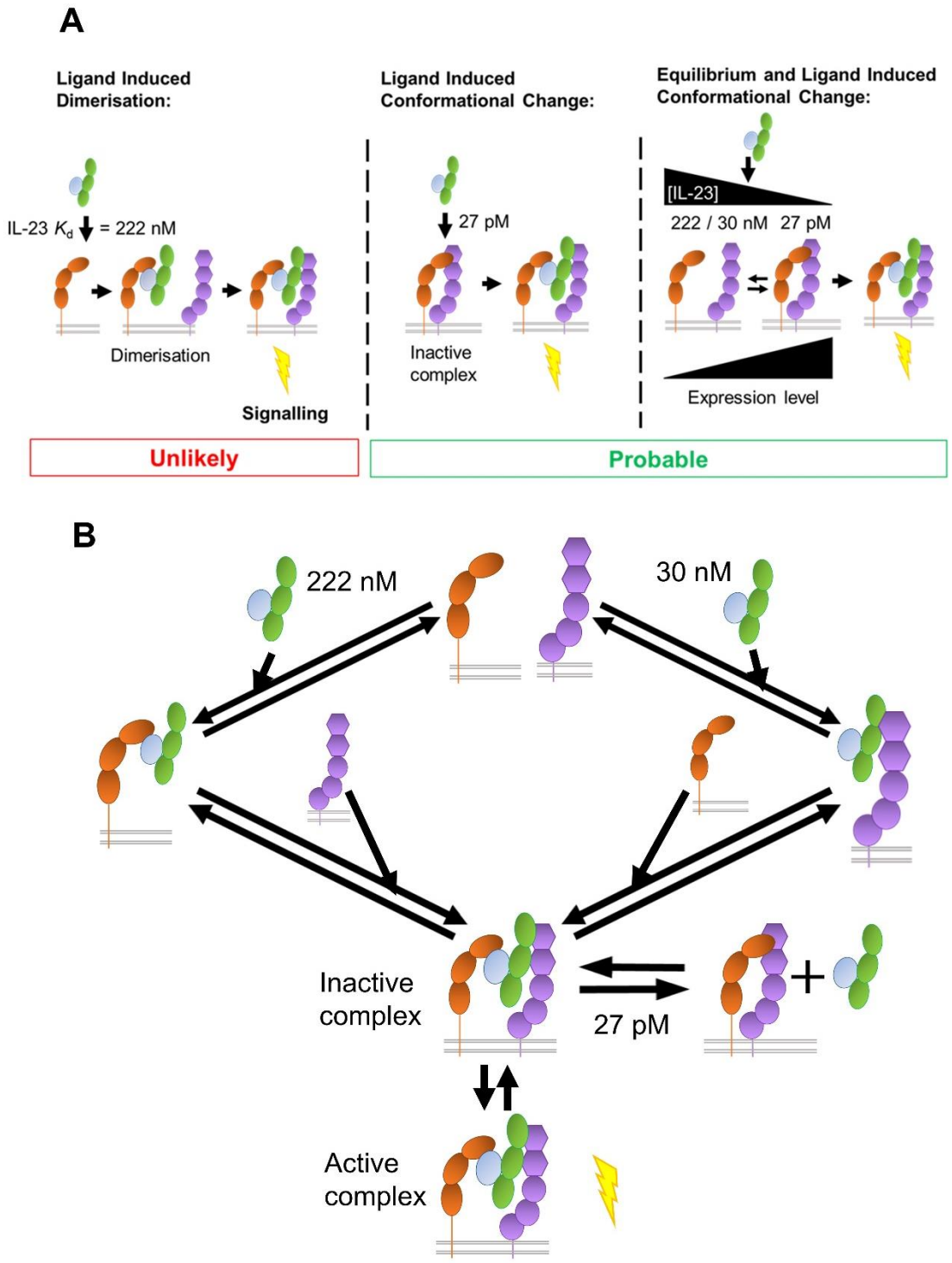

Figure 6-1: A schematic summarising the probable mechanisms of IL-23 receptor activation. (A) (Left) Ligand induced dimerisation in which IL-23 first binds to IL23R and then recruits IL12Rβ1 to induce signalling by dimerisation. This is unlikely as in this thesis it is demonstrated that dimerisation alone is not sufficient for receptor activation. (Centre) Ligand induced conformational change in which the receptor is always pre-formed and ligand binding induces signalling. This is consistent with the results of this thesis, however because endogenous levels of expression were not used, the existence of a further equilibrium between monomers

and complexes cannot be ruled out. (Right) Ligand induced conformational change with an equilibrium between monomers and complexes that is related to the membrane concentration and affinity of the receptor components. Black triangles outline possible implications of this model, namely that higher expression may make the cells more sensitive to IL-23 by producing more high affinity binding sites and high concentrations of IL-23 could potentially increase the response of low expressing cells by engaging low affinity binding sites on IL23R and IL12Rβ1. (B) A reaction scheme demonstrating the hypothesis of receptor activation discussed in the right side of (A).

To fully test the hypotheses set forward here it will be vital to measure cytokine receptors under endogenous promoter-driven expression. Current single molecule imaging studies have focussed on minimal expression systems to aid resolution of individual complexes (Moraga et al., 2015a; Wilmes et al., 2020), and proximity-based technique studies (such as the one outlined in this work) have used over-expression due to the ease of introduction of tagged constructs (Brooks et al., 2014; Krause et al., 2013; Malka et al., 2008). A useful next step in the study of IL-23 receptor activation would be to conduct single molecule imaging studies (such as TIRF-M or FCS) and proximity-based techniques (such as those outlined in this study) on endogenously expressed proteins using either a tag introduced at the endogenous locus through CRISPR or by labelling untagged protein with a fluorescent nanobody or peptide, as has been reported for GPCRs (Soave et al., 2021). This approach, whilst more time intensive, would give a more complete answer as to the true ligand binding and activation mechanism.

In the final part of this study the techniques developed to probe the association and activation of the IL-23 receptor were applied to the characterisation of receptor antagonists and disease relevant mutants. The IL-23 cytokine is a vital drug target for the treatment of several auto-inflammatory diseases and there is a strong industrial focus on the pathway due to the commercial success of Ustekinumab (the 7th highest selling drug in 2021; Chyuan and Lai, 2020; Urquhart, 2021). This has led to the development of a new generation of receptor antagonists specific to IL23R, which could improve upon the current antibody based therapies (Bourne et al., 2017; Kong et al., 2020; Kuchař et al., 2014; Pandya et al., 2020; Quiniou et al., 2014). The successful development and licencing of such an antagonist could serve as a blueprint for further cytokine

receptor specific treatments, much as the initial success of biologic drugs such as infliximab accelerated the development of the field (Lu et al., 2020). There are, however, significant hurdles to establishing such as receptor antagonist, chief amongst these are the lack of knowledge on the pharmacology of cytokine receptors and the predicted poor tractability for small molecules (Wilson and Arkin, 2010).

To aid the pharmacological characterisation of the IL-23 receptor, this study demonstrated that a fluorescent probe competition assay, equivalent to those described for highly characterised GPCR targets (Soave et al., 2020c), could be conducted at a cytokine receptor using competition with both labelled IL-23 (IL23-TMR) and a novel fluorescently tagged peptide that bound to the IL-23:IL23R interface (P630-TMR). Remarkably whilst the affinity of IL23-TMR was modulated by over 8000-fold by the presence of IL12Rβ1, the affinity of P630-TMR was unchanged by the presence of the co-receptor. Similarly, whilst the association and dissociation kinetics of IL23-TMR were relatively slow leading to IL23-TMR having a residence time of 20.3 min at the receptor and 36.8 min at binary complexes, the kinetics of P630-TMR were comparatively quick with a residence time of just 39.7 s at IL23R. A key limitation of the characterisation of these probes was the poor availability of commercial test compounds, with each competitor having to be custom synthesised. To compensate for this, suspected endogenously produced antagonists of IL-23 signalling were tested, demonstrating that IL-12, IL12p80 and IL12p40 all compete with IL23-TMR for the IL-23 receptor.

Previously reported peptide antagonists of the IL-23 receptor have been characterised using downstream assays such as transducer phosphorylation or purified protein assays such as SPR or ELISA (Bourne et al., 2017; Kong et al., 2020; Kuchař et al., 2014; Pandya et al., 2020; Varghese et al., 2020). The NanoBRET competition assays described here are more specific than the downstream inhibition assays and more biologically relevant than the purified protein approaches previously applied. The assay platforms outlined here enable a validated route to screen and characterise novel antagonists. The assays also enable the quantification of the interaction between IL23R and IL12Rβ1. Indeed, it was shown that HT-IL12Rβ1 could competitively displace LgBit-

IL12Rβ1 from SmBit-IL23R in a ligand independent manner. This observation raises the possibility that therapies that allosterically disrupt IL-23 signalling by preventing IL23R and IL12Rβ1 association could be developed and that these could be tested in an analogous assay set up.

Disease linked mutants of IL23R were also profiled using the assays generated in this project, allowing the identification of the mechanism of action of the C115Y IL23R mutation. This could have implications for patients who have immunodeficiencies caused by this variant, as the results indicate that whilst the mutation reduces surface expression, development of a chaperone treatment would be unlikely to restore functionality due to the additional disruption of IL-23 binding caused by the mutation. Indeed, lowered surface expression alone may be beneficial, as it was shown that the IBD protective variant R381Q (Duerr et al., 2006) had lowered surface expression but maintained functionality. The lowered surface expression of R381Q is in agreement with literature reports that the mutation leads to impaired recycling and increased degradation of the receptor (Sun et al., 2020).

Despite the IL-23 receptor being a well-validated drug target for auto-inflammatory disease, at the beginning of this project the mechanisms of ligand binding and activation were unclear and there were limited tools to study the receptor in live cells. This study measured the binding affinity of IL-23 for its receptor components expressed on living cells for the first time and revealed that receptor components associated before ligand engagement to form a high affinity binding site. Further work demonstrated that IL-23 engagement led to a conformational change in the *N*-terminal regions of the receptor and that this could be synthetically reproduced through high affinity crosslinking in specific conformations. Finally, the tools developed were applied to characterise disease linked mutants and reported receptor antagonists, demonstrating that the immunodeficiency associated C115Y mutation abrogated ligand engagement. Several receptor antagonists were characterised and the competitive peptide P630 was developed into a fluorescent probe for the IL23R:IL23p19 interface to be used alongside IL23-TMR for the characterisation of further receptor antagonists. It is hoped that the work outlined here will be of use for the

development of further anti-inflammatory therapeutics targeting the IL-23 pathway.

References

Abroun, S., Saki, N., Ahmadvand, M., Asghari, F., Salari, F., and Rahim, F. (2015). STATs: An old story, yet mesmerizing. Cell J. *17*, 395–411.

Acosta-Rodriguez, E. V., Napolitani, G., Lanzavecchia, A., and Sallusto, F. (2007). Interleukins 1β and 6 but not transforming growth factor-β are essential for the differentiation of interleukin 17-producing human T helper cells. Nat. Immunol. *8*, 942–949.

Ahern, P.P., Schiering, C., Buonocore, S., McGeachy, M.J., Cua, D.J., Maloy, K.J., and Powrie, F. (2010). Interleukin-23 Drives Intestinal Inflammation through Direct Activity on T Cells. Immunity *33*, 279–288.

Akdis, M., Aab, A., Altunbulakli, C., Azkur, K., Costa, R.A., Crameri, R., Duan, S., Eiwegger, T., Eljaszewicz, A., Ferstl, R., et al. (2016). Interleukins (from IL-1 to IL-38), interferons, transforming growth factor β, and TNF-α: Receptors, functions, and roles in diseases. J. Allergy Clin. Immunol. *138*, 984–1010.

Álvarez-Salamero, C., Castillo-González, R., Pastor-Fernández, G., Mariblanca, I.R., Pino, J., Cibrian, D., and Navarro, M.N. (2020). IL-23 signaling regulation of pro-inflammatory T-cell migration uncovered by phosphoproteomics. PLoS Biol. *18*, 1–33.

Angelini, J., Talotta, R., Roncato, R., Fornasier, G., Barbiero, G., Cin, L.D., Brancati, S., and Scaglione, F. (2020). JAK-inhibitors for the treatment of rheumatoid arthritis: A focus on the present and an outlook on the future. Biomolecules *10*, 1002–1042.

Arbiser, J.L., and Elsey, J. (2018). Targeting the Plasticity of Psoriasis. J. Invest. Dermatol. *138*, 734–736.

Vander Ark, A., Cao, J., and Li, X. (2018). TGF-β receptors: In and beyond TGF-β signaling. Cell. Signal. *52*, 112–120.

Atwa, M.A., Emara, A.S., Youssef, N., and Bayoumy, N.M. (2014). Serum concentration of IL-17, IL-23 and TNF-α among patients with chronic spontaneous urticaria: Association with disease activity and autologous serum

skin test. J. Eur. Acad. Dermatology Venereol. *28*.

Babon, J.J., Sabo, J.K., Zhang, J.G., Nicola, N.A., and Norton, R.S. (2009). The SOCS Box Encodes a Hierarchy of Affinities for Cullin5: Implications for Ubiquitin Ligase Formation and Cytokine Signalling Suppression. J. Mol. Biol. *387*, 162–174.

Baeten, D., and Adamopoulos, I.E. (2021). IL-23 Inhibition in Ankylosing Spondylitis: Where Did It Go Wrong? Front. Immunol. *11*, 1–4.

Baker, K.F., and Isaacs, J.D. (2018). Novel therapies for immune-mediated inflammatory diseases: What can we learn from their use in rheumatoid arthritis, spondyloarthritis, systemic lupus erythematosus, psoriasis, Crohn's disease and ulcerative colitis? Ann. Rheum. Dis. *77*, 175–187.

Beizavi, Z., Zohouri, M., Asadipour, M., and Ghaderi, A. (2021). IL-27, a pleiotropic cytokine for fine-tuning the immune response in cancer. Int. Rev. Immunol. *40*, 319–329.

Belladonna, M.L., Renauld, J.-C., Bianchi, R., Vacca, C., Fallarino, F., Orabona, C., Fioretti, M.C., Grohmann, U., and Puccetti, P. (2002). IL-23 and IL-12 Have Overlapping, but Distinct, Effects on Murine Dendritic Cells. J. Immunol. *168*, 5448–5454.

Bello, A.M., Wei, L., Majchrzak-Kita, B., Salum, N., Purohit, M.K., Fish, E.N., and Kotra, L.P. (2014). Small molecule mimetics of an interferon-α receptor interacting domain. Bioorganic Med. Chem. *22*, 978–985.

Benedek, T.G. (2011). History of the development of corticosteroid therapy. Clin. Exp. Rheumatol. *29*, 5–12.

Beyer, B.M., Ingram, R., Ramanathan, L., Reichert, P., Le, H. V., Madison, V., and Orth, P. (2008). Crystal Structures of the Pro-Inflammatory Cytokine Interleukin-23 and Its Complex with a High-Affinity Neutralizing Antibody. J. Mol. Biol. *382*, 942–955.

Bharadwaj, U., Kasembeli, M.M., Robinson, P., and Tweardy, D.J. (2020). Targeting janus kinases and signal transducer and activator of transcription 3 to treat inflammation, fibrosis, and cancer: Rationale, progress, and caution.

Pharmacol. Rev. *72*, 486–526.

Bhattacharya, S., and Schindler, C. (2003). Regulation of Stat3 nuclear export. J. Clin. Invest. *111*, 553–559.

Bhaumik, S., and Basu, R. (2017). Cellular and molecular dynamics of Th17 differentiation and its developmental plasticity in the intestinal immune response. Front. Immunol. *8*, 1–20.

Bieber, T., Simpson, E.L., Silverberg, J.I., Thaçi, D., Paul, C., Pink, A.E., Kataoka, Y., Chu, C.-Y., DiBonaventura, M., Rojo, R., et al. (2021). Abrocitinib versus Placebo or Dupilumab for Atopic Dermatitis. N. Engl. J. Med. *384*, 1101–1112.

Bilik, M.Z., Kaplan, I., Polat, N., Akil, M.A., Akyüz, A., Acet, H., Yüksel, M., Inci, U., Kayan, F., and Toprak, N. (2016). Serum levels of IL-17 and IL-23 in patients with rheumatic mitral stenosis. Med. (United States) *95*.

Bloch, Y., Bouchareychas, L., Merceron, R., Składanowska, K., Van den Bossche, L., Detry, S., Govindarajan, S., Elewaut, D., Haerynck, F., Dullaers, M., et al. (2018). Structural Activation of Pro-inflammatory Human Cytokine IL-23 by Cognate IL-23 Receptor Enables Recruitment of the Shared Receptor IL-12Rβ1. Immunity *48*, 45–58.

Bohnacker, S., Hildenbrand, K., Aschenbrenner, I., Müller, S.I., Bieren, J.E. von, and Feige, M.J. (2020). Influence of glycosylation on IL-12 family cytokine biogenesis and function. Mol. Immunol. *126*, 120–128.

Borg, F.A.Y., and Isenberg, D.A. (2007). Syndromes and complications of interferon therapy. Curr. Opin. Rheumatol. *19*, 61–66.

Borgarelli, C., Klingl, Y.E., Escamilla-Ayala, A., Munck, S., Van Den Bosch, L., De Borggraeve, W.M., and Ismalaj, E. (2021). Lighting Up the Plasma Membrane: Development and Applications of Fluorescent Ligands for Transmembrane Proteins. Chem. - A Eur. J. *27*, 8605–8641.

Boulanger, M.J., Chow, D. chone, Brevnova, E.E., and Garcia, K.C. (2003). Hexameric structure and assembly of the interieukin-6/IL-6 α-receptor/gp130 complex. Science. *300*, 2101–2104.

Bourne, G.T., Bhandari, A., Cheng, X., Frederick, B.T., Zhang, J., Patel, D. V., and Lui, D. (2017). Oral peptide inhibitors of interleukin-23 receptor and their use to treat inflammatory bowel diseases (United States of America: US patent office).

Bousoik, E., and Montazeri Aliabadi, H. (2018). “Do We Know Jack” About JAK? A Closer Look at JAK/STAT Signaling Pathway. Front. Oncol. *8*, 1–20.

Braisted, A.C., Oslob, J.D., Delano, W.L., Hyde, J., McDowell, R.S., Waal, N., Yu, C., Arkin, M.R., and Raimundo, B.C. (2003). Discovery of a potent small molecule IL-2 inhibitor through fragment assembly. J. Am. Chem. Soc. *125*, 3714–3715.

Braunstein, J., Brutsaert, S., Olson, R., and Schindler, C. (2003). STATs Dimerize in the Absence of Phosphorylation. J. Biol. Chem. *278*, 34133–34140.

Briddon, S.J., Middleton, R.J., Cordeaux, Y., Flavin, F.M., Weinstein, J.A., George, M.W., Kellam, B., and Hill, S.J. (2004). Quantitative analysis of the formation and diffusion of A 1-adenosine receptor-antagonist complexes in single living cells. Proc. Natl. Acad. Sci. U. S. A. *101*, 4673–4678.

Bridgewood, C., Alase, A., Watad, A., Wittmann, M., Cuthbert, R., and McGonagle, D. (2019). The IL-23p19/EBI3 heterodimeric cytokine termed IL-39 remains a theoretical cytokine in man. Inflamm. Res. *68*, 423–426.

Brocker, C., Thompson, D., Matsumoto, A., Nebert, D.W., and Vasiliou, V. (2010). Evolutionary divergence and functions of the human interleukin (IL) gene family. Hum. Genomics *5*, 30–55.

Brooks, A.J., Dai, W., O’Mara, M.L., Abankwa, D., Chhabra, Y., Pelekanos, R.A., Gardon, O., Tunny, K.A., Blucher, K.M., Morton, C.J., et al. (2014). Mechanism of activation of protein kinase JAK2 by the growth hormone receptor. Science. *344*, 1–12.

Brown, R.J., Adams, J.J., Pelekanos, R.A., Wan, Y., McKinstry, W.J., Palethorpe, K., Seeber, R.M., Monks, T.A., Eidne, K.A., Parke, M.W., et al. (2005). Model for growth hormone receptor activation based on subunit

rotation within a receptor dimer. Nat. Struct. Mol. Biol. *12*, 814–821.

Bustamante, J., Boisson-Dupuis, S., Abel, L., and Casanova, J.L. (2014). Mendelian susceptibility to mycobacterial disease: Genetic, immunological, and clinical features of inborn errors of IFN-γ immunity. Semin. Immunol. *26*, 454–470.

Bylund, D.B., and Enna, S.J. (2018). Receptor Binding Assays and Drug Discovery. In Advances in Pharmacology, (Elsevier), pp. 21–34.

Campos, L.W., Zenatti, P.P., Pissinato, L.G., Rodrigues, G.O.L., Artico, L.L., Guimarães, T.R., Archangelo, L.F., Martínez, L., Brooks, A.J., and Yunes, J.A. (2019). Oncogenic basic amino acid insertions at the extracellular juxtamembrane region of IL7RA cause receptor hypersensitivity. Blood *133*, 1259–1263.

Capone, A., and Volpe, E. (2020). Transcriptional Regulators of T Helper 17 Cell Differentiation in Health and Autoimmune Diseases. Front. Immunol. *11*, 1–8.

Cargill, M., Schrodi, S.J., Chang, M., Garcia, V.E., Brandon, R., Callis, K.P., Matsunami, N., Ardlie, K.G., Civello, D., Catanese, J.J., et al. (2007). A Large-Scale Genetic Association Study Confirms IL12B and Leads to the Identification of IL23R as Psoriasis-Risk Genes. Am. J. Hum. Genet. *80*, 273–290.

Caspi, R.R. (1998). IL-12 in autoimmunity. Clin. Immunol. Immunopathol. *88*, 4–13.

Chan, K.W., Zhang, H., and Logothetis, D.E. (2003). N-terminal transmembrane domain of the SUR controls trafficking and gating of Kir6 channel subunits. EMBO J. *22*.

Chehboun, S., Labrecque-Carbonneau, J., Pasquin, S., Meliani, Y., Meddah, B., Ferlin, W., Sharma, M., Tormo, A., Masson, J.F., and Gauchat, J.F. (2017). Epstein-Barr virus-induced gene 3 (EBI3) can mediate IL-6 trans-signaling. J. Biol. Chem. *292*, 6644–6656.

Chen, Y., Müller, J.D., So, P.T.C., and Gratton, E. (1999). The photon

counting histogram in fluorescence fluctuation spectroscopy. Biophys. J. *77*, 553–567.

Chen, Y., Ouyang, J., Yan, R., Maarouf, M.H., Wang, X., Chen, B., Liu, S., Hu, J., Guo, G., Zhang, J., et al. (2018). Silencing SOCS3 markedly deteriorates spondyloarthritis in mice induced by minicircle DNA expressing IL23. Front. Immunol. *9*, 1–13.

Chen, Z., Laurence, A., Kanno, Y., Pacher-Zavisin, M., Zhu, B.-M., Tato, C., Yoshimura, A., Hennighausen, L., and O'Shea, J.J. (2006). Selective regulatory function of Socs3 in the formation of IL-17-secreting T cells. Proc. Natl. Acad. Sci. *103*, 8137–8142.

Cheng, Y.-C., and Prusoff, W.H. (1973). Relationship between the inhibition constant (KI) and the concentration of inhibitor which causes 50 per cent inhibition (I50) of an enzymatic reaction. Biochem. Pharmacol. *22*, 3099–3108.

Cheng, X., Lee, T.-Y., Ledet, G., Zemade, G., Tovera, J., Campbell, R., Purro, N., Annamalai, T., Masjedizadeh, M., Liu, D., et al. (2019). Safety, Tolerability, and Pharmacokinetics of PTG-200, an Oral GI-Restricted Peptide Antagonist of IL-23 Receptor, in Normal Healthy Volunteers. Am. J. Gastroenterol. *114*, 439–440.

Cheung, P.F.Y., Wong, C.K., and Lam, C.W.K. (2008). Molecular Mechanisms of Cytokine and Chemokine Release from Eosinophils Activated by IL-17A, IL-17F, and IL-23: Implication for Th17 Lymphocytes-Mediated Allergic Inflammation. J. Immunol. *180*, 5625–5635.

Chizzonite, R., Truitt, T., Desai, B.B., Nunes, P., Podlaski, F.J., Stern, A.S., and Gately, M.K. (1992). IL-12 receptor. I. Characterization of the receptor on phytohemagglutinin-activated human lymphoblasts. J Immunol. *148*, 3117–3124.

Cho, M.-L., Kang, J.-W., Moon, Y.-M., Nam, H.-J., Jhun, J.-Y., Heo, S.-B., Jin, H.-T., Min, S.-Y., Ju, J.-H., Park, K.-S., et al. (2006). STAT3 and NF-κB Signal Pathway Is Required for IL-23-Mediated IL-17 Production in Spontaneous Arthritis Animal Model IL-1 Receptor Antagonist-Deficient

Mice. J. Immunol. *176*, 5652–5661.

Chua, A.O., Chizzonite, R., Desai, B.B., Truitt, T.P., Nunes, P., Minetti, L.J., Warrier, R.R., Presky, D.H., Levine, J.F., Gately, M.K., et al. (1994). Expression cloning of a human IL-12 receptor component: A new member of the cytokine receptor superfamily with strong homology to gp130. J. Immunol. *153*, 128–136.

Chyuan, I.T., and Lai, J.H. (2020). New insights into the IL-12 and IL-23: From a molecular basis to clinical application in immune-mediated inflammation and cancers. Biochem. Pharmacol. *175*, 1–9.

Ciric, B., El-behi, M., Cabrera, R., Zhang, G.-X., and Rostami, A. (2009). IL-23 Drives Pathogenic IL-17-Producing CD8 + T Cells. J. Immunol. *182*, 5296–5305.

Clegg, R.M. (1995). Fluorescence resonance energy transfer. Curr. Opin. Biotechnol. *6*, 103–110.

Cochet, C., Kashles, O., Chambaz, E.M., Borrello, I., King, C.R., and Schlessinger, J. (1988). Demonstration of epidermal growth factor-induced receptor dimerization in living cells using a chemical covalent cross-linking agent. J. Biol. Chem. *263*, 3290–3295.

Cohen, P., Cross, D., and Jänne, P.A. (2021). Kinase drug discovery 20 years after imatinib: progress and future directions. Nat. Rev. Drug Discov. *20*, 551–569.

Collison, L.W., Delgoffe, G.M., Guy, C.S., Vignali, K.M., Chaturvedi, V., Fairweather, D., Satoskar, A.R., Garcia, K.C., Hunter, C.A., Drake, C.G., et al. (2012). The composition and signaling of the IL-35 receptor are unconventional. Nat. Immunol. *13*, 290–299.

Cooper, S.L., Soave, M., Jörg, M., Scammells, P.J., Woolard, J., and Hill, S.J. (2019). Probe dependence of allosteric enhancers on the binding affinity of adenosine A 1 -receptor agonists at rat and human A 1 -receptors measured using NanoBRET. Br. J. Pharmacol. *176*, 864–878.

Corbett, M.S.P., Poger, D., and Mark, A.E. (2016). Revisiting the scissor-like

mechanism of activation for the erythropoietin receptor. FEBS Lett. *590*, 3083–3088.

Couturier, C., and Jockers, R. (2003). Activation of the leptin receptor by a ligand-induced conformational change of constitutive receptor dimers. J. Biol. Chem. *278*, 26604–26611.

Crivat, G., and Taraska, J.W. (2012). Imaging proteins inside cells with fluorescent tags. Trends Biotechnol. *30*, 8–16.

Cua, D.J., and Tato, C.M. (2010). Innate IL-17-producing cells: The sentinels of the immune system. Nat. Rev. Immunol. *10*, 479–489.

Cua, D.J., Sherlock, J., Chen, Y., Murphy, C.A., Joyce, B., Seymour, B., Lucian, L., To, W., Kwan, S., Churakova, T., et al. (2003). Interleukin-23 rather than interleukin-12 is the critical cytokine for autoimmune inflammation of the brain. Nature *421*, 744–748.

Curtis, M.M., Way, S.S., and Wilson, C.B. (2009). IL-23 Promotes the Production of IL-17 by Antigen-Specific CD8 T Cells in the Absence of IL-12 and Type-I Interferons. J. Immunol. *183*, 381–387.

Dacres, H., Michie, M., Wang, J., Pfleger, K.D.G., and Trowell, S.C. (2012). Effect of enhanced Renilla luciferase and fluorescent protein variants on the Förster distance of Bioluminescence resonance energy transfer (BRET). Biochem. Biophys. Res. Commun. *425*, 625–629.

Dale, N.C., Johnstone, E.K.M., White, C.W., and Pfleger, K.D.G. (2019). NanoBRET: The bright future of proximity-based assays. Front. Bioeng. Biotechnol. *7*, 1–13.

Damasceno, L.E.A., Prado, D.S., Veras, F.P., Fonseca, M.M., Toller-Kawahisa, J.E., Rosa, M.H., Públio, G.A., Martins, T.V., Ramalho, F.S., Waismaz, A., et al. (2020). PKM2 promotes Th17 cell differentiation and autoimmune inflammation by fine-tuning STAT3 activation. J. Exp. Med. *217*, 1–16.

Dawson, M.A., Bannister, A.J., Göttgens, B., Foster, S.D., Bartke, T., Green, A.R., and Kouzarides, T. (2009). JAK2 phosphorylates histone H3Y41 and

excludes HP1α from chromatin. Nature *461*, 819–822.

Detry, S., Składanowska, K., Vuylsteke, M., Savvides, S.N., and Bloch, Y. (2019). Revisiting the combinatorial potential of cytokine subunits in the IL-12 family. Biochem. Pharmacol. *165*, 240–248.

Dhillon, S. (2017). Tofacitinib: A Review in Rheumatoid Arthritis. Drugs *77*, 1987–2001.

Dinarello, C.A. (2007). Historical insights into cytokines. Eur. J. Immunol. *37*, 34–45.

Ding, J., Komatsu, H., Iida, S., Yano, H., Kusumoto, S., Inagaki, A., Mori, F., Ri, M., Ito, A., Wakita, A., et al. (2009). The Asn505 mutation of the c-MPL gene, which causes familial essential thrombocythemia, induces autonomous homodimerization of the c-Mpl protein due to strong amino acid polarity. Blood *114*, 3325–3328.

Dixon, A.S., Schwinn, M.K., Hall, M.P., Zimmerman, K., Otto, P., Lubben, T.H., Butler, B.L., Binkowski, B.F., Machleidt, T., Kirkland, T.A., et al. (2016). NanoLuc Complementation Reporter Optimized for Accurate Measurement of Protein Interactions in Cells. ACS Chem. Biol. *11*, 400–408.

Doisne, J.-M., Soulard, V., Bécourt, C., Amniai, L., Henrot, P., Havenar-Daughton, C., Blanchet, C., Zitvogel, L., Ryffel, B., Cavaillon, J.-M., et al. (2011). Cutting Edge: Crucial Role of IL-1 and IL-23 in the Innate IL-17 Response of Peripheral Lymph Node NK1.1 − Invariant NKT Cells to Bacteria. J. Immunol. *186*, 662–666.

Dömling, A., and Li, X. (2022). TNF-α: The shape of small molecules to come? Drug Discov. Today *27*, 3–7.

Dong, H., Li, Q., Zhang, Y., Tan, W., and Jiang, Z. (2013). IL23R Gene Confers Susceptibility to Ankylosing Spondylitis Concomitant with Uveitis in a Han Chinese Population. PLoS One *8*, 1–5.

Dostert, C., Grusdat, M., Letellier, E., and Brenner, D. (2019). The TNF family of ligands and receptors: Communication modules in the immune system and beyond. Physiol. Rev. *99*, 115–160.

Duan, Y.G., Zhang, Q., Liu, Y., Mou, L., Li, G., Gui, Y., and Cai, Z. (2014). Dendritic cells in semen of infertile men: Association with sperm quality and inflammatory status of the epididymis. Fertil. Steril. *101*, 70–77.

Dubnika, A., Manoukian, M.A.C., Mohammadi, M.R., Parekh, M.B., Gurjarpadhye, A.A., Inayathullah, M., Dubniks, V., Lakey, J.R.T., and Rajadas, J. (2018). Cytokines as therapeutic agents and targets in heart disease. Cytokine Growth Factor Rev. *43*, 54-68.

Duerr, R.H., Taylor, K.D., Brant, S.R., Rioux, J.D., Silverberg, M.S., Daly, M.J., Steinhart, A.H., Abraham, C., Regueiro, M., Griffiths, A., et al. (2006). A genome-wide association study identifies IL23R as an inflammatory bowel disease gene. Science. *314*, 1461–1463.

Eberl, G., Colonna, M., Santo, J.P.D., and McKenzie, A.N.J. (2015). Innate lymphoid cells: A new paradigm in immunology. Science. *348*, 879–888.

Eichacker, P.Q., Parent, C., Kalil, A., Esposito, C., Cui, X., Banks, S.M., Gerstenberger, E.P., Fitz, Y., Danner, R.L., and Natanson, C. (2002). Risk and the efficacy of antiinflammatory agents: Retrospective and confirmatory studies of sepsis. Am. J. Respir. Crit. Care Med. *166*, 1197–1205.

El-Behi, M., Ciric, B., Dai, H., Yan, Y., Cullimore, M., Safavi, F., Zhang, G.X., Dittel, B.N., and Rostami, A. (2011). The encephalitogenicity of TH 17 cells is dependent on IL-1- and IL-23-induced production of the cytokine GM-CSF. Nat. Immunol. *12*, 568–575.

Elliott, S., Lorenzini, T., Yanagihara, D., Chang, D., and Elliott, G. (1996). Activation of the erythropoietin (EPO) receptor by bivalent anti-EPO receptor antibodies. J. Biol. Chem. *271*, 24691–24697.

Engelowski, E., Schneider, A., Franke, M., Xu, H., Clemen, R., Lang, A., Baran, P., Binsch, C., Knebel, B., Al-Hasani, H., et al. (2018). Synthetic cytokine receptors transmit biological signals using artificial ligands. Nat. Commun. *9*, 1–15.

Espígol-Frigolé, G., Planas-Rigol, E., Ohnuki, H., Salvucci, O., Kwak, H., Ravichandran, S., Luke, B., Cid, M.C., and Tosato, G. (2016). Identification of

IL-23p19 as an endothelial proinflammatory peptide that promotes gp130-STAT3 signaling. Sci. Signal. *9*, 28.

Eulenfeld, R., Dittrich, A., Khouri, C., Müller, P.J., Mütze, B., Wolf, A., and Schaper, F. (2012). Interleukin-6 signalling: More than Jaks and STATs. Eur. J. Cell Biol. *91*, 486–495.

Fassbender, K., Ragoschke, A., Rossol, S., Schwartz, A., Mielke, O., Paulig, A., and Hennerici, M. (1998). Increased release of interleukin-12p40 in MS: Association with intracerebral inflammation. Neurology *51*, 753–758.

Fereshteh, M.P., Li, X., Li, S., Fan, Y., Zhang, R., Farr, G.A., Kolodin, G., Lippy, J., Naglich, J.G., Schieven, G., et al. (2016). Development of a Human Whole Blood Screening Platform to Monitor JAK/STAT Signaling Using High-Throughput Flow Cytometry. J. Biomol. Screen. *21*, 866–874.

Ferrao, R., and Lupardus, P.J. (2017). The Janus Kinase (JAK) FERM and SH2 domains: Bringing specificity to JAK-receptor interactions. Front. Endocrinol. (Lausanne). *8*, 1–11.

Ferrao, R.D., Wallweber, H.J., and Lupardus, P.J. (2018). Receptor-mediated dimerization of JAK2 FERM domains is required for JAK2 activation. Elife *7*, 1–21.

Filer, C., Ho, P., Smith, R.L., Griffiths, C., Young, H.S., Worthington, J., Bruce, I.N., and Barton, A. (2008). Investigation of association of the IL12B and IL23R genes with psoriatic arthritis. Arthritis Rheum. *58*, 3705–3709.

Flores, R.R., Kim, E., Zhou, L., Yang, C., Zhao, J., Gambotto, A., and Robbins, P.D. (2015). IL-Y, a synthetic member of the IL-12 cytokine family, suppresses the development of type 1 diabetes in NOD mice. Eur. J. Immunol. *45*, 3114–3125.

Floss, D.M., Mrotzek, S., Klöcker, T., Schröder, J., Grötzinger, J., Rose-John, S., and Scheller, J. (2013). Identification of canonical tyrosine-dependent and non-canonical tyrosine-independent STAT3 activation sites in the intracellular domain of the interleukin 23 receptor. J. Biol. Chem. *288*, 19386–19400.

Floss, D.M., Schröder, J., Franke, M., and Scheller, J. (2015). Insights into IL-

23 biology: From structure to function. Cytokine Growth Factor Rev. *26*, 569–578.

Floss, D.M., Klocker, T., Schroder, J., Lamertz, L., Mrotzek, S., Strobl, B., Hermanns, H., and Scheller, J. (2016). Defining the functional binding sites of interleukin 12 receptor 1 and interleukin 23 receptor to Janus kinases. Mol. Biol. Cell *27*, 2301–2316.

Floss, D.M., Moll, J.M., and Scheller, J. (2020). IL-12 and IL-23-Close Relatives with Structural Homologies but Distinct Immunological Functions. Cells *9*, 1–24.

Ford, N.R., Miller, H.E., Reeme, A.E., Waukau, J., Bengtson, C., Routes, J.M., and Robinson, R.T. (2012). Inflammatory Signals Direct Expression of Human IL12RB1 into Multiple Distinct Isoforms. J. Immunol. *189*, 4684–4694.

França, L.T.C., Carrilho, E., and Kist, T.B.L. (2002). A review of DNA sequencing techniques. Q. Rev. Biophys. *35*, 169–200.

Franke, M., Schröder, J., Monhasery, N., Ackfeld, T., Hummel, T.M., Rabe, B., Garbers, C., Becker-Pauly, C., Floss, D.M., and Scheller, J. (2016). Human and murine interleukin 23 receptors are novel substrates for a disintegrin and metalloproteases ADAM10 and ADAM17. J. Biol. Chem. *291*, 10551-10561.

Fuh, G., Cunningham, B.C., Fukunaga, R., Nagata, S., Goeddel, D. V., and Wells, J.A. (1992). Rational design of potent antagonists to the human growth hormone receptor. Science. *256*, 1677–1680.

Gandhi, H., Worch, R., Kurgonaite, K., Hintersteiner, M., Schwille, P., Bökel, C., and Weidemann, T. (2014). Dynamics and interaction of Interleukin-4 receptor subunits in living cells. Biophys. J. *107*, 2515–2527.

Garbers, C., Spudy, B., Aparicio-Siegmund, S., Waetzig, G.H., Sommer, J., Hölscher, C., Rose-John, S., Grötzinger, J., Lorenzen, I., and Scheller, J. (2013). An lnterleukin-6 receptor-dependent molecular switch mediates signal transduction of the IL-27 cytokine subunit p28 (IL-30) via a gp130 protein receptor homodimer. J. Biol. Chem. *288*, 4346–4354.

Gaudino, S.J., and Kumar, P. (2019). Cross-talk between antigen presenting

cells and T cells impacts intestinal homeostasis, bacterial infections, and tumorigenesis. Front. Immunol. *10*, 1–14.

Gent, J., Van Kerkhof, P., Roza, M., Bu, G., and Strous, G.J. (2002). Ligand-independent growth hormone receptor dimerization occurs in the endoplasmic reticulum and is required for ubiquitin system-dependent endocytosis. Proc. Natl. Acad. Sci. U. S. A. *99*, 9858–9863.

Geremia, A., Arancibia-Cárcamo, C. V., Fleming, M.P.P., Rust, N., Singh, B., Mortensen, N.J., Travis, S.P.L., and Powrie, F. (2011). IL-23-responsive innate lymphoid cells are increased in inflammatory bowel disease. J. Exp. Med. *208*, 1127–1133.

Gerenova, J., Manolova, I., and Stanilova, S. (2019). Serum levels of interleukin - 23 and interleukin - 17 in hashimoto's thyroiditis. Acta Endocrinol. (Copenh). *15*.

Gesztelyi, R., Zsuga, J., Kemeny-Beke, A., Varga, B., Juhasz, B., and Tosaki, A. (2012). The Hill equation and the origin of quantitative pharmacology. Arch. Hist. Exact Sci. *66*, 427–438.

Gherbi, K., May, L.T., Baker, J.G., Briddon, S.J., and Hill, S.J. (2015). Negative cooperativity across β1-adrenoceptor homodimers provides insights into the nature of the secondary low-affinity CGP 12177 β1-adrenoceptor binding conformation. FASEB J. *29*, 2859–2871.

Ghoreschi, K., Laurence, A., Yang, X.P., Tato, C.M., McGeachy, M.J., Konkel, J.E., Ramos, H.L., Wei, L., Davidson, T.S., Bouladoux, N., et al. (2010). Generation of pathogenic TH 17 cells in the absence of TGF-β 2 signalling. Nature *467*, 967–971.

Gibson, S.A., Yang, W., Yan, Z., Liu, Y., Rowse, A.L., Weinmann, A.S., Qin, H., and Benveniste, E.N. (2017). Protein Kinase CK2 Controls the Fate between Th17 Cell and Regulatory T Cell Differentiation. J. Immunol. *198*, 4244–4254.

Gillessen, S., Carvajal, D., Ling, P., Podlaski, F.J., Stremlo, D.L., Familletti, P.C., Gubler, U., Presky, D.H., Stern, A.S., and Gately, M.K. (1995). Mouse

interleukin-12 (IL-12) p40 homodimer: a potent IL-12 antagonist. Eur. J. Immunol. *25*, 200–206.

Glassman, C.R., Mathiharan, Y.K., Jude, K.M., Su, L., Panova, O., Lupardus, P.J., Spangler, J.B., Ely, L.K., Thomas, C., Skiniotis, G., et al. (2021). Structural basis for IL-12 and IL-23 receptor sharing reveals a gateway for shaping actions on T versus NK cells. Cell *184*, 983–999.

Goffe, B., and Cather, J.C. (2003). Etanercept: An overview. J. Am. Acad. Dermatol. *49*, 105–111.

Gresser, I. (1977). On the varied biologic effects of interferon. Cell. Immunol. *34*, 406–415.

Guilhot, F., Elson, G., Lefouili, F., Gauchat, J.-F., Tormo, A.J., Duluc, D., Guay-Giroux, A., Jeannin, P., Crabe, S., Lissilaa, R., et al. (2009). The IL-27 p28 Subunit Binds Cytokine-Like Factor 1 to Form a Cytokine Regulating NK and T Cell Activities Requiring IL-6R for Signaling. J. Immunol. *183*, 7692–7702.

Haan, S., Kortylewsk, M., Behrmann, I., Müller-Esterl, W., Heinrich, P.C., and Schaper, F. (2015). Cytoplasmic STAT proteins associate prior to activation. Biochem. J. *354*, 417–421.

Hall, M.P., Unch, J., Binkowski, B.F., Valley, M.P., Butler, B.L., Wood, M.G., Otto, P., Zimmerman, K., Vidugiris, G., MacHleidt, T., et al. (2012). Engineered luciferase reporter from a deep sea shrimp utilizing a novel imidazopyrazinone substrate. ACS Chem. Biol. *7*, 1848–1857.

Hamilton, J.A. (2008). Colony-stimulating factors in inflammation and autoimmunity. Nat. Rev. Immunol. *8*, 533–544.

Hasegawa, H., Mizoguchi, I., Chiba, Y., Ohashi, M., Xu, M., and Yoshimoto, T. (2016). Expanding diversity in molecular structures and functions of the IL-6/IL-12 heterodimeric cytokine family. Front. Immunol. *7*, 1–10.

Hassani, M., and Koenderman, L. (2018). Immunological and hematological effects of IL-5(Rα)-targeted therapy: An overview. Allergy Eur. J. Allergy Clin. Immunol. *73*, 1979–1988.

He, X., Tan, C., Wang, F., Wang, Y., Zhou, R., Cui, D., You, W., Zhao, H., Ren, J., and Feng, B. (2016). Knock-in of large reporter genes in human cells via CRISPR/Cas9-induced homology-dependent and independent DNA repair. Nucleic Acids Res. *44*, 85–99.

Hedner, T., and Everts, B. (1998). The early clinical history of salicylates in rheumatology and pain. Clin. Rheumatol. *17*, 17–25.

Herrmann, A., Vogt, M., Monnigmann, M., Clahsen, T., Sommer, U., Haan, S., Poli, V., Heinrich, P.C., and Muller-Newen, G. (2007). Nucleocytoplasmic shuttling of persistently activated STAT3. J. Cell Sci. *120*, 3249–3261.

Himani, G.S., Prabhuji, M.L.V., and Karthikeyan, B. V. (2014). Gingival crevicular fluid and interleukin-23 concentration in systemically healthy subjects: Their relationship in periodontal health and disease. J. Periodontal Res. *49*.

Hinck, A.P. (2012). Structural studies of the TGF-βs and their receptors - Insights into evolution of the TGF-β superfamily. FEBS Lett. *586*, 1860–1870.

Hinks, T.S.C., and Zhang, X.W. (2020). MAIT Cell Activation and Functions. Front. Immunol. *11*, 1–10.

Ho, S.M., Lewis, J.D., Mayer, E.A., Plevy, S.E., Chuang, E., Rappaport, S.M., Croitoru, K., Korzenik, J.R., Krischer, J., Hyams, J.S., et al. (2019). Challenges in IBD Research: Environmental Triggers. Inflamm. Bowel Dis. *25*, 13–23.

Hoelzel, C.A., and Zhang, X. (2020). Visualizing and Manipulating Biological Processes by Using HaloTag and SNAP-Tag Technologies. ChemBioChem *21*, 1935-1946.

Hohenberger, M., Cardwell, L.A., Oussedik, E., and Feldman, S.R. (2018). Interleukin-17 inhibition: role in psoriasis and inflammatory bowel disease. J. Dermatolog. Treat. *29*, 13–18.

Horioka, M., Huber, T., and Sakmar, T.P. (2020). Playing Tag with Your Favorite GPCR Using CRISPR. Cell Chem. Biol. *27*, 642–644.

Hou, Y., Zhu, L., Tian, H., Sun, H.X., Wang, R., Zhang, L., and Zhao, Y.

(2018). IL-23-induced macrophage polarization and its pathological roles in mice with imiquimod-induced psoriasis. Protein Cell *9*, 1027-1038.

Hu, W., Troutman, T.D., Edukulla, R., and Pasare, C. (2011). Priming Microenvironments Dictate Cytokine Requirements for T Helper 17 Cell Lineage Commitment. Immunity *35*, 1010–1022.

Hu, X., Li, J., Fu, M., Zhao, X., and Wang, W. (2021). The JAK/STAT signaling pathway: from bench to clinic. Signal Transduct. Target. Ther. *6*, 1–33.

Huber, K.V.M. (2017). Target engagement: Shining a light. Nat. Chem. Biol. *13*, 133–134.

Hummel, T.M., Ackfeld, T., Schönberg, M., Ciupka, G., Schulz, F., Oberdoerster, A., Grötzinger, J., Scheller, J., and Floss, D.M. (2017). Synthetic Deletion of the Interleukin 23 Receptor (IL-23R) Stalk Region Led to Autonomous IL-23R Homodimerization and Activation. Mol Cell Biol *37*, 14–17.

Hwang, J.R., Byeon, Y., Kim, D., and Park, S.G. (2020). Recent insights of T cell receptor-mediated signaling pathways for T cell activation and development. Exp. Mol. Med. *52*, 750–761.

Isaacs, A., and Lindenmann, J. (1957). Virus interference. I. The interferon. J. Interferon Res. *7*, 258–267.

Jana, M., and Pahan, K. (2009). IL-12 p40 homodimer, but not IL-12 p70, induces the expression of IL-16 in microglia and macrophages. Mol. Immunol. *46*, 773–783.

Jana, M., Dasgupta, S., Pal, U., and Pahan, K. (2009). IL-12 P40 homodimer, the so-called biologically inactive molecule, induces nitric oxide synthase in microglia via IL-12Rβ1. Glia *57*, 1553–1565.

Jaschinski, F., Rothhammer, T., Jachimczak, P., Seitz, C., Schneider, A., and Schlingensiepen, K.-H. (2011). The Antisense Oligonucleotide Trabedersen (AP 12009) for the Targeted Inhibition of TGF-Beta2. Curr. Pharm. Biotechnol. *12*, 2203–2213.

Jaszczura, M., Mizgała-Izworska, E., Świętochowska, E., and Machura, E. (2019). Serum levels of selected cytokines [interleukin (IL)-17A, IL-18, IL-23] and chemokines (RANTES, IP10) in the acute phase of immunoglobulin A vasculitis in children. Rheumatol. Int. *39*.

Jetten, A.M., and Cook, D.N. (2020). (Inverse) agonists of retinoic acid-related orphan receptor γ: Regulation of immune responses, inflammation, and autoimmune disease. Annu. Rev. Pharmacol. Toxicol. *60*, 371–390.

Jia, R., Balligand, T., Atamanyuk, V., Nivarthi, H., Xu, E., Kutzner, L., Weinzierl, J., Nedelec, A., Kubicek, S., Lesyk, R., et al. (2021). Hematoxylin binds to mutant calreticulin and disrupts its abnormal interaction with thrombopoietin receptor. Blood *137*, 1920–1931.

Jin, H.Y., Tudor, Y., Choi, K., Shao, Z., Sparling, B.A., McGivern, J.G., and Symons, A. (2020). High-Throughput Implementation of the NanoBRET Target Engagement Intracellular Kinase Assay to Reveal Differential Compound Engagement by SIK2/3 Isoforms. SLAS Discov. *25*, 215–222.

Jones, S.A., and Jenkins, B.J. (2018). Recent insights into targeting the IL-6 cytokine family in inflammatory diseases and cancer. Nat. Rev. Immunol. *18*, 773–789.

Ju, J.H., Cho, M.-L., Moon, Y.-M., Oh, H.-J., Park, J.-S., Jhun, J.-Y., Min, S.-Y., Cho, Y.-G., Park, K.-S., Yoon, C.-H., et al. (2008). IL-23 Induces Receptor Activator of NF-κB Ligand Expression on CD4 + T Cells and Promotes Osteoclastogenesis in an Autoimmune Arthritis Model. J. Immunol. *181*, 1507–1518.

Jullien, D., Prinz, J.C., and Nestle, F.O. (2015). Immunogenicity of biotherapy used in psoriasis: The science behind the scenes. J. Invest. Dermatol. *135*, 31-38.

Jumper, J., Evans, R., Pritzel, A., Green, T., Figurnov, M., Ronneberger, O., Tunyasuvunakool, K., Bates, R., Žídek, A., Potapenko, A., et al. (2021). Highly accurate protein structure prediction with AlphaFold. Nature *596*, 583–589.

Kalkhof, S., and Sinz, A. (2008). Chances and pitfalls of chemical cross-linking with amine-reactive N-hydroxysuccinimide esters. Anal. Bioanal. Chem. *392*, 305–312.

Kan, S.H., Mancini, G., and Gallagher, G. (2008). Identification and characterization of multiple splice forms of the human interleukin-23 receptor α chain in mitogen-activated leukocytes. Genes Immun. *9*, 631–639.

Karlsson, M., Zhang, C., Méar, L., Zhong, W., Digre, A., Katona, B., Sjöstedt, E., Butler, L., Odeberg, J., Dusart, P., et al. (2021). A single–cell type transcriptomics map of human tissues. Sci. Adv. *7*, 1–9.

Ke, Y., Lesperance, J., Zhang, E.E., Bard-Chapeau, E.A., Oshima, R.G., Muller, W.J., and Feng, G.S. (2006). Conditional deletion of Shp2 in the mammary gland leads to impaired lobulo-alveolar outgrowth and attenuated Stat5 activation. J. Biol. Chem. *281*, 34374–34380.

Keppler, A., Gendreizig, S., Gronemeyer, T., Pick, H., Vogel, H., and Johnsson, K. (2003). A general method for the covalent labeling of fusion proteins with small molecules in vivo. Nat. Biotechnol. *21*, 86–89.

Khoury, T., and Ilan, Y. (2019). Introducing Patterns of Variability for Overcoming Compensatory Adaptation of the Immune System to Immunomodulatory Agents: A Novel Method for Improving Clinical Response to Anti-TNF Therapies. Front. Immunol. *10*, 1–13.

Kikly, K., Liu, L., Na, S., and Sedgwick, J.D. (2006). The IL-23/Th17 axis: therapeutic targets for autoimmune inflammation. Curr. Opin. Immunol. *18*, 670–675.

Kilpatrick, L.E., Friedman-Ohana, R., Alcobia, D.C., Riching, K., Peach, C.J., Wheal, A.J., Briddon, S.J., Robers, M.B., Zimmerman, K., Machleidt, T., et al. (2017). Real-time analysis of the binding of fluorescent VEGF165a to VEGFR2 in living cells: Effect of receptor tyrosine kinase inhibitors and fate of internalized agonist-receptor complexes. Biochem. Pharmacol. *136*, 62–75.

Kim, H.R., Kim, H.S., Park, M.K., Cho, M.L., Lee, S.H., and Kim, H.Y. (2007). The clinical role of IL-23p19 in patients with rheumatoid arthritis.

Scand. J. Rheumatol. *36*.

Kim, Y., Ho, S.O., Gassman, N.R., Korlann, Y., Landorf, E. V., Collart, F.R., and Weiss, S. (2008). Efficient site-specific labeling of proteins via cysteines. Bioconjug. Chem. *19*, 786–791.

Kong, X.D., Moriya, J., Carle, V., Pojer, F., Abriata, L.A., Deyle, K., and Heinis, C. (2020). De novo development of proteolytically resistant therapeutic peptides for oral administration. Nat. Biomed. Eng. *4*, 560–571.

Koontz, L. (2013). Explanatory chapter: How plasmid preparation kits work. In Methods in Enzymology, (Academic press), pp. 23–28.

Kowalski-Jahn, M., Schihada, H., Turku, A., Huber, T., Sakmar, T.P., and Schulte, G. (2021). Frizzled BRET sensors based on bioorthogonal labeling of unnatural amino acids reveal WNT-induced dynamics of the cysteine-rich domain. Sci. Adv. *7*, 1–15.

Krause, C.D., Digioia, G., Izotova, L.S., Xie, J., Kim, Y., Schwartz, B.J., Mirochnitchenko, O. V., and Pestka, S. (2013). Ligand-independent interaction of the type I interferon receptor complex is necessary to observe its biological activity. Cytokine *64*, 286–297.

Kretzschmar, A.K., Dinger, M.C., Henze, C., Brocke-Heidrich, K., and Horn, F. (2004). Analysis of Stat3 (signal transducer and activator of transcription 3) dimerization by fluorescence resonance energy transfer in living cells. Biochem. J. *377*, 289–297.

Kuchař, M., Vaňková, L., Petroková, H., Černý, J., Osička, R., Pelák, O., Šípová, H., Schneider, B., Homola, J., Šebo, P., et al. (2014). Human interleukin-23 receptor antagonists derived from an albumin-binding domain scaffold inhibit IL-23-dependent ex vivo expansion of IL-17-producing T-cells. Proteins Struct. Funct. Bioinforma. *82*, 975–989.

Kumar, B. V., Connors, T.J., and Farber, D.L. (2018). Human T Cell Development, Localization, and Function throughout Life. Immunity *48*, 202–213.

Lambert, Q.T., Pradhan, A., Roll, J.D., and Reuther, G.W. (2011). Mutations

in the transmembrane and juxtamembrane domains enhance IL27R transforming activity. Biochem. J. *438*, 155-164.

Langdon, Y., Tandon, P., Paden, E., Duddy, J., Taylor, J.M., and Conlon, F.L. (2012). SHP-2 acts via ROCK to regulate the cardiac actin cytoskeleton. Development *139*, 948–957.

Langrish, C.L., Chen, Y., Blumenschein, W.M., Mattson, J., Basham, B., Sedgwick, J.D., McClanahan, T., Kastelein, R.A., and Cua, D.J. (2005). IL-23 drives a pathogenic T cell population that induces autoimmune inflammation. J. Exp. Med. *201*, 233–240.

Lau, E.S., and Oakley, T.H. (2021). Multi-level convergence of complex traits and the evolution of bioluminescence. Biol. Rev. *96*, 673–691.

Lay, C.S., Bridges, A., Goulding, J., Briddon, S.J., Soloviev, Z., Craggs, P.D., and Hill, S.J. (2022). Probing the binding of interleukin-23 to individual receptor components and the IL-23 heteromeric receptor complex in living cells using NanoBRET. Cell Chem. Biol. *29*, 19–29.

Learmouth, R., Scott, K., and Kenneth, G. (2009). Basics of Fluorescence. In Fluorescence Applications in Biotechnology and Life Sciences, (Wiley and sons), pp. 1–22.

Lee, S.Y., Moon, S.J., Moon, Y.M., Seo, H.B., Ryu, J.G., Lee, A.R., Lee, C.R., Kim, D.S., Her, Y.M., Choi, J.W., et al. (2022). A novel cytokine consisting of the p40 and EBI3 subunits suppresses experimental autoimmune arthritis via reciprocal regulation of Th17 and Treg cells. Cell. Mol. Immunol. *19*, 79–91.

Liongue, C., Sertori, R., and Ward, A.C. (2016). Evolution of Cytokine Receptor Signaling. J. Immunol. *197*, 11–18.

Liu, L., McBride, K.M., and Reich, N.C. (2005). STAT3 nuclear import is independent of tyrosine phosphorylation and mediated by importin- 3. Proc. Natl. Acad. Sci. *102*, 8150–8155.

Liu, W., Kawahara, M., Ueda, H., and Nagamune, T. (2009). The influence of domain structures on the signal transduction of chimeric receptors derived from the erythropoietin receptor. J. Biochem. *145*, 575–584.

Liu, Y., Song, Y., Lin, D., Lei, L., Mei, Y., Jin, Z., Gong, H., Zhu, Y., Hu, B., Zhang, Y., et al. (2019). NCR − group 3 innate lymphoid cells orchestrate IL-23/IL-17 axis to promote hepatocellular carcinoma development. EBioMedicine *41*, 333–344.

Livnah, O. evidence for preformed dimers of erythropoietin receptor before ligand activation, Stura, E.A., Middleton, S.A., Johnson, D.L., Jolliffe, L.K., and Wilson, I.A. (1999). Crystallographic evidence for preformed dimers of erythropoietin receptor before ligand activation. Science. *283*, 987–990.

Lochmatter, C., Fischer, R., Charles, P.D., Yu, Z., Powrie, F., and Kessler, B.M. (2016). Integrative Phosphoproteomics Links IL-23R Signaling with Metabolic Adaptation in Lymphocytes. Sci. Rep. *6*, 1–12.

Lopes, J.E., Fisher, J.L., Flick, H.L., Wang, C., Sun, L., Ernstoff, M.S., Alvarez, J.C., and Losey, H.C. (2020). ALKS 4230: A novel engineered IL-2 fusion protein with an improved cellular selectivity profile for cancer immunotherapy. J. Immunother. Cancer *8*, 673–686.

Los, G. V., Encell, L.P., McDougall, M.G., Hartzell, D.D., Karassina, N., Zimprich, C., Wood, M.G., Learish, R., Ohana, R.F., Urh, M., et al. (2008). HaloTag: A novel protein labeling technology for cell imaging and protein analysis. ACS Chem. Biol. *3*, 373–382.

Lu, R.M., Hwang, Y.C., Liu, I.J., Lee, C.C., Tsai, H.Z., Li, H.J., and Wu, H.C. (2020). Development of therapeutic antibodies for the treatment of diseases. J. Biomed. Sci. *27*, 1–30.

Lu, X., Gross, A.W., and Lodish, H.F. (2006). Active conformation of the erythropoietin receptor: Random and cysteine-scanning mutagenesis of the extracellular juxtamembrane and transmembrane domains. J. Biol. Chem. *281*, 7002–7011.

Luban, J., and Goff, S.P. (1995). The yeast two-hybrid system for studying protein-protein interactions. Curr. Opin. Biotechnol. *6*, 59–64.

Lucaciu, L.A., Ilieș, M., Vesa, Ștefan C., Seicean, R., Din, S., Iuga, C.A., and Seicean, A. (2021). Serum interleukin (Il)-23 and il-17 profile in inflammatory

bowel disease (ibd) patients could differentiate between severe and non-severe disease. J. Pers. Med. *11*.

Lupardus, P.J., and Garcia, K.C. (2008). The Structure of Interleukin-23 Reveals the Molecular Basis of p40 Subunit Sharing with Interleukin-12. J. Mol. Biol. *382*, 931–941.

Lupardus, P.J., Ultsch, M., Wallweber, H., Bir Kohli, P., Johnson, A.R., and Eigenbrot, C. (2014). Structure of the pseudokinase-kinase domains from protein kinase TYK2 reveals a mechanism for Janus kinase (JAK) autoinhibition. Proc. Natl. Acad. Sci. *111*, 8025–8030.

Ma, Y., Zhao, S., Shen, S., Fang, S., Ye, Z., Shi, Z., and Hong, A. (2015). A novel recombinant slow-release TNF α-derived peptide effectively inhibits tumor growth and angiogensis. Sci. Rep. *5*, 1–17.

Machleidt, T., Woodroofe, C.C., Schwinn, M.K., Méndez, J., Robers, M.B., Zimmerman, K., Otto, P., Daniels, D.L., Kirkland, T.A., and Wood, K. V. (2015). NanoBRET-A Novel BRET Platform for the Analysis of Protein-Protein Interactions. ACS Chem. Biol. *10*, 1797–1804.

Maehle, A.H. (2004). "Receptive Substances": John Newport Langley (1852-1925) and his Path to a Receptor Theory of Drug Action. Med. Hist. *48*, 153–174.

Maguire, J.J., Kuc, R.E., and Davenport, A.P. (2012). Radioligand binding assays and their analysis. Methods Mol. Biol. *897*, 31–77.

Mahdaviani, S.A., Mansouri, D., Jamee, M., Zaki-Dizaji, M., Aghdam, K.R., Mortaz, E., Khorasanizadeh, M.H., Eskian, M., Movahedi, M., Ghaffaripour, H., et al. (2020). Mendelian Susceptibility to Mycobacterial Disease (MSMD): Clinical and Genetic Features of 32 Iranian Patients. J. Clin. Immunol. *40*, 872–882.

Mahil, S.K., Ezejimofor, M.C., Exton, L.S., Manounah, L., Burden, A.D., Coates, L.C., de Brito, M., McGuire, A., Murphy, R., Owen, C.M., et al. (2020). Comparing the efficacy and tolerability of biologic therapies in psoriasis: an updated network meta-analysis. Br. J. Dermatol. *183*, 638–649.

Malka, Y., Hornakova, T., Royer, Y., Knoops, L., Renauld, J.C., Constantinescu, S.N., and Henis, Y.I. (2008). Ligand-independent homomeric and heteromeric complexes between interleukin-2 or -9 receptor subunits and the γ chain. J. Biol. Chem. *283*, 33569–33577.

Mancini, G., Kan, S.H., and Gallagher, G. (2008). A novel insertion variant of the human IL-23 receptor-α chain transcript. Genes Immun. *9*, 566-569.

Mangan, P.R., Harrington, L.E., O'Quinn, D.B., Helms, W.S., Bullard, D.C., Elson, C.O., Hatton, R.D., Wahl, S.M., Schoeb, T.R., and Weaver, C.T. (2006). Transforming growth factor-β induces development of the T H17 lineage. Nature *441*, 231-234.

Martin, B., Hirota, K., Cua, D.J., Stockinger, B., and Veldhoen, M. (2009). Interleukin-17-Producing γδ T Cells Selectively Expand in Response to Pathogen Products and Environmental Signals. Immunity *31*, 321–330.

Martínez-barricarte, R., Markle, J.G., Ma, C.S., Deenick, E.K., Ramírez-alejo, N., Mele, F., Latorre, D., Mahdaviani, S.A., Aytekin, C., Mansouri, D., et al. (2018). Human IFNγ immunity to mycobacteria is governed by both IL-12 and IL-23. Sci. Immunol. *3*, 1–13.

Maruyama, I.N. (2015). Activation of transmembrane cell-surface receptors via a common mechanism? The "rotation model." BioEssays *37*, 959–967.

Matthews, E.E., Thévenin, D., Rogers, J.M., Gotow, L., Lira, P.D., Reiter, L.A., Brissette, W.H., and Engelman, D.M. (2011). Thrombopoietin receptor activation: transmembrane helix dimerization, rotation, and allosteric modulation. FASEB J. *25*, 2234–2244.

Mazzoni, A., Maggi, L., Liotta, F., Cosmi, L., and Annunziato, F. (2019). Biological and clinical significance of T helper 17 cell plasticity. Immunology *158*, 287–295.

McElroy, C.A., Holland, P.J., Zhao, P., Lim, J.M., Wells, L., Eisenstein, E., and Walsh, S.T.R. (2012). Structural reorganization of the interleukin-7 signaling complex. Proc. Natl. Acad. Sci. U. S. A. *109*, 2503–2508.

McGonagle, D., Watad, A., Sharif, K., and Bridgewood, C. (2021). Why

Inhibition of IL-23 Lacked Efficacy in Ankylosing Spondylitis. Front. Immunol. *12*, 1–9.

Metcalfe, R.D., Putoczki, T.L., and Griffin, M.D.W. (2020). Structural Understanding of Interleukin 6 Family Cytokine Signaling and Targeted Therapies: Focus on Interleukin 11. Front. Immunol. *11*, 1–26.

Michnick, S.W., Remy, I., Campbell-Valois, F.X., Vallee-Belisle, A., and Pelletier, J.N. (2000). Detection of protein-protein interactions by protein fragment complementation strategies. Methods Enzymol. *328*, 208–230.

Miyano, K., Sudo, Y., Yokoyama, A., Hisaoka-Nakashima, K., Morioka, N., Takebayashi, M., Nakata, Y., Higami, Y., and Uezono, Y. (2014). History of the G protein-coupled receptor (GPCR) assays from traditional to a state-of-the-art biosensor assay. J. Pharmacol. Sci. *126*, 302–309.

Mizoguchi, I., Ohashi, M., Hasegawa, H., Chiba, Y., Orii, N., Inoue, S., Kawana, C., Xu, M., Sudo, K., Fujita, K., et al. (2020). EBV-induced gene 3 augments IL-23Rα protein expression through a chaperone calnexin. J. Clin. Invest. *130*, 6124–6140.

Mocellin, S., Pasquali, S., Rossi, C.R., and Nitti, D. (2010). Interferon alpha adjuvant therapy in patients with high-risk melanoma: A systematic review and meta-analysis. J. Natl. Cancer Inst. *102*, 493–501.

Mohr, A., Chatain, N., Domoszlai, T., Rinis, N., Sommerauer, M., Vogt, M., and Müller-Newen, G. (2012). Dynamics and non-canonical aspects of JAK/STAT signalling. Eur. J. Cell Biol. *91*, 6–7.

Monaco, G., Lee, B., Xu, W., Mustafah, S., Hwang, Y.Y., Carré, C., Burdin, N., Visan, L., Ceccarelli, M., Poidinger, M., et al. (2019). RNA-Seq Signatures Normalized by mRNA Abundance Allow Absolute Deconvolution of Human Immune Cell Types. Cell Rep. *26*, 1627-1640.

Mondal, S., Kundu, M., Jana, M., Roy, A., Rangasamy, S.B., Modi, K.K., Wallace, J., Albalawi, Y.A., Balabanov, R., and Pahan, K. (2020). IL-12 p40 monomer is different from other IL-12 family members to selectively inhibit IL-12Rβ1 internalization and suppress EAE. Proc. Natl. Acad. Sci. U. S. A.

117, 21557–21567.

Moraga, I., Wernig, G., Wilmes, S., Gryshkova, V., Richter, C.P., Hong, W.J., Sinha, R., Guo, F., Fabionar, H., Wehrman, T.S., et al. (2015a). Tuning cytokine receptor signaling by re-orienting dimer geometry with surrogate ligands. Cell *160*, 1196-1208.

Moraga, I., Richter, D., Wilmes, S., Winkelmann, H., Jude, K., Thomas, C., Suhoski, M.M., Engleman, E.G., Piehler, J., and Garcia, K.C. (2015b). Instructive roles for agonist binding parameters in determining the functional bandwidth of cytokine receptor signaling. Sci. Signal. *8*, 1–36.

Moriki, T., Maruyama, H., and Maruyama, I.N. (2001). Activation of preformed EGF receptor dimers by ligand-induced rotation of the transmembrane domain. J. Mol. Biol. *311*, 1011–1026.

Morris, R., Kershaw, N.J., and Babon, J.J. (2018). The molecular details of cytokine signaling via the JAK/STAT pathway. Protein Sci. *27*, 1984–2009.

Namour, F., Diderichsen, P.M., Cox, E., Vayssière, B., Van der Aa, A., Tasset, C., and Van't Klooster, G. (2015). Pharmacokinetics and Pharmacokinetic/Pharmacodynamic Modeling of Filgotinib (GLPG0634), a Selective JAK1 Inhibitor, in Support of Phase IIB Dose Selection. Clin. Pharmacokinet. *54*, 859-874.

Nanda, J.S., and Lorsch, J.R. (2014). Labeling a protein with fluorophores using NHS ester derivitization. In Methods in Enzymology, (Elsevier), pp. 87–94.

Nederveen-Schippers, L.M., Pathak, P., Keizer-Gunnink, I., Westphal, A.H., van Haastert, P.J.M., Borst, J.W., Kortholt, A., and Skakun, V. (2021). Combined fcs and pch analysis to quantify protein dimerization in living cells. Int. J. Mol. Sci. *22*, 7300–7319.

Ng, D.C.H., Bao, H.L., Cheh, P.L., Huang, G., Zhang, T., Poli, V., and Cao, X. (2006). Stat3 regulates microtubules by antagonizing the depolymerization activity of stathmin. J. Cell Biol. *172*, 245–257.

Nogueira, E., Hamour, S., Sawant, D., Henderson, S., Mansfield, N., Chavele,

K.M., Pusey, C.D., and Salama, A.D. (2010). Serum IL-17 and IL-23 levels and autoantigen-specific Th17 cells are elevated in patients with ANCA-associated vasculitis. Nephrol. Dial. Transplant. *25*.

Oh, C.K., Geba, G.P., and Molfino, N. (2010). Investigational therapeutics targeting the IL-4/IL-13/STAT-6 pathway for the treatment of asthma. Eur. Respir. Rev. *19*, 46–54.

Olsen, J.G., and Kragelund, B.B. (2014). Who climbs the tryptophan ladder? On the structure and function of the WSXWS motif in cytokine receptors and thrombospondin repeats. Cytokine Growth Factor Rev. *25*, 337–341.

Panda, S.K., and Colonna, M. (2019). Innate lymphoid cells in mucosal immunity. Front. Immunol. *10*, 1–13.

Pandya, P., Sayers, R.O., Ting, J.P., Morshedian, S., Torres, C., Cudal, J.S., Zhang, K., Fitchett, J.R., Zhang, Q., Zhang, F.F., et al. (2020). Integration of phage and yeast display platforms: A reliable and cost effective approach for binning of peptides as displayed on-phage. PLoS One *15*, 1–19.

Pang, X., and Zhou, H.X. (2012). A common model for cytokine receptor activation: Combined scissor-like rotation and self-rotation of receptor dimer induced by class I cytokine. PLoS Comput. Biol. *8*, 1–10.

Parascandola, J., and Jasensky, R. (1974). Origins of the receptor theory of drug action. Bull. Hist. Med. *48*, 199–220.

Parham, C., Chirica, M., Timans, J., Vaisberg, E., Travis, M., Cheung, J., Pflanz, S., Zhang, R., Singh, K.P., Vega, F., et al. (2002). A Receptor for the Heterodimeric Cytokine IL-23 Is Composed of IL-12Rβ1 and a Novel Cytokine Receptor Subunit, IL-23R. J. Immunol. *168*, 5699–5708.

Parigi, T.L., and Iacucci, M. (2022). Blockade of IL-23 : What is in the Pipeline ? J. Crohn's Colitis *16*, 64–72.

Paton, W., and Rang, H. (1965). The uptake of atropine and related drugs by intestinal smooth muscle of the guinea-pig in relation to acetylcholine receptors. Proc. R. Soc. London. Ser. B. Biol. Sci. *163*, 1–44.

Paul, M.D., and Hristova, K. (2019). The transition model of RTK activation:

A quantitative framework for understanding RTK signaling and RTK modulator activity. Cytokine Growth Factor Rev. *49*, 23–31.

Paulmurugant, R., and Gambhir, S.S. (2003). Monitoring protein-protein interactions using split synthetic renilla luciferase protein-fragment-assisted complementation. Anal. Chem. *75*, 1584–1589.

Pawlak-buś, K., Schmidt, W., and Leszczyński, P. (2021). Lack of association between serum interleukin-23 and interleukin-27 levels and disease activity in patients with active systemic lupus erythematosus. J. Clin. Med. *10*, 2–14.

Peach, C.J., Kilpatrick, L.E., Woolard, J., and Hill, S.J. (2021). Use of NanoBiT and NanoBRET to monitor fluorescent VEGF-A binding kinetics to VEGFR2/NRP1 heteromeric complexes in living cells. Br. J. Pharmacol. *178*, 2393–2411.

Pecquet, C., Chachoua, I., Roy, A., Balligand, T., Vertenoeil, G., Leroy, E., Albu, R.I., Defour, J.P., Nivarthi, H., Hug, E., et al. (2019). Calreticulin mutants as oncogenic rogue chaperones for TpoR and traffic-defective pathogenic TpoR mutants. Blood *133*, 2669–2681.

Pfleger, K.D.G., and Eidne, K.A. (2006). Illuminating insights into protein-protein interactions using bioluminescence resonance energy transfer (BRET). Nat. Methods *3*, 165–174.

Pidasheva, S., Trifari, S., Phillips, A., Hackney, J.A., Ma, Y., Smith, A., Sohn, S.J., Spits, H., Little, R.D., Behrens, T.W., et al. (2011). Functional studies on the IBD susceptibility gene IL23R implicate reduced receptor function in the protective genetic variant R381Q. PLoS One *6*, 1–9.

Pillet, A.H., Lavergne, V., Pasquier, V., Gesbert, F., Thèze, J., and Rose, T. (2010). IL-2 induces conformational changes in its preassembled receptor core, which then migrates in lipid raft and binds to the cytoskeleton meshwork. J. Mol. Biol. *403*, 671–692.

Potjewijd, J., de Paus, R.A., van Wengen, A., Damoiseaux, J., Verbon, A., and de Vosse, E. van (2012). Disseminated Mycobacterium genavense infection in a patient with a novel partial interleukin-12/23 receptor β1 deficiency. Clin.

Immunol. *144*.

Praveen Rao, P.N., and Knaus, E.E. (2008). Evolution of nonsteroidal anti-inflammatory drugs (NSAIDs): Cyclooxygenase (COX) inhibition and beyond. J. Pharm. Pharm. Sci. *11*, 81–110.

Qi, Q., Liu, Y., Cheng, Y., Glanville, J., Zhang, D., Lee, J.Y., Olshen, R.A., Weyand, C.M., Boyd, S.D., and Goronzy, J.J. (2014). Diversity and clonal selection in the human T-cell repertoire. Proc. Natl. Acad. Sci. U. S. A. *111*, 13139–13144.

Qian, L., Sun, G., Zhou, B., Wang, G., Song, J., and He, H. (2011). Study on the relationship between different cytokines in the semen of infertility patients. Am. J. Reprod. Immunol. *66*, 157–161.

Quiniou, C., Domínguez-Punaro, M., Cloutier, F., Erfani, A., Ennaciri, J., Sivanesan, D., Sanchez, M., Chognard, G., Hou, X., Rivera, J.C., et al. (2014). Specific targeting of the IL-23 receptor, using a novel small peptide noncompetitive antagonist, decreases the inflammatory response. Am. J. Physiol. Integr. Comp. Physiol. *82*, 1216–1230.

Rabalski, A.J., Gyenis, L., and Litchfield, D.W. (2016). Molecular pathways: Emergence of protein kinase CK2 (CSNK2) as a potential target to inhibit survival and DNA damage response and repair pathways in cancer cells. Clin. Cancer Res. *22*, 2840–2847.

Rafat, S., Mohamed, Y.Y., Ahmed, M.E., and Abdelaleem, E.A. (2022). Interleukin-23 serum level in systemic lupus erythematosus patients: Relation to disease activity and different disease parameters. Egypt. Rheumatol. *44*.

Rahmati, S., Tsoi, L., O'Rielly, D., Chandran, V., and Rahman, P. (2020). Complexities in Genetics of Psoriatic Arthritis. Curr. Rheumatol. Rep. *22*, 1–8.

Rana, A., Minz, R.W., Aggarwal, R., Anand, S., Pasricha, N., and Singh, S. (2012). Gene expression of cytokines (TNF-α, IFN-γ), serum profiles of IL-17 and IL-23 in paediatric systemic lupus erythematosus. Lupus *21*.

Ray, A.A., Fountain, J.J., Miller, H.E., Cooper, A.M., and Robinson, R.T. (2015). IL12Rβ1ΔTM is a secreted product of il12rb1 that promotes control of

extrapulmonary tuberculosis. Infect. Immun. *83*, 560-571.

Rectenwald, J.M., Hardy, P.B., Norris-Drouin, J.L., Cholensky, S.H., James, L.I., Frye, S. V., and Pearce, K.H. (2019). A General TR-FRET Assay Platform for High-Throughput Screening and Characterizing Inhibitors of Methyl-Lysine Reader Proteins. SLAS Discov. *24*, 693–700.

Remmers, E.F., Cosan, F., Kirino, Y., Ombrello, M.J., Abaci, N., Satorius, C., Le, J.M., Yang, B., Korman, B.D., Cakiris, A., et al. (2010). Genome-wide association study identifies variants in the MHC class I, IL10, and IL23R-IL12RB2 regions associated with Behçet's disease. Nat. Genet. *42*, 698-702.

Remy, I., Wilson, I.A., and Michnick, S.W. (1999). Erythropoietin receptor activation by a ligand-induced conformation change. Science. *283*, 990–993.

Riviere, Y., Cresser, I., Guillon, J.C., and Tovey, M.G. (1977). Inhibition by anti interferon serum of lymphocyte choriomeningitis virus disease in suckling mice. Proc. Natl. Acad. Sci. U. S. A. *74*, 2135–2139.

Robers, M.B., Dart, M.L., Woodroofe, C.C., Zimprich, C.A., Kirkland, T.A., Machleidt, T., Kupcho, K.R., Levin, S., Hartnett, J.R., Zimmerman, K., et al. (2015). Target engagement and drug residence time can be observed in living cells with BRET. Nat. Commun. *6*, 1–10.

Robinson, R.T., Khader, S.A., Martino, C.A., Fountain, J.J., Teixeira-Coelho, M., Pearl, J.E., Smiley, S.T., Winslow, G.M., Woodland, D.L., Walter, M.J., et al. (2010). Mycobacterium tuberculosis infection induces il12rb1 splicing to generate a novel IL-12Rβ1 isoform that enhances DC migration. J. Exp. Med. *207*, 591-605.

Roda, A., Pasini, P., Mirasoli, M., Michelini, E., and Guardigli, M. (2004). Biotechnological applications of bioluminescence and chemiluminescence. Trends Biotechnol. *22*, 295–303.

Rose-John, S. (2012). IL-6 trans-signaling via the soluble IL-6 receptor: Importance for the proinflammatory activities of IL-6. Int. J. Biol. Sci. *8*, 1237–1247.

Rostami, M., Haidari, K., and Shahbazi, M. (2018). The Human IL-23 Decoy

Receptor Inhibits T-Cells Producing IL-17 by Genetically Engineered Mesenchymal Stem Cells. Int. J. Cell Biol. *2018*, 1–15.

Rowlinson, S.W., Behncken, S.N., Rowland, J.E., Clarkson, R.W., Strasburger, C.J., Wu, Z., Baumbach, W., and Waters, M.J. (1998). Activation of chimeric and full-length growth hormone receptors by growth hormone receptor monoclonal antibodies: A specific conformational change may be required for full-length receptor signaling. J. Biol. Chem. *273*, 5307-5314.

Rui, H., Lebrun, J.J., Kirken, R.A., Kelly, P.A., and Farrar, W.L. (1994). JAK2 activation and cell proliferation induced by antibody-mediated prolactin receptor dimerization. Endocrinology *135*, 1299–1306.

Ruiz de Morales, J.M.G., Puig, L., Daudén, E., Cañete, J.D., Pablos, J.L., Martín, A.O., Juanatey, C.G., Adán, A., Montalbán, X., Borruel, N., et al. (2020). Critical role of interleukin (IL)-17 in inflammatory and immune disorders: An updated review of the evidence focusing in controversies. Autoimmun. Rev. *19*, 1–15.

Saleki, K., Yaribash, S., Banazadeh, M., Hajihosseinlou, E., Gouravani, M., Saghazadeh, A., and Rezaei, N. (2021). Interferon therapy in patients with SARS, MERS, and COVID-19: A systematic review and meta-analysis of clinical studies. Eur. J. Pharmacol. *906*, 1–32.

Sasaki, A., Yasukawa, H., Suzuki, A., Kamizono, S., Syoda, T., Kinjyo, I., Sasaki, M., Johnston, J.A., and Yoshimura, A. (1999). Cytokine-inducible SH2 protein-3 (CIS3/SOCS3) inhibits Janus tyrosine kinase by binding through the N-terminal kinase inhibitory region as well as SH2 domain. Genes to Cells *4*, 339-351.

Sayago, C., Gonzalez Valcarcel, I.C., Qian, Y., Lee, J., Alsina-Fernandez, J., Fite, N.C., Carrillo, J.J., Zhang, F.F., Chalmers, M.J., Dodge, J.A., et al. (2018). Deciphering Binding Interactions of IL-23R with HDX-MS: Mapping Protein and Macrocyclic Dodecapeptide Ligands. ACS Med. Chem. Lett. *9*, 912–916.

Scheide-Noeth, J.P., Rosen, M., Baumstark, D., Dietz, H., and Mueller, T.D. (2019). Structural Basis of Interleukin-5 Inhibition by the Small Cyclic Peptide

AF17121. J. Mol. Biol. *431*, 714–731.

Scheinecker, C., Redlich, K., and Smolen, J.S. (2008). Cytokines as Therapeutic Targets: Advances and Limitations. Immunity *28*, 440-444.

Schiele, F., Ayaz, P., and Fernández-Montalván, A. (2015). A universal homogeneous assay for high-throughput determination of binding kinetics. Anal. Biochem. *468*, 42–49.

Schlüter, T., Schelmbauer, C., Karram, K., and Mufazalov, I.A. (2018). Regulation of IL-1 signaling by the decoy receptor IL-1R2. J. Mol. Med. *96*, 983–992.

Schmidt, T., Ye, F., Situ, A.J., An, W., Ginsberg, M.H., and Ulmer, T.S. (2016). A conserved ectodomain-transmembrane domain linker motif tunes the allosteric regulation of cell surface receptors. J. Biol. Chem. *291*, 17536–17546.

Schmiedel, B.J., Singh, D., Madrigal, A., Valdovino-Gonzalez, A.G., White, B.M., Zapardiel-Gonzalo, J., Ha, B., Altay, G., Greenbaum, J.A., McVicker, G., et al. (2018). Impact of Genetic Polymorphisms on Human Immune Cell Gene Expression. Cell *175*, 1701–1715.

Schreiber, G., and Walter, M.R. (2010). Cytokine-receptor interactions as drug targets. Curr. Opin. Chem. Biol. *14*, 511–519.

Schroder, J., Moll, J.M., Baran, P., Grotzinger, J., Scheller, J., and Floss, D.M. (2015). Non-canonical interleukin 23 receptor complex assembly: P40 protein recruits interleukin 12 receptor β1 via site II and induces P19/interleukin 23 receptor interaction via site III. J. Biol. Chem. *290*, 359–370.

Schröder, M., Kroeger, K.M., Volk, H.-D., Eidne, K.A., and Grütz, G. (2004). Preassociation of nonactivated STAT3 molecules demonstrated in living cells using bioluminescence resonance energy transfer: a new model of STAT activation? J. Leukoc. Biol. *75*, 792–797.

Schürmann, M., Janning, P., Ziegler, S., and Waldmann, H. (2016). Small-Molecule Target Engagement in Cells. Cell Chem. Biol. *23*, 435–441.

Schust, J., Sperl, B., Hollis, A., Mayer, T.U., and Berg, T. (2006). Stattic: A

Small-Molecule Inhibitor of STAT3 Activation and Dimerization. Chem. Biol. *13*, 1235–1242.

Schuster, B., Meinert, W., Rose-John, S., and Kallen, K.J. (2003). The human interleukin-6 (IL-6) receptor exists as a preformed dimer in the plasma membrane. FEBS Lett. *538*, 113–116.

Schütt, A., Zacharias, M., Schneider, N., Horn, S., Grötzinger, J., Rose-John, S., and Schmidt-Arras, D. (2013). Gp130 activation is regulated by D2-D3 interdomain connectivity. Biochem. J. *450*, 487-496.

Seiffert, P., Bugge, K., Nygaard, M., Haxholm, G.W., Martinsen, J.H., Pedersen, M.N., Arleth, L., Boomsma, W., and Kragelund, B.B. (2020). Orchestration of signaling by structural disorder in class 1 cytokine receptors. Cell Commun. Signal. *18*, 1–30.

Seubert, N., Royer, Y., Staerk, J., Kubatzky, K.F., Moucadel, V., Krishnakumar, S., Smith, S.O., and Constantinescu, S.N. (2003). Active and inactive orientations of the transmembrane and cytosolic domains of the erythropoietin receptor dimer. Mol. Cell *12*, 1239–1250.

Shan, Y., Gnanasambandan, K., Ungureanu, D., Kim, E.T., Hammarén, H., Yamashita, K., Silvennoinen, O., Shaw, D.E., and Hubbard, S.R. (2014). Molecular basis for pseudokinase-dependent autoinhibition of JAK2 tyrosine kinase. Nat. Struct. Mol. Biol. *21*, 579–584.

Shigehara, K., Shijubo, N., Ohmichi, M., Kamiguchi, K., Takahashi, R., Morita-Ichimura, S., Ohchi, T., Tatsuno, T., Hiraga, Y., Abe, S., et al. (2003). Increased circulating interleukin-12 (IL-12) p40 in pulmonary sarcoidosis. Clin. Exp. Immunol. *132*, 152-157.

Shimomura, O. (2010). Bioluminescence - Chemical Principles and Methods (World Scientific).

Shuai, K., Ziemiecki, A., Wilks, A.F., Harpur, A.G., Sadowski, H.B., Gilman, M.Z., and Darnell, J.E. (1993). Polypeptide signalling to the nucleus through tyrosine phosphorylation of Jak and Stat proteins. Nature *366*, 580–583.

Sivanesan, D., Beauchamp, C., Quinou, C., Lee, J., Lesage, S., Chemtob, S.,

Rioux, J.D., and Michnick, S.W. (2016). IL23R (Interleukin 23 Receptor) variants protective against inflammatory bowel diseases (IBD) display loss of function due to impaired protein stability and intracellular trafficking. J. Biol. Chem. *291*, 8673–8685.

Soave, M., Kellam, B., Woolard, J., Briddon, S.J., and Hill, S.J. (2020a). NanoBiT Complementation to Monitor Agonist-Induced Adenosine A1 Receptor Internalization. SLAS Discov. *25*, 186–194.

Soave, M., Heukers, R., Kellam, B., Woolard, J., Smit, M.J., Briddon, S.J., and Hill, S.J. (2020b). Monitoring Allosteric Interactions with CXCR4 Using NanoBiT Conjugated Nanobodies. Cell Chem. Biol. *27*, 1250–1261.

Soave, M., Briddon, S.J., Hill, S.J., and Stoddart, L.A. (2020c). Fluorescent ligands: Bringing light to emerging GPCR paradigms. Br. J. Pharmacol. *177*, 978–991.

Soave, M., Stoddart, L.A., White, C.W., Kilpatrick, L.E., Goulding, J., Briddon, S.J., and Hill, S.J. (2021). Detection of genome-edited and endogenously expressed G protein-coupled receptors. FEBS J. *288*, 2585-2601.

Spangler, J.B., Moraga, I., Mendoza, J.L., and Garcia, K.C. (2015). Insights into cytokine-receptor interactions from cytokine engineering. Annu. Rev. Immunol. *33*, 139–167.

Staels, F., Lorenzetti, F., Keukeleere, K. De, Willemsen, M., Gerbaux, M., Neumann, J., Tousseyn, T., Pasciuto, E., Munter, P. De, Bossuyt, X., et al. (2022). A Novel Homozygous Stop Mutation in IL23R Causes Mendelian Susceptibility to Mycobacterial Disease. J. Clin. Immunol. *42*, 1638–1652.

Stoddart, L.A., White, C.W., Nguyen, K., Hill, S.J., and Pfleger, K.D.G. (2016). Fluorescence- and bioluminescence-based approaches to study GPCR ligand binding. Br. J. Pharmacol. *173*, 3028–3037.

Stoddart, L.A., Kilpatrick, L.E., and Hill, S.J. (2018). NanoBRET Approaches to Study Ligand Binding to GPCRs and RTKs. Trends Pharmacol. Sci. *39*, 136–147.

Stone, T.A., and Deber, C.M. (2017). Therapeutic design of peptide modulators of protein-protein interactions in membranes. Biochim. Biophys. Acta - Biomembr. *1859*, 577–585.

Sulkowski, M.S., Cooper, C., Hunyady, B., Jia, J., Ogurtsov, P., Peck-Radosavljevic, M., Shiffman, M.L., Yurdaydin, C., and Dalgard, O. (2011). Management of adverse effects of Peg-IFN and ribavirin therapy for hepatitis C. Nat. Rev. Gastroenterol. Hepatol. *8*, 212–223.

Sun, R., Hedl, M., and Abraham, C. (2020). IL23R recycling and amplifies innate receptor-induced signalling and cytokines in human macrophages, and the IBD-protective IL23R R381Q variant modulates these outcomes. Gut *69*, 264–273.

Sutton, C.E., Lalor, S.J., Sweeney, C.M., Brereton, C.F., Lavelle, E.C., and Mills, K.H.G. (2009). Interleukin-1 and IL-23 Induce Innate IL-17 Production from γδ T Cells, Amplifying Th17 Responses and Autoimmunity. Immunity *31*, 331–341.

Takatori, H., Kanno, Y., Watford, W.T., Tato, C.M., Weiss, G., Ivanov, I.I., Littman, D.R., and O'Shea, J.J. (2009). Lymphoid tissue inducer-like cells are an innate source of IL-17 and IL-22. J. Exp. Med. *206*, 35–41.

Tanaka, K., Ichiyama, K., Hashimoto, M., Yoshida, H., Takimoto, T., Takaesu, G., Torisu, T., Hanada, T., Yasukawa, H., Fukuyama, S., et al. (2008). Loss of Suppressor of Cytokine Signaling 1 in Helper T Cells Leads to Defective Th17 Differentiation by Enhancing Antagonistic Effects of IFN-γ on STAT3 and Smads. J. Immunol. *180*, 3746–3756.

Teng, M.W.L., Bowman, E.P., McElwee, J.J., Smyth, M.J., Casanova, J.L., Cooper, A.M., and Cua, D.J. (2015). IL-12 and IL-23 cytokines: From discovery to targeted therapies for immune-mediated inflammatory diseases. Nat. Med. *21*, 719–729.

Tenhumberg, S., Schuster, B., Zhu, L., Kovaleva, M., Scheller, J., Kallen, K.J., and Rose-John, S. (2006). gp130 dimerization in the absence of ligand: Preformed cytokine receptor complexes. Biochem. Biophys. Res. Commun. *346*, 649–657.

Thimaradka, V., Hoon Oh, J., Heroven, C., Radu Aricescu, A., Yuzaki, M., Tamura, T., and Hamachi, I. (2021). Site-specific covalent labeling of His-tag fused proteins with N-acyl-N-alkyl sulfonamide reagent. Bioorganic Med. Chem. *30*, 1–6.

Tsurushita, N., Hinton, P.R., and Kumar, S. (2005). Design of humanized antibodies: From anti-Tac to Zenapax. Methods *36*, 69–83.

Ugur, M., Baygutalp, N.K., Melikoglu, M.A., Baygutalp, F., Altas, E.U., and Seferoglu, B. (2015). Elevated serum interleukin-23 levels in ankylosing spondylitis patients and the relationship with disease activity. Nagoya J. Med. Sci. *77*.

Uhlen, M., Karlsson, M.J., Zhong, W., Tebani, A., Pou, C., Mikes, J., Lakshmikanth, T., Forsström, B., Edfors, F., Odeberg, J., et al. (2019). A genome-wide transcriptomic analysis of protein-coding genes in human blood cells. Science. *366*, 1–13.

Ulgesa, A., Witsch, E.J., Pramanik, G., Klein, M., Birkner, K., Bühler, U., Wasser, B., Luessi, F., Stergiou, N., Dietzen, S., et al. (2016). Protein kinase CK2 governs the molecular decision between encephalitogenic TH 17 cell and Treg cell development. Proc. Natl. Acad. Sci. U. S. A. *113*, 10145–10150.

Urquhart, L. (2021). Top product forecasts for 2021. Nat. Rev. Drug Discov. *20*, 10–11.

Varghese, T.M., Dudas, P.L., Allen, S.J., Schneeweis, J.E., and Finley, M.F.A. (2020). Optimization of a High-Throughput Cell-Based Screening Strategy to Identify Small-Molecule Inhibitors of IL-23 Signaling. SLAS Discov. *26*, 122–129.

Verreck, F.A.W., De Boer, T., Langenberg, D.M.L., Hoeve, M.A., Kramer, M., Vaisberg, E., Kastelein, R., Kolk, A., De Waal-Malefyt, R., and Ottenhoff, T.H.M. (2004). Human IL-23-producing type 1 macrophages promote but IL-10-producing type 2 macrophages subvert immunity to (myco)bacteria. Proc. Natl. Acad. Sci. U. S. A. *101*, 4560-4565.

Vignali, D.A.A., and Kuchroo, V.K. (2012). IL-12 family cytokines:

immunological playmakers. Nat. Immunol. *13*, 722–728.

Vila-Coro, A.J., Rodríguez-Frade, J.M., Martín De Ana, A., Moreno-Ortíz, M.C., Martínez-A, C., and Mellado, M. (1999). The chemokine SDF-1alpha triggers CXCR4 receptor dimerization and activates the JAK/STAT pathway. FASEB J. *13*, 1699–1710.

Vilček, J., and Feldmann, M. (2004). Historical review: Cytokines as therapeutics and targets of therapeutics. Trends Pharmacol. Sci. *25*, 201–209.

Virtanen, A.T., Haikarainen, T., Raivola, J., and Silvennoinen, O. (2019). Selective JAKinibs: Prospects in Inflammatory and Autoimmune Diseases. BioDrugs *33*, 15–32.

van de Vosse, E., de Paus, R.A., van Dissel, J.T., and Ottenhoff, T.H.M. (2005). Molecular complementation of IL-12Rβ1 deficiency reveals functional differences between IL-12Rβ1 alleles including partial IL-12Rβ1 deficiency. Hum. Mol. Genet. *14*.

van de Vosse, E., Haverkamp, M.H., Ramirez-Alejo, N., Martinez-Gallo, M., Blancas-Galicia, L., Metin, A., Garty, B.Z., Sun-Tan, Ç., Broides, A., de Paus, R.A., et al. (2013). IL-12Rβ1 deficiency: Mutation update and description of the IL12RB1 variation database. Hum. Mutat. *34*, 1329–1339.

Walker, J.R., Hall, M.P., Zimprich, C.A., Robers, M.B., Duellman, S.J., Machleidt, T., Rodriguez, J., and Zhou, W. (2017). Highly Potent Cell-Permeable and Impermeable NanoLuc Luciferase Inhibitors. ACS Chem. Biol. *12*, 1028–1037.

Wallweber, H.J.A., Tam, C., Franke, Y., Starovasnik, M.A., and Lupardus, P.J. (2014). Structural basis of recognition of interferon-α receptor by tyrosine kinase 2. Nat. Struct. Mol. Biol. *21*, 443–448.

Walter, M.R. (2020). The Role of Structure in the Biology of Interferon Signaling. Front. Immunol. *11*, 1–12.

Wang, H., Kjer-Nielsen, L., Shi, M., D'Souza, C., Pediongco, T.J., Cao, H., Kostenko, L., Lim, X.Y., Eckle, S.B.G., Meehan, B.S., et al. (2019). IL-23 costimulates antigen-specific MAIT cell activation and enables vaccination

against bacterial infection. Sci. Immunol. *4*, 1–14.

Wang, X., Wei, Y., Xiao, H., Liu, X., Zhang, Y., Han, G., Chen, G., Hou, C., Ma, N., Shen, B., et al. (2016). A novel IL-23p19/Ebi3 (IL-39) cytokine mediates inflammation in Lupus-like mice. Eur. J. Immunol. *46*, 1343–1350.

Waters, M.J., and Brooks, A.J. (2015). JAK2 activation by growth hormone and other cytokines. Biochem. J. *466*, 1–11.

Waters, M.J., Brooks, A.J., and Chhabra, Y. (2014). A new mechanism for growth hormone receptor activation of JAK2, and implications for related cytokine receptors. JAK-STAT *3*, 2162–3996.

Waugh, J., and Perry, C.M. (2005). Anakinra: A review of its use in the management of rheumatoid arthritis. BioDrugs *19*, 1095–1119.

Wegrzyn, J., Potla, R., Chwae, Y.J., Sepuri, N.B.V., Zhang, Q., Koeck, T., Derecka, M., Szczepanek, K., Szelag, M., Gornicka, A., et al. (2009). Function of mitochondrial Stat3 in cellular respiration. Science. *323*, 793–797.

Werner, J.L., Gessner, M.A., Lilly, L.M., Nelson, M.P., Metz, A.E., Horn, D., Dunaway, C.W., Deshane, J., Chaplin, D.D., Weaver, C.T., et al. (2011). Neutrophils produce interleukin 17A (IL-17A) in a Dectin-1- and IL-23-dependent manner during invasive fungal infection. Infect. Immun. *79*, 3966–3977.

Westerfield, J.M., and Barrera, F.N. (2020). Membrane receptor activation mechanisms and transmembrane peptide tools to elucidate them. J. Biol. Chem. *295*, 1792–1814.

Wilmes, S., Beutel, O., Li, Z., Francois-Newton, V., Richter, C.P., Janning, D., Kroll, C., Hanhart, P., Hötte, K., You, C., et al. (2015). Receptor dimerization dynamics as a regulatory valve for plasticity of type I interferon signaling. J. Cell Biol. *209*, 579–593.

Wilmes, S., Hafer, M., Vuorio, J., Tucker, J.A., Winkelmann, H., Löchte, S., Stanly, T.A., Pulgar Prieto, K.D., Poojari, C., Sharma, V., et al. (2020). Mechanism of homodimeric cytokine receptor activation and dysregulation by oncogenic mutations. Science. *367*, 643–652.

Wilson, C.G.M., and Arkin, M.R. (2010). Small-molecule inhibitors of IL-2/IL-2R: Lessons learned and applied. Curr. Top. Microbiol. Immunol. *348*, 25–59.

Wu, T.R., Kate Hong, Y., Wang, X.D., Ling, M.Y., Dragoi, A.M., Chung, A.S., Campbell, A.G., Han, Z.Y., Feng, G.S., and Chin, Y.E. (2002). SHP-2 is a dual-specificity phosphatase involved in Stat1 dephosphorylation at both tyrosine and serine residues in nuclei. J. Biol. Chem. *277*, 47572–47580.

Yang, K., Oak, A.S.W., and Elewski, B.E. (2021). Use of IL-23 Inhibitors for the Treatment of Plaque Psoriasis and Psoriatic Arthritis: A Comprehensive Review. Am. J. Clin. Dermatol. *22*, 173–192.

Yang, L., Anderson, D.E., Baecher-Allan, C., Hastings, W.D., Bettelli, E., Oukka, M., Kuchroo, V.K., and Hafler, D.A. (2008). IL-21 and TGF-β are required for differentiation of human T H17 cells. Nature *454*, 350–352.

Yoon, C., Johnston, S.C., Tang, J., Stahl, M., Tobin, J.F., and Somers, W.S. (2000). Charged residues dominate a unique interlocking topography in the heterodimeric cytokine interleukin-12. EMBO J. *19*, 3530–3541.

Yoshida, H., and Hunter, C.A. (2015). The immunobiology of interleukin-27. Annu. Rev. Immunol. *33*, 417-443.

Youssef, T., Saleh, S.A., Rund, A., Montasser, I., Mohsen, M., and Hazem, O. (2018). Evaluation of interleukin 23 (IL-23) as a non-invasive test of disease severity in patients with ulcerative colitis. Arab J. Gastroenterol. *19*.

Zeng, R., Aoki, Y., Yoshida, M., Arai, K. -i., and Watanabe, S. (2014). Stat5B Shuttles Between Cytoplasm and Nucleus in a Cytokine-Dependent and -Independent Manner. J. Immunol. *168*, 4567–4575.

Zhang, N., and Bevan, M.J. (2011). CD8+ T Cells: Foot Soldiers of the Immune System. Immunity *35*, 161–168.

Zhang, J., Zhang, Y., Wang, Q., Li, C., Deng, H., Si, C., and Xiong, H. (2019). Interleukin-35 in immune-related diseases: protection or destruction. Immunology *157*, 13–20.

Zhang, X.Y., Zhang, H.J., Zhang, Y., Fu, Y.J., He, J., Zhu, L.P., Wang, S.H.,

and Liu, L. (2006). Identification and expression analysis of alternatively spliced isoforms of human interleukin-23 receptor gene in normal lymphoid cells and selected tumor cells. Immunogenetics *57*, 934–943.

Zhao, R., Xing, S., Li, Z., Fu, X., Li, Q., Krantz, S.B., and Zhao, Z.J. (2005). Identification of an acquired JAK2 mutation in polycythemia vera. J. Biol. Chem. *280*, 22788–22792.

Zheng, Y., Qin, H., Frank, S.J., Deng, L., Litchfield, D.W., Tefferi, A., Pardanani, A., Lin, F.T., Li, J., Sha, B., et al. (2011). A CK2-dependent mechanism for activation of the JAK-STAT signaling pathway. Blood *118*, 156–166.

Zhou, L., Ivanov, I.I., Spolski, R., Min, R., Shenderov, K., Egawa, T., Levy, D.E., Leonard, W.J., and Littman, D.R. (2007). IL-6 programs TH-17 cell differentiation by promoting sequential engagement of the IL-21 and IL-23 pathways. Nat. Immunol. *8*, 967–974.

Ziblat, A., Nuñez, S.Y., Iraolagoitia, X.L.R., Spallanzani, R.G., Torres, N.I., Sierra, J.M., Secchiari, F., Domaica, C.I., Fuertes, M.B., and Zwirner, N.W. (2018). Interleukin (IL)-23 stimulates IFN-γ secretion by CD56bright natural killer cells and enhances IL-18-driven dendritic cells activation. Front. Immunol. *8*, 1–11.

Zlotnik, A., and Yoshie, O. (2012). The Chemokine Superfamily Revisited. Immunity *36*, 705–716.